České vysoké učení technické v Praze
Fakulta jaderná a fyzikálně inženýrská

HABILITAČNÍ PRÁCE

2014 Jiří Mikyška

CZECH TECHNICAL UNIVERSITY IN PRAGUE

faculty of nuclear sciences and physical engineering

HABILITAČNÍ PRÁCE

Matematické modelování transportu směsí v porézním prostředí

Jiří Mikyška

Obsah

Kapitola 1

Předmluva

Matematické modely transportu směsí chemických látek v porézním prostředí hrají důležitou roli při studiu mnoha procesů v přírodě i technice [5, 47, 89]. Z různých aplikací můžeme jmenovat např. vtláčení CO_2 do podzemí za účelem trvalého uložení v horninovém masivu (prevence skleníkového efektu pomocí technologie Carbon Capture and Storage – CCS), injektáž plynu do ropných ložisek za účelem zvýšení jejich výtěžnosti [80, 12, 3], či řešení ekologických problémů vznikajících průnikem kontaminace do horninového prostředí [38, 1, 98]. Při řešení těchto problémů je potřebné simulovat transport komponent vícesložkové směsi v pórézním prostředí. Např. při vtlačování CO_2 do podzemí se superkritický CO_2 vtlačuje do rezervoáru, který obsahuje vodu a/nebo ropu. V závislosti na vnějších podmínkách může směs být homogenní (CO_2 se plně rozpustí ve vodě, resp. ropě) nebo se směs může rozdělit na dvě nebo více fází, které mají navzájem rozdílné hustoty a chemická složení [82, 78]. Pokud se směs rozdělí do dvou fází (v případě ropy např. plyn obsahující převážně CO_2 a lehčí alkany a kapalinu obsahující převážně těžší alkany a menší množství rozpuštěného CO_2) může dojít k tomu, že lehčí fáze bude mít výrazně nižší viskozitu než původní jednofázová směs, což povede ke zlepšení výtěžnosti rezervoáru.

Při ukládání CO_2 do podzemí za účelem trvalého uložení v hlubinných uložištích lze využít jedinečných vlastností směsí obsahujících CO_2. Je dobře známo, že při směšování CO_2 a vody při zadané teplotě a tlaku výsledná směs zaujme obecně jiný objem než je součet objemů vody a CO_2 před směšováním [30]. Směšování vody a CO_2 obecně vede ke změně hustoty směsi, jedná se tedy o silně neideální směsi. Stavové chování takovýchto směsí je třeba popisovat prostředky rovnovážné termodynamiky. Zároveň je potřeba konzistentně propojit tyto termodynamické výpočty s výpočtem proudění vícefázové směsi. To vede k modelům popisujícím transport komponent vícesložkových směsí, přičemž komponenty mohou přecházet mezi fázemi. Přestože jak termodynamika směsí, tak simulace transportu v pórézním prostředí jsou dobře rozvinuté disciplíny, ukazuje se, že propojení těchto dvou disciplín není triviální a je zdrojem mnoha problémů, které je potřeba řešit. Jedná se tedy o interdisciplinární problematiku propojující znalosti z termodynamiky směsí, mechaniky tekutin a termodynamiky kontinua spolu s poznatky z numerické matematiky a matematického modelování.

Cílem této práce je stručně popsat současný stav a shrnout příspěvky autora k této problematice. Nejprve bude popsána konvenční formulace kompozičního modelu a budou představeny některé její nedostatky, které bývají v literatuře často opomíjeny. Zkušenosti s těmito modely, které získal autor této práce během svého osmiměsíčního pobytu v Reservoir Engineering Research Institute v Palo Alto v Kalifornii, potom vedly k návrhu různých modifikací formulace konvenčního modelu i k návrhu alternativních přístupů řešení transportního modelu. Tyto nové formulace a metody jsou základem přiložených publikací. Popis těchto příspěvků autora je hlavní částí této práce.

Kapitola 2

Modelování transportu směsí v porézním prostředí

2.1 Fyzikální formulace konvenčního transportního modelu

2.1.1 Transportní rovnice

Budeme vyšetřovat dvoufázové stlačitelné proudění směsi n chemických komponent v porézním prostředí vymezeném oblastí Ω. Omezíme se na případ nestlačitelného porézního prostředí s porozitou ϕ, která může obecně záviset na poloze, tj. $\phi = \phi(\mathbf{x})$. Budeme uvažovat isotermální případ – tj. proudění při konstantní teplotě T. Bilanci hmoty pro každou komponentu lze zapsat ve tvaru

$$\frac{\partial(\phi c_i)}{\partial t} + \nabla \cdot \mathbf{q}_i = F_i, \qquad i = 1, \ldots, n, \tag{2.1}$$

kde $c_i = c_i(\mathbf{x}, t)$ jsou neznámé celkové molární koncentrace jednotlivých komponent směsi, $\mathbf{q}_i$ je hustota molárního toku i-té komponenty a zdrojový člen F_i popisuje objemovou hustotu vtláčení, resp. čerpání i-té komponenty ve vyšetřované oblasti (počet molů dodaných do jednotkového objemu zeminy za jednotku času). V každém bodě $\mathbf{x} \in \Omega$ (a každém čase t) jsou v daném bodě definovány koncentrace c_i všech komponent $i = 1, \ldots, n$. Jedná se tedy o model směsi pomocí překrývajících se kontinuí.

V závislosti na vnějších podmínkách se může v daném bodě směs vyskytovat buď v jedné nebo více fázích. Každá fáze α je charakterizována svým chemickým složením (přesněji souborem molárních koncentrací jednotlivých komponent ve fázi α), saturací (objemovým zlomkem) S_α a rychlostí. Na pórové úrovni jsou fáze prostorově oddělené podoblasti pórového prostoru. Na makroskopickém měřítku však nevidíme lokální detaily a pracujeme s průměrovanými veličinami přes vhodně zvolené reprezentativní elementární objemy. Saturace je tedy makroskopická veličina, která udává podíl objemu pórového prostoru obsazený fází α na celkovém pórovém prostoru. Veličiny S_α jsou tak definovány v každém bodě oblasti a tvoří překrývající se kontinua.

Z definice saturace plyne, že

$$\sum_{\alpha} S_\alpha = 1. \tag{2.2}$$

Neuvažujeme-li difuzi, pak rychlost všech komponent v dané fázi je stejná. Celková hustota molárního toku i-té komponenty je tedy dána předpisem

$$\mathbf{q}_i = \sum_{\alpha} c_{\alpha,i}\mathbf{v}_\alpha, \tag{2.3}$$

kde se sčítá přes všechny fáze α, $c_{\alpha,i}$ je molární koncentrace i-té komponenty ve fázi α a $\mathbf{v}_\alpha$ je rychlost fáze α. Předpokládáme, že rychlost fáze α je dobře popsána Darcyho zákonem tvaru [22, 5]

$$\mathbf{v}_\alpha = -\lambda_\alpha \mathbf{K}(\nabla p - \varrho_\alpha \mathbf{g}), \quad \lambda_\alpha = \frac{k_{r\alpha}}{\eta_\alpha}, \tag{2.4}$$

kde $\mathbf{K} = \mathbf{K}(\mathbf{x})$ označuje vlastní propustnost zeminy, p je tlak, $\varrho_\alpha = \sum_{i=1}^{n} c_{\alpha,i}M_i$ je hustota fáze α, M_i je molární hmotnost i-té komponenty a $\mathbf{g}$ označuje vektor gravitačního zrychlení. Mobilita λ_α fáze α je definována jako podíl relativní permeability $k_{r\alpha}$ fáze α a dynamické viskozity η_α fáze α. Relativní permeabilita $k_{r\alpha} : \langle 0, 1\rangle \mapsto \langle 0, 1\rangle$ je veličina popisující redukci permeability z důvodu přítomnosti ostatních fází. Obecně závisí na saturaci S_α fáze α

$$k_{r\alpha} = k_{r\alpha}\left(S_\alpha\right) \tag{2.5}$$

a k jejímu modelování používáme buď lineární ($k_{r\alpha}\left(S_\alpha\right) = S_\alpha$) nebo kvadratický ($k_{r\alpha}\left(S_\alpha\right) = S_\alpha^2$) model. Podle zvoleného modelu závisí dynamická viskozita η_α fáze α na teplotě a molárních koncentracích fáze α, příp. tlaku p, teplotě T a molárních zlomcích jednotlivých komponent $x_{\alpha,i} = c_{\alpha,i}/c_\alpha$, kde $c_\alpha = \sum_{i=1}^{n} c_{\alpha,i}$ je celková molární koncentrace fáze α, tedy

$$\eta_\alpha = \eta_\alpha(T, c_{\alpha,1}, \ldots, c_{\alpha,n}), \qquad \text{resp.} \qquad \eta_\alpha = \eta_\alpha(p, T, x_{\alpha,1}, \ldots, x_{\alpha,n}). \tag{2.6}$$

Pro modelování této závislosti používáme model LBC (Lohrenz-Bray-Clark) [60], který je stručně popsán v příloze článku [Č5].

2.1.2 Přestup komponent mezi fázemi

Uvedený model je třeba doplnit konstitutivními vztahy, které popíší vazby mezi celkovými koncentracemi c_i a počtem fází, fázovými koncentracemi $c_{\alpha,i}$ všech komponent ve všech fázích a saturacemi S_α všech fází. K modelování přestupu komponent mezi fázemi se běžně používá předpoklad lokální termodynamické rovnováhy, který je v daném kontextu dobře fyzikálně obhajitelný, neboť proudění v porézním prostředí je typicky velmi pomalé v porovnání s rychlostí přestupu komponent mezi fázemi. Podmínka stabilní termodynamické rovnováhy vede

k minimalizaci celkové Gibbsovy energie složeného systému při zadané teplotě, tlaku a celkových molárních zlomcích jednotlivých komponent směsi [30, 63, 65]. Označme $z_i = c_i/c$, kde $c = \sum_{i=1}^{n} c_i$ je celková molární koncentrace směsi, celkové molární zlomky jednotlivých komponent pro $i = 1, \ldots, n$. Dále zaveďme molární zlomky jednotlivých komponent ve fázi α předpisem $x_{\alpha,i} = c_{\alpha,i}/c_\alpha$, kde $c_\alpha = \sum_{i=1}^{n} c_{\alpha,i}$ je celková koncentrace fáze α. Podmínka fázové rovnováhy vede k následující soustavě nelineárních algebraických rovnic

$$f_{oi}(p, T, x_{o,1}, \ldots, x_{o,n}) = f_{gi}(p, T, x_{g,1}, \ldots, x_{g,n}), \qquad i = 1, \ldots, n, \tag{2.7a}$$

$$z_i = (1 - \nu)x_{o,i} + \nu x_{g,i}, \qquad i = 1, \ldots, n, \tag{2.7b}$$

$$\sum_{i=1}^{n} z_i = \sum_{i=1}^{n} x_{o,i} = \sum_{i=1}^{n} x_{g,i} = 1, \tag{2.7c}$$

kde $f_{\alpha i}$ je fugacita komponenty i ve fázi α a $\nu \in (0, 1)$ označuje molární zlomek plynné fáze (tj. počet molů plynné fáze ku celkovému počtu molů směsi). Zde uvažujeme pouze dvoufázový případ a formulujeme podmínku termodynamické rovnováhy pouze mezi dvěma fázemi označenými jako o (oil) a g (gas). Vyjádření fugacit pomocí stavové rovnice popíšeme v následující kapitole.

Pro zadané hodnoty tlaku p, teploty T a celkových molárních zlomků z_i všech komponent lze řešením soustavy (2.7) určit molární zlomky $x_{\alpha,i}$ všech komponent v obou fázích a molární zlomek plynné fáze ν. Dále lze určit fázové koncentrace c_α řešením stavové rovnice

$$p = p(T, 1/c_\alpha, x_{\alpha,1}, \ldots, x_{\alpha,n}), \qquad \alpha \in \{o, g\} \tag{2.8}$$

a dopočítat fázové saturace S_α řešením soustavy rovnic

$$c_o S_o + c_g S_g = c, \tag{2.9}$$

$$S_o + S_g = 1. \tag{2.10}$$

Koncentrace $c_{\alpha,i}$ jsou pak dány vzorcem $c_{\alpha,i} = c_\alpha x_{\alpha,i}$. Pokud je za daných podmínek (tj. tlaku p, teplotě T a celkových molárních zlomcích $z_1, \ldots, z_n$) směs stabilní, pak nedojde k rozkladu směsi na fáze. V tomto případě není třeba řešit systém (2.7), protože stačí položit $c_{\alpha,i} = c_i$ a $S_\alpha = 1$.

2.1.3 Stavová rovnice a fugacita

Předpokládáme, že stavové chování libovolné fáze je popsáno stavovou rovnicí tvaru

$$p = p(T, V, N_1, \ldots, N_n), \tag{2.11}$$

kde p označuje tlak, T je teplota, V je objem a $N_1, \ldots, N_n$ jsou látková množství jednotlivých komponent v dané fázi. Pro směsi nepolárních uhlovodíků a CO_2 se dobře osvědčila Pengova-Robinsonova rovnice [81] tvaru

$$p = \frac{RT}{v_\alpha - b_\alpha} - \frac{a_\alpha}{v_\alpha^2 + 2b_\alpha v_\alpha - b_\alpha^2}, \tag{2.12}$$

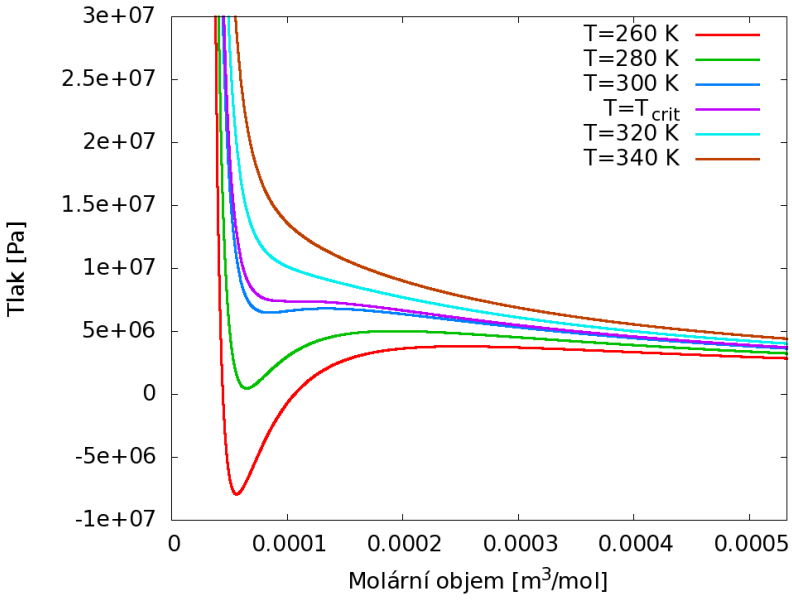

Obrázek 2.1: Závislost tlaku p na molárním objemu v pro čistý CO_2 za různých teplot. Kritická teplota CO_2 je $T_{crit} = 304$ K.

kde koeficient $v_\alpha = 1/c_\alpha$ označuje molární objem fáze α, R je univerzální plynová konstanta a koeficienty a_α a b_α jsou dány následujícími vzorci

$$a_\alpha = \sum_{i=1}^{n}\sum_{j=1}^{n} a_{ij}x_{\alpha,i}x_{\alpha,j}, \qquad b_\alpha = \sum_{i=1}^{n} b_i x_{\alpha,i}, \tag{2.13}$$

$$a_{ij} = (1-\delta_{ij})\sqrt{a_i a_j}, \qquad b_i = 0{,}0778\frac{RT_{i,crit}}{p_{i,crit}}, \tag{2.14}$$

$$a_i = 0{,}45724\frac{R^2T_{i,crit}^2}{p_{i,crit}}[1+m_i(1-\sqrt{T/T_{i,crit}})]^2, \tag{2.15}$$

$$m_i = \begin{cases} 0{,}37464 + 1{,}54226\omega_i - 0{,}26992\omega_i^2 & \text{pro } \omega_i < 0{,}5, \\ 0{,}3796 + 1{,}485\omega_i - 0{,}1644\omega_i^2 + 0{,}01667\omega_i^3 & \text{pro } \omega_i \geq 0{,}5. \end{cases} \tag{2.16}$$

V těchto rovnicích δ_{ij} označuje binární interakční koeficient mezi komponentami i a j, $p_{i,crit}$ a $T_{i,crit}$ jsou kritický tlak a kritická teplota i-té komponenty a ω_i označuje tzv. excentrický faktor i-té komponenty. Pro směsi uhlovodíků s vodou je potřeba Pengovu-Robinsonovu rovnici doplnit dodatečným členem popisujícím asociaci molekul vody. Konkrétní tvar této stavové rovnice je možno nalézt v [59] nebo v příloze článku [Č4].

Pengova-Robinsonova stavová rovnice patří do třídy tzv. kubických rovnic, jejichž obecné vlastnosti lze snadno ilustrovat na jednoduchém případu čisté látky ($n = 1$). Index i budeme v tomto případě vynechávat. Rozebereme 2 případy. Nechť je nejprve $T \geq T_{crit}$. V tomto případě

je tlak p ostře klesající funkcí V (viz Obr. 2.1) a lze tedy pro každý tlak z oboru hodnot stavové rovnice jednoznačně určit odpovídající objem V. Při nadkritické teplotě tedy v případě čisté látky nedochází k fázovému přechodu. Pokud je ovšem $T < T_{crit}$, pak má rovnice (2.12) pro každý tlak v určitém rozmezí tlaků až 3 reálné kořeny V – nejmenší z nich odpovídá objemu kapalné fáze (V_L), největší z nich odpovídá objemu plynné fáze (V_G) a prostřední odpovídá nestabilnímu řešení, které nemá fyzikální význam. Pro $T \to T_{crit}$ a $p \to p_{crit}$ zdola se oba kořeny přibližují a setkají se v kritickém bodě, kde nelze obě fáze od sebe rozlišit (v kritickém bodě je např. hustota kapaliny i její páry stejná). Protože funkce p je homogenní funkce stupně nula v proměnných V, $N_1, \ldots, N_n$, lze tlak dané fáze vyjádřit pomocí fázových koncentrací jako

$$p = p(T, 1, c_{\alpha,1}, \ldots, c_{\alpha,n}). \tag{2.17}$$

Zavedeme-li tzv. koeficient chemické stlačitelnosti fáze α vztahem $Z_\alpha = pv_\alpha/RT$, pak lze tento koeficient považovat za míru neideality směsi (pro ideální plyn je $Z_\alpha = 1$). Dále označme

$$A_\alpha = \frac{a_\alpha p}{R^2T^2} \qquad \text{a} \qquad B_\alpha = \frac{b_\alpha p}{RT}, \qquad \alpha \in \{o, g\}. \tag{2.18}$$

Fugacitu komponenty i ve fázi α lze potom vyjádřit ve tvaru [30]

$$f_{\alpha i}(p, T, x_{\alpha,1}, \ldots, x_{\alpha,n}) = p x_{\alpha,i} \varphi_{\alpha,i}, \tag{2.19}$$

kde $\varphi_{\alpha,i}$ označuje fugacitní koeficient komponenty i ve fázi α, jehož logaritmus lze pro Pengovu-Robinsonovu stavovou rovnici vyjádřit ve tvaru [30]

$$\begin{aligned} \ln \varphi_{\alpha,i} =& \frac{b_i}{b_\alpha}(Z_\alpha - 1) - \ln(Z_\alpha - B_\alpha) - \\ & - \frac{A_\alpha}{2\sqrt{2}B_\alpha}\left(\frac{2}{a_\alpha}\sum_{j=1}^{n} a_{ij}x_{\alpha,j} - \frac{b_i}{b_\alpha}\right) \ln \frac{Z_\alpha + (\sqrt{2}+1)B_\alpha}{Z_\alpha - (\sqrt{2}-1)B_\alpha}. \end{aligned} \tag{2.20}$$

2.1.4 Příspěvek k matematické formulaci modelu: počáteční a okrajové podmínky

Výše uvedený systém rovnic řešených na omezené d-rozměrné oblasti Ω je třeba doplnit o vhodné počáteční a okrajové podmínky, které je potřeba zvolit tak, aby výsledná úloha byla formulována korektně – tj. aby za daných podmínek existovalo právě jedno řešení, které bude spojitě záviset na vstupních datech úlohy. Navzdory své důležitosti je tato problematika v dostupné literatuře často opomíjena. Některé knihy, např. [16], se problematice okrajových podmínek nevěnují vůbec. V mnoha článcích se okrajové podmínky zmiňují pouze v souvislosti s konstrukcí numerického schématu, přičemž korektnost různých formulací okrajových podmínek je přinejmenším sporná. V přiloženém článku [Č1] je ukázáno, že často používaná nulová Neumannova podmínka tvaru

$$\mathbf{v}_\alpha \cdot \mathbf{n} = -\lambda_\alpha \mathbf{K}(\nabla p - \varrho_\alpha \mathbf{g}) \cdot \mathbf{n} = 0, \qquad \forall \alpha \in \{o, g\}, \tag{2.21}$$

která vyjadřuje podmínku nepropustnosti pro každou fázi α na některé části hranice $\partial\Omega$, není korektní. Z podmínky (2.21) lze totiž ve dvoufázovém systému (kdy je $\lambda_\alpha \neq 0$ pro obě fáze $\alpha \in \{o, g\}$) odvodit, že

$$\nabla p \cdot \mathbf{n} = \varrho_g \mathbf{g} \cdot \mathbf{n} \qquad \text{a zároveň} \qquad \nabla p \cdot \mathbf{n} = \varrho_o \mathbf{g} \cdot \mathbf{n}, \tag{2.22}$$

které nemohou být splněny zároveň ve dvoufázovém systému s gravitací, pokud mají obě fáze různé hustoty. Nelze tedy vynucovat nulovou Neumannovu podmínku pro každou fázovou rychlost, ale pouze pro celkový tok každé komponenty. Na základě zkušeností získaných s tímto modelem doplňujeme tedy rovnice kompozičního modelu následujícími počátečními a okrajovými podmínkami

$$c_i(\mathbf{x}, 0) = c_i^0(\mathbf{x}), \quad \mathbf{x} \in \Omega,\ i = 1, \ldots, n, \tag{2.23a}$$

$$p(\mathbf{x}, t) = p^D(\mathbf{x}, t), \quad \mathbf{x} \in \Gamma_p,\ t \in I, \tag{2.23b}$$

$$\mathbf{q}_i(\mathbf{x}, t) \cdot \mathbf{n}(\mathbf{x}) = 0, \quad \mathbf{x} \in \Gamma_q,\ t \in I,\ i = 1, \ldots, n, \tag{2.23c}$$

v nichž $\mathbf{n}$ označuje jednotkový vektor vnější normály definovaný skoro všude na $\partial\Omega$, $\Gamma_p \cup \Gamma_q = \partial\Omega$, a $\Gamma_p \cap \Gamma_q = \emptyset$. Rovnice (2.23a) popisuje počáteční rozložení molárních koncentrací, (2.23b) je Dirichletova okrajová podmínka předepisující tlak p^D na části hranice Γ_p, a (2.23c) je homogenní Neumannova okrajová podmínka popisující nepropustnou část hranice Γ_q. Předpokládáme, že Γ_p je odtoková část hranice, takže na ní není třeba předepisovat žádné okrajové podmínky pro molární koncentrace.

2.2 Numerické řešení kompozičního modelu

2.2.1 Strategie řešení konvenčního kompozičního modelu

V této kapitole uvedeme přehled základní strategie řešení kompozičního modelu. Vzhledem k rozsahu práce nebude cílem popsat veškeré detaily používaných metod, ale spíše ukázat problémy, které se při řešení kompozičního modelu vyskytují nezávisle na tom, kterou metodu prostorové či časové diskretizace použijeme.

Implicitní schéma

Systém rovnic (2.1)–(2.9) představuje soustavu nelineárních diferenciálně-algebraických rovnic doplněný o počáteční a okrajové podmínky (2.23). Pro řešení tohoto systému je možno použít více přístupů [68]. Prvním z nich je tzv. plně implicitní metoda, kdy se časové derivace aproximují diferencemi a koeficienty rovnic se vyčíslují na nové časové hladině. Po diskretizaci v prostoru musíme řešit obrovský systém nelineárních rovnic, který se zpravidla řeší Newtonovou metodou. Tato metoda linearizuje zároveň diskretizované transportní rovnice (2.1) i rovnice fázové rovnováhy (2.7) na každém elementu vzhledem k vybraným primárním proměnným.

V literatuře lze najít různé volby primárních proměnných, nejčastěji se používá tlak p a molární zlomky $x_{\alpha,i}$ vybrané fáze $\alpha \in \{o, g\}$. Tato metoda však vyžaduje, aby zvolená fáze α byla přítomna v každém výpočetním elementu sítě. Pokud toto nelze zaručit, pak se volba primárních proměnných provádí na každém elementu K adaptivně tak, aby se za primární proměnné volily molární zlomky $x_{\alpha,i}$ té fáze α, která je na elementu K v nadbytku (tj. má maximální saturaci). Sada primárních proměnných se tedy mění za běhu simulace podle toho, jak se vyvíjí v čase dané řešení, což výpočet poněkud komplikuje. Vzhledem k velikosti výsledné soustavy rovnic (v problémech souvisejících s těžbou ropy se běžně vyšetřují směsi několika desítek komponent) se však plně implicitní přístup v kompoziční simulaci mnohasložkových směsí nepoužívá a je nahrazován tzv. sekvenčními přístupy.

Sekvenční řešení – schéma IMPEC

Při sekvenčním řešení se časová diskretizace a linearizace systému (2.1)–(2.9) provádí tak, aby bylo možno řešit jednotlivé rovnice systému postupně (viz např. [80, 15, 94]). V metodě IMPEC (IMplicit Pressure, Explicit Concentrations) se nejprve zformuluje rovnice popisující evoluci tlaku. Tato rovnice se potom řeší implicitně a výsledný tlak na nové časové hladině se použije k výpočtu toků (s využitím koncentrací ze staré časové hladiny). Tyto toky se pak použijí při řešení transportních rovnic (2.1), které se řeší explicitně. Tím obdržíme celkové koncentrace c_i na nové časové vrstvě, přičemž v každém časovém kroku je potřeba řešit jen systém pro tlak, jehož velikost nezávisí na počtu komponent směsi.

K formulaci rovnic popisujících evoluci tlaku je v literatuře dostupných několik metod [2, 99, 19, 20, 18, 95], které ovšem v zásadě vycházejí ze dvou základních přístupů. Prvním z nich je metoda založená na linearizaci systému rovnic (2.1)–(2.9) Newtonovou metodou, kdy se z diskrétní podoby rovnic pro přírůstky zvolených primárních proměnných (mezi nimiž je vždy tlak) eliminací ostatních proměnných odvodí redukovaný systém pouze pro přírůstky tlaku. Po vyřešení systému pro přírůstky tlaku se již přírůstky ostatních primárních proměnných neřeší, získané aproximace tlaků se použijí k výpočtu toků a pak se přejde k explicitnímu řešení transportních rovnic pro jednotlivé komponenty. Tuto verzi predikce tlaku v kompoziční simulaci poprvé použili Young a Stephenson [99]. Alternativní metodou pro predikci vývoje tlaku je metoda, kterou poprvé použili Ács, Farkas a Doleschell v práci [2], ve které se vhodnou kombinací transportních rovnic (2.1) odvodí evoluční rovnice pro tlak tvaru

$$\phi c_f \frac{\partial p}{\partial t} + \sum_{i=1}^{n} \overline{v_i}\, \nabla \cdot (c_{o,i}\mathbf{v}_o + c_{g,i}\mathbf{v}_g) = \sum_{i=1}^{n} \overline{v_i} F_i, \tag{2.24}$$

kde c_f označuje koeficient celkové (dvoufázové) stlačitelnosti směsi a $\overline{v_i}$ je celkový (tj. dvoufázový) parciální molární objem i-té komponenty. Tyto koeficienty jsou funkcemi tlaku, teploty a molárních zlomků. Postup jejich výpočtu ze stavové rovnice je uveden v knize [30].

V následujících odstavcích popíšeme řešení systému rovnic (2.1)–(2.9) na dvourozměrné oblasti Ω pokryté obdélníkovou sítí s využitím rovnice pro tlak (2.24), kterou diskretizujeme

smíšenou hybridní verzí metody konečných prvků nejnižšího řádu [8, 88]. V této metodě aproximujeme tlak současně s celkovým tokem, který je dále využit pro výpočet transportu. Tento přístup navazuje na práce [67, 40, 41, 42]. Transportní rovnice jsou řešeny nespojitou Galerkinovou metodou využívající po částech lineární nespojité bazické funkce [44, 21, 14]. Při použití metody vyššího řádu přesnosti je obecně nutné výsledná data poupravit s využitím vhodné omezující funkce, která zabrání vzniku nefyzikálních oscilací. Podrobnosti tohoto přístupu jsou uvedeny v [53, 54, 55, 56, 57, 39].

2.2.2 Diskretizace celkového molárního toku

Celkový molární tok $\mathbf{q}$ zavedeme předpisem

$$\mathbf{q} = c_o \mathbf{v}_o + c_g \mathbf{v}_g = -\sum_{\alpha'} c_{\alpha'} \lambda_{\alpha'} \mathbf{K}(\nabla p - \widetilde{\varrho}\mathbf{g}), \tag{2.25}$$

kde $\widetilde{\varrho} = f_o \varrho_o + f_g \varrho_g$ a $f_\alpha = c_\alpha \lambda_\alpha / \sum_{\alpha'} c_{\alpha'} \lambda_{\alpha'}$. Koeficient $\sum_{\alpha'} c_{\alpha'} \lambda_{\alpha'}$ v rovnici (2.25) je vždy kladný, protože alespoň jedna fáze má vždy nenulovou mobilitu. Z rovnice (2.25) lze tedy vyjádřit gradient tlaku

$$\nabla p = -\frac{1}{\sum_{\alpha'} c_{\alpha'} \lambda_{\alpha'}} \mathbf{K}^{-1} \mathbf{q} + \widetilde{\varrho}\mathbf{g}. \tag{2.26}$$

a ten dosadit do Darcyho zákona (2.4). Takto lze odvodit vyjádření celkových fázových toků pomocí celkového toku ve tvaru

$$\mathbf{q}_\alpha \equiv c_\alpha \mathbf{v}_\alpha = f_\alpha(\mathbf{q} - \mathbf{G}_\alpha), \tag{2.27}$$

kde

$$\mathbf{G}_\alpha = \begin{cases} c_o \lambda_o (\varrho_o - \varrho_g)\mathbf{K}\mathbf{g} & \alpha = g, \\ c_g \lambda_g (\varrho_g - \varrho_o)\mathbf{K}\mathbf{g} & \alpha = o. \end{cases} \tag{2.28}$$

Aproximaci celkového molárního toku hledáme v prostoru $RT_0(K)$ – tj. Raviartově-Thomasově prostoru nejnižšího stupně na každém elementu K (pro podrobnosti viz [88, 97, 13]). Aproximace celkového toku na elementu K je tedy tvaru

$$\mathbf{q}_K = \sum_{E \in \partial K} q_{K,E} \mathbf{w}_{K,E}, \tag{2.29}$$

kde koeficient $q_{K,E}$ udává celkový molární tok ve směru vnější normály přes hranu E z elementu K a $\mathbf{w}_{K,E}$ označuje bazické funkce prostoru $RT_0(K)$. Vlastnosti těchto bazických funkcí i podrobné odvození jejich tvaru lze najít v přiloženém článku [Č1]. S použitím vlastností těchto bazických funkcí lze odvodit vyjádření koeficientů celkového molárního toku na libovolném elementu K pomocí průměrného tlaku na daném elementu p_K a průměrných tlaků na všech hranách elementu K (tzv. stopy tlaku) označených jako $\hat{p}_{K,E}$ ve tvaru

$$q_{K,E} = a_{K,E} p_K - \sum_{E' \in \partial K} b_{K,E,E'} \hat{p}_{K,E'} + d_{K,E}. \tag{2.30}$$

Koeficienty $a_{K,E}$, $b_{K,E,E'}$ a $d_{K,E}$ v této rovnici závisejí na geometrii sítě a na lokálních hodnotách celkové mobility. Vyjádření těchto koeficientů lze najít v přiloženém článku [Č1]. Zákon zachování hmoty na hraně $E = K \cap K'$ oddělující dva sousední elementy K and K' vede k podmínce

$$q_{K,E} + q_{K',E} = 0, \qquad K \cap K' = E. \tag{2.31}$$

Dosazením z (2.30) dostaneme

$$\begin{aligned} a_{K,E}p_K - \sum_{E' \in \partial K} b_{K,E,E'}\hat{p}_{K,E'} + d_{K,E} + \\ + a_{K',E}p_{K'} - \sum_{E' \in \partial K'} b_{K',E,E'}\hat{p}_{K',E'} + d_{K',E} = 0, \end{aligned} \tag{2.32}$$

Na hranách E ležící na neumannovské části hranice z rovnice (2.23c) odvodíme

$$q_{K,E} = 0, \tag{2.33}$$

a tedy

$$a_{K,E}p_K - \sum_{E' \in \partial K} b_{K,E,E'}\hat{p}_{K,E'} + d_{K,E} = 0. \tag{2.34}$$

Systém rovnic (2.32) a (2.34) lze zapsat v maticovém tvaru

$$R^T P - M\hat{P} = V, \tag{2.35}$$

kde

$$R \in \mathbb{R}^{N_K, N_E}, \qquad R_{K,E} = a_{K,E}, \tag{2.36a}$$

$$M \in \mathbb{R}^{N_E, N_E}, \qquad M_{E,E'} = \sum_{K : E,E' \in \partial K} b_{K,E,E'}, \tag{2.36b}$$

$$V \in \mathbb{R}^{N_E}, \qquad V_E = \sum_{K : E \in \partial K} d_{K,E}. \tag{2.36c}$$

V těchto rovnicích N_K označuje počet elementů, N_E je celkový počet hran, $P \in \mathbb{R}^{N_K}$ je vektor průměrných tlaků na jednotlivých elementech a $\hat{P} \in \mathbb{R}^{N_E}$ je vektor stop tlaků na jednotlivých hranách.

2.2.3 Aproximace rovnice pro tlak

Rovnici pro tlak (2.24) lze přeformulovat do následujícího tvaru

$$\phi c_f \frac{\partial p}{\partial t} + \sum_{i=1}^{n} \overline{v_i} \, \nabla \cdot (m_i \mathbf{q} - \mathbf{s}_i) = \sum_{i=1}^{n} \overline{v_i} F_i, \tag{2.37}$$

kde $m_i = x_{o,i} f_o + x_{g,i} f_g$ a $\mathbf{s}_i = x_{o,i} f_o \mathbf{G}_o + x_{g,i} f_g \mathbf{G}_g$. Tuto rovnici lze integrovat přes libovolný element K. Předpokládáme-li, že koeficienty c_f a $\overline{v_i}$ jsou po elementech konstantní, odvodíme s využitím divergenční věty

$$\phi_K c_{f,K} |K| \frac{\partial p_K}{\partial t} + \sum_{i=1}^{n} \overline{v_{i,K}} \sum_{E \in \partial K} \int_E (m_{i,K,E} q_{K,E} - \mathbf{s}_{i,K,E} \cdot \mathbf{n}_{K,E}) = \sum_{i=1}^{n} \overline{v_{i,K}} F_{i,K} |K|, \quad (2.38)$$

kde $|K|$ označuje plochu elementu K. Dosazením celkového toku z (2.30) a použitím zpětné Eulerovy metody odvodíme následující schéma

$$DP^{n+1} - \tilde{R}\hat{P}^{n+1} = G, \quad (2.39)$$

kde horní index $n+1$ označuje časovou hladinu, $D \in \mathbb{R}^{N_K, N_K}$ je diagonální matice s elementy

$$D_K = \frac{\phi_K c_{f,K} |K|}{\Delta t} + \sum_{i=1}^{n} \overline{v_{i,K}} \sum_{E \in \partial K} \int_E m_{i,K,E} a_{K,E},$$

$\tilde{R} \in \mathbb{R}^{N_K, N_E}$ je obdélníková matice s prvky

$$\tilde{R}_{K,E'} = \sum_{i=1}^{n} \overline{v_{i,K}} \sum_{E \in \partial K} \int_E m_{i,K,E} b_{K,E,E'},$$

a $G \in \mathbb{R}^{N_K}$ je vektor se složkami

$$G_K = \frac{\phi_K c_{f,K} |K|}{\Delta t} p_K^n - \sum_{i=1}^{n} \overline{v_{i,K}} \sum_{E \in \partial K} \int_E (m_{i,K,E} d_{K,E} - \mathbf{s}_{i,K,E} \cdot \mathbf{n}_{K,E}) + |K| \sum_{i=1}^{n} \overline{v_{i,K}} F_{i,K}.$$

Koeficienty c_f, $\overline{v_i}$, $m_{i,K,E}$ a $\mathbf{s}_{i,K,E}$ se vyčíslují pomocí průměrných hodnot fázových koncentrací a saturací na elementu K ve staré časové vrstvě n.

2.2.4 Příspěvek k aproximaci fázových toků

Důležitým krokem v metodě IMPEC je korektní aproximace fázových toků $\mathbf{q}_\alpha = f_\alpha(\mathbf{q} - \mathbf{G}_\alpha)$. V přiloženém článku [Č1] zobecňujeme metodu, kterou dříve Sammon [91] použil při simulaci dvoufázového nemísitelného proudění, na problém kompoziční simulace. Nejprve je třeba vyřešit soustavu rovnic (2.35) a (2.39). Tím získáme tlaky na jednotlivých elementech P a stopy tlaku na hranách $\hat{P}$ na nové časové hladině. Protože matice D je diagonální a invertovatelná, je možno redukovat soustavu (2.35) a (2.39) na soustavu rovnic pro stopy tlaku tvaru [66]

$$(M - R^T D^{-1} \tilde{R}) \hat{P}^{n+1} = V - R^T D^{-1} G \quad (2.40)$$

Soustavu (2.40) řešíme pomocí přímého řešiče UMFPACK [23, 24, 25, 26]. Řešením tohoto systému získáme stopy tlaků $\hat{P}^{n+1}$ na nové časové hladině. Průměrné hodnoty tlaků na jednotlivých

elementech P^{n+1} lze potom získat z rovnice (2.39). Potom můžeme vypočítat celkový molární tok pomocí rovnice (2.30). Rovnice (2.31) zaručuje splnění bilance celkového molárního toku na každé vnitřní hraně mezi dvěma elementy sítě. Pokud bychom ovšem chtěli vypočítat fázové toky pomocí (2.27), zjistíme, že při použití lokálních hodnot koeficientů f_α a $\mathbf{G}_\alpha$ na elementu K dostaneme rozdílné hodnoty normálové složky fázových toků na hraně E podle toho, z které strany hrany E koeficienty vyčíslujeme. Abychom dostali konzervativní pole, průměrujeme hodnoty ϱ_α používané pro výpočet $\mathbf{G}_\alpha$ v rovnici (2.27) pomocí aritmetického průměru hodnot na sousedících elementech, zatímco hodnoty koeficientů $c_\alpha\lambda_\alpha$ a $c_{\alpha'}\lambda_{\alpha'}$ při vyčíslení f_α se berou ze strany, která je proti směru k toku $\mathbf{q}_\alpha$ (tzv. upwind). Zde ovšem narážíme na problém, že směr $\mathbf{q}_\alpha$ ještě není znám. Tento problém lze vyřešit následujícím postupem. Označme symbolem α fázi, pro kterou platí, že

$$\operatorname{sgn} q_{K,E} = -\operatorname{sgn} \mathbf{G}_\alpha \cdot \mathbf{n}_{K,E}, \tag{2.41}$$

kde $c_\alpha\lambda_\alpha$ a $c_{\alpha'}\lambda_{\alpha'}$ se zvolí libovolně, např. $c_\alpha\lambda_\alpha = c_{\alpha'}\lambda_{\alpha'} = 1$. Symbolem α' označíme zbývající fázi. Alespoň jedna z přítomných fází vždy splní podmínku (2.41), protože celkový tok je předem dán a vektory $\mathbf{G}_\alpha$ a $\mathbf{G}_{\alpha'}$ ukazují do navzájem opačných směrů, viz (2.28). Z podmínky (2.41) plyne, že fáze α směřuje stejným směrem jako celkový tok, přesněji $\operatorname{sgn} q_{\alpha,K,E} = \operatorname{sgn} q_{K,E}$ nezávisle na tom, jaké jsou skutečné hodnoty nezáporného koeficientu $c_{\alpha'}\lambda_{\alpha'}$ v rovnici (2.27). Známé znaménko $q_{\alpha,K,E}$ umožňuje najít upwindovou hodnotu výrazu $c_\alpha\lambda_\alpha$, který se vyskytuje ve výpočtu vektoru $\mathbf{G}_{\alpha'}$. Je tedy možno vypočítat $q_{\alpha',K,E}$ a stanovit upwindovou hodnotu koeficientu $\lambda_{\alpha'}$ (koeficient bereme ze strany proti směru $q_{\alpha',K,E}$) a nakonec stanovit skutečnou hodnotu $q_{\alpha,K,E}$. V posledním kroku se změní pouze hodnota toku, nikoliv však jeho směr. Proto nakonec dostaneme konzistentní aproximaci fázových toků takovou, že koeficienty $c_\alpha\lambda_\alpha$ a $c_{\alpha'}\lambda_{\alpha'}$ při vyčíslení f_α se berou ze strany, která je proti směru příslušného fázového toku, jak jsme chtěli. Tyto fázové toky dále využijeme při řešení transportních rovnic. Poznamenejme, že prosté průměrování hodnot toků z obou stran není možné, protože vede ke schématu, které je nepodmíněně nestabilní.

2.2.5 Aproximace transportních rovnic

Transportní rovnice (2.1) diskretizujeme nespojitou Galerkinovou metodou konečných prvků [44, 21, 14, 29]. Na každém obdélníkovém elementu K aproximujeme neznámé koncentrace jednotlivých komponent lineárními funkcemi, které ovšem nemusí být spojité přes hranice elementů. Na každém elementu tedy máme pro každou koncentraci 3 stupně volnosti – hodnotu koncentrace uprostřed elementu a hodnoty složek gradientu ve směru os x a y. Aproximace tedy uvažujeme ve tvaru

$$c_{i,K} = \sum_{l=1}^{3} c_{i,K}^l \varphi_{K,l}, \qquad c_{\alpha,i,K} = \sum_{l=1}^{3} c_{\alpha,i,K}^l \varphi_{K,l}, \tag{2.42}$$

kde $\varphi_{K,l}$ jsou bazické funkce lokálního prostoru lineárních funkcí na elementu K. Detailní odvození tvaru těchto funkcí je provedeno v přiloženém článku [Č1]. Násobením transportních rovnic testovací funkcí, integrací přes element K a použitím Greenovy věty lze odvodit následující schéma nespojité Galerkinovy metody

$$\int_K \phi \frac{\partial c_{i,K}}{\partial t}\varphi_{K,j} - \int_K (x_{o,i,K}\mathbf{q}_o + x_{g,i,K}\mathbf{q}_g)\cdot\nabla\varphi_{K,j} + \\ + \sum_{E\in\partial K}\int_E \left(\widetilde{x_{o,i,K,E}}\mathbf{q}_o + \widetilde{x_{g,i,K,E}}\mathbf{q}_g\right)\cdot\mathbf{n}_{K,E}\varphi_{K,j} = \int_K F_i\varphi_{K,j}, \tag{2.43}$$

které platí pro každý stupeň volnosti $j \in \{1,2,3\}$. V integrálu přes hranici elementu označuje $\widetilde{x_{\alpha,i,K,E}}$ pro $\alpha \in \{o,g\}$ hodnotu molárního zlomku z upwindové strany vzhledem k toku $\mathbf{q}_\alpha$, tj.

$$\widetilde{x_{\alpha,i,K,E}} = \begin{cases} x_{\alpha,i,K,E} & \text{pokud } q_{\alpha,K,E} \equiv \mathbf{q}_\alpha\cdot\mathbf{n}_{K,E}|E| \geq 0, \\ x_{\alpha,i,K',E} & \text{pokud } q_{\alpha,K,E} \equiv \mathbf{q}_\alpha\cdot\mathbf{n}_{K,E}|E| < 0, \end{cases} \tag{2.44}$$

kde předpokládáme, že $E = K\cap K'$ je společná hrana mezi sousedními elementy K a K'. Pokud hrana E leží na hranici, pak lze na vtokové části hranice použít Dirichletovy okrajové podmínky. Hodnoty $x_{\alpha,i,K,E}$ a $x_{\alpha,i,K',E}$ v rovnici (2.44) získáme řešením lokální fázové rovnováhy na hranách elementů při teplotě T, tlaku $\hat{p}_{K,E}$ a celkových molárních koncentracích z_i na příslušné hraně. Hodnoty z_i na hraně se spočte pomocí hodnot z_i uprostřed elementu a složek gradientů, které jsou k dispozici při použití nespojité Galerkinovy metody. Hodnoty $x_{\alpha,i,K}$ v integrálu přes element K v rovnici (2.43) vypočítáme řešením lokální termodynamické rovnováhy při teplotě T, tlaku p_K a celkových molárních zlomcích z_i uprostřed elementu. K dosažení vyššího řádu přesnosti je tedy potřeba na každém elementu řešit 5 problémů fázové rovnováhy.

Dosazením (2.42) do (2.43) odvodíme následující semidiskrétní schéma

$$\phi_K\sum_{l=1}^{3}\frac{dc_{i,K}^l}{dt}M_{j,l}^K - \sum_{\alpha\in\{o,g\}}\sum_{l=1}^{3}x_{\alpha,i,K}\sum_{E\in\partial K}q_{\alpha,K,E}M_{j,l}^{K,E} + \\ + \sum_{E\in\partial K}\sum_{\alpha\in\{o,g\}}\widetilde{x_{\alpha,i,K,E}}q_{\alpha,K,E}M_j^E = \int_K F_i\varphi_{K,j}. \tag{2.45}$$

Matice M^K, M^E, a $M^{K,E}$ obsahují integrály bazických funkcí a jsou odvozeny v přiloženém článku [Č1]. Protože matice M^K je diagonální, vede aproximace časové derivace dopřednou diferencí k explicitnímu schématu pro 3 neznámé stupně volnosti $c_{i,K}^l$ na každém elementu K.

2.2.6 Příspěvek k implementaci omezující funkce

Výše popsané schéma nespojité Galerkinovy metody je potřeba stabilizovat použitím omezující funkce (tzv. limiter), která zabrání vzniku umělých oscilací numerického řešení. Na obdélníkové síti lze omezení sklonů provádět nezávisle na sobě pro oba směry x a y. Podstata metody spočívá

v tom, že sklony získané použitím nespojité Galerkinovy metody po každém časovém kroku modifikujeme tak, aby se průměrná hodnota numerického řešení na každém elementu nezměnila a aby hodnoty celkových koncentrací na každé hraně ležely mezi minimem a maximem hodnot příslušné koncentrace uprostřed sousedních buněk. Vzhledem k tomu, že jako stupně volnosti na každém elementu používáme 1) průměrné hodnoty celkových molárních koncentrací, 2) rozdíly hodnot koncentrací na pravé hraně a uprostřed elementu a 3) rozdíly hodnot koncentrací na horní hraně a uprostřed elementu, lze uvedenou metodu snadno implementovat. Zároveň lze snadno získat metodu konečných objemů, pokud oba sklony nastavíme na nulu.

Při implementaci tohoto limiteru narážíme na zajímavý problém. Při kompoziční simulaci se běžně místo původního systému rovnic (2.1) pro všechny komponenty $i \in \{1, 2, \ldots, n\}$ formuluje ekvivalentní úloha ve tvaru

$$\frac{\partial(\phi c_i)}{\partial t} + \nabla \cdot \mathbf{q}_i = F_i, \qquad i = 1, \ldots, n-1, \tag{2.46}$$

$$\frac{\partial(\phi c)}{\partial t} + \nabla \cdot \mathbf{q} = F \equiv \sum_{i=1}^{n} F_i, \tag{2.47}$$

což jsou bilanční rovnice pro prvních $n-1$ komponent doplněné bilanční rovnicí celé směsi. Při použití metod prvního řádu přesnosti (např. metody konečných objemů) jsou obě formulace ekvivalentní a fungují stejně dobře. Při použití metody vyššího řádu se obě formulace začnou odlišovat ve způsobu aplikace limiteru. Limiter lze snadno aplikovat v případě původní formulace (2.1) pro $i \in \{1, 2, \ldots, n\}$. Po každém kroku nespojité Galerkinovy metody limiter definuje horní a dolní meze $c^E_{i,max}$ a $c^E_{i,min}$ hodnot celkových koncentrací na každé hraně E následujícím způsobem

$$c^E_{i,max} = \max\{c_{i,K}, c_{i,K'}\}, \qquad c^E_{i,min} = \min\{c_{i,K}, c_{i,K'}\}, \tag{2.48}$$

kde K a K' jsou elementy sítě přiléhající k hraně E. Pokud je potřeba, sklon numerického řešení na každém elementu K se redukuje tak, aby na každé hraně byly splněny nerovnosti

$$c^E_{i,min} \leq c^{K,E}_i \leq c^E_{i,max}, \tag{2.49}$$

kde $c^{K,E}_i$ označuje hodnotu celkové molární koncentrace i-té komponenty uprostřed hrany E zrekonstruované pomocí 3 stupňů volnosti na elementu K. Vyščítáním nerovností (2.49) přes $i \in \{1, 2, \ldots, n\}$ dostaneme pro celkovou molární koncentraci směsi omezení

$$\sum_{i=1}^{n} c^E_{i,min} \leq c^{K,E} \equiv \sum_{i=1}^{n} c^{K,E}_i \leq \sum_{i=1}^{n} c^E_{i,max}. \tag{2.50}$$

Pokud stejný postup použijeme v alternativní formulaci (2.46), pak limiter bude definovat dolní a horní meze $c^E_{i,min}$ a $c^E_{i,max}$ omezující hodnoty celkových molárních koncentrací c_i pro

$i = 1, \ldots, n-1$ a dále meze c^E_{min} a c^E_{max} omezující hodnoty celkové koncentrace c na každé hraně E. Sklony těchto proměnných se budou případně redukovat tak, aby

$$\begin{aligned} c^E_{i,min} \leq c^{K,E}_i \leq c^E_{i,max}, \qquad i = 1, \ldots, n-1 \\ c^E_{min} \leq c^{K,E} \leq c^E_{max}. \end{aligned} \tag{2.51}$$

Z těchto nerovností můžeme pro poslední komponentu c_n odvodit nerovnost

$$c^E_{min} - \sum_{i=1}^{n-1} c^E_{i,max} \leq c^{K,E}_n = c^{K,E} - \sum_{i=1}^{n-1} c^{K,E}_i \leq c^E_{max} - \sum_{i=1}^{n-1} c^E_{i,min}. \tag{2.52}$$

Tato nerovnost však není v souladu s podmínkou (2.49) pro $i = n$. Použití metody vyššího řádu a limiteru ve formulaci (2.46) vede ke vzniku nefyzikálních oscilací koncentrace poslední komponenty, které se během několika málo časových kroků rozšíří i do dalších komponent. Problém lze vyřešit konstrukcí speciálního limiteru, který bude nastavovat meze celkové koncentrace tak, aby byly zajištěny správné meze hodnot poslední komponenty c_n. Tento postup však vede ke zbytečně složitému kódu. Jednodušší řešení je vycházet z původní formulace (2.1) pro $i \in \{1, 2, \ldots, n\}$, ve které splnění nerovností (2.49) zajistí stabilitu řešení pro dostečně malé časové kroky (při splnění tzv. CFL-podmínky).

2.2.7 Řešení rovnic fázové rovnováhy

Nedílnou součástí řešení transportních rovnic je výpočet lokální termodynamické rovnováhy na každém elementu. Pro zadané hodnoty tlaku p, teploty T a celkových molárních zlomků z_i ($i \in \{1, 2, \ldots, n\}$ je potřeba nejdříve rozhodnout, zda je směs za těchto podmínek stabilní nebo zda se rozdělí na fáze. Ve dvoufázovém případě je potřeba stanovit molární zlomky $x_{\alpha,i}$ jednotlivých komponent v každé fázi, koncentrace c_α a saturace S_α obou fází řešením soustavy (2.7).

Testování fázové stability

Pro testování stability fáze při zadaném tlaku p, teplotě T a celkových molárních zlomcích z_i, kde $i \in \{1, 2, \ldots, n\}$, je možno použít Gibbsovo kritérium fázové stability [30], které testuje, zda lze odloučením malého množství zkušební fáze s molárními zlomky x_i z počáteční fáze při konstantní teplotě T a tlaku p vytvořit dvoufázový stav s nižší hodnotou celkové Gibbsovy energie systému než je energie hypotetického jednofázového stavu. Počáteční fáze je při zadaném tlaku p, teplotě T a celkových molárních zlomcích z_i stabilní, právě když

$$TPD(x_1, \ldots, x_n) \equiv \sum_{i=1}^{n} x_i(\mu_i(p, T, x_1, \ldots, x_n) - \mu_i(p, T, z_1, \ldots, z_n)) \geq 0 \tag{2.53}$$

pro všechny přípustné molární zlomky x_i zkušební fáze. V poslední rovnici μ_i označuje chemický potenciál i-té komponenty, který souvisí s fugacitou následujícím způsobem

$$\mu_i(p,T,x_1,\ldots,x_n) - \mu_i(p,T,z_1,\ldots,z_n) = RT \ln \frac{f_i(p,T,x_1,\ldots,x_n)}{f_i(p,T,z_1,\ldots,z_n)}. \tag{2.54}$$

Podaří-li se najít molární zlomky $x_1,\ldots,x_n$ tak, aby $TPD(x_1,\ldots,x_n) < 0$, pak je směs při daných podmínkách nestabilní a rozdělí se na fáze. Hodnoty $x_1,\ldots,x_n$ pak udávají složení nové fáze, která, pokud se odloučí v malém množství z počáteční fáze s molárními zlomky $z_1,\ldots,z_n$, povede k dvoufázovému systému s nižší Gibbsovou energií v porovnání s původním jednofázovým stavem. Hodnoty $x_1,\ldots,x_n$ pak lze využít pro konstrukci počátečního rozkladu směsi na fáze při následném výpočtu rovnovážného stavu.

Pro vyšetřování stability bylo navrženo mnoho numerických metod. Michelsen v práci [62] využil toho, že k ověření podmínky (2.53) stačí vyšetřit hodnoty funkce TPD pouze ve všech stacionárních bodech a stabilitu systému stanovit podle hodnoty funkce TPD v bodě globálního minima. Soustavu rovnic

$$\frac{\partial TPD}{\partial x_i}(x_1,\ldots,x_n) = 0, \qquad i = 1,\ldots,n-1, \tag{2.55}$$

$$\sum_{i=1}^{n} x_i = 1, \tag{2.56}$$

lze řešit iteračně s využitím více počátečních nástřelů, které mají za cíl pokrýt stavový prostor tak, aby byl nalezen bod globálního minima funkce TPD. Počáteční nástřely bývají konstruovány na základě fyzikálně motivovaných heuristik [96]. Podrobnosti lze najít v [62, 30, 43].

V souvislosti s dalším výkladem zdůrazněme, že chemické potenciály a fugacity v rovnicích (2.53) a (2.54) závisejí nejen na tlaku, teplotě a molárních zlomcích, ale i na tom, kterou fázi vyšetřujeme. Při výpočtu koeficientu Z_α vyskytujícím se ve vzorci pro fugacitu (2.20) je totiž potřeba volit správný kořen stavové rovnice – viz kapitola 2.1.3. Při testování fázové stability však často předem nevíme, zda počáteční fáze je kapalná nebo plynná (a v případě dvoufázového systému toto označení ani nemá rozumný smysl). Proto se testují obě možnosti – nejprve se předpokládá, že počáteční fáze je kapalná a hledaná testovací fáze je plynná a potom se zkouší opačná alternativa, kdy k plynné počáteční fázi hledáme kapalnou testovací fázi. Uvedené možnosti odpovídají případu, kdy vyšetřujeme dvoufázové systémy typu kapalina-plyn, které jsou z hlediska teorie i numerického řešení nejlépe prozkoumané. Ve složitějších případech (vícefázové proudění, dvoufázové proudění dvou kapalin, apod.) je pak testování stability složitější.

Výpočet dvoufázového rovnovážného stavu

Pokud zjistíme, že při zadaném tlaku p, teplotě T a celkových molárních zlomcích z_i je směs nestabilní, potřebujeme stanovit rovnovážný dvoufázový stav řešením rovnic (2.7). Vzhledem

k tomu, že výpočet fázové rovnováhy v dvoufázovém vícekomponentním systému při zadaném tlaku, teplotě a molárních zlomcích patří mezi základní úlohy chemického inženýrství s mnoha praktickými aplikacemi, bylo pro řešení soustavy (2.7) vyvinuto mnoho iteračních metod, z nichž jmenujme zejména metodu SSI (succesive substitution method – metoda postupného dosazování) a Newtonovu metodu. Jako počáteční nástřel se používají buď heuristické nástřely zkonstruované na základě studia rovnováh za ideálních podmínek (ideální plyn a ideální roztok) nebo aproximace získaná pomocí výše popsaného testu stability. Podrobnosti lze najít v [62], [63], [65] a [30].

Výhodou metody SSI je její robustnost, nevýhodou pomalá (lineární) konvergence. Newtonova metoda dosahuje v blízkosti kořene kvadratické konvergence, ale vyžaduje dobrou počáteční aproximaci, jinak nemusí konvergovat. Obě metody se často kombinují, kdy se několik iterací metody SSI použije k nalezení vhodného počátečního nástřelu pro Newtonovu metodu. Poznamenejme, že stejně jako při testování stability je i zde při výpočtu fugacit (příp. i jejich derivací v Newtonově metodě) potřeba rozlišovat, jaký druh fáze (kapalina nebo plyn) vyšetřujeme a podle toho správně volit kořeny stavové rovnice.

2.2.8 Shrnutí výpočetního algoritmu

Výpočet transportu lze popsat následujícími kroky:

1. Načti vstupní data úlohy – teplotu, počáteční rozložení tlaku a molárních zlomků všech komponent.
2. Proveď výpočet fázové rovnováhy při počátečním tlaku, teplotě a molárních zlomcích.
3. Vypočti viskozity všech fází na všech elementech.
4. Opakuj následující časové kroky, dokud simulace neskončí v zadaném čase:
   (a) Sestav a vyřeš soustavu (2.40) pro stopy tlaků $\hat{P}$.
   (b) Vypočti tlaky uvnitř elementů P pomocí (2.39).
   (c) Vypočti celkové molární toky a fázové toky pomocí postupu popsaného v kapitole 2.2.4.
   (d) Vypočti hodnoty celkových koncentrací všech komponent na nové časové hladině použitím jednoho kroku explicitního Eulerova schématu nespojité Galerkinovy metody (2.45).
   (e) Oprav gradienty numerického řešení aplikací limiteru.
   (f) Otestuj stabilitu směsi a na dvoufázových elementech proveď výpočet fázové rovnováhy směsi. Výsledkem jsou hodnoty fázových vlastností na nové časové hladině.
   (g) Aktualizuj viskozity všech fází na všech elementech.

2.3 Příspěvky k formulaci kompozičního modelu

V předcházejících kapitolách jsme uvedli konvenční formulaci kompozičního transportního modelu, jehož součástí je řešení dvou základních úloh termodynamiky vícesložkových směsí, a sice problému testování fázové stability a výpočtu fázové rovnováhy při zadaných vnějších podmínkách. Jedná se o základní problémy chemického inženýrství, které se obvykle řeší při předepsaném tlaku, teplotě a celkových molárních zlomcích jednotlivých komponent směsi (viz např. [87, 4, 62, 63, 37, 77]). Ukazuje se však, že pro účely využití těchto metod v transportních modelech se vzhledem k tvaru stavových rovnic více hodí jiná formulace – a sice při předepsaném objemu, teplotě a celkovém látkovém množství každé komponenty. Možnost odvození takovýchto alternativních formulací byla sice příležitostně zmiňována v literatuře [65, 64, 11], ale v kompoziční simulaci se do roku 2013 používala výhradně výše uvedená Gibbsova formulace fázové rovnováhy při předepsaném tlaku, teplotě a celkových molárních zlomcích (příp. látkových množstvích) jednotlivých komponent směsi. V literatuře lze najít použití Helmholtzovy energie k odvození obecných podmínek fázové stability [35, 72], či kritéria pro stanovení kritických bodů směsí [36, 73]. Pro výpočet fázové rovnováhy při jiných specifikovaných proměnných (včetně objemu, teploty a látkových množství) Michelsen v práci [64] navrhl použít výpočet fázové rovnováhy při předepsaném tlaku, teplotě a molárních zlomcích, přičemž tlak se stanoví iteračně tak, aby výsledná kriteriální funkce (v našem případě celkový molární objem směsi) nabývala předepsané hodnoty. Tento přístup byl použit v pracech [28] k výpočtu termodynamické rovnováhy v systému, na který působí gravitační síla a [10] ke studiu segregace komponent směsi za působení odstředivých sil. Michelsenův postup umožňuje využít existující řešiče fázové rovnováhy při zadaném tlaku, teplotě a látkových množstvích. Tento postup je však výpočetně náročný, protože pro výpočet jedné fázové rovnováhy při zadaném V, T, N je potřeba provést mnoho výpočtů fázových rovnováh při zadaných p, T, N, než se najde tlak odpovídající objemu V. Další nevýhodou tohoto postupu je, že neřeší problémy, které budeme diskutovat v následujícím odstavci. Přímý výpočet fázové rovnováhy při zadaných V, T, N založený na minimalizaci Helmholtzovy energie použil Cabral a spol. v práci [9], avšak jejich metoda vyžadovala provádět výpočet tlaku a fugacit v komplexní aritmetice. Korektní odvození a vývoj výpočetních metod pro řešení fázové rovnováhy v Helmholtzově formulaci při zadaném objemu, teplotě a celkových látkových množstvích každé komponenty lze tedy považovat za původní příspěvek autora.

2.3.1 Některá omezení konvenční formulace

Pro reprezentaci chemického potenciálu se běžně používají pojmy fugacity a fugacitních koeficientů, což jsou funkce teploty, tlaku, molárních zlomků jednotlivých komponent směsi a fáze, které lze vyjádřit pomocí stavové rovnice [30, 65]. Při použití vzorců uváděných v literatuře je však potřeba invertovat stavovou rovnici – tj. nalézt objem V odpovídající zadanému tlaku p, teplotě T a látkovým množstvím $N_1, \ldots, N_n$ jednotlivých komponent. V případě Pengovy-Robinsonovy rovnice však tento objem není daný jednoznačně a je tedy potřeba ze dvou

fyzikálně významných kořenů vybrat ten, který je právě potřeba. Nejčastěji se vybírá ten kořen, jehož molární Gibbsova energie je nižší, případně kořen odpovídající zadané fázi [79, 83]. Oba přístupy mají svá úskalí, která nejsou běžně v literatuře diskutována.

Pokud vybíráme ten kořen, jehož molární Gibbsova energie je nejmenší, pak není jasné, který kořen vybrat, pokud jsou molární Gibbsovy energie stejné. To nastane např. v případě čisté látky při teplotě T a odpovídajícím saturačním tlaku $p^{sat}(T)$. Např. 1 mol vody při tlaku $p = 1$ atm a teplotě varu $T = 100$ °C může zabírat objem $V = 18{,}8$ cm^3 v kapalné fázi, kdežto v plynné fázi za stejných podmínek $30{,}2$ dm^3 [7]. Ze zadaného tlaku, teploty a počtu molů nelze usoudit, jaký je celkový objem systému, jenž může být ve stavu čistě kapalném nebo čistě plynném nebo ve směsi obou fází. Tlak, teplota a počty molů jednotlivých komponent nejsou tedy dostatečné pro jednoznačné určení všech parametrů rovnovážného stavu.

Pokud vybíráme ten kořen, který odpovídá zadané fázi, pak narážíme na problém fázové identifikace – je nutno předem říci, jestli chceme vyšetřovat stav systému za daných podmínek v plynné fázi (pak vybíráme větší z kořenů) nebo nás zajímá stav systému v kapalné fázi (pak vybíráme menší z kořenů). Tento přístup však může být sporný v případě, že vyšetřujeme chování látky v okolí kritického bodu, kde se vlastnosti obou fází příliš neliší a fázová identifikace může selhat.

Oba dva výše uvedené problémy lze elegantně vyřešit, pokud přeformulujeme úlohu do proměnných V, T, $N_1, \ldots, N_n$. Na rozdíl od tlaku, teploty a látkových množství totiž proměnné objem, teplota a látková množství určují stav systému jednoznačně. Pro reprezentaci chemických potenciálů v proměnných V, T, $N_1, \ldots, N_n$ jsme v článku [Č2] zavedli pojem objemové funkce F_i každé komponenty pomocí následujících rovnic

$$\mu_i(T, V_2, N_1, \ldots, N_n) = \mu_i(T, V_1, N_1, \ldots, N_n) - RT \ln \frac{F_i(T, V_2, N_1, \ldots, N_n)}{F_i(T, V_1, N_1, \ldots, N_n)} \tag{2.57}$$

a

$$\lim_{V \to +\infty} \frac{F_i(T, V, N_1, \ldots, N_n)}{V} = 1. \tag{2.58}$$

Dále definujeme koeficient objemové funkce Φ_i předpisem

$$\Phi_i(T, V, N_1, \ldots, N_n) = \frac{F_i(T, V, N_1, \ldots, N_n)}{V}. \tag{2.59}$$

Takto definované pojmy objemové funkce a koeficientu objemové funkce nahrazují pojmy fugacity a fugacitního koeficientu, které se běžně používají při vyšetřování rovnováh při zadaném tlaku, teplotě a molárních zlomcích. V článku [Č2] je odvozeno vyjádření koeficientu Φ_i ze stavové rovnice ve tvaru

$$\ln \Phi_i(T, V, N_1, \ldots, N_n) = \int_V^{+\infty} \left[\frac{1}{V} - \frac{1}{RT} \frac{\partial p}{\partial N_i}(T, V, N_1, \ldots, N_n) \right] dV. \tag{2.60}$$

Rozdíl chemických potenciálů mezi dvěma stavy $[T, V', N_1', \dots N_n']$ a $[T, V'', N_1'', \dots N_n'']$ je potom dán výrazem

$$\mu_i(T, V'', N_1'', \dots, N_n'') = \mu_i(T, V', N_1', \dots, N_n') + \\ + RT \ln \frac{N_i'' V'}{N_i' V''} \frac{\Phi_i(T, V', N_1', \dots, N_n')}{\Phi_i(T, V'', N_1'', \dots, N_n'')}. \tag{2.61}$$

Podrobnosti odvození těchto vztahů lze najít v přiloženém článku [Č2]. Pro určení rovnovážného stavu zavedeme Helmholtzovu volnou energii systému. Je-li systém n komponent s látkovými množstvími $N_1, \dots, N_n$, objemem V při teplotě T v jedné fázi, pak jeho Helmholtzovu volnou energii zavádíme předpisem

$$A^I = \sum_{i=1}^{n} N_i \mu_i(T, V, N_1, \dots, N_n) - p(T, V, N_1, \dots, N_n)V. \tag{2.62}$$

Pro heterogenní systém složený z více fází je Helmholtzova energie rovna součtu Helmholtzových energií jednotlivých fází, tj.

$$A^\Pi = \sum_{\alpha=1}^{\Pi} A^I(T, V_\alpha, N_{\alpha,1}, \dots, N_{\alpha,n}), \tag{2.63}$$

kde V_α označuje objem fáze α, $N_{\alpha,1}, \dots, N_{\alpha,n}$ jsou počty molů každé komponenty ve fázi α a Π je počet fází. Tyto veličiny musí splňovat podmínky

$$\sum_{\alpha=1}^{\Pi} V_\alpha = V, \qquad \sum_{\alpha=1}^{\Pi} N_{\alpha,i} = N_i, \qquad i = 1, \dots, n. \tag{2.64}$$

V termodynamické rovnováze zaujme systém n komponent s látkovými množstvími $N_1, \dots, N_n$, objemem V při teplotě T takovou konfiguraci, pro kterou je příslušná hodnota Helmholtzovy energie nejnižší mezi všemi přípustnými rozklady na libovolný počet fází splňujícími omezení (2.64). Rovnovážná hodnota Helmholtzovy energie je tedy dána předpisem

$$A(T, V, N_1, \dots, N_n) = \min A^\Pi = \min \sum_{\alpha=1}^{\Pi} A^I(T, V_\alpha, N_{\alpha,1}, \dots, N_{\alpha,n}), \tag{2.65}$$

kde $\min$ se hledá přes všechna $\Pi \in \mathbb{N}$ a všechny přípustné rozklady splňující (2.64).

2.3.2 Vyšetřování fázové stability při zadané teplotě, objemu a látkových množstvích

Uvažujme směs n komponent s látkovými množstvími $N_1, \dots N_n$, které zaujímají objem V při teplotě T. Zajímá nás, zda tato směs zůstane homogenní (tj. jednofázová) nebo se rozdělí na dvě nebo více fází.

Pro jednofázový systém je Helmholtzova energie definována předpisem (2.62). Předpokládejme, že z počáteční fáze odloučíme malé množství zkušební fáze o objemu V' a látkových množstvích $N'_1, \dots N'_n$. Směs je stabilní, pokud odloučení malého množství zkušební fáze libovolného složení z počáteční fáze nepovede ke snížení Helmholtzovy energie systému v porovnání s jednofázovým stavem. V článku [Č3] odvozujeme následující verzi Gibbsova kritéria fázové stability při zadané teplotě, objemu a látkových množstvích (viz též [92]):

Věta 1. *Počáteční fáze je při zadané teplotě T, objemu V a látkových množstvích $N_1, \dots, N_n$ stabilní, právě když*

$$\sum_{i=1}^{n} N'_i(\mu_i(T, V', N'_1, \dots, N'_n) - \mu_i(T, V, N_1, \dots, N_n)) - \\ - (p(T, V', N'_1, \dots, N'_n) - p(T, V, N_1, \dots, N_n))V' \geq 0, \tag{2.66}$$

pro všechny přípustné kombinace V' a $N'_1, \dots, N'_n$.

Zaveďme molární koncentrace jednotlivých komponent směsi každé fáze předpisy

$$c_i = \frac{N_i}{V}, \qquad \text{resp.} \qquad c'_i = \frac{N'_i}{V'} \tag{2.67}$$

Vzhledem k tomu, že tlak a chemické potenciály jsou intenzivní veličiny (pozitivně homogenní funkce stupně nula v proměnných V, $N_1, \dots, N_n$), můžeme přeformulovat kritérium fázové stability do následujícího tvaru.

Věta 2. *Počáteční fáze je při zadané teplotě T a molárních koncentracích $c_1, \dots, c_n$ stabilní, právě když funkce D (tzv. tangent plane distance function) definovaná předpisem*

$$D(c'_1, \dots c'_n) = \sum_{i=1}^{n} c'_i(\mu_i(T, 1, c'_1, \dots, c'_n) - \mu_i(T, 1, c_1, \dots, c_n)) - \\ - (p(T, 1, c'_1, \dots, c'_n) - p(T, 1, c_1, \dots, c_n)), \tag{2.68}$$

je nezáporná pro všechny přípustné koncentrace $c'_1, \dots, c'_n$.

Abychom zjistili, zda existuje stav se zápornou hodnotou funkce D, stačí vyšetřovat hodnoty funkce D ve svých stacionárních bodech. Stacionární body funkce D jsou zadány podmínkami (podrobné odvození je provedeno v [Č3])

$$\frac{\partial D}{\partial c'_j}(c'_1, \dots, c'_n) = \mu_j(T, 1, c'_1, \dots, c'_n) - \mu_j(T, 1, c_1, \dots, c_n) = 0, \qquad j = 1, \dots, n. \tag{2.69}$$

Pokud je ve všech stacionárních bodech hodnota funkce D nezáporná, pak je daná směs stabilní. Pokud v některém ze stacionárních bodů je hodnota funkce D záporná, pak je směs nestabilní.

Z podmínek (2.69) plyne, že hledaná zkušební fáze je tedy v chemické rovnováze s počáteční fází. Tlaky v obou fázích se však mohou lišit. Pokud $c'_1, \dots c'_n$ jsou koncentrace zkušební fáze splňující podmínky stacionarity (2.69), pak z (2.68) plyne, že

$$D(c'_1, \dots c'_n) = p(T, 1, c_1, \dots, c_n) - p(T, 1, c'_1, \dots, c'_n), \tag{2.70}$$

tj. hodnota funkce D ve stacionárním bodě je rovna rozdílu tlaků v počáteční fázi a zkušební fázi. Metody pro hledání stacionárních bodů funkce D je možno rozdělit na dvě skupiny:

1. *metody optimalizační*, kdy se hledá minimum funkce D na dané přípustné oblasti.

2. *metody rovnicové*, kdy se hledá numerické řešení podmínek (2.69).

V optimalizačních metodách založených na minimalizaci funkce D se nejčastěji využívají gradientní metody, Newtonova metoda nebo jejich kombinace, případně kvazi-newtonovské metody. Tyto metody zaručují konvergenci k lokálnímu extrému funkce D. Pokud chceme zaručit konvergenci ke globálnímu minimu funkce D, je nutno používat metody pro globální optimalizaci - např. metody založené na intervalové aritmetice nebo heuristické algoritmy (metoda simulovaného žíhání, diferenciální evoluce, . . .), viz např. [45, 46, 32, 50, 51, 52, 69, 70, 75, 90]. Hledání globálního minima funkce je však obtížná úloha. Algoritmy pro globální minimalizaci vyžadují mnoho vyčíslení funkce D jsou tedy nepoužitelné pro kompoziční simulaci, ve které je potřeba testovat stabilitu směsi v každém konečném elementu diskretizační sítě v každém časovém kroku. V kompoziční simulaci se proto používají lokální metody [31, 86], v nichž se pravděpodobnost konvergence k nesprávnému řešení snižuje použitím více počátečních aproximací, které jsou často konstruovány na základě fyzikálních heuristik získaných řešením problému fázové stability za idealizovaných podmínek. Obdobné problémy se vyskytují i u metod založených na řešení rovnic (2.69). Nalezení *všech* kořenů zadané soustavy rovnic je obecně těžká úloha. Obvykle se tedy používají lokální metody s využitím více počátečních nástřelů. Oproti optimalizačním metodám je nutno počítat i s možností, že algoritmus zkonverguje k řešení, které nebude ani lokálním minimem funkce D, neboť podmínky stacionarity (2.69) jsou splněny i v bodech lokálních maxim a sedlových bodech funkce D. V přiloženém článku [Č3] jsme odvodili metodu pro vyšetřování fázové stability vícesložkové směsi založené na Newtonově metodě pro řešení systému rovnic (2.69) ve tvaru, který se ukázal jako dostačující pro potřeby kompoziční simulace.

2.3.3 Fázová rovnováha dvoufázového systému při zadané teplotě, objemu a látkových množstvích

Uvažujme směs n komponent s látkovými množstvími $N_1, \dots N_n$, které zaujímají objem V při teplotě T a předpokládejme, že tato směs je nestabilní a má se rozdělit na dvě fáze. Cílem je stanovit objemy obou fází V' a V'' a počty molů každé komponenty v obou fázích N'_i a N''_i pro $i \in \{1, 2, \dots, n\}$ a mj. i hodnotu rovnovážného tlaku p. Helmholtzova energie hypotetického

jednofázového stavu je dána předpisem (2.62). Helmholtzova energie dvoufázového stavu je dána předpisem

$$\begin{aligned} A^{II} &= A^I(T, V', N_1', \ldots, N_n') + A^I(T, V'', N_1'', \ldots, N_n'') = \\ &= \sum_{i=1}^{n} N_i' \mu_i(T, V', N_1', \ldots, N_n') - p(T, V', N_1', \ldots, N_n')V' + \\ &+ \sum_{i=1}^{n} N_i'' \mu_i(T, V'', N_1'', \ldots, N_n'') - p(T, V'', N_1'', \ldots, N_n'')V''. \end{aligned} \tag{2.71}$$

Rovnovážný stav dvoufázového systému při zadané teplotě T, celkovém objemu V a celkových látkových množstvích jednotlivých komponent N_i ($i = 1, \ldots n$) je takový stav, pro který je přírůstek Helmholtzovy energie vzhledem k hypotetickému jednofázovému stavu

$$\Delta A \; = A^I(T, V', N_1', \ldots, N_n') + A^I(T, V'', N_1'', \ldots, N_n'') - A^I(T, V, N_1, \ldots, N_n) \tag{2.72}$$

minimální mezi všemi přípustnými rozklady splňujícími omezující podmínky

$$V' + V'' = V, \tag{2.73a}$$
$$N_i' + N_i'' = N_i, \qquad i = 1, \ldots, n. \tag{2.73b}$$

Hledání rovnovážného stavu tedy představuje optimalizační problém – hledání minima funkce ΔA – s vedlejšími podmínkami (2.73). Metodou Lagrangeových multiplikátorů lze odvodit nutné podmínky fázové rovnováhy.

Věta 3. *Nechť systém při zadané teplotě T, celkovém objemu V a celkových látkových množstvích jednotlivých komponent $N_1, \ldots, N_n$ je v rovnováze rozdělen na dvě fáze s objemy V' a V'' a látkovými množstvími N_i' a N_i'' každé komponenty tak, že platí* (2.73)*. Potom*

$$p(T, V', N_1', \ldots, N_n') = p(T, V'', N_1'', \ldots, N_n''), \tag{2.74a}$$
$$\mu_i(T, V', N_1', \ldots, N_n') = \mu_i(T, V'', N_1'', \ldots, N_n'') \qquad i = 1, \ldots, n. \tag{2.74b}$$

Rovnice (2.74a) vyjadřuje podmínku mechanické rovnováhy – obě fáze mají v rovnováze stejný tlak. Rovnice (2.74b) vyjadřuje podmínku chemické rovnováhy – chemické potenciály každé komponenty v obou fázích se rovnají. Označíme-li společnou hodnotu tlaku jako p^{eq} a společnou hodnotu chemického potenciálu i-té komponenty μ_i^{eq}, pak systém rovnic (2.73) a (2.74) představuje definici implicitně zadaných funkcí $p^{eq}(T, V, N_1, \ldots, N_n)$ a $\mu_i^{eq}(T, V, N_1, \ldots, N_n)$ pro $i = 1, 2, \ldots, n$ ve dvoufázové oblasti.

Vyšetřujme systém s látkovými množstvími jednotlivých komponent $N_1, \ldots, N_n$ zaujímající objem V při teplotě T. Zaveďme celkové molární koncentrace $c_i = N_i/V$ každé komponenty $i \in \{1, \ldots, n\}$. Stabilitu jednofázového stavu popsaného teplotou T a koncentracemi $c_1, \ldots, c_n$ lze testovat pomocí kritéria stability (2.68) popsaného v předchozí kapitole. Pokud pro všechny

přípustné hodnoty $c'_1, \ldots, c'_n$ je $D(c'_1, \ldots, c'_n) \geq 0$, pak je jednofázový stav stabilní – systém se nachází v jedné fázi a tlak systému lze vypočítat pomocí stavové rovnice.

Pokud při testování stability nalezneme přípustné hodnoty $c'_1, \ldots, c'_n$, pro které je $D(c'_1, \ldots, c'_n) < 0$, pak je systém nestabilní a má se rozdělit na (alespoň) 2 fáze. V rámci této práce se omezíme na nejvýše dvoufázové systémy. Cílem je pak nalézt objemy V' a V'' obou fází a látková množství $N'_1, \ldots, N'_n$ a $N''_1, \ldots, N''_n$ každé komponenty v obou fázích tak, aby celková změna Helmholtzovy energie oproti hypotetickému jednofázovému stavu daná předpisem (2.72) byla minimální mezi všemi přípustnými rozklady tvaru (2.73). Výpočet rovnovážného stavu bude probíhat ve dvou etapách. Nejprve se zkonstruuje přípustný dvoufázový rozklad s nižší energií, než je energie původního jednofázového stavu. Tento rozklad je dále iteračně vylepšován s cílem dosáhnout minima funkce ΔA při splnění omezujících podmínek (2.73). Takto nalezneme dvoufázový stav s nejnižší Helmholtzovou energií při zadaných omezujících podmínkách.

Konstrukce počátečního dvoufázového rozkladu

Nechť je jednofázový systém nestabilní. Potom algoritmus pro testování fázové stability popsaný v předchozí kapitole nalezne koncentrace $c'_1, \ldots, c'_n$, pro které je $D(c'_1, \ldots, c'_n) < 0$. Z definice funkce D plyne, že pokud z počáteční fáze o objemu V s látkovými množstvími $N_1, \ldots, N_n$ vydělíme dostatečně malé množství zkušební fáze s koncentracemi $c'_1, \ldots, c'_n$, pak dojde k poklesu Helmholtzovy energie systému oproti jednofázovému stavu. Hledáme tedy dostatečně malý objem $V' > 0$ takový, aby

$$A^I(T, V', c'_1V', \ldots, c'_nV') + A^I(T, V - V', N_1 - c'_1V', \ldots, N_n - c'_nV') - A^I(T, V, N_1, \ldots, N_n) < 0. \tag{2.75}$$

Objem V' lze najít metodou půlení intervalu – nejprve zkusíme, zda $V' = V/2$ splňuje podmínku (2.75). Pokud tato podmínka není splněna, půlí se hodnota V' tak dlouho, dokud neplatí (2.75). Protože $D(c'_1, \ldots, c'_n) < 0$, musí tento proces skončit po konečně mnoha krocích. Takto nalezená hodnota V' poskytuje dvoufázový rozklad tvaru

$$N'_i = c'_iV', \qquad N''_i = N_i - c'_iV', \qquad i \in \{1, \ldots, n\}, \tag{2.76}$$

$$V'' = V - V', \tag{2.77}$$

který splňuje podmínky (2.73) a pro který je hodnota Helmholtzovy energie nižší než $A^I(T, V, N_1, \ldots, N_n)$ – viz (2.75).

Hledání dvoufázového rovnovážného stavu

Dvoufázový rozklad zkonstruovaný v předchozím kroku není obecně rovnovážným stavem, tj. stavem s nejnižší hodnotou dvoufázové Helmholtzovy energie mezi všemi přípustnými rozklady

splňujícími podmínky (2.73). Podmínky (2.73) lze přepsat do maticového tvaru

$$\mathbb{A}\mathbf{x} = \mathbf{b}, \tag{2.78}$$

kde matice $\mathbb{A} \in R^{n+1,2n+2}$, vektory $\mathbf{x} \in R^{2n+2}$ a $\mathbf{b} \in R^{n+1}$ jsou dány předpisy

$$\mathbb{A} = (\mathbb{I}_{n+1}\, \mathbb{I}_{n+1}), \tag{2.79}$$

$$\mathbf{x} = [N_1', \ldots, N_n', V', N_1'', \ldots, N_n'', V'']^T, \tag{2.80}$$

$$\mathbf{b} = [N_1, \ldots, N_n, V]^T. \tag{2.81}$$

V těchto rovnicích $\mathbb{I}_{n+1}$ označuje jednotkovou matici na prostoru dimenze $n+1$ a T označuje transpozici vektoru, resp. matice. Cílem je minimalizovat ΔA – funkci $2n+2$ proměnných při $n+1$ omezujích podmínkách daných rovnicemi $\mathbb{A}\mathbf{x} = \mathbf{b}$, což představuje $2n+2-(n+1) = n+1$ stupňů volnosti. Pomocí (2.78) lze např. eliminovat proměnné $V'' = V - V'$ a $N_i'' = N_i - N_i'$ pro $i = 1, \ldots n$ a přeformulovat problém minimalizace funkce ΔA při zadaných omezujících podmínkách na problém bez vazeb pouze v $n+1$ proměnných $N_1', \ldots, N_n', V'$. Tento postup však zanáší do problému nesymetrii – jedna fáze je privilegována na úkor druhé, což může způsobovat problémy v situacích, kdy je např. množství jedné fáze ve dvoufázovém systému velmi malé. Proto popíšeme alternativní postup, který ošetřuje obě fáze naprosto rovnocenně.

Z tvaru matice $\mathbb{A}$, která je v horním stupňovitém tvaru, vidíme, že řádky matice jsou lineárně nezávislé. Matice $\mathbb{A}$ má tedy hodnost $n+1$. Označme $\mathbb{Z} \in R^{2n+2,n+1}$ matici, jejíž sloupce tvoří ortonormální bázi jádra operátoru příslušného matici $\mathbb{A}$. Tuto bázi doplňme na ortonormální bázi prostoru R^{2n+2} pomocí vektorů z R^{2n+2}, které budou tvořit sloupce matice $\mathbb{Y} \in R^{2n+2,n+1}$. Matice $\mathbb{Y}$ a $\mathbb{Z}$ lze zvolit např. ve tvaru

$$\mathbb{Y} = \frac{1}{\sqrt{2}} \begin{pmatrix} \mathbb{I}_{n+1} \\ \mathbb{I}_{n+1} \end{pmatrix}, \qquad \mathbb{Z} = \frac{1}{\sqrt{2}} \begin{pmatrix} \mathbb{I}_{n+1} \\ -\mathbb{I}_{n+1} \end{pmatrix}. \tag{2.82}$$

Protože sloupce matic $\mathbb{Y}$ a $\mathbb{Z}$ tvoří bázi prostoru R^{2n+2}, lze pro každý vektor $\mathbf{x} \in R^{2n+2}$ najít rozklad tvaru

$$\mathbf{x} = \mathbb{Y}\mathbf{x}_{\mathcal{Y}} + \mathbb{Z}\mathbf{x}_{\mathcal{Z}}, \tag{2.83}$$

kde vektory $\mathbf{x}_{\mathcal{Y}}$ a $\mathbf{x}_{\mathcal{Z}}$ z prostoru R^{n+1} jsou vektorem $\mathbf{x}$ jednoznačně určeny. Vektor $\mathbf{x}$ je tímto rozložen na část $\mathbb{Z}\mathbf{x}_{\mathcal{Z}}$, která leží v jádře operátoru příslušného matici $\mathbb{A}$, a na část $\mathbb{Y}\mathbf{x}_{\mathcal{Y}}$, která leží v ortogonálním doplňku jádra operátoru příslušného matici $\mathbb{A}$. Pokud je vektor $\mathbf{x}$ přípustný, tj. splňuje podmínky (2.73), pak

$$\mathbb{A}\mathbf{x} = \mathbb{A}\mathbb{Y}\mathbf{x}_{\mathcal{Y}} + \mathbb{A}\,\mathbb{Z}\mathbf{x}_{\mathcal{Z}} = \mathbb{A}\mathbb{Y}\mathbf{x}_{\mathcal{Y}} = \mathbf{b}, \tag{2.84}$$

protože $\mathbb{A}\mathbb{Z} = 0$. Z konstrukce matice $\mathbb{Y}$ plyne, že součin $\mathbb{A}\mathbb{Y}$ je regulární, a tedy soustava $\mathbb{A}\mathbb{Y}\mathbf{x}_{\mathcal{Y}} = \mathbf{b}$ má právě jedno řešení $\mathbf{x}_{\mathcal{Y}}$. Vektor $\mathbf{x}_{\mathcal{Y}}$ je tedy jednoznačně určen omezujícími podmínkami. Zbývá určit vektor $\mathbf{x}_{\mathcal{Z}}$.

Minimalizaci funkce ΔA za podmínek (2.78) budeme provádět iteračně. Počáteční aproximaci $\mathbf{x}^{(0)}$ získáme pomocí výše uvedeného postupu. Je-li $\mathbf{x}^{(k)}$ aproximace v k-tém kroku, pak další aproximaci hledáme ve tvaru

$$\mathbf{x}^{(k+1)} = \mathbf{x}^{(k)} + \alpha_k \mathbf{d}^{(k)}, \tag{2.85}$$

kde α_k označuje velikost kroku a $\mathbf{d}^{(k)}$ udává směr přírůstku. Předpokládáme, že aproximace $\mathbf{d}^{(k)}$ je přípustná, tj. $\mathbb{A}\mathbf{x}^{(k)} = \mathbf{b}$. Požadujeme-li, aby byla přípustná i $\mathbf{x}^{(k+1)}$, potom vektor $\mathbf{d}^{(k)}$ musí splňovat $\mathbb{A}\mathbf{d}^{(k)} = 0$, neboli $\mathbf{d}^{(k)} = \mathbb{Z}\mathbf{d}_{\mathcal{Z}}^{(k)}$, kde $\mathbf{d}_{\mathcal{Z}}^{(k)} \in R^{n+1}$. Vektor $\mathbf{d}^{(k)}$ je tedy vektor z R^{2n+2}, který leží v podprostoru (jádře operátoru příslušného matici $\mathbb{A}$) dimenze $n+1$. Takto jsme problém optimalizace s $n+1$ vazbami v dimenzi $2n+2$ převedli na problém bez vazeb v prostoru dimenze $n+1$. Vektor $\mathbf{d}_{\mathcal{Z}}^{(k)}$ lze hledat Newtonovou minimalizační metodou využívající kvadratickou aproximaci funkce ΔA v okolí bodu $\mathbf{x}^{(k)}$, tj.

$$\min_{\substack{\mathbf{d}^{(k)} \in R^{2n+2} \\ \mathbb{A}\mathbf{d}^{(k)} = 0}} \Delta A(\mathbf{x}^{(k)} + \mathbf{d}^{(k)}) = \min_{\mathbf{d}_{\mathcal{Z}}^{(k)} \in R^{n+1}} \Delta A(\mathbf{x}^{(k)} + \mathbb{Z}\mathbf{d}_{\mathcal{Z}}^{(k)}) \approx$$

$$\approx \Delta A(\mathbf{x}^{(k)}) + \mathbf{g}(x^{(k)})^T \mathbb{Z}\mathbf{d}_{\mathcal{Z}}^{(k)} + \frac{1}{2}(\mathbb{Z}\mathbf{d}_{\mathcal{Z}}^{(k)})^T \mathbb{H}(\mathbf{x}^{(k)}) \mathbb{Z}\mathbf{d}_{\mathcal{Z}}^{(k)}, \tag{2.86}$$

kde $\mathbf{g}(x^{(k)})$ označuje gradient a $\mathbb{H}(\mathbf{x}^{(k)})$ označuje hessián funkce ΔA vyčíslený v bodě $\mathbf{x}^{(k)}$. Výpočet prvků gradientu a hessiánu je podrobně proveden v přiloženém článku [Č4]. Hledaný vektor $\mathbf{d}_{\mathcal{Z}}^{(k)}$ je tedy argument minima příslušné kvadratické formy. Z nutných podmínek pro extrém plyne, že kvadratická forma v rovnici (2.86) nabývá stacionární hodnoty pro $\mathbf{d}_{\mathcal{Z}}^{(k)}$ splňující

$$\mathbb{H}_{\mathcal{Z}}(\mathbf{x}^{(k)}) \mathbf{d}_{\mathcal{Z}}^{(k)} = -\mathbf{g}_{\mathcal{Z}}(x^{(k)}), \tag{2.87}$$

kde $\mathbb{H}_{\mathcal{Z}}(\mathbf{x}^{(k)}) = \mathbb{Z}^T \mathbb{H}(\mathbf{x}^{(k)}) \mathbb{Z}$ a $\mathbf{g}_{\mathcal{Z}}(x^{(k)}) = \mathbb{Z}^T \mathbf{g}(x^{(k)})$ označují zúžení (projekci) hessiánu, resp. gradientu na jádro zobrazení příslušné matici $\mathbb{A}$. Matice $\mathbb{H}_{\mathcal{Z}}$ má následující strukturu

$$\mathbb{H}_{\mathcal{Z}}(\mathbf{x}^{(k)}) = \frac{1}{2} \begin{pmatrix} \mathbb{B} & \mathbb{C} \\ \mathbb{C}^T & \mathbb{D} \end{pmatrix}, \tag{2.88}$$

kde

$$\mathbb{B} \in \mathrm{R}^{n \times n},\ \mathbb{B}_{ij} = \frac{\partial \mu_i}{\partial N_j'}(T, V', N_1', \ldots, N_n') + \frac{\partial \mu_i}{\partial N_j''}(T, V'', N_1'', \ldots, N_n''),$$

$$\mathbb{C} \in \mathrm{R}^{n},\ \mathbb{C}_j = -\frac{\partial p}{\partial N_j'}(T, V', N_1', \ldots, N_n') - \frac{\partial p}{\partial N_j''}(T, V'', N_1'', \ldots, N_n''),$$

$$\mathbb{D} \in \mathrm{R}^{1},\ \mathbb{D} = -\frac{\partial p}{\partial V'}(T, V', N_1', \ldots, N_n') - \frac{\partial p}{\partial V''}(T, V'', N_1'', \ldots, N_n''),$$

a

$$\mathbf{g}_{\mathcal{Z}}(\mathbf{x}^{(k)}) = \frac{1}{\sqrt{2}} \begin{pmatrix} \mu_1(T, V', N_1', \ldots, N_n') - \mu_1(T, V'', N_1'', \ldots, N_n'') \\ \vdots \\ \mu_n(T, V', N_1', \ldots, N_n') - \mu_n(T, V'', N_1'', \ldots, N_n'') \\ -p(T, V', N_1', \ldots, N_n') + p(T, V'', N_1'', \ldots, N_n'') \end{pmatrix}. \tag{2.89}$$

Při výpočtu prvků matice $\mathbb{H}_{\mathcal{Z}}$ a vektoru $\mathbf{g}_{\mathcal{Z}}$ se tlaky vyčíslí pomocí stavové rovnice a rozdíly chemických potenciálů se vyjádří pomocí koeficientů objemových funkcí popsaných v kapitole 2.3.1 (rovnice (2.60) a (2.61)).

Pokud $\mathbf{d}_{\mathcal{Z}}^{(k)}$ je řešení systému rovnic (2.87) a matice $\mathbb{H}_{\mathcal{Z}}$ je pozitivně definitní, pak vektor $\mathbf{d}_{\mathcal{Z}}^{(k)}$ míří ve směru poklesu funkce ΔA. Pokud hessián není pozitivně definitní, pak upravíme směr $\mathbf{d}_{\mathcal{Z}}^{(k)}$ tak, aby byl zajištěn pokles funkce ΔA v dané iteraci. Vektor $\mathbf{d}_{\mathcal{Z}}^{(k)}$ v tomto případě najdeme řešením pozměněné soustavy rovnic tvaru

$$\widehat{\mathbb{H}_{\mathcal{Z}}}(\mathbf{x}^{(k)})\mathbf{d}_{\mathcal{Z}}^{(k)} = -\mathbf{g}_{\mathcal{Z}}(\mathbf{x}^{(k)}), \tag{2.90}$$

kde $\widehat{\mathbb{H}_{\mathcal{Z}}}(\mathbf{x}^{(k)})$ je pozitivně definitní matice získaná modifikovanou Choleskyho faktorizací matice $\mathbb{H}_{\mathcal{Z}}(\mathbf{x}^{(k)})$. V této variantě se provádí Choleskyho faktorizace původního hessiánu $\mathbb{H}_{\mathcal{Z}}(\mathbf{x}^{(k)})$ do tvaru $\mathbb{H}_{\mathcal{Z}}(\mathbf{x}^{(k)}) = \mathbb{L}\mathbb{L}^T$ kde $\mathbb{L}$ je dolní trojúhelníková matice. Pokud během této faktorizace vznikne na diagonále matice $\mathbb{L}$ nekladný prvek, pak tento prvek uměle přepíšeme na kladné číslo. Takto dostaneme Choleskyho rozklad nějaké pozitivně definitní matice $\widehat{\mathbb{H}_{\mathcal{Z}}}(\mathbf{x}^{(k)})$, která se použije v Newtonově metodě pro výpočet směru $\mathbf{d}_{\mathcal{Z}}^{(k)}$ na místo skutečného hessiánu $\mathbb{H}_{\mathcal{Z}}(\mathbf{x}^{(k)})$. Tato úprava Newtonovy metody zajistí snižování účelové funkce ΔA v každé iteraci, pokud zvolíme velikost kroku α_k dostatečně malou. Hodnotu α_k hledáme opět metodou půlení intervalu – nejprve zkusíme položit $\alpha_k = 1$ a potom testujeme, zda $\Delta A(\mathbf{x}^{(k)} + \mathbf{d}^{(k)}) < \Delta A(\mathbf{x}^{(k)})$. Pokud je tato podmínka splněna, pak položíme $\mathbf{x}^{(k+1)} = \mathbf{x}^{(k)} + \mathbf{d}^{(k)}$. Pokud podmínka není splněna, tak půlíme hodnotu α_k tak dlouho, až je splněna podmínka $\Delta A(\mathbf{x}^{(k)} + \alpha_k\mathbf{d}^{(k)}) < \Delta A(\mathbf{x}^{(k)})$ a potom položíme $\mathbf{x}^{(k+1)} = \mathbf{x}^{(k)} + \alpha_k\mathbf{d}^{(k)}$. Takto se provede jedna iterace Newtonovy metody. Iterace se zastaví, pokud (viz [85])

$$\|\mathbf{d}^{(k)}\|_2 := \left(\sum_{j=1}^{2n+2} \mathbf{d}_j^{(k)\,2} \right)^{\frac{1}{2}} \leq \varepsilon_{tol} = 10^{-7}. \tag{2.91}$$

2.3.4 Nekonvenční formulace kompozičního modelu

Novou formulaci lokální termodynamické rovnováhy využijeme ke konstrukci nové formulace kompozičního modelu. Model je zapsán ve formě bilančních rovnic pro n komponent směsi

$$\frac{\partial(\phi c_i)}{\partial t} + \nabla \cdot \mathbf{q}_i = F_i, \qquad i = 1, \ldots, n, \tag{2.92}$$

$$\mathbf{q}_i = \sum_\alpha c_{\alpha,i} \mathbf{v}_\alpha, \tag{2.93}$$

které jsou doplněny Darcyho zákonem pro každou fázi tvaru

$$\mathbf{v}_\alpha = -\lambda_\alpha \mathbf{K}(\nabla p - \varrho_\alpha \mathbf{g}), \quad \lambda_\alpha = \frac{k_{r\alpha}}{\eta_\alpha}. \tag{2.94}$$

Stejně jako v konvenčním modelu jsou relativní permeabilita $k_{r\alpha}$ fáze α a dynamické viskozity η_α fáze α dány konstitučními vztahy

$$k_{r\alpha} = k_{r\alpha}\left(S_\alpha\right), \tag{2.95}$$

a dynamická viskozita η_α fáze α závisí na teplotě a molárních koncentracích fáze α

$$\eta_\alpha = \eta_\alpha(T, c_{\alpha,1}, \ldots, c_{\alpha,n}). \tag{2.96}$$

Tento systém rovnic doplníme vztahy popisující vazby mezi celkovými koncentracemi c_i a počtem fází, fázovými koncentracemi $c_{\alpha,i}$ všech komponent ve všech fázích a saturacemi S_α všech fází. K tomuto účelu použijeme algoritmy pro testování fázové stability a ve dvoufázovém případě algoritmus pro výpočet fázové rovnováhy směsi při zadaném objemu, teplotě a látkových množstvích z předchozích kapitol. Primárními neznámými budou celkové molární koncentrace všech komponent c_i, které jsou funkcemi prostoru a času, tj. $c_i = c_i(\mathbf{x}, t)$. Za předpokladu lokální termodynamické rovnováhy lze v každém bodě $\mathbf{x}$ a každém čase t testovat stabilitu jednofázového stavu s teplotou T a celkovými koncentracemi $c_1(\mathbf{x}, t), \ldots, c_n(\mathbf{x}, t)$. V jednofázovém případě lze tlak v daném bodě stanovit přímo pomocí stavové rovnice

$$p(\mathbf{x}, t) = p\left(T, 1, c_1(\mathbf{x}, t), \ldots, c_n(\mathbf{x}, t)\right). \tag{2.97}$$

Ve dvoufázovém případě je rozklad komponent mezi fáze dán následujícími podmínkami lokální fázové rovnováhy [Č2]

$$\sum_\alpha c_{\alpha,i}(\mathbf{x}, t) S_\alpha(\mathbf{x}, t) = c_i(\mathbf{x}, t) \qquad i = 1, \ldots, n, \tag{2.98a}$$

$$\sum_\alpha S_\alpha(\mathbf{x}, t) = 1, \tag{2.98b}$$

$$p\left(T, 1, c_{\alpha,1}(\mathbf{x}, t), \ldots, c_{\alpha,n}(\mathbf{x}, t)\right) = p\left(T, 1, c_{\beta,1}(\mathbf{x}, t), \ldots, c_{\beta,n}(\mathbf{x}, t)\right), \quad \forall \alpha \neq \beta, \tag{2.98c}$$

$$\mu_i\left(T, 1, c_{\alpha,1}(\mathbf{x}, t), \ldots, c_{\alpha,n}(\mathbf{x}, t)\right) = \mu_i\left(T, 1, c_{\beta,1}(\mathbf{x}, t), \ldots, c_{\beta,n}(\mathbf{x}, t)\right), \quad \forall \alpha \neq \beta, \quad \forall i = 1, \ldots, n. \tag{2.98d}$$

Tento systém nelineárních algebraických rovnic při zadané teplotě a celkových molárních koncentracích umožňuje stanovit koncentrace všech komponent v obou fázích a fázové saturace. Po vyřešení této soustavy je možno stanovit hodnotu rovnovážného tlaku systému ze stavové rovnice

$$p(\mathbf{x},t) = p\left(T, 1, c_{\alpha,1}(\mathbf{x},t), \ldots, c_{\alpha,n}(\mathbf{x},t)\right), \tag{2.99}$$

kde α je kterákoliv fáze. Hodnota tlaku nezávisí na volbě fáze, neboť pro systém v termodynamické rovnováze jsou tlaky v obou fázích stejné. Rovnice řešíme na omezené oblasti $\Omega \subset \mathbb{R}^d$ ($d \in \mathbb{N}$) a časovém intervalu I. V oblasti $\Omega \times I$ hledáme funkce $c_i = c_i(\mathbf{x},t)$, které řeší soustavu rovnic (2.92)-(2.98) a splňují následující počáteční a okrajové podmínky

$$c_i(\mathbf{x},0) = c_i^0(\mathbf{x}), \quad \mathbf{x} \in \Omega,\ i = 1,\ldots,n, \tag{2.100a}$$

$$p(\mathbf{x},t) = p^D(\mathbf{x},t), \quad \mathbf{x} \in \Gamma_p,\ t \in I, \tag{2.100b}$$

$$\mathbf{q}_i(\mathbf{x},t)\cdot\mathbf{n}(\mathbf{x}) = 0, \quad \mathbf{x} \in \Gamma_q,\ t \in I,\ i = 1,\ldots,n, \tag{2.100c}$$

v nichž $\mathbf{n}$ označuje jednotkový vektor vnější normály definovaný skoro všude na $\partial\Omega$, $\Gamma_p \cup \Gamma_q = \partial\Omega$, a $\Gamma_p \cap \Gamma_q = \emptyset$. Rovnice (2.100a) popisuje počáteční rozložení molárních koncentrací, (2.100b) je Dirichletova okrajová podmínka předepisující tlak p^D na části hranice Γ_p, a (2.100c) je homogenní Neumannova okrajová podmínka popisující nepropustnou část hranice Γ_q. Předpokládáme, že Γ_p je odtoková část hranice, takže na ní není třeba předepisovat žádné okrajové podmínky pro molární koncentrace.

2.4 Numerické řešení nekonvenčního kompozičního modelu

Systém rovnic (2.92)–(2.100) budeme řešit numericky pomocí kombinace smíšené hybridní metody konečných prvků pro aproximaci celkového toku a metody konečných objemů pro aproximaci transportních rovnic. Časová diskretizace bude provedena zpětnou Eulerovou metodou. Výsledný systém nelineárních rovnic bude linearizován Newtonovou metodou. Počet fází na každém elementu bude určován pomocí testování jednofázové stability při konstantní teplotě a celkových molárních koncentracích všech komponent. Ve dvoufázových elementech se rozdělení komponent mezi fáze vypočítá algoritmem pro výpočet fázové rovnováhy při zadané teplotě a celkových koncentracích všech komponent. Výsledkem tohoto výpočtu je i hodnota rovnovážného tlaku v daném elementu. Tento způsob stanovení tlaku při kompoziční simulaci je původním příspěvkem autora.

Numerické schéma odvodíme pro problém ve dvoudimenzionální polygonální oblasti Ω s hranicí $\partial\Omega$, kterou pokryjeme triangulací $\mathcal{T}_\Omega$. Označme K některý element sítě $\mathcal{T}_\Omega$, jeho plochu $|K|$, E bude hrana elementu a $|E|$ její délka. Stejně jako dříve N_K bude označovat počet elementů v síti a N_E celkový počet hran sítě.

2.4.1 Diskretizace celkového toku

Celkový tok $\mathbf{q}$ je zavedený předpisem (2.25). V kapitole 2.2.2 jsme odvodili vyjádření fázového toku pomocí celkového toku (2.27). Obdobným postupem lze odvodit následující vyjádření celkového toku i-té komponenty pomocí celkového toku

$$\mathbf{q}_i = \sum_\alpha \frac{c_{\alpha,i}\lambda_\alpha}{\sum_\beta c_\beta \lambda_\beta} \left(\mathbf{q} - \sum_\beta c_\beta \lambda_\beta \left(\varrho_\beta - \varrho_\alpha \right) \mathbf{K}\mathbf{g} \right). \tag{2.101}$$

Celkový tok $\mathbf{q}$ aproximujeme na každém elementu K funkcí z Raviartova-Thomasova prostoru nejnižšího stupně ($RT_0(K)$) [8]

$$\mathbf{q}|_K = \sum_{E \in \partial K} q_{K,E} \mathbf{w}_{K,E}, \tag{2.102}$$

kde koeficient $q_{K,E}$ má význam celkového toku vektorové funkce $\mathbf{q}$ přes hranu E z elementu K ve směru vnější normály $\mathbf{n}_{K,E}$ a $\mathbf{w}_{K,E}$ označuje po částech lineární bazické funkce prostoru $RT_0(K)$, které v případě trojúhelníkových prvků jsou definovány jako

$$\mathbf{w}_{K,E}(\mathbf{x}) = \frac{1}{2|K|} \left(\mathbf{x} - \mathbf{N}_{K,E} \right), \qquad \forall \mathbf{x} \in K,\ E \in \partial K. \tag{2.103}$$

Zde $\mathbf{N}_{K,E} \in K$ označuje souřadnice vrcholu trojúhelníku K naproti hraně E. Bazické funkce (2.103) mají následující vlastnosti

$$\nabla \cdot \mathbf{w}_{K,E}(\mathbf{x}) = \frac{1}{|K|}, \qquad \mathbf{w}_{K,E}(\mathbf{x}) \cdot \mathbf{n}_{K,E'} = \frac{\delta_{E,E'}}{|E|}. \tag{2.104}$$

Rovnici (2.26) vynásobíme skalárně funkcí $\mathbf{w}_{K,E}$, a výsledek integrujeme přes element K, čímž obdržíme

$$\begin{aligned} \int_K \nabla p \cdot \mathbf{w}_{K,E'} = &- \left(\sum_{\alpha \in \Pi(K)} c_{\alpha,K} \lambda_{\alpha,K} \right)^{-1} \sum_{E \in \partial K} q_{K,E} \int_K \mathbf{K}^{-1} \mathbf{w}_{K,E} \cdot \mathbf{w}_{K,E'} + \\ &+ \widetilde{\varrho}_K \int_K \mathbf{g} \cdot \mathbf{w}_{K,E'}, \end{aligned} \tag{2.105}$$

kde jsme použili (2.102) a větu o střední hodnotě. Symbolem $\Pi(K)$ jsme označili množinu všech fází na elementu K. Použijeme-li Greenovu větu, větu o střední hodnotě a vlastnosti (2.104), odvodíme

$$\begin{aligned} \int_K \nabla p \cdot \mathbf{w}_{K,E'} &= \sum_{E \in \partial K} \int_E p \mathbf{w}_{K,E'} \cdot \mathbf{n}_{K,E} - \int_K p \nabla \cdot \mathbf{w}_{K,E'} = \\ &= \frac{1}{|E'|} \int_{E'} p - \frac{1}{|K|} \int_K p. \end{aligned} \tag{2.106}$$

Označme

$$A_{K,E,E'} = \int_K \mathbf{K}^{-1}\mathbf{w}_{K,E} \cdot \mathbf{w}_{K,E'}, \qquad G_{K,E'} = \int_K \mathbf{g} \cdot \mathbf{w}_{K,E'},$$
$$\widehat{p}_{K,E'} = \frac{1}{|E'|}\int_{E'} p, \qquad p_K = \frac{1}{|K|}\int_K p. \tag{2.107}$$

Potom lze z (2.105) a (2.106) odvodit

$$\left(\sum_{\alpha\in\Pi(K)} c_{\alpha,K}\lambda_{\alpha,K}\right)^{-1} \sum_{E\in\partial K} q_{K,E}A_{K,E,E'} = p_K - \widehat{p}_{K,E'} + \widetilde{\varrho}_K G_{K,E'}. \tag{2.108}$$

Protože vlastní propustnost $\mathbf{K}$ je tenzor splňující podmínku stejnoměrné eliptičnosti (viz [61]), tj.

$$\exists\alpha_0 > 0: \quad \alpha_0 \sum_{i=1}^{d} \boldsymbol{\xi}_i^2 \le \sum_{i,j=1}^{d} [\mathbf{K}(\mathbf{x})]_{i,j}\, \boldsymbol{\xi}_i\, \boldsymbol{\xi}_j, \qquad \forall \boldsymbol{\xi} \in \mathbb{R}^d, \tag{2.109}$$

pro skoro všechna $\mathbf{x} \in \Omega$, existuje inverzní matice k matici $\mathbf{A}_K = (A_{K,E,E'})_{E,E'\in\partial K}$. Přenásobením rovnice (2.108) maticí $\mathbf{A}_K^{-1}$, dostaneme pro každý element $K \in \mathcal{T}_\Omega$ a každou hranu $E \in \partial K$

$$q_{K,E} = \sum_{\alpha\in\Pi(K)} c_{\alpha,K}\lambda_{\alpha,K}\left(\alpha_E^K p_K - \sum_{E'\in\partial K} \beta_{E,E'}^K \widehat{p}_{K,E'} + \gamma_E^K \widetilde{\varrho}_K\right), \qquad E \in \partial K, \tag{2.110}$$

což je diskrétní analogie Darcyho zákona pro totální tok. Koeficienty α_E^K , $\beta_{E,E'}^K$, a γ_E^K jsou dány následujcími předpisy

$$\alpha_E^K = \sum_{E'\in\partial K} A_{K,E,E'}^{-1}, \qquad \beta_{E,E'}^K = A_{K,E,E'}^{-1}, \qquad \gamma_E^K = \sum_{E'\in\partial K} A_{K,E,E'}^{-1} G_{K,E'}, \tag{2.111}$$

přičemž $A_{K,E,E'}^{-1}$ označuje prvek inverzní matice $\mathbf{A}_K^{-1}$. Tyto koeficienty závisejí na geometrii sítě a na lokálních hodnotách propustnosti prostředí. Hodnota p_K odpovídá průměrnému tlaku na elementu K, $\widehat{p}_{K,E'}$ je průměrný tlak na hraně E na elementu K (tzv. stopa tlaku). Symboly $c_{\alpha,K}$, $\lambda_{\alpha,K}$, $\widetilde{\varrho}_K$ označují průměrné hodnoty koncentrací, mobility fáze α a průměrné hustoty na elementu K. Veličiny průměrované přes element K jsou funkcemi celkových molárních koncentrací a teploty na elementu K. Vyčíslení těchto veličin bude popsáno dále v kapitole 2.4.3.

Na každé vnitřní hraně E mezi sousedními elementy $K, K' \in \mathcal{T}_\Omega$ požadujeme, aby příslušné stopy tlaku z obou stran byly stejné, tj. $\widehat{p}_{K,E} = \widehat{p}_{K',E}$. Společnou hodnotu tlaku na hraně E budeme značit $\widehat{p}_E$. Spojitost normálových komponent totálního toku na každé vnitřní hraně E mezi sousedními elementy $K, K' \in \mathcal{T}_\Omega$ vede k podmínce

$$q_{K,E} + q_{K',E} = 0. \tag{2.112}$$

Na hranách E ležících na $\partial\Omega$ lze předepsat okrajové podmínky (2.100b), (2.100c)

$$\widehat{p}_E = p^D(E), \qquad \forall E \subset \Gamma_p, \tag{2.113a}$$

$$q_{K,E} = 0, \qquad \forall E, K : E \subset \Gamma_q, E \in \partial K, \tag{2.113b}$$

kde $p^D(E)$ označuje předepsanou hodnotu tlaku p na hraně E.

Dosazením (2.110) do (2.112) a (2.113b) lze eliminovat tok $q_{K,E}$. Abychom odvodili plně implicitní schéma, budeme vyčíslovat všechny veličiny závisející na čase v čase t_{n+1}, což bude vyznačeno horním indexem $n+1$. Rovnice (2.110)–(2.113) lze tedy přepsat jako systém N_E algebraických rovnic tvaru $\mathcal{F}_E = 0$, kde

$$\mathcal{F}_E = \begin{cases} \displaystyle\sum_{K:E\in\partial K} \left(\sum_{\alpha\in\Pi(K)} c_{\alpha,K}^{n+1}\, \lambda_{\alpha,K}^{n+1} \right) \left(\alpha_E^K p_K^{n+1} - \sum_{E'\in\partial K} \beta_{E,E'}^K \widehat{p}_{E'}^{n+1} + \gamma_E^K \widetilde{\varrho}_K^{n+1} \right), \\ \qquad\qquad\qquad\qquad\qquad\qquad\qquad\qquad \forall E \subset \Gamma_p, \\ \widehat{p}_E^{n+1} - p^D(E)\,, \quad \forall E \subset \Gamma_p. \end{cases} \tag{2.114}$$

Symbol $\sum_{K:E\in\partial K}$ označuje sčítání přes elementy K po stranách hrany E.

2.4.2 Příspěvek k aproximaci transportních rovnic – výpočet toku bez nutnosti fázové identifikace

Transportní rovnice (2.92) s počátečními a okrajovými podmínkami (2.100) budeme diskretizovat metodou konečných objemů (viz [58]). Integrací (2.92) přes libovolný element $K \in \mathcal{T}_\Omega$ a použitím Greenovy věty odvodíme

$$\frac{\mathrm{d}}{\mathrm{d}t} \int_K \phi(\mathbf{x}) c_i(\mathbf{x},t) + \int_{\partial K} \mathbf{q}_i(\mathbf{x},t) \cdot \mathbf{n}_{\partial K}(\mathbf{x}) = \int_K F_i(\mathbf{x}), \qquad i = 1,\ldots,n. \tag{2.115}$$

Označíme-li $\phi_K\,, c_{i,K}\,, F_{i,K}\,,$ průměrné hodnoty $\phi, c_i\,, F_i$ $(i = 1,\ldots,n)$ přes element K, pak lze semi-diskrétní aproximaci rovnice (2.92) zapsat ve tvaru

$$\frac{\mathrm{d}(\phi_K c_{i,K})}{\mathrm{d}t}|K| + \sum_{E\in\partial K} q_{i,K,E} = F_{i,K}|K|, \tag{2.116}$$

kde $q_{i,K,E}$ je numerická aproximace toku $\int_E \mathbf{q}_i \cdot \mathbf{n}_{K,E}$ přes hranu $E \in \partial K$. Numerický tok $q_{i,K,E}$ vyčíslíme následujícím způsobem

$$q_{i,K,E} = \begin{cases} \displaystyle\sum_{\alpha\in\Pi(K,E)^+} q_{\alpha,i,K,E} - \sum_{\beta\in\Pi(K',E)^+} q_{\beta,i,K',E}\,, & \forall E \notin \partial\Omega\,, \\ \displaystyle\sum_{\alpha\in\Pi(K,E)^+} q_{\alpha,i,K,E}, & \forall E \in \Gamma_p, \\ 0, & \forall E \in \Gamma_q. \end{cases} \tag{2.117}$$

V těchto rovnicích $\Pi(K,E)^+ = \{\alpha \in \Pi(K) \,|\, q_{\alpha,i,K,E} > 0\}$ označuje množinu fází na elementu K, které procházejí hranou $E \in \partial K$, z elementu K směrem ven a $q_{\alpha,i,K,E}$ je diskrétní podoba toku i-té komponenty ve fázi α (2.101)

$$q_{\alpha,i,K,E} = \frac{c_{\alpha,i,K}\,\lambda_{\alpha,K}}{\sum\limits_{\beta\in\Pi(K)} c_{\beta,K}\,\lambda_{\beta,K}} \left(q_{K,E} - \sum_{\beta\in\Pi(K)} c_{\beta,K}\,\lambda_{\beta,K}\,(\varrho_{\beta,K} - \varrho_{\alpha,K})\,\gamma_E^K \right). \tag{2.118}$$

Pro výpočet toku (2.117) se tedy používají jen fáze protékající hranou E ze sousedních elementů směrem ven. Tato metoda nezávisí na identitě fází a přirozeným způsobem propojí i elementy s různým počtem/identitou fází. V rovnici (2.118) je $q_{K,E}$ dáno pomocí (2.110). Hodnoty $c_{\alpha,i,K}$ a $S_{\alpha,K}$ se vypočtou lokálně na každém elementu řešením lokální termodynamické rovnováhy za předepsané teploty T a celkových molárních koncentrací c_i všech komponent.

Předpokládáme, že porézní prostředí je nestlačitelné, a tedy porozita nezávisí na čase. Časovou derivaci $c_{i,K}$ v (2.116) lze pak aproximovat diferencí s časovým krokem Δt_n. Pomocí zpětné Eulerovy metody [58] odvodíme plně implicitní schéma tvaru $\mathcal{F}_{K,i} = 0$, kde

$$\mathcal{F}_{K,i} = \phi_K |K| \frac{c_{i,K}^{n+1} - c_{i,K}^n}{\Delta t_n} + \sum_{E\in\partial K} q_{i,K,E}^{n+1} - F_{i,K}^{n+1}|K|, \tag{2.119}$$

kde tok $q_{i,K,E}$ je vyčíslen pomocí (2.117). Počáteční podmínky (2.100a) lze diskretizovat následovně

$$c_{i,K}^0 = c_i^0(K), \qquad \forall K \in \mathcal{T}_\Omega,\ i = 1,\dots,n, \tag{2.120}$$

kde $c_i^0(K)$ označuje průměrnou hodnotu c_i^0 na elementu K.

2.4.3 Sestavení soustavy rovnic

V rovnicích (2.114) a (2.119) jsme označili $\mathcal{F}_E$ a $\mathcal{F}_{K,i}$ výrazy reprezentující složky vektoru $\boldsymbol{\mathcal{F}}$. K výpočtu hodnot $c_{\alpha,K}^{n+1}$, $\lambda_{\alpha,K}^{n+1}$, $\widetilde{\varrho}_K^{n+1}$, které jsou potřeba v (2.114) a další hodnoty průměrované přes element, které závisejí na vlastnostech fází v (2.117)–(2.119), provedeme výpočet lokální termodynamické rovnováhy na elementu K při zadaných hodnotách koncentrací $c_{1,K}^{n+1},\dots,c_{n,K}^{n+1}$ a teploty T. Tímto výpočtem obdržíme i hodnotu průměrného tlaku p_K^{n+1}. Budeme tedy řešit systém $N_K \cdot n + N_E$ nelineárních algebraických rovnic

$$\boldsymbol{\mathcal{F}} = [\mathcal{F}_{1,1},\dots,\mathcal{F}_{1,n},\dots,\mathcal{F}_{N_K,1},\dots,\mathcal{F}_{N_K,n}\,;\mathcal{F}_1,\dots,\mathcal{F}_{N_E}]^T = \mathbf{0} \tag{2.121}$$

pro neznámé primární proměnné, kterými budou celkové molární koncentrace $c_{1,K}^{n+1},\dots,c_{n,K}^{n+1}$, $K \in \{1,\dots,N_K\}$ a stopy tlaků na hranách $\widehat{p}_E^{n+1}$, $E \in \{1,\dots,N_E\}$. Tento systém budeme řešit Newtonovou metodou, která vede v každé iteraci k řešení následujícího systému lineárních algebraických rovnic

$$\mathbf{J}\,\boldsymbol{\delta} = -\boldsymbol{\mathcal{F}}\,. \tag{2.122}$$

Jakobiho matice $\mathbf{J}$ systému (2.122) je řídká a nesymetrická. Jakobián lze rozdělit na 4 bloky, jejichž prvky lze napočítat analyticky pomocí následujících vztahů

$$(\mathbf{J}_{K,K'})_{i,j} = \frac{\partial \mathcal{F}_{K,i}}{\partial c_{j,K'}^{n+1}},\ (\mathbf{J}_{K,E})_i = \frac{\partial \mathcal{F}_{K,i}}{\partial \widehat{p}_E^{n+1}},\ (\mathbf{J}_{E,K})_j = \frac{\partial \mathcal{F}_E}{\partial c_{j,K}^{n+1}},\ J_{E,E'} = \frac{\partial \mathcal{F}_E}{\partial \widehat{p}_{E'}^{n+1}}. \tag{2.123}$$

V těchto rovnicích $J_{E,E'}$ je prvek matice $\mathbf{J}_{E,E'}$, $i,j = 1,\ldots,n;\ K,K' = 1,\ldots,N_K\,;\ E,E' = 1,\ldots,N_E$. Soustavu (2.122) řešíme přímým řešičem UMFPACK [23, 24, 25, 26]. Řešení této soustavy $\boldsymbol{\delta}$ je vektor obsahující korekce molárních koncentrací $\delta c_{i,K}^{n+1}$ a stop tlaků na hranách $\delta \widehat{p}_E^{n+1}$. Přičtením těchto korekcí k hodnotám $c_{i,K}^{n+1}$ a $\widehat{p}_E^{n+1}$ z předchozí iterace dostaneme novou aproximaci primárních proměnných. Iterační proces zastavíme, je-li splněna podmínka

$$\|\boldsymbol{\mathcal{F}}\| < \varepsilon \tag{2.124}$$

pro zvolenou hodnotu $\varepsilon > 0$ [85]. Obdobně jako při výpočtu dvoufázové rovnováhy může být robustnost této metody zvýšena použitím techniky hledání ve směru (line-search) [85]. Časový krok je volen adaptivně v závislosti na průběhu konvergence Newtonovy metody. Pokud při výpočtu daného časového kroku nezkonverguje Newtonova metoda do 10 iterací nebo pokud line-search nevede k redukci $\|\boldsymbol{\mathcal{F}}\|$ do 10 iterací, pak se daný časový krok zrestartuje s poloviční hodnotou Δt_n. Pokud Newtonova metoda zkonverguje za méně než 4 iterace, pak se daný časový krok přijme a v následujícím časovém kroku se délka časového kroku prodlouží ($\Delta t_{n+1} = 1.2\Delta t_n$).

Nakonec zdůrazněme, že linearizace je provedena vzhledem k celkovým molárním koncentracím na každém elementu a stopám tlaku na každé hraně, což jsou proměnné, které jsou vždy dobře definovány bez ohledu na počet a identitu fází na elementu K. Není tedy potřeba měnit v průběhu simulace primární proměnné podle toho, zda se objeví nová fáze nebo některá z fází vymizí (viz např. [6, 17, 76]).

2.4.4 Shrnutí výpočetního algoritmu

Numerické řešení probíhá v následujících krocích:

1. Načti vstupní data úlohy – teplotu a počáteční rozložení celkových koncentrací všech komponent.

2. Proveď výpočet lokální termodynamické rovnováhy na každém elementu při zadané teplotě a celkových molárních koncentracích. Výsledkem výpočtu bude mimo jiné i hodnota tlaku na každém elementu.

3. Vypočti viskozity všech fází na každém elementu.

4. Opakuj následující časové kroky, dokud simulace neskončí v zadaném čase:

(a) použij Newtonovu metodu na řešení systému (2.121), tj. opakuj následující kroky, dokud není splněno kritérium konvergence (2.124):

i. Proveď výpočet lokální termodynamické rovnováhy na každém elementu.

ii. Vyčísli fázové mobility $\lambda_{\alpha,K}^{n+1}$ pomocí (2.94), (2.95) a (2.96) na každém elementu.

iii. Na každém elementu K vypočti průměrné hodnoty tlaku p_K^{n+1} pomocí (2.97) nebo (2.98c) v závislosti na počtu fází na elementu K.

iv. Vypočti celkové toky $q_{K,E}^{n+1}$ pomocí (2.110) a toků $q_{\alpha,i,K,E}^{n+1}$ s využitím (2.118).

v. Sestav a vyřeš soustavu lineárních algebraických rovnic (2.122) pro korekce molárních koncentrací $\delta c_{i,K}^{n+1}$ a tlaků $\delta \widehat{p}_E^{n+1}$.

vi. Přičti korekce $\delta c_{i,K}^{n+1}$ a $\delta \widehat{p}_E^{n+1}$ k $c_{i,K}^{n+1}$ a $\widehat{p}_E^{n+1}$, a zkontroluj normu defektu (2.124). V případě potřeby použij modifikaci Newtonovy metody s prohledáváním ve směru (line search).

(b) Pokud Newtonova metoda zkonvergovala za max. 10 iterací, přijmi současnou aproximaci a pokračuj ve výpočtu další časové hladiny ($n \to n+1$).

(c) Pokud Newtonova metoda nekonverguje, výpočet v daném čase se restartuje s nižší hodnotou časového kroku.

2.5 Numerické výsledky

V této kapitole ukážeme výsledky numerických simulací dokládající vybrané aspekty příspěvků autora.

2.5.1 Využití metod vyššího řádu přesnosti

V této části ukážeme výsledky numerických simulací získané konvenční metodou. Výsledky získané metodou vyššího řádu (kombinace smíšené hybridní metody konečných prvků a nespojité Galerkinovy metody – MHFE/DG) porovnáme s metodou prvního řádu založené na kombinaci smíšené hybridní metody konečných prvků a metody konečných objemů (MHFE/FV). Výhodou metody vyššího řádu je podstatná redukce numerické difuze při zachování stability schématu, což demonstrujeme na následujících příkladech.

Příklad 1

V prvním příkladu simulujeme vytlačování propanu metanem ve vodorovné 2D oblasti o velikosti 50×50 m bez gravitace při konstantní teplotě $T = 397$ K. Porozita rezervoáru je $\phi = 0{,}2$ a vlastní propustnost $K = 10$ mD. Metan je vtláčen v levém dolním rohu, zatímco směs je čerpána v pravém horním rohu, kde je udržován konstantní tlak 50 bar. Za těchto podmínek směs zůstává v jedné fázi po celou dobu simulace. Rychlost vtláčení je 42,5 m^2/den při tlaku

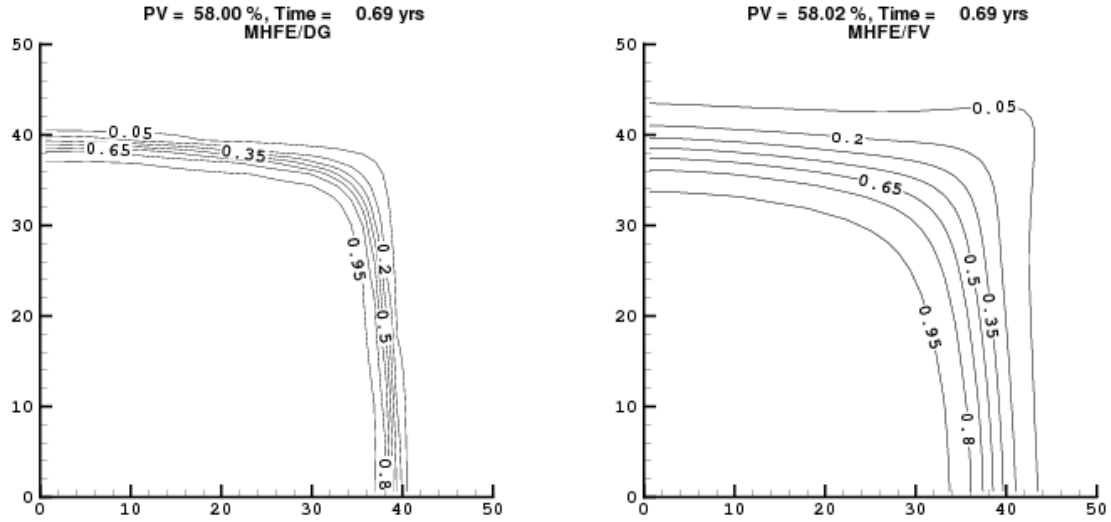

Obrázek 2.2: Celkové molární zlomky metanu po injektáži 58% pórového objemu metanu (0,69 roku) vypočtené na síti 40×40 pomocí metod MHFE/DG (vlevo) a MHFE/FV (vpravo): Příklad 1 bez gravitace.

$p = 1$ atm a teplotě $T = 293$ K. Pro tuto simulaci používáme lineární model relativní permeability ($k_{r\alpha}(S_\alpha) = S_\alpha$). Na obrázku 2.2 vidíme molární zlomky metanu po injektáži 58% pórového objemu metanu vypočtené oběma metodami na čtvercové síti 40×40, odkud je vidět ostřejší reprezentace postupujícího rozhraní při použití metody vyššího řádu v porovnání s metodou prvního řádu, která je podstatně difuznější. Pokud stejný problém řešíme na svislé oblasti (tj. uvažujeme vliv gravitace), pak dostaneme výsledky zobrazené na obrázku 2.3, kde jsou zobrazeny molární zlomky metanu po vtlačení 20% pórového prostoru metanu. I v tomto případě metoda vyššího řádu přesnosti má podstatně nižší numerickou difuzi v porovnání s metodou prvního řádu.

Příklad 2

Opět simulujeme vytlačování propanu metanem ve 2D oblasti o velikosti 50×50 m při konstantní teplotě $T = 311$ K. Porozita rezervoáru je $\phi = 0{,}2$ a vlastní propustnost $K = 10$ mD. Metan je vtláčen v levém dolním rohu a směs je odčerpávána v pravém horním rohu, kde je udržován tlak $p = 69$ bar. Za těchto podmínek se v části oblasti objeví dvoufázová oblast. Rychlost vtláčení je 0,017 m^2/den při tlaku $p = 1$ atm a teplotě $T = 293$ K. Opět používáme lineární model relativní permeability. Na obrázku 2.4 vidíme molární zlomky metanu po vtlačení 50% pórového objemu metanu vypočtené oběma metodami na čtvercové síti 20×20 v případě, že neuvažujeme gravitaci (vodorovná oblast). Pokud uvažujeme vliv gravitace (svislá oblast), pak

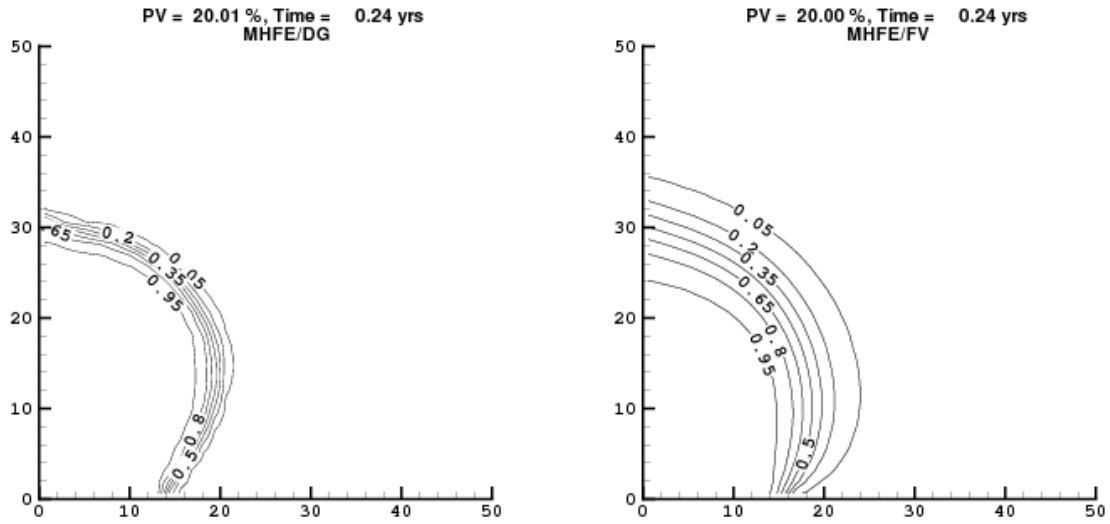

Obrázek 2.3: Celkové molární zlomky metanu po injektáži 20% pórového objemu metanu (0,24 roku) vypočtené na síti 40×40 pomocí metod MHFE/DG (vlevo) a MHFE/FV (vpravo): Příklad 1 s gravitací.

získáme výsledky zobrazené na obrázku 2.5. I v těchto příkladech jasně vidíme podstatnou redukci numerické difuze při použití metody vyššího řádu přesnosti.

2.5.2 Výpočty fázové rovnováhy při zadané teplotě, objemu a látkových množstvích

Z velkého množství výpočtů stability a fázové rovnováhy při zadané teplotě, objemu a látkových množstvích vybíráme několik příkladů, které mají ukázat výhodu této formulace oproti klasické formulaci předepisující tlak, teplotu a celkové molární zlomky všech komponent směsi.

Příklad 1 – čistý CO_2

V prvním příkladě budeme vyšetřovat stabilitu a fázovou rovnováhu čistého oxidu uhličitého (CO_2). Nejprve vyšetřujeme jednofázovou stabilitu při zadané teplotě, objemu a látkovém množství pro teploty $T \in \langle 180; 320 \rangle$ K v celém rozsahu přípustných molárních koncentrací c. Na obrázku 2.6 (vlevo) jsou vyznačeny hodnoty minima funkce D v každém bodě (c, T) v závislosti na teplotě T a celkové molární koncentraci c. Na obrázku 2.6 (vpravo) je vyznačena hranice mezi jednofázovou a dvoufázovou oblastí v prostoru proměnných c, T. Z obrázku 2.6 (vpravo) je vidět, že při teplotě $T = 280$ K zůstává CO_2 v jedné fázi pro nízké molární koncentrace. Při izotermální kompresi se v jistém rozmezí koncentrací CO_2 rozděluje mezi 2 fáze a při celkové

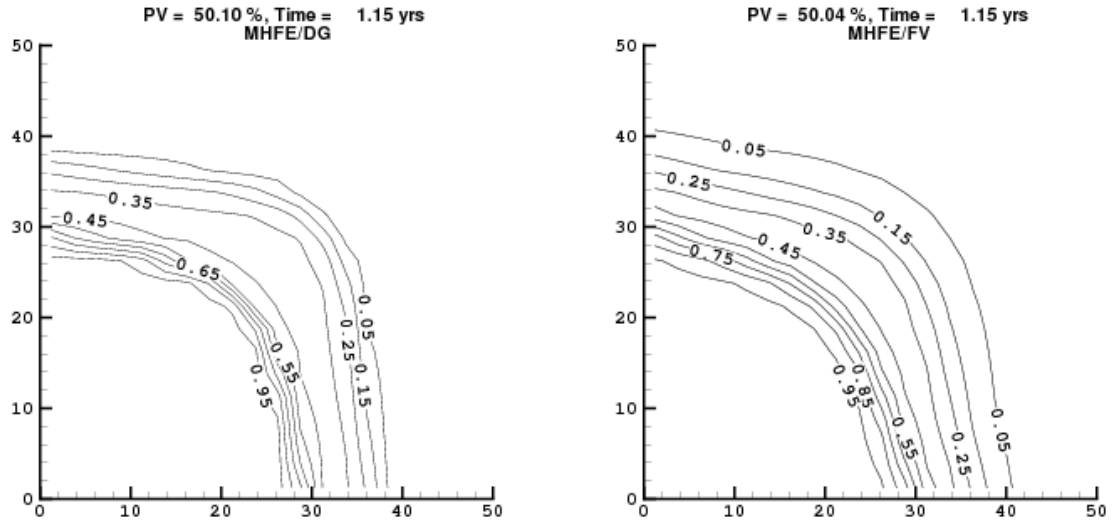

Obrázek 2.4: Celkové molární zlomky metanu po injektáži 50% pórového objemu metanu (1,15 roku) vypočtené na síti 20×20 pomocí metod MHFE/DG (vlevo) a MHFE/FV (vpravo): Příklad 2 bez gravitace.

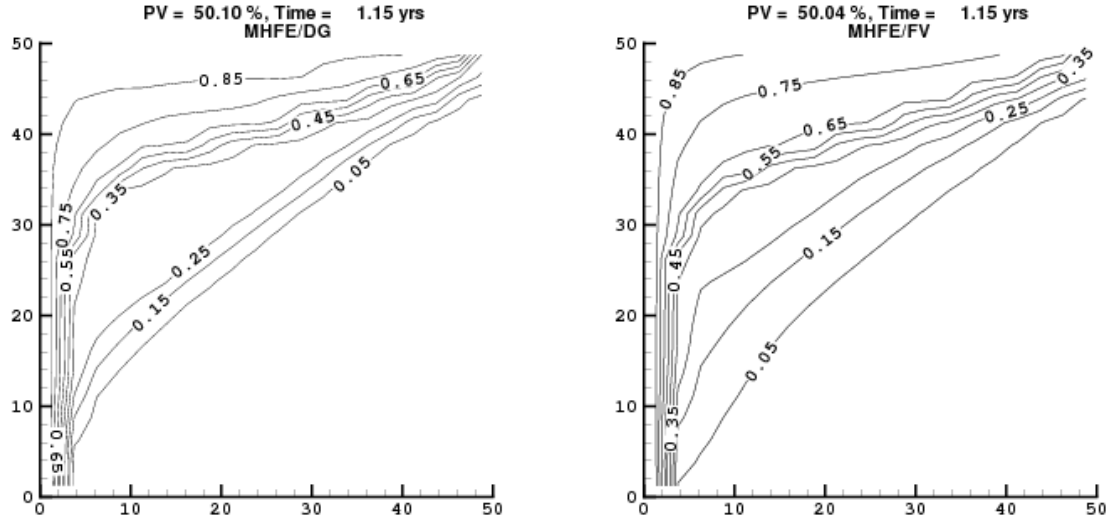

Obrázek 2.5: Celkové molární zlomky metanu po injektáži 50% pórového objemu metanu (1,15 roku) vypočtené na síti 20×20 pomocí metod MHFE/DG (vlevo) a MHFE/FV (vpravo): Příklad 2 s gravitací.

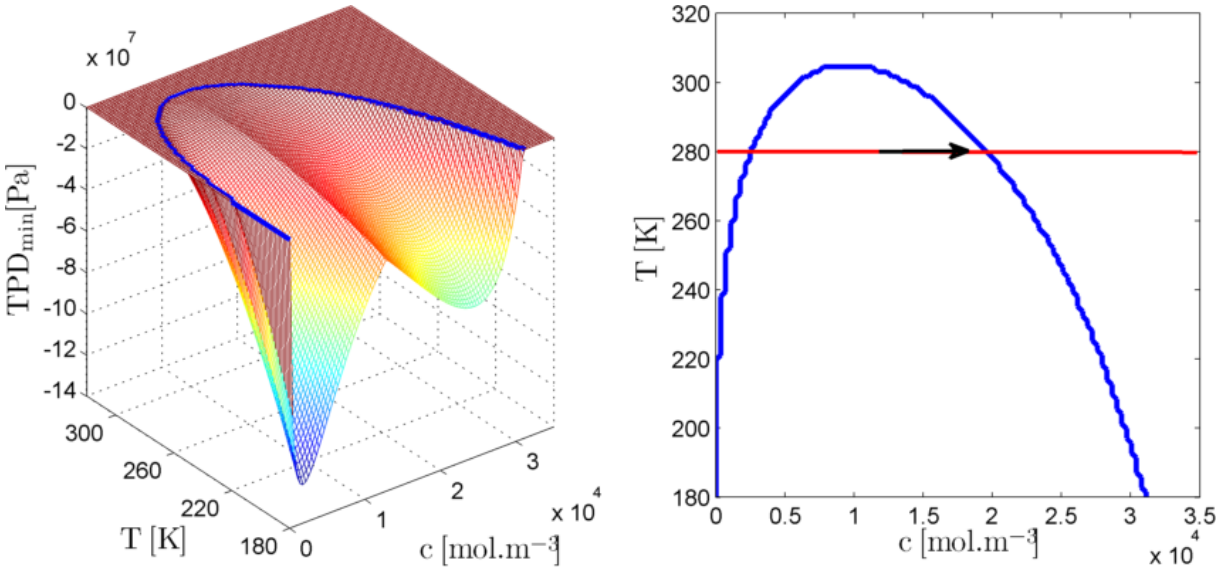

Obrázek 2.6: Globální minimum funkce D (v grafu označené jako TPD) v závislosti na celkové molární koncentraci c a teplotě T (vlevo) a hranice mezi jednofázovou a dvoufázovou oblastí v prostoru proměnných c, T-space (vpravo). Příklad 1: čistý oxid uhličitý $\mathrm{CO_2}$.

molární koncentraci vyšší než cca 20000 mol.m^{-3} přejde CO_2 opět do jednofázového stavu. Na obrázku 2.7 jsou znázorněny saturace a hustoty obou fází v závislosti na celkové koncentraci. Na obrázku 2.8, je znázorněn rovnovážný tlak systému v závislosti na celkové molární koncentraci c. Protože ve dvoufázové oblasti (oblast mezi body A a B na obrázku 2.8) je tlak konstantní, není možno jednotlivé dvoufázové stavy rozlišit pomocí proměnných p, T, a N. Všechny dvoufázové stavy a oba krajní body jsou sice nerozlišitelné pomocí proměnných p, T, N, lze je však rozlišit v proměnných V, T, N, protože každý z těchto stavů má odlišný objem. Tento příklad ukazuje výhodu použití proměnných V, T, N.

Příklad 2 – směs CO_2 a nC_{10}

Budeme vyšetřovat fázovou stabilitu a fázovou rovnováhu směsi oxidu uhličitého ($\mathrm{CO_2}$) a normálního dekanu ($\mathrm{nC_{10}}$) s molárními zlomky $z_{\mathrm{CO_2}} = 0{,}547413$ a $z_{\mathrm{nC_{10}}} = 0{,}452587$. Binární interakční koeficient je $\delta_{\mathrm{CO_2-nC_{10}}} = 0{,}15$. Nejprve byla vyšetřována fázová stabilita při zadané teplotě a celkové koncentraci směsi v rozsahu teplot $T \in \langle 250; 650 \rangle$ K a v celém rozsahu přípustných molárních koncentrací c. Na obrázku 2.9 (vlevo), můžeme vidět hodnoty minima funkce D jako funkci teploty T a celkové molární koncentrace c. Hranice mezi jednofázovou a dvoufázovou oblastí v prostoru proměnných c, T je znázorněna na obrázku 2.9 (vpravo). Odtud vidíme, že při izotermální kompresi směsi při teplotě $T = 311$ K se směs rozděluje na 2 fáze od nejnižších hodnot celkové koncentrace c až do přibližně $c = 8000$ mol.m^{-3}, kdy směs přechází

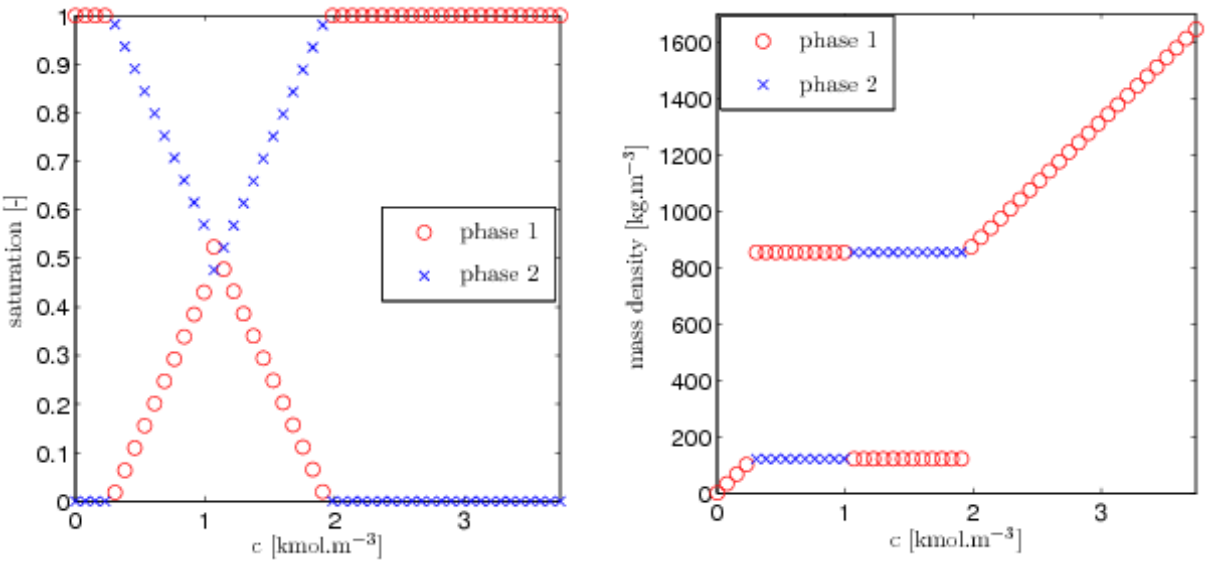

Obrázek 2.7: Saturace (vlevo) a hustoty (vpravo) obou fází v závislosti na celkové molární koncentraci c při teplotě $T = 280$ K. Příklad 1: čistý oxid uhličitý CO_2.

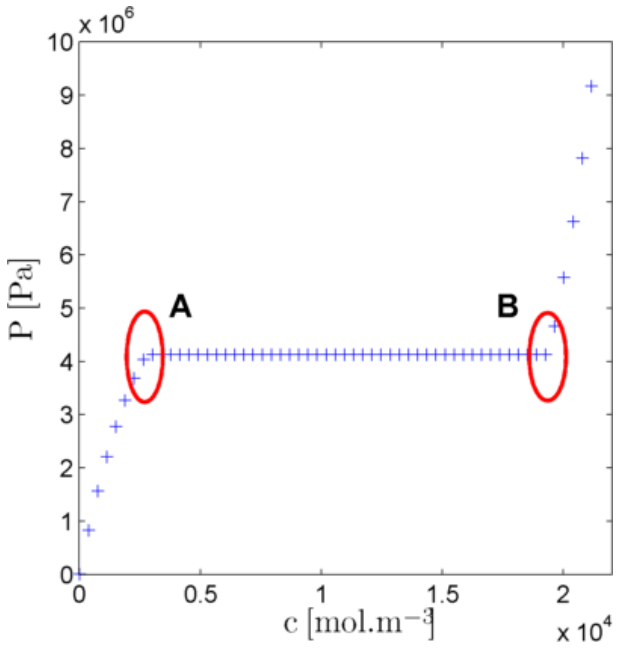

Obrázek 2.8: Rovnovážný tlak jako funkce celkové molární koncentrace c při teplotě $T = 280$ K. Příklad 1: čistý oxid uhličitý CO_2.

do jedné fáze, zatímco při molárních koncentracích vyšších než přibližně 9500 mol.m^{-3} je směs opět rozdělena mezi 2 fáze.

Na obrázku 2.11 jsou znázorněny saturace a hustoty obou fází v závislosti na celkové koncentraci c. Molární zlomky obou komponent v obou fázích pro jednotlivé molární koncentrace c jsou znázorněny na obrázku 2.12. Na obrázku 2.10 je znázorněn rovnovážný tlak jako funkce celkové molární koncentrace směsi. Na rozdíl od předchozího příkladu není tlak ve dvoufázové oblasti konstantní, protože v průběhu fázového přechodu mění fáze své chemické složení. Zároveň můžeme pozorovat prudký nárůst tlaku pro molární koncentrace větší než 8000 mol.m^{-3}, kdy už je vyčerpána plynná (dobře stlačitelná) fáze. Pro vysoké hodnoty molárních koncentrací c a nízké teploty T můžeme pozorovat druhou dvoufázovou oblast.

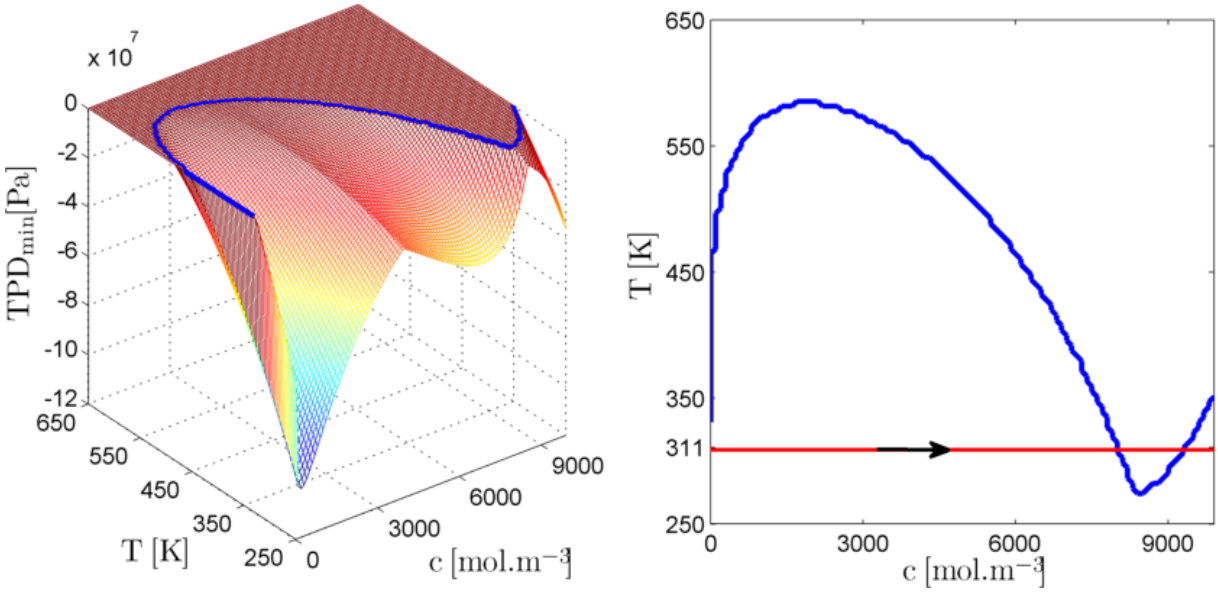

Obrázek 2.9: Globální minimum funkce D (v obrázku značené jako TPD) v závislosti na celkové molární koncentraci c a teplotě T (vlevo) a hranice mezi jednofázovou a dvoufázovou oblastí v prostoru proměnných c, T (vpravo). Příklad 2: směs CO_2 a nC_{10}.

Příklad 3 – směs CO_2 a nC_{10} s třífázovou oblastí

Algoritmy pro testování fázové stability a výpočet fázové rovnováhy popsané v této práci lze zobecnit i na systémy, které se rozkládají do více než dvou fází. Takové zobecnění bylo provedeno v diplomové práci [48] a je předmětem připravované publikace [49]. Zde uvedeme pouze jeden příklad dokládající výhodnost nové formulace fázové rovnováhy. Stejně jako v minulém příkladu budeme vyšetřovat rovnováhu směsi CO_2 a nC_{10}. Při podrobnějším rozboru stability směsi zjistíme, že pro nízké teploty existuje v prostoru proměnných c, T třífázová oblast – viz

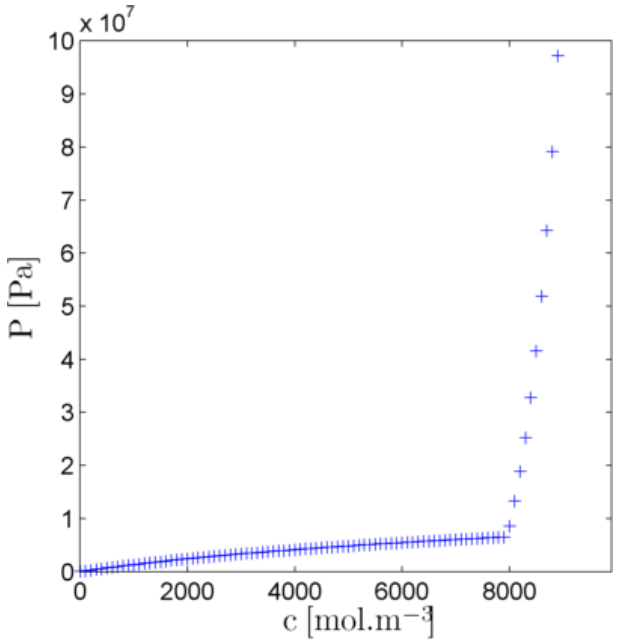

Obrázek 2.10: Rovnovážný tlak v závislosti na celkové molární koncentraci c při teplotě $T = 311$ K. Příklad 2: směs CO_2 a nC_{10}.

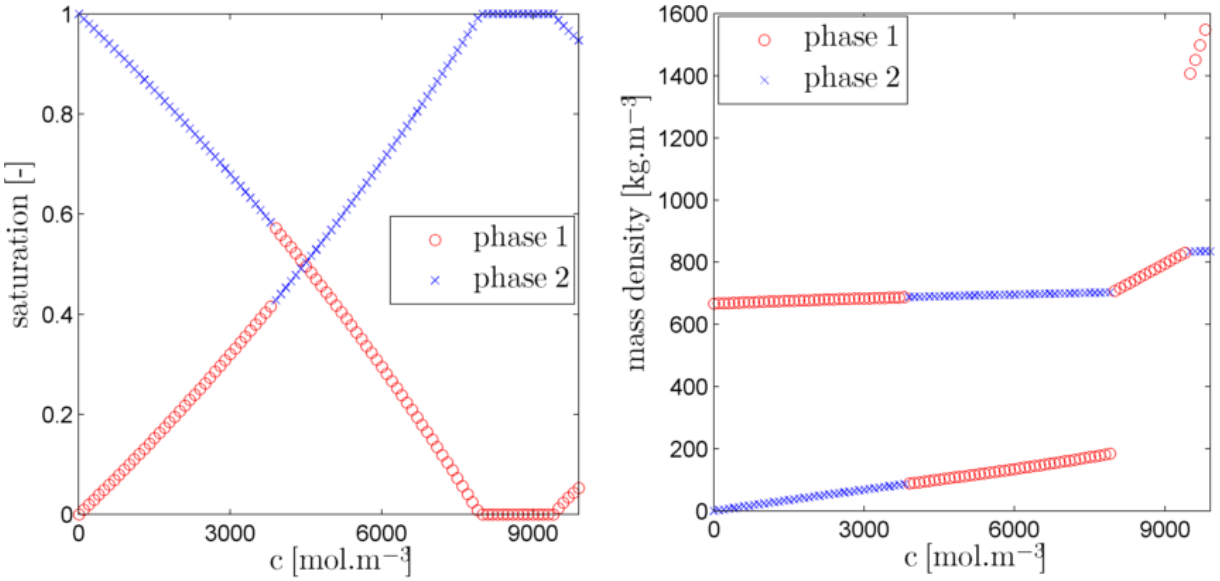

Obrázek 2.11: Saturace (vlevo) a hustoty (vpravo) obou fází v závislosti na celkové molární koncentraci c při teplotě $T = 311$ K. Příklad 2: směs CO_2 a nC_{10}.

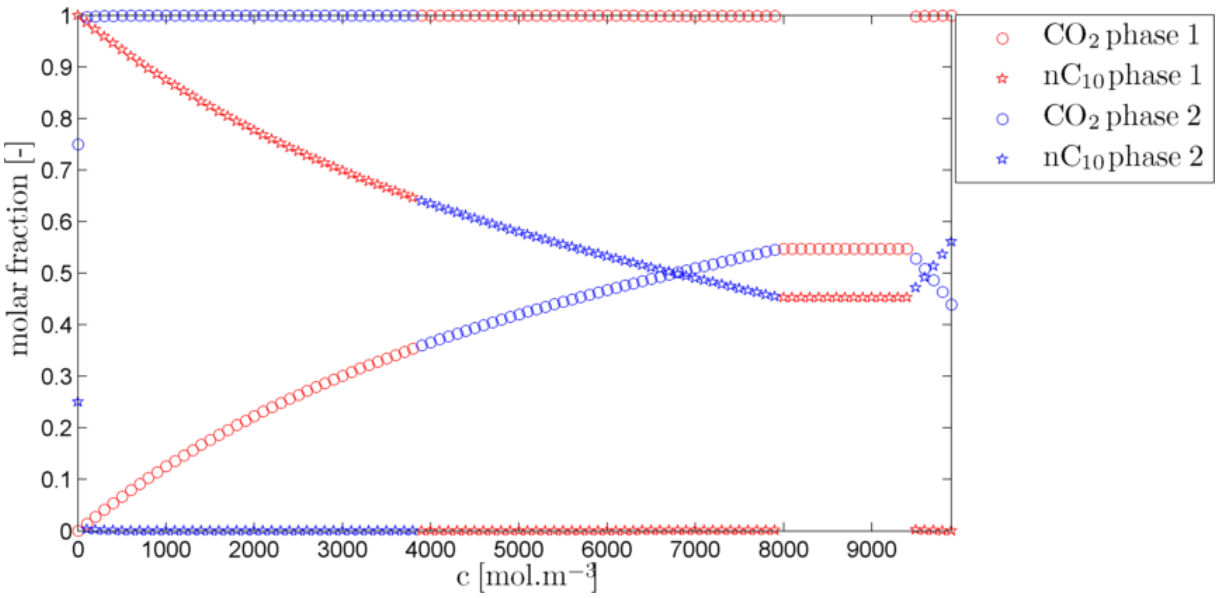

Obrázek 2.12: Molární zlomky obou komponent v obou fázích v závislosti na celkové molární koncentraci c při teplotě $T = 311$ K. Příklad 2: směs CO_2 a nC_{10}.

obrázek 2.13, na kterém vidíme hranici mezi jednofázovou (červená), dvoufázovou (modrá) a třífázovou oblastí (zelená). Při izotermální kompresi při teplotě $T = 260$ K, se nejprve směs rozděluje mezi 2 fáze od nejnižších celkových molárních koncentrací až do přibližně $c = 5000$ mol.m^{-3}, kdy systém přechází do 3 fází. Při celkové molární koncentraci vyšší než 8000 mol.m^{-3} se směs rozděluje opět jen do 2 fází.

Na obrázku 2.15 jsou znázorněny saturace a hustoty obou fází v závislosti na celkové molární koncentraci c. Molární zlomky obou komponent ve všech fázích jsou znázorněny jako funkce celkové molární koncentrace c na obrázku 2.16. Na obrázku 2.14 je znázorněn rovnovážný tlak systému v závislosti na celkové molární koncentraci c. Zde můžeme pozorovat pomalý nárůst tlaku během izotermální komprese ve dvoufázové oblasti následovaný konstantní hodnotou tlaku ve třífázové oblasti (molární hustoty cca od 5000 mol.m^{-3} do 8000 mol.m^{-3}) a strmý nárůst tlaku pro molární koncentrace vyšší než 8000 mol.m^{-3}, kdy už není přítomna plynná fáze. Ve třífázové oblasti je konstantní nejen tlak, ale i molární zlomky jednotlivých komponent v každé fázi a hustoty všech fází. Konstantní hodnota tlaku ve třífázové oblasti připomíná chování čisté látky. Podobně jako v případě čisté látky nelze pomocí proměnných tlak, teplota a látková množství jednoznačně rozlišit třífázové stavy. Tento příklad ukazuje, že problém nejednoznačnosti určení rovnovážného stavu není jen problémem čisté látky, ale může se vyskytnout i u směsí. Zde jsme tento problém pozorovali u binární směsi ve 3 fázích. Našli jsme i příklady dalších systémů, které vykazují stejné chování (např. ternární směs sirovodíku, oxidu uhličitého a metanu ve 3 i 4 fázích, viz [49]).

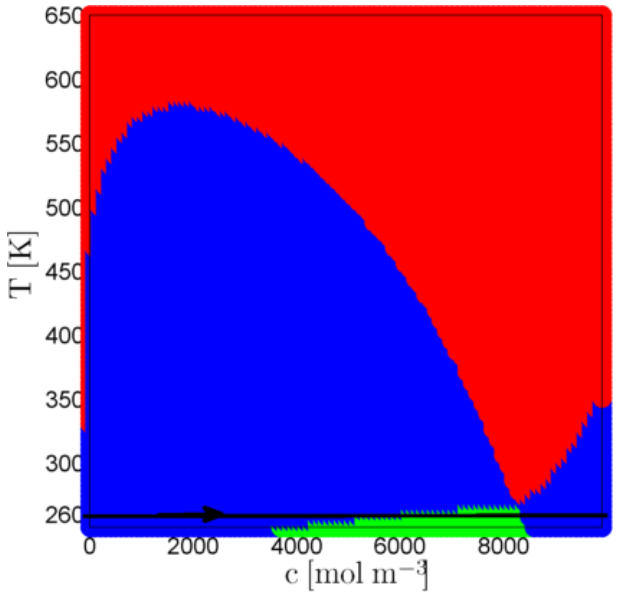

Obrázek 2.13: Hranice mezi jednofázovou (červená), dvoufázovou (modrá) a třífázovou (zelená) oblastí v prostoru proměnných c, T. Příklad 3: směs CO_2–nC_{10}.

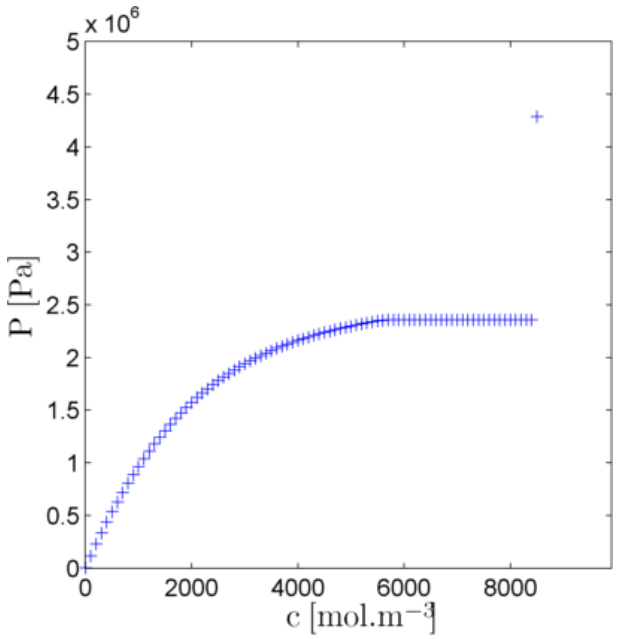

Obrázek 2.14: Rovnovážný tlak v závislosti na celkové molární koncentraci c při teplotě $T = 260$ K. Příklad 3: směs CO_2–nC_{10}.

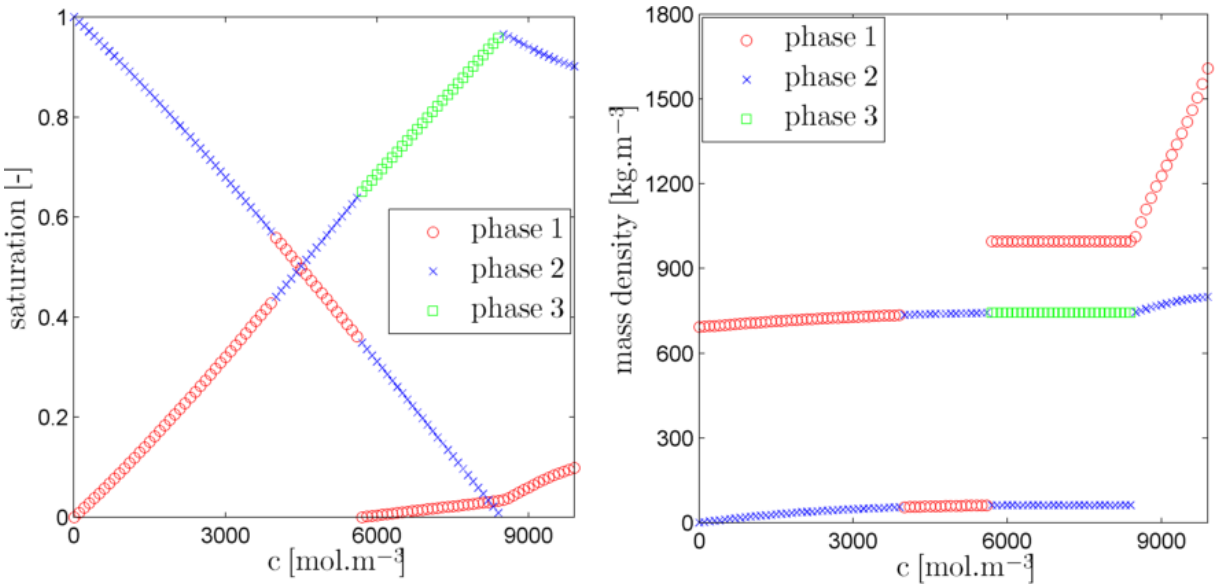

Obrázek 2.15: Saturace (vlevo) a hustoty (vpravo) všech fází v závislosti na celkové molární koncentraci c při teplotě $T = 260$ K. Příklad 3: směs CO_2–nC_{10}.

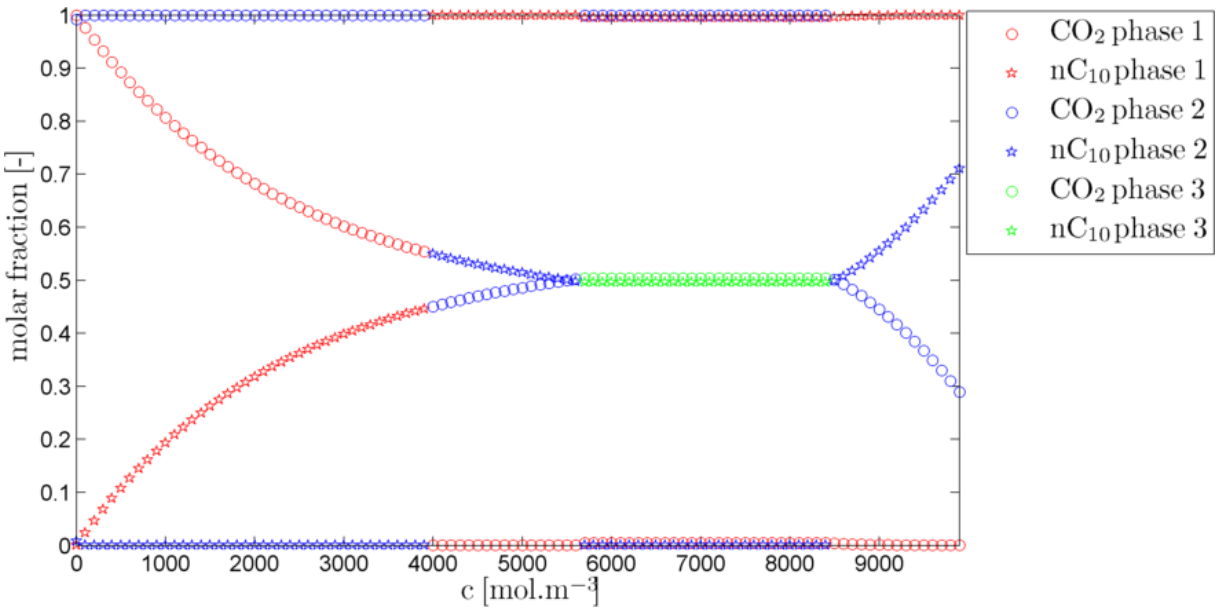

Obrázek 2.16: Molární zlomky obou komponent ve všech fázích v závislosti na celkové molární koncentraci c při teplotě $T = 260$ K. Příklad 3: směs CO_2–nC_{10}.

2.5.3 Nekonvenční formulace kompozičního modelu

Nově navržená formulace kompozičního modelu byla testována na mnoha modelových příkladech. Zde uvedeme jen příklad jednoduché simulace, která pomocí konvenčního modelu není dobře řešitelná. Budeme simulovat izotermální vtláčení CO_2 do vodorovného dvourozměrného rezervoáru tvaru čtverce o hraně 50 m, který již obsahuje CO_2 při teplotě $T = 280\,\mathrm{K}$ a tlaku $p = 4\,\mathrm{MPa}$. Saturační tlak CO_2 při $280\,\mathrm{K}$ je $4{,}13\,\mathrm{MPa}$. CO_2 je vtlačován do oblasti v levém dolním rohu a odčerpáván v pravém horním rohu, kde je udržován tlak $p = 4\,\mathrm{MPa}$. Rychlost vtláčení je $42{,}5\,\mathrm{m}^2/\mathrm{den}$ při tlaku 1 atm a teplotě $293\,\mathrm{K}$.

Propustnost prostředí je $\mathbf{K} = 9{,}87 \cdot 10^{-17}\,\mathrm{m}^2$ a porozita je $\phi = 0{,}2$. Hranice oblasti je nepropustná s výjimkou rohu oblasti, kde je udržován tlak $p = 4\,\mathrm{MPa}$. Používáme linární model pro relativní permeabilitu ($k_{r\alpha}(S_\alpha) = S_\alpha$ pro každou fázi α). V důsledku vtláčení roste tlak v okolí vtláčecího elementu na hodnoty vyšší než je saturační tlak CO_2 při zadané teplotě, což vede ke vzniku kapalné fáze. Na obrázku 2.17 je zobrazen výsledek výpočtu v různých časech. Kapalný CO_2 s hustotou přibližně $873\,\mathrm{kg\,m}^{-3}$ vytlačuje vlastní plynný CO_2 s hustotou přibližně $118\,\mathrm{kg\,m}^{-3}$. Na obrázku 2.17 je též znázorněna izočára saturačního tlaku, jejíž poloha velmi dobře koresponduje s oblastí, kde se nacházejí dvoufázové elementy. Při pokusu řešit tuto úlohu pomocí kódu založeném na konvenční formulaci (viz kapitoly 2.1 a 2.2, příp. [40, 41], [Č1]) dojde k selhání programu v důsledku chyb vznikajících z důvodu nesprávné fázové identifikace. V nové formulaci se tyto problémy neobjevují, neboť fázová identifikace není potřeba.

2.6 Shrnutí příspěvků autora

Z výše uvedeného přehledu studovaného problému a přiložených publikací vyplývá, že autor dosáhl původních výsledků v následujících oblastech:

- Formulace okrajových podmínek popisujících nepropustnou hranici v konvenčním kompozičním modelu.
- Návrh stabilního schématu pro výpočet fázových rychlostí v konvenčním kompozičním modelu.
- Vývoj metod vyššího řádu přesnosti v konvenční formulaci a řešení problémů konstrukce vhodného limiteru.
- Návrh nové formulace kompozičního modelu využívající netradiční formulaci problému fázové rovnováhy.
- Vývoj numerických metod pro řešení problému testování fázové stability a výpočet fázové rovnováhy při zadaném objemu, teplotě a látkových množstvích.
- Vývoj numerického modelu založeného na nové formulaci.

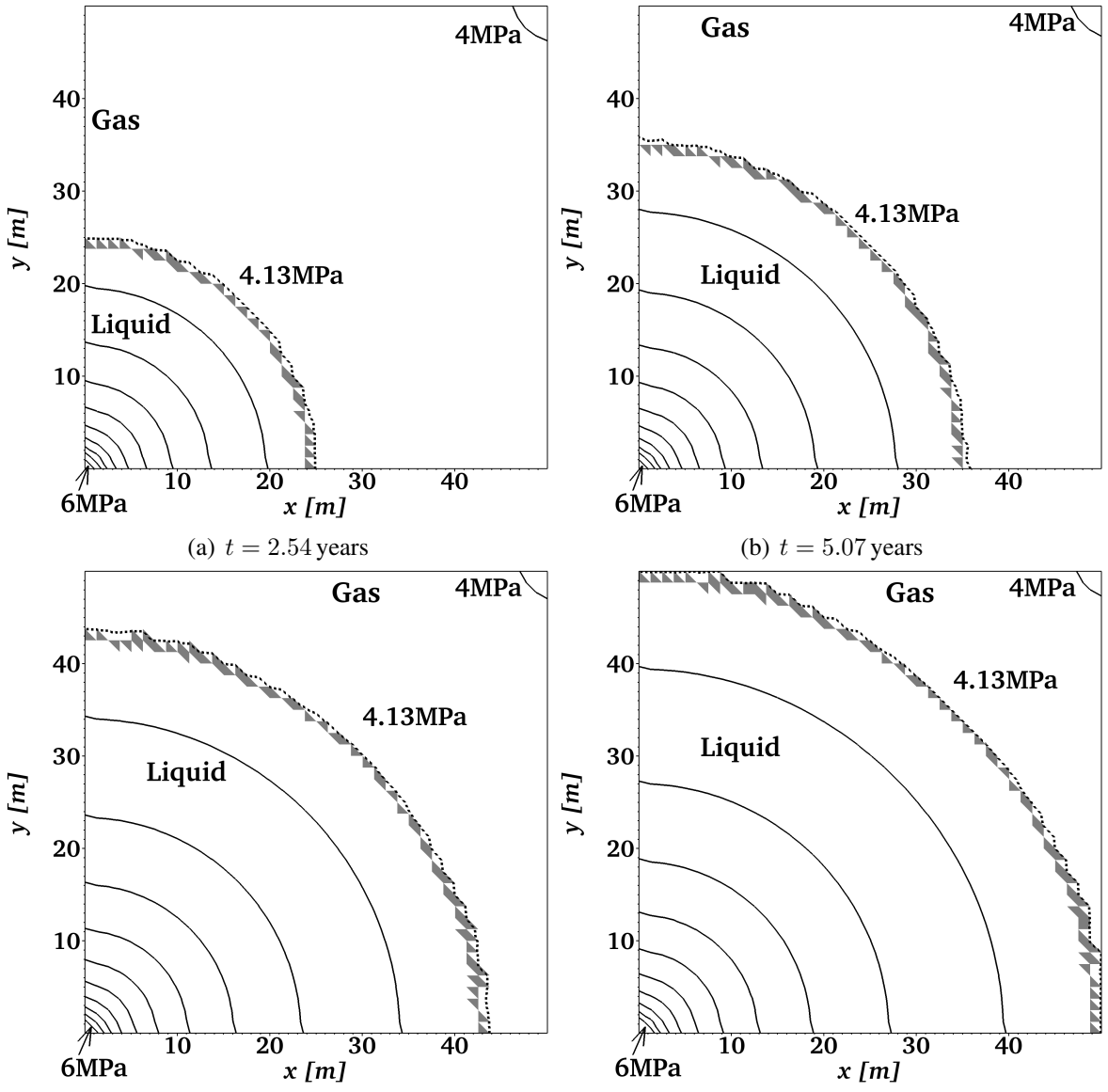

(a) $t = 2.54$ years

(b) $t = 5.07$ years

(c) $t = 7.61$ years

(d) $t = 10.14$ years

Obrázek 2.17: Izočáry průměrných tlaků na elementech p_K ve čtyřech různých časech. Šedivě jsou vyznačeny dvoufázové elementy. Plné izočáry jsou rovnoměrně rozloženy mezi vyznačené hodnoty. Čárkovaná izočára ukazuje saturační tlak a odděluje oblasti kapalné a plynné fáze.

2.7 Současný výzkum a mezinárodní spolupráce

Problematika simulace transportu komponent v porézním prostředí s přestupem komponent mezi fázemi je zdrojem mnoha problémů, které je potřeba řešit. Jedním z problémů je např. výpočetní náročnost přístupu popsaného v kapitole 2.4, která je dána velikostí soustav rovnic vznikajících při použití plně implicitního schématu. Lze očekávat, že podstatného zrychlení bude možno dosáhnout použitím sekvenčního přístupu (viz schéma IMPEC z kapitoly 2.2.1). Konstrukce schématu IMPEC však není v případě nové formulace triviální záležitost a je předmětem současného výzkumu autora. Mnoho otázek zůstává v této oblasti stále otevřených – např. jak do modelu zahrnout difuzi nebo kapilaritu. V tradičně používaných modelech (viz např. [71, 93, 74, 33, 34]) jsou tyto jevy popisovány pomocí konceptů, které byly původně vyvinuty pro nemísitelné proudění. Zdá se, že i v této oblasti může popis směsi pomocí proměnných V, T, N poskytovat jisté výhody oproti tradičním proměnným p, T, z, ale současné teorie kapilarity se nutně opírají o fázovou identifikaci. Autor věří, že konceptuální model, který byl popsán v této práci může být upraven tak, že do něj bude možné zahrnout i difuzi a kapilaritu, i když možná za cenu netriviální reformulace základních pojmů, kterými popisujeme tyto jevy. Vývoj takových formulací je předmětem budoucího výzkumu. Z hlediska praktických aplikací bude zajímavé studovat i rozšíření modelu na neizotermální případ [27]. Daná problematika tedy stále poskytuje mnoho příležitostí a výzkumných témat do budoucna.

Výzkum v této oblasti se přirozeně odehrává ve spolupráci s domácími i zahraničními pracovišti. V první řadě je třeba uvést úspěšnou intenzivní spolupráci s prof. Abbasem Firoozabadi (Reservoir Engineering Research Institute, Palo Alto, California a Yale University, New Haven, Connecticut) a prof. Tissou H. Illangasekarem z Center of Experimental Study of Subsurface Environmental Processes na Colorado School of Mines (Golden, Colorado), do kterých jsou zapojováni i magisterští studenti a doktorandi FJFI ČVUT. Dále zmiňme kontakty s prof. Peterem Bastianem (Heidelberg), s prof. Shuyu Sunem (King Abdullah University of Science and Technology, Saudská Arábie), Dr. Jorge Monteagudo (ConocoPhillips, Houston, Texas), doc. Peterem Frolkovičem ze Slovenské technické univerzity v Bratislavě a Dr. Janem Hrubým z Ústavu termomechaniky Akademie věd České republiky. Z řady projektů, na kterých autor pracoval, uveďme zejména:

- Development of Computational Models for Simulation of CO_2 Sequestration, projekt č. P105/11/1507 Grantové agentury České republiky, 2011-2013,

- Computational Methods in Thermodynamics of Multicomponent Mixtures, projekt Ministerstva školství mládeže a tělovýchovy České republiky KONTAKT LH12064, 2012-2015,

- Mathematical Modelling of Multi-Phase Porous Media Flow, projekt č. 201/08/P567 Grantové agentury České republiky, 2008-2010,

- Development and Validation of Porous Media Flow and Transport Models for Subsurface Environmental Application, projekt Ministerstva školství mládeže a tělovýchovy České republiky KONTAKT ME878, 2006-2009,
- Numerical Methods for Multiphase Flow and Transport in Subsurface Environmental Applications, projekt Ministerstva školství mládeže a tělovýchovy České republiky, KONTAKT ME10009, 2010-2012, hlavní řešitel prof. Dr. Ing. Michal Beneš,
- Jindřich Nečas Center for Mathematical Modelling, výzkumné centrum Ministerstva školství mládeže a tělovýchovy České republiky, LC06052, hlavní řešitel prof. RNDr. Josef Málek, CSc., Univerzita Karlova, 2006-2011.

Kapitola 3

Přiložené publikace

3.1 Stručný přehled přiložených článků

Přílohou práce je následujících šest článků.

[Č1]: Mikyška, J., and Firoozabadi, A., Implementation of Higher-Order Methods for Robust and Efficient Compositional Simulation, Journal of Computational Physics, 229(8): 2898-2913, 2010

V článku jsou zkoumány problémy vznikající při pokusu o použití metod vyššího řádu přesnosti pro simulaci kompozičního proudění. V této práci popisujeme korektní formulaci transportních rovnic a okrajových podmínek, které v dřívějších formulacích bránily využití metod vyššího řádu. Dále popisujeme metodu aproximace fázových toků ve smíšené hybridní metodě konečných prvků, která umožňuje efektivní využití metod vyššího řádu pro simulaci dvoufázového vícekomponentního proudění s přestupem komponent mezi fázemi.

[Č2]: Mikyška, J., and Firoozabadi, A., A New Thermodynamic Function for Phase-Splitting at Constant Temperature, Moles, and Volume, AIChE Journal, 57(7):1897-1904, 2011

V tomto článku zavádíme novou termodynamickou funkci pro popis fázové rovnováhy při konstantní teplotě, objemu a látkových množstvích – tzv. objemovou funkci. Tato funkce přirozeným způsobem nahrazuje běžně používaný pojem fugacity a umožňuje najít reprezentaci chemického potenciálu v těchto proměnných. Dále odvozujeme tvar podmínek fázové rovnováhy pomocí objemových funkcí a navrhujeme první numerický algoritmus pro vyšetřování dvoufázové rovnováhy založený na kombinaci metody postupných iterací a Newtonovy metody.

[Č3]: Mikyška, J., and Firoozabadi, A., Investigation of Mixture Stability at Given Volume, Temperature, and Number of Moles, Fluid Phase Equilibria, Vol. 321 (May 15, 2012), pp. 1–9, 2012

V práci odvozujeme kritérium fázové stability při předepsané teplotě, objemu a látkových množstvích jednotlivých komponent směsi. V tomto přístupu využíváme Helmholtzovu energii systému a reprezentaci chemického potenciálu pomocí objemových funkcí, což vede k návrhu numerického algoritmu pro vyšetřování stability jedné fáze založené na Newtonově metodě. Robustnost a efektivnost metody je demonstrována na mnoha příkladech vícekomponentních směsí.

[Č4]: Jindrová, T., and Mikyška, J., Fast and Robust Algorithm for Calculation of Two-Phase Equilibria at Given Volume, Temperature, and Moles, Fluid Phase Equilibria, Vol. 353 (Sep 15, 2013), pp. 101–114, 2013

V článku je vyvinut rychlý a robustní algoritmus pro výpočet fázové rovnováhy při zadaném objemu, teplotě a látkových množstvích jednotlivých komponent. Metoda je založena na přímé minimalizaci celkové Helmholtzovy energie směsi při zadaných vazebních podmínkách popisujících bilanci hmoty a objemu. Algoritmus využívá modifikovanou Newtonovu metodu s prohledáváním v zadaném směru a modifikovanou Choleskyho faktorizaci Hessovy matice tak, aby byl zajištěn pokles celkové Helmholtzovy energie v každé iteraci. Algoritmus využívá počáteční aproximaci, která se konstruuje s využitím výsledků získaných během testování stability směsi. Efektivnost a robustnost je demonstrována na mnoha příkladech výpočtů dvoufázové rovnováhy vícekomponentních směsí.

[Č5]: Polívka, O., and Mikyška, J., Numerical Simulation of Multicomponent Compressible Flow in Porous Medium, Journal of Math-for-Industry, Vol. 3 (2011C-7), pp. 53–60, 2011

V článku se zabýváme numerickou simulací stlačitelného proudění jednofázové vícekomponentní směsi (viz též [84]). Problém je formulován pomocí bilančních rovnic pro jednotlivé komponenty, Darcyho zákona, stavové rovnice a vhodných počátečních a okrajových podmínek. Problém se řeší numericky pomocí kombinace smíšené hybridní metody konečných prvků pro diskretizaci Darcyho zákona a metody konečných objemů pro diskretizaci transportních rovnic. Časová diskretizace je provedena Eulerovou metodou. Výsledná soustava nelineárních algebraických rovnic je řešena Newtonovou metodou. Navržená metoda umožňuje redukovat velikost výsledných soustav lineárních algebraických rovnic na rozměr, který nezávisí na počtu komponent směsi. Konvergence numerického schématu je ověřena na dvou modelových problémech.

[Č6]: Polívka, O., and Mikyška, J., Compositional Modeling in Porous Media using Constant Volume Flash and Flux Computation without the Need for Phase Identification, Journal of Computational Physics 272: 149–169, 2014

V článku představujeme novou formulaci kompozičního modelu popisujícího stlačitelné dvoufázové proudění směsi několika chemických komponent v porézním prostředí s přestupem komponent mezi fázemi. Model je formulován pomocí Darcyho zákona pro všechny fáze, rovnic kontinuity pro každou komponentu, konstitučních vztahů a vhodných počátečních a okrajových podmínek. Rozklad komponent mezi fáze je popsán novou formulací lokální termodynamické rovnováhy za předepsané teploty, objemu a látkových množství. Problém je řešen numericky pomocí kombinace smíšené hybridní metody konečných prvků pro diskretizaci celkového toku a metody konečných objemů pro diskretizaci transportních rovnic. Dále je navržena nová metoda pro výpočet numerického toku každé komponenty, která na rozdíl od dřívějších přístupů nezávisí na fázové identifikaci a nevyžaduje párování fázových toků na sousedních výpočetních elementech.

3.2 [Č1]: Mikyška, J., and Firoozabadi, A., Implementation of Higher-Order Methods for Robust and Efficient Compositional Simulation, Journal of Computational Physics, 229(8): 2898-2913, 2010

Journal of Computational Physics 229 (2010) 2898–2913

Contents lists available at ScienceDirect

Journal of Computational Physics

journal homepage: www.elsevier.com/locate/jcp

Implementation of higher-order methods for robust and efficient compositional simulation

Jiří Mikyška [a,b], Abbas Firoozabadi [a,*]

[a] Reservoir Engineering Research Institute, 385 Sherman Avenue, Suite 5, Palo Alto, CA 94306, USA
[b] Czech Technical University in Prague, Faculty of Nuclear Sciences and Physical Engineering, Department of Mathematics, Trojanova 13, 120 00 Prague, Czech Republic

ARTICLE INFO

Article history:
Received 13 February 2009
Received in revised form 10 December 2009
Accepted 21 December 2009
Available online 4 January 2010

Keywords:
Compositional flow
Two-phase flow
Mixed finite-elements
Discontinuous Galerkin method
Monotone upwind scheme for conservation laws
Slope limiter
Gas injection

ABSTRACT

Numerical simulation of two-phase multicomponent flow in permeable media with species transfer between the phases often requires use of higher-order methods. Unlike first-order methods, higher-order methods may be very sensitive to problem formulation. The sensitivity to problem formulation and lack of recognition have hindered the widespread use of higher-order methods in various problems including improved oil recovery and sequestration from CO_2 injection. In this work, we offer proper formulation of species balance equations and boundary conditions which overcome problems of formulations used previously that were detrimental to the efficiency of higher-order methods. We also present proper approximation of phase fluxes in the mixed finite element method. Our proposals remove major deficiencies in using higher-order methods in two-phase multicomponent flow. Numerical examples are presented to demonstrate robustness and efficiency of our approach.

1. Introduction

Injection of gases such as CO_2 in the subsurface has broad applications in oil recovery and in sequestration. In such injection schemes in addition to transfer of species between the phases, there can be substantial changes in density and viscosity of the phases from solubility and vaporization of species. For CO_2, there is often an increase in liquid phase density from solubility. There is also decrease in liquid viscosity. CO_2 solubility may also result in swelling of the liquid phase. Depending on the transfer of species between the phases, there may be also the opposite effects. Despite much progress in the last thirty years in numerical simulation of gas injection schemes in the subsurface, efficient numerical simulation of compositional effects remains a challenging task.

There are two types of numerical schemes used for compositional simulation. In one scheme, first-order finite-difference and finite-volume methods are used. The latter is fit for unstructured grids while the former is for structured grids. One serious issue with the first-order schemes is severe numerical dispersion. Another limitation is the accuracy of flow field calculations. First-order finite-volume methods [1] have been used for two-phase flow in permeable media. Despite powerful features, these methods have inherent limitations when applied to fractured media [2].

Higher-order methods have been used in compositional models. The two main advantageous features of these methods are: (1) low numerical dispersion, and (2) accurate flow field calculations. Finite element method is the main approach in

* Corresponding author. Tel.: +1 650 326 9172; fax: +1 650 326 9277.
E-mail addresses: jiri.mikyska@fjfi.cvut.cz (J. Mikyška), abbas.firoozabadi@yale.edu (A. Firoozabadi).

0021-9991/$ - see front matter © 2009 Published by Elsevier Inc.
doi:10.1016/j.jcp.2009.12.022

higher-order method for complex compositional modeling. Unlike the first-order methods, higher-order methods, especially the finite element methods, are very sensitive to proper problem formulation and proper physics. This aspect is often ignored in the literature.

In two recent papers [3,4], Hoteit and Firoozabadi have advanced the use of the combined discontinuous Galerkin (DG) and mixed-hybrid finite element (MHFE) methods for compositional modeling. The combined algorithm provides a powerful tool for multicomponent flow modeling of two phases in complex permeable media. In an earlier work [5], Chen et al. have applied the combined method for the electric field and convection. In the problem of interest to us, the DG has low numerical dispersion and the MHFE gives accurate calculation of the flow field. In further testing of the combined approach we have found that in some cases the code crashes. We have also seen some oscillations in contour plot of the species concentration. A close examination has shown that there may exist some fundamental issues with formulation in the literature and in our own work [3,4]. These issues may not affect first-order finite-difference and finite-volumes methods, but can affect higher-order methods. Proper formulation of the problem has not been discussed in the literature to the best of our knowledge. These issues are common to any higher-order method. In this work, we will use a combination of mixed-hybrid finite element method for the pressure equation and either discontinuous Galerkin finite element method or higher-order finite-volume (FV) scheme of the MUSCL (monotone upwind-centered scheme for conservation laws) type for the transport equations.

In this paper, for the sake of completeness, we present the formulation of two-phase flow with species transfer between the phases in permeable media. We first provide the flow equations, and then present boundary conditions. Boundary conditions in two-phase compositional flow are subtle issues. Next we derive the numerical schemes and then introduce the numerical algorithm for computations. Upwinding of different coefficients in the equations is discussed in detail. This issue also deserves much attention. At the end, we provide six numerical examples to demonstrate the performance of both algorithms. The results reveal that proper implementation of physical concepts allows efficient calculation and robustness of the algorithm. The work is ended with summary and conclusions.

2. Model equations

Consider two-phase (oil and gas) flow with n_c-components in permeable media without capillarity and diffusion at a constant temperature T. The transport of the components is described by the following molar balance equations

$$\phi\frac{\partial cz_i}{\partial t}+\nabla\cdot(c_o x_{oi}\mathbf{v}_o+c_g x_{gi}\mathbf{v}_g)=F_i,\quad i=1,\dots,n_c, \tag{1}$$

where ϕ is the porosity, c is the overall molar density, z_i is the mole fraction of ith component, c_o, c_g, x_{oi} and x_{gi} are the oil and gas molar densities and oil and gas molar fractions, respectively, and F_i describes distribution of the sources/sinks of the ith component. Other symbols will be defined shortly.

The above system is written in the following form for numerical implementation [3–6]

$$\phi\frac{\partial cz_i}{\partial t}+\nabla\cdot(c_o x_{oi}\mathbf{v}_o+c_g x_{gi}\mathbf{v}_g)=F_i,\quad i=1,\dots,n_c-1, \tag{2a}$$

$$\phi\frac{\partial c}{\partial t}+\nabla\cdot(c_o\mathbf{v}_o+c_g\mathbf{v}_g)=F\equiv\sum_{i=1}^{n}F_i. \tag{2b}$$

The species balance equations in the form presented in (2a) and (2b) is fit for implementation in the first-order finite-difference and first-order finite-volume schemes. This is the form that all the works in the literature is based on. However, after much examination we suspected that (2a) and (2b) give oscillation in species profile in the implementation of the higher-order method used in our work. The problem was definitively solved when the species balance equations in the form given by (1) was implemented. We also observed larger time steps in our implementation. Later in this work we will discuss the reasoning behind use of (1).

The oil and gas phase velocities $\mathbf{v}_o$ and $\mathbf{v}_g$ are described by Darcy's laws,

$$\mathbf{v}_\alpha=-\lambda_\alpha(S_\alpha)\mathbf{K}(\nabla p-\rho_\alpha\mathbf{g}),\quad \alpha\in\{o,g\}, \tag{3}$$

where λ_α is the α-phase mobility, $\mathbf{K}$ is the permeable medium intrinsic permeability, p is the pressure, ρ_α is the α-phase density, and $\mathbf{g}$ is the gravity acceleration vector. In (1), (2a) and (2b), t denotes the time. The viscosities hidden in the mobility terms are estimated based on the methodology of Lohrentz et al. [7].

Using the concept of volume-balance, one can derive the following pressure equation (see [6]),

$$\phi c_f\frac{\partial p}{\partial t}+\sum_{i=1}^{n_c}\overline{v_i}\nabla\cdot(c_o x_{oi}\mathbf{v}_o+c_g x_{gi}\mathbf{v}_g)=\sum_{i=1}^{n_c}\overline{v_i}F_i, \tag{4}$$

where c_f is the total fluid compressibility and $\overline{v_i}$ is the total partial molar volume of the ith component (see [8] for details).

The splitting of components between the phases is given by the following thermodynamic equilibrium equations

$$f_{oi}(x_{o1},\dots,x_{on_c-1},p;T) = f_{gi}(x_{g1},\dots,x_{gn_c-1},p;T), \quad i=1,\dots,n_c, \tag{5a}$$

$$z_i = (1-v)x_{oi} + v x_{gi}, \quad i=1,\dots,n_c, \tag{5b}$$

$$\sum_{i=1}^{n_c} x_{oi} = \sum_{i=1}^{n_c} x_{gi} = \sum_{i=1}^{n_c} z_i = 1, \tag{5c}$$

where f_{oi} and f_{gi} represent fugacities of the ith component in the respective phase, and v is the gas mole fraction.

The phase and volumetric behavior is modeled using the Peng–Robinson equation of state (PR-EOS) [9] in the form

$$\begin{aligned} &\rho_\alpha = c_\alpha \sum_{i=1}^{n_c} x_{\alpha i} M_i, \quad c_\alpha = \frac{p}{Z_\alpha RT}, \\ &Z_\alpha^3 - (1-B_\alpha)Z_\alpha^2 + (A_\alpha - 3B_\alpha^2 - 2B_\alpha)Z_\alpha - (A_\alpha B_\alpha - B_\alpha^2 - B_\alpha^3) = 0, \end{aligned} \tag{6}$$

where M_i is the molar weight of the ith component, R is the universal gas constant, and A_α and B_α are the parameters of the PR-EOS which depend on pressure, temperature and respective phase composition (see [8]).

For evaluation of the phase mobilities in (3), the phase saturations are calculated from

$$S_o = \frac{c}{c_o}(1-v), \quad S_g = \frac{c}{c_g} v. \tag{7}$$

The saturation constraint $S_o + S_g = 1$ then provides an additional condition

$$1 - c\left(\frac{1-v}{c_o} + \frac{v}{c_g}\right) = 0, \tag{8}$$

from which we can evaluate c independent of the transport equation (1). Obviously, the system is over determined; we have one more equation than the unknowns. In the computations, the value of c is determined from Eq. (1) and the constraint equation (8) is used as a criterion for the selection of a time step.

The above equations pertain to the condition when both phases are present. When the system is only in a single-phase, then the equation system must be modified. When only α-phase is present, the fugacity equality (5a) has no relevance and the rest of the equations are transformed into a simpler system by identifying c_α with c, z_i with $x_{\alpha i}$, setting S_α to one and v to either one or zero depending on the phase identity.

3. Initial and boundary conditions

In this work we found that the implementation of boundary conditions at the horizontal impermeable walls in two-phase was critical for successful computations. We also found that the current implementation based on literature formulation gives inconsistent pressure in the grid cells at the horizontal impermeable walls.

To define a well-posed problem, the system of equations formulated in the previous section must be completed by appropriate initial and boundary conditions. The pressure equation (4) is parabolic with respect to pressure. Therefore, we have to provide an initial condition for pressure at each point of the domain Ω. As we will use the total molar flux formulation (introduced later), we have to provide either pressure (Dirichlet boundary condition) or normal component of total molar flux (Neumann boundary condition) at each boundary point $\mathbf{x} \in \partial\Omega$. The transport equation (1) are hyperbolic type and of the first-order with respect to cz_i. It is, therefore, necessary to prescribe initial molar density and mole fractions of all components in the mixture at all points inside the domain Ω. The boundary values of molar density and composition can be prescribed at the inflow boundary. On the other hand, the values at the outflow boundary will be computed.

The injection/production wells can be represented by the source/sink terms, respectively. The whole boundary can then be represented by impermeable walls. The condition for impermeable walls is specified in the literature by

$$\mathbf{v}_\alpha \cdot \mathbf{n} = -\lambda_\alpha(S_\alpha)\mathbf{K}(\nabla p - \rho_\alpha \mathbf{g}) \cdot \mathbf{n} = 0, \quad \alpha \in \{o,g\}, \tag{9}$$

where $\mathbf{n}$ is the outer normal vector. Use of the above equation in two-phase region (where $\lambda_\alpha \neq 0$ for both $\alpha \in \{o,g\}$) gives

$$\nabla p \cdot \mathbf{n} = \rho_o \mathbf{g} \cdot \mathbf{n} \quad \text{and} \quad \nabla p \cdot \mathbf{n} = \rho_g \mathbf{g} \cdot \mathbf{n}. \tag{10}$$

Note that there are two distinct pressure gradients at the wall when the phase densities are not the same. While there is no issue for a vertical impermeable wall due to absence of gravity term, there is a problem when (9) is used at the horizontal boundaries. An appropriate boundary condition in two-phase state is the use of

$$(c_o \mathbf{v}_o + c_g \mathbf{v}_g) \cdot \mathbf{n} = 0, \tag{11}$$

which prescribes the normal component of the total molar flux to be zero. The boundary condition (11) can be readily enforced using the MHFE formulation to be presented in the following section. Condition given by (11) implies that if one phase is flowing out of the domain Ω, the other phase is flowing in at the same point. According to the above discussion, the composition of the inflow phase can be prescribed, while the composition of the outflow phase is computed. The molar balance for each component at the wall is prescribed as

$$c_o x_{oi} \mathbf{v}_o \cdot \mathbf{n} + c_g x_{gi} \mathbf{v}_g \cdot \mathbf{n} = 0. \tag{12}$$

The condition given by (12) states that the total molar flux of each individual component at the boundary is zero. The composition of the inflow phase is computed from the composition of the outflow phase so that (12) holds.

4. Numerical solution

The system of Eqs. (1)–(5c) is discretized using the implicit pressure explicit composition (IMPEC) scheme. The pressure equation is solved using the mixed-hybrid finite element (MHFE) method of the lowest order providing accurate approximations of phase fluxes that are consequently used in transport modeling. The transport equations are treated either by the discontinuous Galerkin (DG) method or a higher-order finite-volume scheme such as the monotonic upwind-centered scheme for conservation laws (MUSCL, see [10–14]). Higher-order methods generally require data reconstruction using a slope limiter that must be carried out to avoid spurious oscillations. In this section we will give details of the methods for a 2D rectangular grid.

4.1. Discretization of the total molar flux

We use the concept of total molar flux rather than total velocity that was used in [4]. This is due to the fact that total volumetric velocity is not preserved when composition is not the same on the two sides of the interface. Because the mobility λ_α can be zero at extreme saturations, the total molar flux $\mathbf{q}$ is introduced

$$\mathbf{q} = c_o \mathbf{v}_o + c_g \mathbf{v}_g = -\sum_{\alpha'} c_{\alpha'} \lambda_{\alpha'} \mathbf{K}(\nabla p - \rho \mathbf{g}), \tag{13}$$

where $\rho = f_o \rho_o + f_g \rho_g$, and $f_\alpha = c_\alpha \lambda_\alpha / \sum_{\alpha'} c_{\alpha'} \lambda_{\alpha'}$. Note that unlike coefficients $c_\alpha \lambda_\alpha$ in the phase fluxes, the coefficient $\sum_{\alpha'} c_{\alpha'} \lambda_{\alpha'}$ in (13) is always positive as at least one of the phases is mobile. We then solve (13) in terms of the pressure gradient

$$\nabla p = -\frac{1}{\sum_{\alpha'} c_{\alpha'} \lambda_{\alpha'}} \mathbf{K}^{-1} \mathbf{q} + \rho \mathbf{g}. \tag{14}$$

Eq. (14) can be substituted in Darcy's laws given by (3) to obtain the following expression for phase molar fluxes

$$\mathbf{q}_\alpha \equiv c_\alpha \mathbf{v}_\alpha = f_\alpha (\mathbf{q} - \mathbf{G}_\alpha), \tag{15}$$

where

$$\mathbf{G}_\alpha = \begin{cases} c_o \lambda_o (\rho_o - \rho_g) \mathbf{K} \mathbf{g} & \alpha = g, \\ c_g \lambda_g (\rho_g - \rho_o) \mathbf{K} \mathbf{g} & \alpha = o. \end{cases} \tag{16}$$

The total molar flux is approximated using the lowest order Raviart–Thomas elements as

$$\mathbf{q}_K = \sum_{E \in \partial K} q_{K,E} \mathbf{w}_{K,E}, \tag{17}$$

where $q_{K,E}$ is the normal component of the total molar flux over the edge E of element K with respect to outer normal, and $\mathbf{w}_{K,E}$ denotes the RT_0 basis functions (see Appendix A). The total flux can be expressed as a function of cell-average pressure p_K, traces of pressure on element faces $tp_{K,E}$ as follows

$$q_{K,E} = a_{K,E} p_K - \sum_{E' \in \partial K} b_{K,E,E'} tp_{K,E'} + d_{K,E}, \tag{18}$$

where $a_{K,E}$, $b_{K,E,E'}$, and $d_{K,E}$ are coefficients which depend on the mesh geometry and on the local values of total mobility. Evaluation of these coefficients is detailed in Appendix A. The total flux continuity leads to the following equation on edge $E = K \cap K'$ between neighboring elements K and K'

$$q_{K,E} + q_{K',E} = 0, \quad K \cap K' = E. \tag{19}$$

Using (18), we derive

$$a_{K,E} p_K - \sum_{E' \in \partial K} b_{K,E,E'} tp_{K,E'} + d_{K,E} + a_{K',E} p_{K'} - \sum_{E' \in \partial K'} b_{K',E,E'} tp_{K',E'} + d_{K',E} = 0, \tag{20}$$

In this work, we use Eq. (11) to obtain the following condition for boundary edges $E \subset \partial\Omega$ adjacent to an element K

$$q_{K,E} = 0, \tag{21}$$

whence

$$a_{K,E} p_K - \sum_{E' \in \partial K} b_{K,E,E'} tp_{K,E'} + d_{K,E} = 0. \tag{22}$$

The system of Eqs. (20) and (22) can be rewritten in the matrix form as

$$R^T P - MTP = V, \tag{23}$$

where

$$R \in \mathbb{R}^{N_K,N_E}, \quad R_{K,E} = a_{K,E}, \tag{24a}$$

$$M \in \mathbb{R}^{N_E,N_E}, \quad M_{E,E'} = \sum_{K:E,E' \in \partial K} b_{K,E,E'}, \tag{24b}$$

$$V \in \mathbb{R}^{N_E}, \quad V_E = \sum_{K:E \in \partial K} d_{K,E}, \tag{24c}$$

N_K denotes the number of element cells, N_E number of mesh edges, $P \in \mathbb{R}^{N_K}$ is the vector of cell-average pressures (indexed by elements), and $TP \in \mathbb{R}^{N_E}$ is the vector of pressure traces indexed by mesh edges.

4.2. Approximation of the pressure equation

We use (15) to rewrite the pressure equation given by (4) in terms of the total molar flux as

$$\phi c_f \frac{\partial p}{\partial t} + \sum_{i=1}^{n_c} \overline{v_i} \nabla \cdot (m_i \mathbf{q} - \mathbf{s}_i) = \sum_{i=1}^{n_c} \overline{v_i} F_i, \tag{25}$$

where $m_i = x_{oi} f_o + x_{gi} f_g$, and $\mathbf{s}_i = x_{oi} f_o \mathbf{G}_o + x_{gi} f_g \mathbf{G}_g$. This equation is integrated over each element K of the mesh. Assuming that the total compressibility and the total partial molar volumes are element-wise constant, we use the divergence theorem to rewrite the last equation in the following form

$$\phi_K c_{f,K} |K| \frac{\partial p_K}{\partial t} + \sum_{i=1}^{n_c} \overline{v_{i,K}} \sum_{E \in \partial K} \int_E (m_{i,K,E} q_{K,E} - \mathbf{s}_{i,K,E} \cdot \mathbf{n}_{K,E}) = \sum_{i=1}^{n_c} \overline{v_{i,K}} F_{i,K} |K|, \tag{26}$$

where $|K|$ is the area of element K. The flux in this equation can be eliminated using (18). The backward Euler scheme for discretization of the time derivative is employed, in which all coefficients are evaluated explicitly using the values from previous time level. We end up with the following system

$$DP^{n+1} - \widetilde{R} TP^{n+1} = G, \tag{27}$$

where the index $n+1$ denotes the time level, $D \in \mathbb{R}^{N_K,N_K}$ is a diagonal matrix with diagonal components

$$D_K = \frac{\phi_K c_{f,K} |K|}{\Delta t} + \sum_{i=1}^{n_c} \overline{v_{i,K}} \sum_{E \in \partial K} \int_E m_{i,K,E} a_{K,E},$$

$\widetilde{R} \in \mathbb{R}^{N_K,N_E}$ is a rectangular matrix with components

$$\widetilde{R}_{K,E'} = \sum_{i=1}^{n_c} \overline{v_{i,K}} \sum_{E \in \partial K} \int_E m_{i,K,E} b_{K,E,E'},$$

and $G \in \mathbb{R}^{N_K}$ is a right side vector with components

$$G_K = \frac{\phi_K c_{f,K} |K|}{\Delta t} p_K^n - \sum_{i=1}^{n_c} \overline{v_{i,K}} \sum_{E \in \partial K} \int_E (m_{i,K,E} d_{K,E} - \mathbf{s}_{i,K,E} \cdot \mathbf{n}_{K,E}) + |K| \sum_{i=1}^{n_c} \overline{v_{i,K}} F_{i,K}.$$

All the coefficients $m_{i,K,E}$ and $\mathbf{s}_{i,K,E}$ are evaluated using the average values inside element K, i.e. we should write $m_{i,K}$, and $\mathbf{s}_{i,K}$ instead of $m_{i,K,E}$ and $\mathbf{s}_{i,K,E}$, respectively. Note that no upwinding is possible here because of implicit treatment of pressure. Moreover, the pressure equation (4) is not in the divergence form which implies that the volume-balance (which is the basis of the pressure equation) is not satisfied exactly by the numerical solution. This should not influence the balance of total molar flux explicitly enforced using (19).

4.3. Approximation of the phase fluxes

One of the most important issues in this work is proper approximation of the phase fluxes $\mathbf{q}_\alpha = f_\alpha(\mathbf{q} - \mathbf{G}_\alpha)$. In this respect we have advanced the procedure outlined in [15]. At first the system of Eqs. (23) and (27) for pressures P and traces of pressure TP at a new time level must be solved. Here we can take advantage of the fact that the matrix D is diagonal with nonzero diagonal elements, and thus invertible. Therefore, we can combine (23) and (27) to derive the following system of equations for pressure traces

$$(M - R^T D^{-1} \widetilde{R}) TP^{n+1} = R^T D^{-1} \widetilde{R}. \tag{28}$$

Once we solve for traces of pressure TP^{n+1}, the cell-average pressure P can be updated using (27). Then we can evaluate the total molar flux from (18). Eq. (19) guarantees the balance of total molar flux over the element edges. However, when evaluating the phase fluxes using (15), the local values of f_α and $\mathbf{G}_\alpha$ cannot be used as this would lead to non-matching phase fluxes at element edges. To obtain phase fluxes that are balanced at the mesh edges, the values of ρ_α used in $\mathbf{G}_\alpha$ in (15) are taken as an arithmetic average of the neighboring cell values, while $c_\alpha\lambda_\alpha$, and $c_{\alpha'}\lambda_{\alpha'}$ in f_α are taken from the upwind side with respect to $\mathbf{v}_\alpha$. In computing phase fluxes (note that $\mathbf{q}_\alpha$ is not available yet), we denote by α the phase for which

$$\operatorname{sgn}\mathbf{q}_{K,E}\cdot\mathbf{n}_{K,E} = -\operatorname{sgn}\mathbf{G}_\alpha\cdot\mathbf{n}_{K,E},$$

where $c_\alpha\lambda_\alpha$ and $c_{\alpha'}\lambda_{\alpha'}$, are evaluated arbitrarily, e.g. by setting $c_\alpha\lambda_\alpha = c_{\alpha'}\lambda_{\alpha'} = 1$; the primed phase α' denotes the other phase. The use of the above expression is always possible because the total flux has been evaluated and $\mathbf{G}_\alpha$ and $\mathbf{G}_{\alpha'}$ (with $c_\alpha\lambda_\alpha$ and $c_{\alpha'}\lambda_{\alpha'}$ set to 1) are pointing in the opposite directions. Now we can predict the sign of $q_{\alpha,K,E}$, which has the same sign as of $q_{K,E}$, independent of the actual value of $c_{\alpha'}\lambda_{\alpha'}$, which is always non-negative, in (15). Using the known sign of $q_{\alpha,K,E}$, we can choose the upwind value of $c_\alpha\lambda_\alpha$ used in the computation of $\mathbf{G}_{\alpha'}$. We can now evaluate $q_{\alpha',K,E}$ and finally the actual value of $\lambda_{\alpha'}$ is estimated and then the actual value of $q_{\alpha,K,E}$ can be determined. Note that this procedure is not consistent with the way we treated flux in the discretizaton of pressure equation, but it ensures the balance of phase velocities, which is important for correct treatment of mass balance in the transport. Our suggested procedure for calculation of individual interface phase velocities allows robust calculations and alleviates a deficiency in previous work [4].

4.4. Approximation of components transport

We discuss two methods for approximation of the components transport equations: (1) the discontinuous Galerkin finite element method, and (2) the MUSCL-type finite-volume scheme.

4.4.1. Discontinuous Galerkin finite element method

The components transport equation (1) are discretized using the discontinuous Galerkin finite element method. On each rectangular element K, the unknown concentration is approximated using a linear function. Note that in a rectangular element, there is no need for 4 degrees of freedom because the interpolant is allowed to be discontinuous in DG method. Assuming such an approximation in the form

$$cz_{i,K} = \sum_{l=1}^{3} cz_{i,K}^l\varphi_{K,l}, \quad c_\alpha x_{\alpha i,K} = \sum_{l=1}^{3} c_\alpha x_{\alpha i,K}^l\varphi_{K,l}, \tag{29}$$

where functions $\varphi_{K,l}$ form a basis of a local approximation space (detailed in Appendix B), we multiply (1) by a test function, integrate over the element K and integrate by parts to obtain

$$\int_K \phi\frac{\partial cz_{i,K}}{\partial t}\varphi_{K,j} - \int_K (x_{oi,K}\mathbf{q}_o + x_{gi,K}\mathbf{q}_g)\cdot\nabla\varphi_{K,j} + \sum_{E\in\partial K}\int_E (\widetilde{x_{oi,K,E}}\mathbf{q}_o + \widetilde{x_{gi,K,E}}\mathbf{q}_g)\cdot\mathbf{n}_{K,E}\varphi_{K,j} = \int_K F_i\varphi_{K,j} \tag{30}$$

for each $j\in\{1,2,3\}$. In the surface integral, the $\widetilde{x_{\alpha i,K,E}}$ ($\alpha\in\{o,g\}$) denotes the value of concentration upwinded with respect to $\mathbf{q}_\alpha$ defined as

$$\widetilde{x_{\alpha i,K,E}} = \begin{cases} x_{\alpha i,K,E} & \text{if } q_{\alpha,K,E}\equiv\mathbf{q}_\alpha\cdot\mathbf{n}_{K,E}|E| \geqslant 0,\\ x_{\alpha i,K',E} & \text{if } q_{\alpha,K,E}\equiv\mathbf{q}_\alpha\cdot\mathbf{n}_{K,E}|E| < 0,\end{cases} \tag{31}$$

where we assume that $E = K\cap K'$ is a common edge between the neighboring elements K and K'. If E is a boundary edge, then the Dirichlet boundary conditions on the influx part of the boundary can be applied readily at this stage. Note that the values $x_{\alpha i,K,E}$ and $x_{\alpha i,K',E}$ in (31) result from the evaluation of the two-phase flash at the element edges using the values of temperature T, pressure trace TP and overall molar composition z_i at that edge. The value of z_i at the edge is computed from the value of z_i in the element center using the slopes provided by the DG method. On the other hand, the values $x_{\alpha i,K}$ in the second integral on the left hand side of (29) is evaluated by the two-phase flash at temperature T, average element pressure P and overall molar composition z_i at the element center. This implies that five flashes must be performed on every element.

Substituting (29) into (30), we derive the following semi-discrete scheme

$$\phi_K\sum_{l=1}^{3}\frac{dcz_{i,K}^l}{dt}M_{j,l}^K - \sum_{\alpha\in\{o,g\}}\sum_{l=1}^{3}x_{\alpha i,K}\sum_{E\in\partial K}q_{\alpha,K,E}M_{j,l}^{K,E} + \sum_{E\in\partial K}\sum_{\alpha\in\{o,g\}}\widetilde{x_{\alpha i,K,E}}q_{\alpha,K,E}M_j^E = \int_K F_i\varphi_{K,j}. \tag{32}$$

The matrices M^K, M^E, and $M^{K,E}$ are defined and their elements are evaluated in Appendix B. The matrix M^K is diagonal, and thus the forward Euler scheme leads to an explicit scheme in terms of $cz_{i,K}^l$ with 3 degrees of freedom per element.

4.4.2. Higher-order finite-volume method of the MUSCL-type

An alternative method for the discretization of the transport equation (1) is the higher-order finite-volume method. There are plenty of methods available (see [1]); in this paper we will discuss the monotonic upwind-centered scheme for conservation laws (MUSCL) by van Leer developed in a series of papers [10–14].

To develop the scheme, Eq. (1) are integrated over an arbitrary rectangular element K. After using the divergence theorem, we have

$$\int_K \phi \frac{\partial cz_{i,K}^1}{\partial t} + \sum_{E\in\partial K} \int_E (\widetilde{x_{oi,K,E}}\mathbf{q}_o + \widetilde{x_{gi,K,E}}\mathbf{q}_g)\cdot\mathbf{n}_{K,E} = \int_K F_i, \tag{33}$$

where the $\widetilde{x_{\alpha i,K,E}}$ ($\alpha\in\{o,g\}$) denotes the value of concentration upwinded with respect to $\mathbf{q}_\alpha$ defined by (31). Eq. (33) describes evolution of the average values of the overall molar densities $cz_{i,K}$ at every element. Unlike the DG scheme, the slopes of the solution are not described by an evolution equation as in (30), but rather reconstructed by using the average values of cz_i in the neighboring elements. In case of the rectangular mesh, the reconstruction carried out using central difference quotients as

$$cz_{i,K}^2 = \frac{cz_{i,R} - cz_{i,L}}{4}, \quad cz_{i,K}^3 = \frac{cz_{i,T} - cz_{i,B}}{4}, \tag{34}$$

where K denotes an element and R, L, T, B are its right, left, top, and right neighbor, respectively. The upper index $l\in\{1,2,3\}$ in $cz_{i,K}^l$ is used to distinguish between the central value ($l=1$) and gradients of $cz_{i,K}$ in the x and y direction ($l=2,3$) to keep the notation consistent with the one used in the derivation of the DG scheme (see also Appendix B). At boundary elements, the slope in the direction perpendicular to the boundary is set to zero for simplicity. After the slopes of cz_i have been reconstructed, the five flashes at every elements are performed to obtain equilibrium compositions $x_{\alpha,i,K}$ at element centers (using the average element pressure and overall composition) and $x_{\alpha i,K,E}$ at element faces (using the traces of pressures, and overall composition evaluated at element faces evaluated in terms of the average values and reconstructed slopes). The values $x_{\alpha i,K,E}$ are then used to evaluate $\widetilde{x_{\alpha i,K,E}}$ needed in (33) using upwinding (31). Finally, the resulting FV-MUSCL scheme reads as

$$\phi_K \frac{dcz_{i,K}^1}{dt}|K| + \sum_{E\in\partial K}\sum_{\alpha\in\{o,g\}} \widetilde{x_{\alpha i,K,E}} q_{\alpha,K,E} = \int_K F_i. \tag{35}$$

4.5. Slope limiter

To avoid unphysical oscillations in the numerical solution, both methods are stabilized by using an appropriate slope limiter. In case of the discontinuous element-wise linear approximation on a rectangular grid, the slope limiting can be carried out in a simple way using two 1D limiters in the directions of x and y axes. The idea of the method is to modify the solution resulting from the DG step after each time step so that the average value of each molar concentration is not modified and the slopes are adjusted so that the values of concentrations at any edge are between the minimum and maximum values of concentrations in adjacent cells. The implementation follows closely the description in Appendix B1 in [3]. As mentioned in Appendix B, our degrees of freedom at each element are: (1) the average value of molar concentration, (2) the difference between the value in the center of the element and the value on the right edge, and (3) the difference between the value in the center of the element and the value on the top edge, which allows for a straightforward implementation of the limiter. Also, the classical first-order finite-volume upwind method can be mimicked easily by setting the differences between the two edge values and the central value to zero.

As mentioned above, the formulation given by (2) is used instead of the original system given by (1) in the literature. When using the first-order finite-volume method, both formulations work equally well. However, there is a complication when (2) is employed in a higher-order method, such as DG or MUSCL, that requires the use of a slope limiter. Here, the use of the original system of Eq. (1) is more straightforward. After each step of DG method the limiter provides bounds $cz_{i,min}$ and $cz_{i,max}$ for each boundary value of cz_i and the slope may be manipulated so that the inequalities

$$cz_{i,min} \leqslant cz_i \leqslant cz_{i,max} \tag{36}$$

hold for each $i=1,\ldots,n_c$. The value of overall molar concentration is then evaluated as

$$c = \sum_{i=1}^{n_c} cz_i, \tag{37}$$

which fulfills

$$\sum_{i=1}^{n_c} cz_{i,min} \leqslant c \leqslant \sum_{i=1}^{n_c} cz_{i,max}. \tag{38}$$

If the alternative formulation based on (2) is used, then the limiter would provide bounds $cz_{i,min}$ and $cz_{i,max}$ on cz_i for $i=1,\ldots,n_c-1$ and bounds c_{min} and c_{max} on c. The slopes of these variables would be manipulated so that

$$\begin{aligned} &cz_{i,min} \leqslant cz_i \leqslant cz_{i,max}, \quad i=1,\ldots,n_c-1,\\ &c_{min} \leqslant c \leqslant c_{max}. \end{aligned} \tag{39}$$

From these inequalities we can derive the following bounds on cz_{n_c}

$$c_{max} - \sum_{i=1}^{n_c-1} cz_{i,min} \leqslant cz_{n_c} = c - \sum_{i=1}^{n_c-1} cz_i \leqslant c_{max} - \sum_{i=1}^{n_c-1} cz_{i,min}, \tag{40}$$

which are inconsistent with the bounds given by Eq. (36) for $i = n_c$ and lead to creation of unphysical oscillations in the last component molar concentration. After several time steps, these oscillations spoil the other components profiles too. The problem could be solved by a special version of limiter for c that would enforce the correct bounds on cz_{n_c}, but this would lead to an unnecessary complicated code which would be more difficult to debug. The straightforward solution is to use the original system of Eq. (1).

5. Computational algorithm

The computation proceeds in the following steps:

1. Read the initial temperature and distribution of pressure and overall molar concentrations of all components. There is only one value of temperature for the whole domain.
2. Perform the flash calculations to obtain number of phases and phase composition at the initial pressure, temperature, and overall composition at element centers and at element faces.
3. Use the Lohrentz et al. method to evaluate the phase viscosities.
4. Repeat the following steps until a predetermined simulation time is reached.
   (a) Assemble and solve the system (28) for traces of pressure TP.
   (b) Evaluate cell-average pressures P locally on each element using (27).
   (c) Calculate fluxes using the procedure described in Section 4.3.
   (d) Compute new overall composition using one explicit Euler time step of the DG scheme (32) or FV-MUSCL scheme (35).
   (e) If the FV-MUSCL scheme was used, reconstruct the slopes of cz_i at every element using (34).
   (f) Apply the slope limiter.
   (g) Perform the phase stability analysis and flash calculation to obtain number of phases and phase composition at the new pressure, temperature and overall composition at element centers and at element faces.
   (h) Update phase viscosities.

6. Results of numerical computations

In this section, we present results of six examples that were carried out using the implementation of the method described in this paper. All the problems were solved on a 2D rectangular domain 50×50 m with a rectangular grid using a HP xw9400 RedHat WS 4 workstation with the Dual-Core AMD Opteron 2216 CPU at 2.4 GHz and 4 GB memory. The relative permeability data for all examples are given in Table 1.

6.1. Example 1

The first problem is the displacement of propane by methane in a horizontal 2D domain (i.e. no gravity). Methane is injected in the lower left corner, displacing propane that is produced in the upper right corner. The initial data of the problem

Table 1
Relative permeability used in Examples 1–6.

Examples	1–4	5 and 6
Relative permeability model type	Linear	Quadratic
Residual gas saturation	0	0.0
Residual oil saturation	0	0.3

Table 2
Relevant data for Examples 1 and 2.

Injection fluid (mole fraction)	1.0 C_1	0.0 C_3
Initial fluid (mole fraction)	0.0 C_1	1.0 C_3
Initial pressure at the bottom (bar)	50	
Temperature (K)	397	
Porosity (fraction)	0.2	
Permeability (md)	10	
Injection rate (m^2/day) at $p = 1$ atm, $T = 293$ K	42.5	

given in Table 2 are chosen so that the mixture stays in single-phase gas state during whole simulation. We fix the injection rate (given in Table 2) and the pressure in the production well at 50 bar.

Fig. 1 shows methane mole fraction at 58% of PVI computed using the MHFE/DG and MHFE/FV methods on a 40×40 mesh. The computation time (to 100% PVI) is 2 min for both methods. As can be seen from the figure, both methods provide very similar results. We have carried out calculations for Example 1 and the next three examples using the first-order finite-volume method for the transport equations. The numerical dispersion is very significant compared to the DG and higher-order finite-volume method. For the sake of brevity, these results are not shown.

6.2. Example 2

The second problem is the displacement of propane by methane in a vertical 2D domain (i.e. with gravity). Methane is injected in the lower left corner, displacing propane that is produced in the upper right corner. The data of the problem are given in Table 2. The initial pressure is fixed in the production well. The pressure and temperature are chosen so that the mixture stays in single-phase gas state during the whole simulation. The computation time to 100% of PVI on a 40×40 grid is 8 min for both methods. Fig. 2 shows methane mole fraction at 20% of PVI computed using the MHFE/DG and MHFE/FV methods. Note the non-symmetry due to gravity effect. Again, both methods provide similar results.

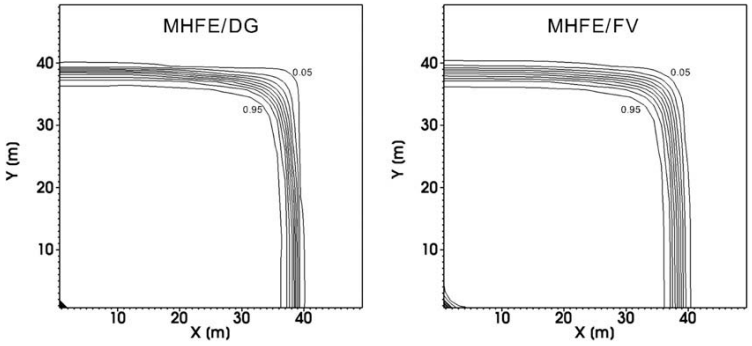

Fig. 1. Methane mole fraction at PVI = 58% (0.69 years) computed on a 40×40 mesh by the MHFE/DG method (left) and the MHFE/FV method (right): Example 1.

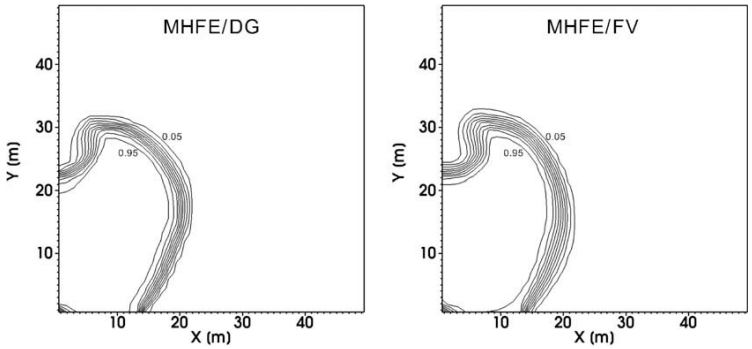

Fig. 2. Methane mole fraction at PVI = 20% (0.24 years) computed by the MHFE/DG (left) and the MHFE/FV (right) methods on a 40×40 mesh: Example 2.

Table 3
Relevant data for Examples 3 and 4.

Injection fluid composition (mole fraction)	1.0 C_1	0.0 C_3
Initial fluid composition (mole fraction)	0.0 C_1	1.0 C_3
Initial pressure at the bottom (bar)	69	
Temperature (K)	311	
Porosity (fraction)	0.2	
Permeability (md)	10	
Injection rate (m^2/day) at $p = 1$ atm, $T = 293$ K	42.5	

6.3. Example 3

The third problem is the displacement of propane by methane in a horizontal 2D domain (i.e. without gravity). Methane is injected in the lower left corner, displacing propane that is produced in the upper right corner. The relevant data are shown in Table 3. Unlike Example 1, the pressure and the temperature are chosen so that a two-phase region develops. In this example, methane, similar to Examples 1 and 2, is a gas but propane, unlike Examples 1 and 2, is in liquid state.

Fig. 3 shows the overall methane mole fraction at 50% of PVI computed using the MHFE/DG and MHFE/FV methods on a 40×40 mesh. The computation time was 2 min for MHFE/DG and 3 min for MHFE/FV methods. Both methods provide results that match almost perfectly.

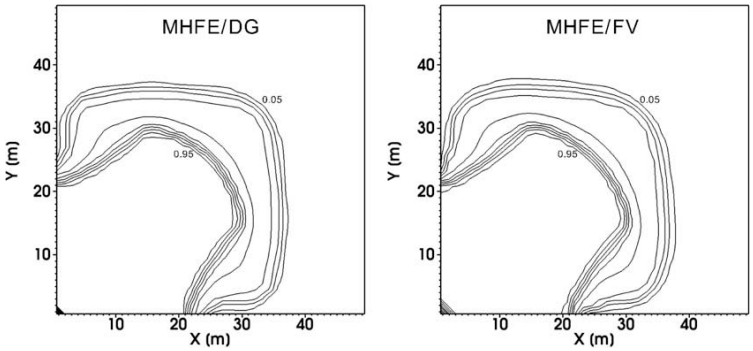

Fig. 3. Overall methane mole fraction at PVI = 50% (1.15 years) computed on a 40×40 mesh by the MHFE/DG method (left) and the MHFE/FV method (right): Example 3.

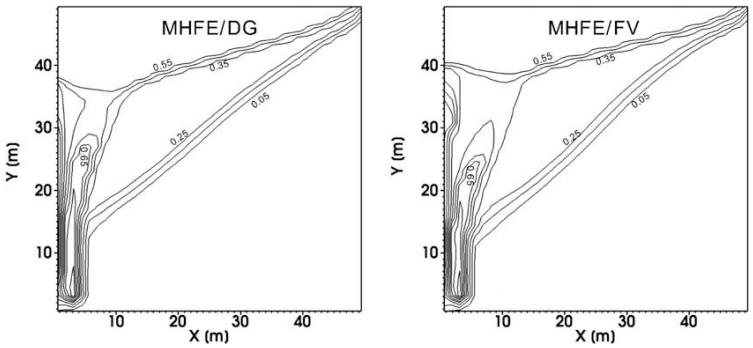

Fig. 4. Overall methane mole fraction at PVI = 50% (1.15 years) computed on a 40×40 mesh by the MHFE/DG method (left) and the MHFE/FV method (right): Example 4.

Table 4
Relevant data for Examples 5 and 6.

Injection gas composition (mole fraction)	1.0 CO_2	0.0 N_2
	0.0 C_1	0.0 C_2–C_3
	0.0 C_4–C_5	0.0 C_6–C_{10}
	0.0 C_{11}–C_{24}	0.0 C_{25+}
Initial fluid composition (mole fraction)	0.0086 CO_2	0.0028 N_2
	0.4451 C_1	0.1207 C_2–C_3
	0.0505 C_4–C_5	0.1328 C_6–C_{10}
	0.1660 C_{11}–C_{24}	0.0735 C_{25+}
Initial pressure at the bottom (bar)	276	
Temperature (K)	403.15	
Porosity (fraction)	0.2	
Permeability (md)	10	
Injection rate (m^2/day) at $p = 1$ atm, $T = 293$ K	133.33	

Table 5
Properties of the eight-component mixture in Examples 5 and 6.

Property	CO_2	N_2	C_1	C_2-C_3	C_4-C_5	C_6-C_{10}	$C_{11}-C_{24}$	C_{25+}
Accentric factor	0.23900	0.03900	0.01100	0.11783	0.21032	0.41752	0.66317	1.72763
Critical temperature (K)	304.14	126.21	190.56	327.81	435.62	574.42	708.95	891.47
Critical pressure (bar)	73.75	33.90	45.99	46.54	36.09	25.04	15.02	7.60
Molar weight (g/mol)	44	28	16	34.96	62.98	110.21	211.91	462.79
Critical volume (m^3/kg)	0.00214	0.00321	0.00615	0.00474	0.437	0.00425	0.00443	0.00417
Volume shift parameter	0.0600	−0.2885	−0.0154	−0.0949	−0.0598	0.0466	0.1494	0.4950
Binary interaction coefficients								
CO_2	0							
N_2	0	0						
C_1	0.15	0.1	0					
C_2-C_3	0.15	0.1	0.0346	0				
C_4-C_5	0.15	0.1	0.0392	0	0			
C_5-C_{10}	0.15	0.1	0.0469	0	0	0		
$C_{11}-C_{24}$	0.15	0.1	0.0635	0	0	0	0	
C_{25+}	0.08	0.1	0.1052	0	0	0	0	0

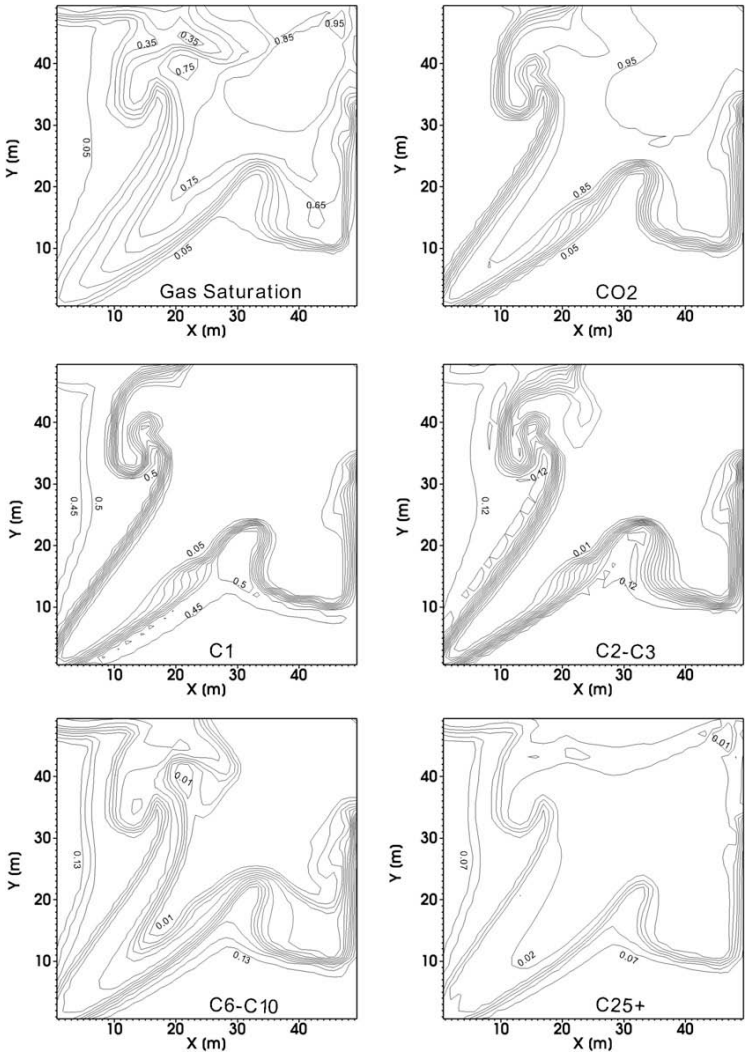

Fig. 5. Results at PVI = 50% (1.37 years) computed on a 40×40 mesh by the MHFE/DG method showing gas saturation, and overall mole fractions of CO_2, C_1, C_2-C_3, C_6-C_{10}, and C_{25+} pseudocomponent: Example 5.

6.4. Example 4

The fourth example, the displacement of propane by methane is studied in a vertical 2D domain (i.e. with gravity). Methane is injected in the lower left corner, displacing propane that is produced in the upper right corner. The data of the problem are given in Table 3. The pressure in the production well is fixed at the initial pressure. Unlike in Example 2, the pressure and the temperature are chosen so that a two-phase region develops. Fig. 4 shows the methane overall mole fraction at 50% of PVI computed on a 40×40 grid. The match between the two methods is again very good. The computation time for both methods to 100% of PVI is approximately 45 min for MHFE/DG and 47 min for MHFE/FV.

6.5. Example 5

In this example, we simulate the injection of CO_2 in a domain saturated with an 8-component hydrocarbon mixture. The initial fluid mixture is in liquid state. The domain is a vertical cross-section of size 50×50 m. The components, the composition of the initial and the injected fluid, and other parameters are specified in Tables 4 and 5. CO_2 is injected in the upper

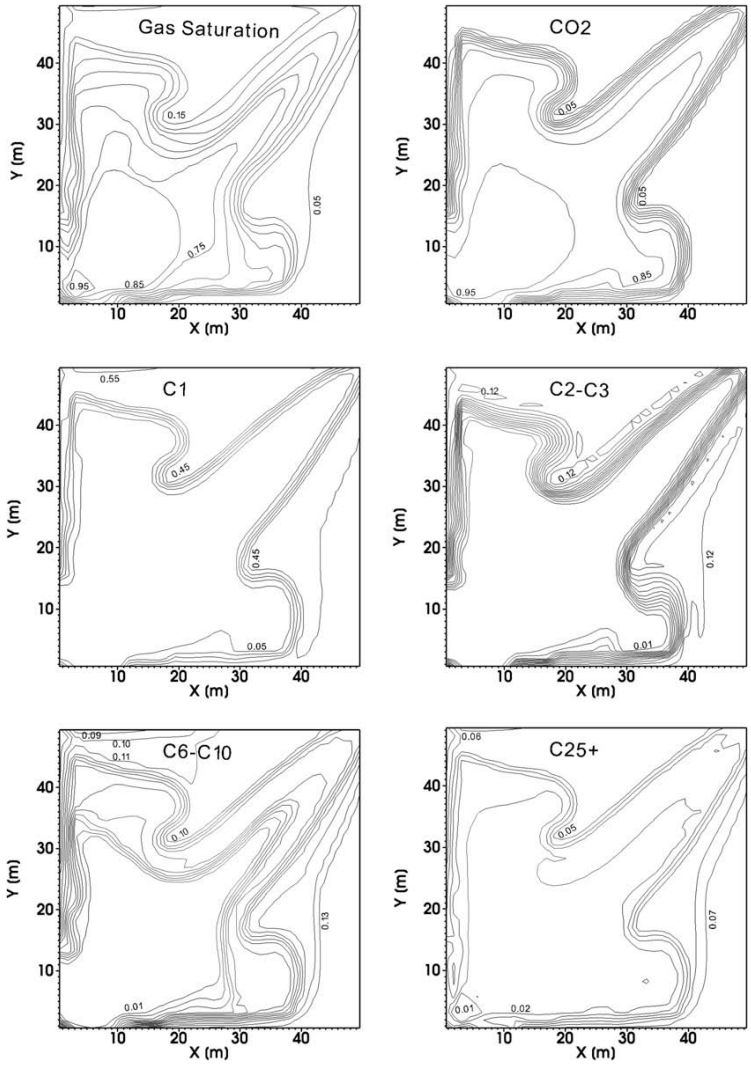

Fig. 6. Results at PVI = 50% (1.37 years) computed on a 40×40 mesh by the MFE/DG method showing gas saturation, overall mole fractions of CO_2, C_1, C_2—C_3, C_6—C_{10}, and C_{25+} pseudocomponents: Example 6.

right corner, displacing the hydrocarbon mixture towards the lower left corner. The pressure is fixed in the production well at 276 bar. Under these conditions a two-phase region develops.

Fig. 5 shows gas saturation and overall molar fractions of selected components at 50% of PVI. It is only with the formulation in this paper that the run can be performed. Without our modification the code would break down before achievement of 100% of PVI. The computation time of the MHFE/DG method to 100% of PVI is 60 min on a 40×40 grid.

6.6. Example 6

In the last example, we simulate the injection of CO_2 in the bottom of the vertical domain. The components, the composition of the initial and the injected fluid, and other physical parameters are the same as in the previous example (see Tables 4 and 5). The only difference is that this time the injection and production wells are interchanged, i.e. the injection well is located at the bottom of the domain in the lower left corner, and the production is at the top in the upper right corner. The pressure in the production well is fixed at the initial pressure.

Fig. 6 shows the gas saturation and overall molar fractions of selected components at 50% of PVI. The computational time of MHFE/DG method to 100% of PVI is 2 h and 32 min on a 40×40 grid.

7. Discussion and concluding remarks

In this work, as a result of use of individual component balance equations, we have suppressed spurious oscillations in composition that were leading to crash of the code in the previous works [3,4]. While our suggestion for the use of Eq. (1) rather than Eq. (2) is deceptively simple, the effect on the robustness of the code is significant. This suggestion affects only the higher-order methods, such as discontinuous Galerkin or MUSCL-type finite-volume methods, which require stabilization using a slope limiter.

The use of boundary conditions for total molar flux and total individual component fluxes are also straightforward and result in substantial improved efficiency of the code. Our suggestion in the boundary condition makes the problem formulation consistent. Proper treatment of boundary conditions allows to increase time steps and leads to significant speed up of the code in both MHFE/FV and MHFE/DG methods.

The approximation of phase fluxes described in our work is a key in MHFE method. Without our implementation we have seen code crash.

All aspects of our suggestions relate to two-phase flows, where without them, the use of higher-order methods will not be widespread in some applications such as CO_2 injection in the subsurface.

In order to show robustness and efficiency of the proposed algorithm, we present six examples of various degree of complexity. The comparison of MHFE/DG and MHFE/FV shows that both methods provide similar results. Generally, FV scheme of MUSCL-type is considered to be cheaper than DG because of lower number of degrees of freedom per element in the case of FV method, but our experiments show that the CPU time difference between the two methods is practically negligible. The two methods are very similar; they only differ in the evaluation of the gradients of the concentrations at the elements. While the DG method provides an evolution equation for the gradients, in higher-order finite-volume methods, the gradient is reconstructed from the neighboring cells. In case of the orthogonal grid, this reconstruction is particularly simple, but this may not be the case when more general unstructured grids are used (see e.g. [20]). The FV method is expected to be faster because it does not include the evaluation of the integral over the element (the second term on the left hand side of (32)) as in DG. However, this step has very little effect on the overall efficiency of the code. The explicit solution of the transport equation requires about 5% of the CPU time while the flash and linear solver take 80–85% and 5–10% of the CPU, respectively. These data correspond to Examples 1–4. In some cases we observed that the computation time of DG was even lower than for FV (see Examples 2 and 3). We have used the MHFE/FV to compute results for Example 6 (results not presented for the sake of brevity). The computation time is 2 h and 28 min which is less then 2 h and 32 min for MHFE/DG. We have presented results of two simulations of CO_2 injection in a multicomponent hydrocarbon mixture; these are new results that could not be obtained using previous work in the literature in which inappropriate upwinding of mobility coefficients created numerical problems leading to breakdown of the computation at the very beginning.

Acknowledgments

This work was supported by the member companies of the Reservoir Engineering Research Institute (RERI), Qatar Foundation, and by the project Mathematical Modelling of Multi-Phase Porous Media Flow, number 201/08/P567 of the Czech Science Foundation.

Appendix A. Raviart–Thomas basis functions and details of the MHFE discretization

We use the lowest order Raviart–Thomas elements [16,17] for which the functions $\mathbf{w}_{K,E}$ are associated with the rectangle edges of each element K. These functions defined on a reference element $K = (0, l_x) \times (0, l_y)$ read as

$$\begin{aligned}\mathbf{w}_{K,B}(x,y) &= \left(0,\frac{y-l_y}{|K|}\right), \quad \mathbf{w}_{K,T}(x,y) = \left(0,\frac{y}{|K|}\right),\\ \mathbf{w}_{K,L}(x,y) &= \left(\frac{x-l_x}{|K|},0\right), \quad \mathbf{w}_{K,R}(x,y) = \left(\frac{x}{|K|},0\right),\end{aligned} \tag{41}$$

where the $B,\ T,\ L$, and R denote the bottom, top, left, and right edge in the element K, respectively. These function are linearly independent and satisfy the following properties

$$\nabla\cdot\mathbf{w}_{K,E} = \frac{1}{|K|}, \quad \mathbf{w}\cdot\mathbf{n}_{K,E'} = \frac{1}{|E|}\delta_{E,E'}, \tag{42}$$

where $|K|$ denotes the surface area of the element K and $|E|$ stands for the length of the edge E.

Assume that the total molar flux $\mathbf{q}$ and the vector $\mathbf{Kg}$ can be represented on the element K as

$$\mathbf{q}(\mathbf{x},t)|_K = \sum_{E'\in\partial K} q_{K,E'}\mathbf{w}_{K,E'}(\mathbf{x}), \quad \mathbf{Kg}|_K = \sum_{E'\in\partial K} q^{Kg}_{K,E'}\mathbf{w}_{K,E'}(\mathbf{x}), \tag{43}$$

where $q_{K,E'} = \int_E \mathbf{q}\cdot\mathbf{n}_{K,E'}$ and $q^{Kg}_{K,E} = \int_E \mathbf{Kg}\cdot\mathbf{n}_{K,E} = \mathbf{Kg}\cdot\mathbf{n}_{K,E}|E|$. Multiplying (14) by $\mathbf{w}_{K,E}$, integrating the result over the element K, and using the Gauss theorem, one obtains

$$\int_K \frac{\mathbf{w}_{K,E}\cdot\mathbf{K}^{-1}\mathbf{q}}{\sum_{\alpha'} c_{\alpha'}\lambda_{\alpha'}} = -\int_K \mathbf{w}_{K,E}\cdot\nabla p + \int_K \rho\mathbf{w}_{K,E}\cdot\mathbf{g} = \int_K p\nabla\cdot\mathbf{w}_{K,E} - \int_{\partial K} p\mathbf{w}_{K,E}\cdot\mathbf{n}_{K,E} + \int_K \rho\mathbf{w}_{K,E}\cdot\mathbf{K}^{-1}\mathbf{Kg}. \tag{44}$$

The right side can be further simplified using the properties of basis functions (42) into

$$\int_K \frac{\mathbf{w}_{K,E}\cdot\mathbf{K}^{-1}\mathbf{q}}{\sum_{\alpha'} c_{\alpha'}\lambda_{\alpha'}} = \frac{1}{|K|}\int_K p - \frac{1}{|E|}\int_E p + \int_K \rho\mathbf{w}_{K,E}\cdot\mathbf{K}^{-1}\mathbf{Kg}. \tag{45}$$

Let p_K and $tp_{K,E}$ denote the cell and edge average pressure, respectively. Assuming that the mobilities and densities are constant over the element K, and using (43), (45) is approximated by

$$\sum_{E'\in\partial K} \frac{q_{K,E'}}{\sum_{\alpha'} c_{\alpha',K}\lambda_{\alpha',K}}\mathbf{A}_{K,E,E'} = p_K - tp_{K,E} + \sum_{E'\in\partial K}\rho_K q^{Kg}_{K,E'}\mathbf{A}_{K,E,E'}, \tag{46}$$

where

$$\mathbf{A}_{K,E,E'} = \int_K \mathbf{w}_{K,E}\cdot\mathbf{K}_K^{-1}\mathbf{w}_{K,E'}. \tag{47}$$

By inverting the matrix $\mathbf{A}_K = [\mathbf{A}_{K,E,E'}]_{E,E'\in\partial K}$, the flux $q_{K,E}$ can be expressed as

$$q_{K,E} = a_{K,E}p_K - \sum_{E'\in\partial K} b_{K,E,E'}tp_{K,E'} + d_{K,E}, \tag{48}$$

where

$$a_{K,E} = \sum_{\alpha'} c_{\alpha',K}\lambda_{\alpha',K}\sum_{E'\in\partial K}\mathbf{A}^{-1}_{K,E,E'}, \tag{49}$$

$$b_{K,E,E'} = \sum_{\alpha'} c_{\alpha',K}\lambda_{\alpha',K}\mathbf{A}^{-1}_{K,E,E'}, \tag{50}$$

$$d_{K,E} = \mathbf{Kg}\cdot\mathbf{n}_{K,E}|E|\sum_{\alpha'} c_{\alpha',K}\lambda_{\alpha',K}\rho_{\alpha,K}. \tag{51}$$

Note that in our implementation, $\mathbf{K}$ is assumed to be a scalar constant over the element. If the integral on the right side is computed exactly, we have to invert the 4×4-matrix which is block-diagonal with full 2×2 diagonal blocks that reads as

$$\mathbf{A}_K = \left[\frac{1}{\mathbf{K}}\int_K \mathbf{w}_{K,E}\cdot\mathbf{w}_{K,E'}\right]_{E,E'} = \frac{1}{6\mathbf{K}}\begin{pmatrix} 2\frac{l_x}{l_y} & -\frac{l_x}{l_y} & 0 & 0\\ -\frac{l_x}{l_y} & 2\frac{l_x}{l_y} & 0 & 0\\ 0 & 0 & 2\frac{l_y}{l_x} & -\frac{l_y}{l_x}\\ 0 & 0 & -\frac{l_y}{l_x} & 2\frac{l_y}{l_x}\end{pmatrix}, \tag{52}$$

where l_x and l_y are the lengths of the rectangle sides parallel to x and y axis, respectively. This matrix is non-singular and can be inverted as

$$\mathbf{A}_K^{-1} = \mathbf{K}\begin{pmatrix} 4\frac{l_y}{l_x} & 2\frac{l_y}{l_x} & 0 & 0\\ 2\frac{l_y}{l_x} & 4\frac{l_y}{l_x} & 0 & 0\\ 0 & 0 & 4\frac{l_x}{l_y} & 2\frac{l_x}{l_y}\\ 0 & 0 & 2\frac{l_x}{l_y} & 4\frac{l_x}{l_y}\end{pmatrix}. \tag{53}$$

The rows and columns of both matrices correspond to the edges of the elements in the rank right, left, top and bottom. It is known that the resulting matrix of the MHFE method is not the M-matrix which can lead to oscillations in the solution (see [18]). Chavent and Roberts [19] have recommended to evaluate the integral in (52) using the following low-order quadrature rule

$$\int_K \varphi(x)\,\mathrm{d}x \approx \frac{|K|}{4}\sum_{j=1}^{4}\varphi(x_i), \tag{54}$$

where x_i denotes coordinates of the element vertices. With this mass-lumping technique, the matrix $\mathbf{A}_K$ is approximated by

$$\mathbf{A}_K = \left[\frac{1}{\mathbf{K}}\int_K \mathbf{w}_{K,E}\cdot\mathbf{w}_{K,E'}\right]_{E,E'} \approx \frac{1}{2\mathbf{K}}\begin{pmatrix} \frac{l_x}{l_y} & 0 & 0 & 0\\ 0 & \frac{l_x}{l_y} & 0 & 0\\ 0 & 0 & \frac{l_y}{l_x} & 0\\ 0 & 0 & 0 & \frac{l_y}{l_x}\end{pmatrix} \tag{55}$$

whose inversion is

$$\mathbf{A}_K^{-1} \approx \mathbf{K}\begin{pmatrix} 2\frac{l_y}{l_x} & 0 & 0 & 0\\ 0 & 2\frac{l_y}{l_x} & 0 & 0\\ 0 & 0 & 2\frac{l_x}{l_y} & 0\\ 0 & 0 & 0 & 2\frac{l_x}{l_y}\end{pmatrix}. \tag{56}$$

Appendix B. Basis functions and details of the discontinuous Galerkin FEM discretization

The basis functions $\varphi_{K,l}$ defined on a reference element $K = (0,l_x)\times(0,l_y)$ read as

$$\varphi_{K,1}(x,y) = 1, \quad \varphi_{K,2}(x,y) = \frac{2}{l_x}\left(x-\frac{l_x}{2}\right), \quad \varphi_{K,3}(x,y) = \frac{2}{l_y}\left(y-\frac{l_y}{2}\right). \tag{57}$$

The weighting factors $cz^l_{i,K}$ $(l = 1,2,3)$ can be then interpreted as the average value of molar concentration over the element K, and differences between the central value and the values at the right and top edges, respectively. The matrix elements appearing in (32) are defined by the following integrals

$$M^K_{j,l} = \int_K \varphi_{K,j}\varphi_{K,l}, \quad M^E_j = \frac{1}{|E|}\int_E \varphi_{K,j},$$
$$M^{K,E}_{j,l} = \int_K \varphi_{K,l}\mathbf{w}_{K,E}\cdot\nabla\varphi_{K,j},$$

where we assume that the phase fluxes fields on the element K can be approximated as

$$\mathbf{q}_{\alpha,K} = \sum_{E\in\partial K} q_{\alpha,K,E}\mathbf{w}_{K,E}$$

using the vector basis functions from the mixed-hybrid finite-elements. The integrals can be readily evaluated to obtain

$$M^K = \left[M^K_{j,l}\right] = \begin{pmatrix} 1 & 0 & 0\\ 0 & \frac{1}{3} & 0\\ 0 & 0 & \frac{1}{3}\end{pmatrix}|K| \tag{58}$$

for matrix M^K. The matrices M^E, where the edges E are denoted by $T,\ B,\ L$, and R (top, bottom, left, and right, respectively), read as

$$M^T = \left[M^T_j\right] = \begin{pmatrix}1\\0\\1\end{pmatrix}, \quad M^B = \left[M^B_j\right] = \begin{pmatrix}1\\0\\-1\end{pmatrix}, \tag{59}$$

$$M^R = \left[M^R_j\right] = \begin{pmatrix}1\\1\\0\end{pmatrix}, \quad M^L = \left[M^L_j\right] = \begin{pmatrix}1\\-1\\0\end{pmatrix}. \tag{60}$$

Using the same notation for the edges, the elements of matrices $M^{K,E}$ are evaluated as

$$M^{K,T} = \left[M^{K,T}_{j,l}\right] = \begin{pmatrix} 0 & 0 & 0 \\ 0 & 0 & 0 \\ 1 & 0 & \frac{1}{3} \end{pmatrix}, \quad M^{K,B} = \left[M^{K,B}_{j,l}\right] = \begin{pmatrix} 0 & 0 & 0 \\ 0 & 0 & 0 \\ -1 & 0 & \frac{1}{3} \end{pmatrix},$$
$$M^{K,R} = \left[M^{K,R}_{j,l}\right] = \begin{pmatrix} 0 & 0 & 0 \\ 1 & \frac{1}{3} & 0 \\ 0 & 0 & 0 \end{pmatrix}, \quad M^{K,L} = \left[M^{K,L}_{j,l}\right] = \begin{pmatrix} 0 & 0 & 0 \\ -1 & \frac{1}{3} & 0 \\ 0 & 0 & 0 \end{pmatrix}. \tag{61}$$

References

[1] R.J. Leveque, Finite volume methods for hyperbolic problems, Cambridge Texts in Applied Mathematics, Cambridge University Press, 2002.
[2] J.E.P. Monteagudo, A. Firoozabadi, Control-volume model for simulation of water injection in fractured media: incorporating matrix heterogeneity and reservoir wettability effects, SPEJ (2007).
[3] H. Hoteit, A. Firoozabadi, Multicomponent fluid flow by discontinuous Galerkin and mixed methods in unfractured and fractured media, Water Resour. Res. 41 (2005) W11412, doi:10.1029/2005WR004339.
[4] H. Hoteit, A. Firoozabadi, Compositional modeling by the combined discontinuous Galerkin and mixed methods, SPEJ (2006).
[5] Z. Chen, B. Cockburn, J.W. Jerome, C.-W. Shu, Mixed-RKDG finite element methods for the 2D hydrodynamic model for semiconductor device simulation, VLSI Des. 3 (2) (1995) 145–158.
[6] G. Ács, S. Doleschall, É. Farkas, General purpose compositional model, SPEJ 25 (4) (1985) 543–553 (SPE-10515-PA).
[7] J. Lohrentz, B. Bary, R. Clark, Calculating viscosities of reservoir fluids from their compositions, J. Pet. Technol. 16 (1964) 1171–1176.
[8] A. Firoozabadi, Thermodynamics of Hydrocarbon Reservoirs, McGraw-Hill, New York, 1999.
[9] D.-Y. Peng, D.B. Robinson, A new two-constant equation of state, Ind. Eng. Chem. Fundam. 15 (1) (1976) 59–64.
[10] B. van Leer, Towards the ultimate conservative difference scheme. I. The quest of monotonicity, Springer Lect. Note Phys. 18 (1973) 163–168.
[11] B. van Leer, Towards the ultimate conservative difference scheme. II. Monotonicity and conservation combined in a second order scheme, J. Comput. Phys. 14 (1974) 361–370.
[12] B. van Leer, Towards the ultimate conservative difference scheme. III. Upstream-centered finite-difference schemes for ideal compressible flow, J. Comput. Phys. 23 (1977) 263–275.
[13] B. van Leer, Towards the ultimate conservative difference scheme. IV. A new approach to numerical convection, J. Comput. Phys. 23 (1977) 276–299.
[14] B. van Leer, Towards the ultimate conservative difference scheme. V. A second order sequel to Godunov's method, J. Comput. Phys. 32 (1979) 101–136.
[15] P.H. Sammon, An analysis of upstream differencing, SPE Reserv. Eng. (1988) 1053–1056.
[16] F. Brezzi, M. Fortin, Mixed and Hybrid Finite Element Methods, Springer, New York, 1991.
[17] P. Raviart, J. Thomas, A mixed hybrid finite element method for the second order elliptic problem, Lect. Note Math. Ser., vol. 606, Springer, New York, 1977.
[18] A. Younes, P. Ackerer, F. Lehmann, A new mass lumping scheme for the mixed hybrid finite element method, Int. J. Numer. Method Eng. 67 (2006) 89–107.
[19] G. Chavent, J.E. Roberts, A unified physical presentation of mixed, mixed-hybrid finite elements and standard finite difference approximations for the determination of velocities in waterflow problems, Adv. Water Resour. 14 (6) (1991) 329–348.
[20] M. Feistauer, J. Felcman, Straškraba, Mathematical and Computational Methods for Compressible Flow, Clarendon Press, Oxford, 2003.

3.3 [Č2]: Mikyška, J., and Firoozabadi, A., A New Thermodynamic Function for Phase-Splitting at Constant Temperature, Moles, and Volume, AIChE Journal, 57(7):1897-1904, 2011

[Č2]: AIChE Journal, 57(7):1897-1904, 2011

AIChE

A New Thermodynamic Function for Phase-Splitting at Constant Temperature, Moles, and Volume

Jiří Mikyška
Dept. of Mathematics, Faculty of Nuclear Sciences and Physical Engineering, Czech Technical University in Prague, Trojanova 13, 120 00 Prague 2, Czech Republic

Abbas Firoozabadi
Yale University, Yale School of Engineering and Applied Science, Dept. of Chemical Engineering & Environmental Science, 9 Hillhouse Avenue, ML 103, New Haven, CT 06511

Reservoir Engineering Research Institute, 595 Lytton Ave., Suite B, Palo Alto, CA 94301

DOI 10.1002/aic.12387
Published online August 31, 2010 in Wiley Online Library (wileyonlinelibrary.com).

We introduce a new thermodynamic function for phase-split computations at constant temperature, moles, and volume. The new volume function F_i introduced in this work is a natural choice under these conditions. Phase equilibrium conditions in terms of the volume functions are derived using the Helmholtz free energy. We present a numerical algorithm to investigate two-phase equilibrium based on the fixed point iteration and Newton method. We demonstrate usefulness and powerful features of the new thermodynamic function for a number of examples in two-phase equilibrium calculations. © 2010 American Institute of Chemical Engineers *AIChE J,* 57: 1897–1904, 2011
Keywords: two-phase equilibrium, constant volume flash, VT-flash, Helmholtz free energy, volume function

Introduction

Consider a closed system of constant volume V in which there is a mixture of c components with mole numbers $n_1,\ldots,n_c$ at temperature T. Assuming that the system is in two-phase, we want to establish compositions and amounts of both phases. This is the problem of two-phase phase-split (the so called flash) under the constant temperature, moles, and volume (VT-flash). The motivation for constant volume flash is the equilibrium calculation in a PVT cell in two-phase when two nonequilibrium phases are introduced.[1,2] These cells are used to determine diffusion coefficients in both phases in two-phase state. We have found out that the use of conventional methods is based on ad hoc approaches.

Correspondence concerning this article should be addressed to A. Firoozabadi at abbas.firoozabadi@yale.edu.

The standard problem of constant pressure and temperature (PT-flash) is addressed in many references.[3–6] In this approach, pressure, temperature, and overall chemical composition are given. The phase compositions and molar densities are computed using the minimization of the Gibbs energy. This approach has the shortcoming that it cannot provide an answer when a single component is in two-phase region at temperature T and saturation pressure $P = P^{\text{sat}}(T)$ because the chemical potentials of the component in both phases are the same. Therefore, we cannot determine whether the component at these specific conditions is vapor or liquid or a mixture of both. Althought P and T are the most preferred variables in chemical engineering, we see that specifying pressure and temperature is not sufficient for the unique determination of the state of the system in this case.

The issue can be resolved by reformulating the problem using the minimization of the Helmholtz free energy rather than Gibbs free energy. In this formulation, the volume of

the system, mole numbers, and temperature are given, and the chemical compositions, molar densities of the phases, and pressure in the mixture are computed. The selection of variables V, T, and n_i, ($i \in \{1,\ldots,c\}$) is natural for pressure-explicit equations of state. Unlike in PT-flash, the VT-flash provides a unique answer in any physically admissible situation because when V is known, P can be evaluated readily from say a cubic equation of state. Therefore, we develop a new "volume-based" formulation of equilibrium thermodynamics. The presented derivations lead to a new function F_i, called volume function that plays an analogous role to fugacity that is used in the pressure-based formulation. We present all derivations in details to show that this approach is much more fit for the pressure-explicit equations of state than the standart development using the Gibbs free energy that suffers from the nonuniqueness of volume at given pressure.

A theoretical possibility of other state function-based flash specification (including VT-flash) is mentioned in Refs. 6 and 7, where a nested optimization approach is proposed. This means that in an outer loop we search iteratively for pressure, which is used in PT-flash in the inner loop to evaluate equilibrium state at that pressure. The goal of the iterations is to find a pressure for which the volume constraint is satisfied. This procedure allows to use existing implementations of the PT-flash but, on the other hand, is computationally expensive as it requires many solutions of PT-flashes before the true pressure is found. In this article, we offer an alternative formulation allowing to formulate VT-flash directly without using nested iterations.

The article is structured as follows. In the first section, we introduce the new thermodynamic volume function F_i of variables V, T, and n_i that will be useful in describing thermodynamic behavior of real mixtures under the constant temperature, volume, and moles. Then, we develop an expression for the chemical potential of a component in a mixture in terms of this new function. We reformulate the two-phase equilibrium conditions at constant temperature, volume, and moles using F_i. Next, we propose a numerical algorithm for computation of VT-flash, and, finally, we present examples showing results of phase-equilibrium computations based on the new formulation for a number of mixtures in two-phase state.

Volume Function Coefficient

We will introduce a new thermodynamic volume function that will be useful to derive basic expressions for the chemical potential of a component in a multicomponent mixture from the bulk phase equilibrium thermodynamics. Our derivation will be based on Helmholtz free energy and will use volume, temperature, and moles as primary variables.

Assuming a pressure-explicit equation of state, it is convenient to describe the system using the Helmholtz free energy $A = A(V,T,n_1,\ldots,n_c)$. The general expression for the Helmholtz free energy of a bulk phase is given by

$$A = -PV + \sum_{i=1}^{c} n_i \mu_i, \tag{1}$$

where $P = P(V,T,n_1,\ldots,n_c)$ is the pressure given by an equation of state, and $\mu_i = \mu_i(V,T,n_1,\ldots,n_c)$ is the chemical potential of the i-th component in the mixture. From

Algorithm: Two-Phase VT-Flash Using Fixed Point Iteration

1. Let c, $z_1,\ldots z_c$, and $T > 0$ be given. Evaluate $P_0 = P(1/c,T,z_1,\ldots,z_c)$, initialize K_i's using Wilson correlation,[8] i.e.

$$\ln K_i = 5.37(1+\omega_i)\left[1 - \frac{T_{ci}}{T}\right] + \ln\frac{P_{ci}}{P_0}$$

at the initial pressure P_0 and set the number of iterations, $n = 0$.

2. Evaluate $\alpha \in (0;1)$ by solving the Rachford-Rice equation

$$\sum_{i=1}^{c} \frac{(K_i^n - 1)z_i}{1 + (K_i^n - 1)\alpha} = 0,$$

that can be solved, e.g., by Newton's method.

3. Update chemical compositions of both phases by

$$x'_{i,n+1} = \frac{z_i}{1 + (K_i^n - 1)\alpha}, \quad x''_{i,n+1} = \frac{z_i K_i^n}{1 + (K_i^n - 1)\alpha},$$

4. Use bisection or other method to find $S''_{n+1} \in (0;1)$ satisfying

$$P\left(\frac{1 - S''_{n+1}}{c(1-\alpha)}, T, x'_{1,n+1}, \ldots, x'_{c,n+1}\right) = P\left(\frac{S''_{n+1}}{c\alpha}, T, x''_{1,n+1}, \ldots, x''_{c,n+1}\right),$$

and update the other saturation and molar concentrations by

$$S'_{n+1} = 1 - S''_{n+1}, \quad c'_{n+1} = \frac{c(1-\alpha)}{1 - S''_{n+1}}, \quad c''_{n+1} = \frac{c\alpha}{S''_{n+1}}.$$

5. Update K_i values by

$$K_i^{n+1} = \frac{c'_{n+1}\Phi_i(1,T,c''_{n+1}x''_{1,n+1},\ldots,c''_{n+1}x''_{c,n+1})}{c''_{n+1}\Phi_i(1,T,c'_n x'_{1,n+1},\ldots,c'_n x'_{c,n+1})}.$$

6. Check for convergence. If needed, increase n by one and go to step 2.

$$dA = -SdT - PdV + \sum_{i=1}^{c} \mu_i dn_i,$$

we see that

$$P = -\frac{\partial A}{\partial V}, \qquad \mu_i = \frac{\partial A}{\partial n_i}. \tag{2}$$

Assuming that A is a smooth function of its variables, the mixed second-order derivatives must be interchangeable, which implies

$$\frac{\partial \mu_i}{\partial V} = -\frac{\partial P}{\partial n_i}, \tag{3}$$

with appropriate variables held constant. Integrating (3) between two volumes V_1 and V_2, we derive the following expression describing the change of chemical potential with volume at constant temperature and moles

$$\mu_i(V_2,T,n_1,\ldots,n_c) = \mu_i(V_1,T,n_1,\ldots,n_c) - \int_{V_1}^{V_2} \frac{\partial P}{\partial n_i}(V,T,n_1,\ldots,n_c)dV. \tag{4}$$

For an ideal gas mixture, the equation of state

$$P = \frac{nRT}{V}, \quad \text{where } n = \sum_{i=1}^{c} n_i$$

can be integrated using (4) to yield

$$\mu_i(V_2, T, n_1, \ldots, n_c) = \mu_i(V_1, T, n_1, \ldots, n_c) - RT \ln \frac{V_2}{V_1}. \quad (5)$$

For real mixtures a more general equation than (5) must be used. To simplify our derivations, it is convenient to have a similar form of the expression for the chemical potential of a component in a real mixture as in the ideal case. For this purpose, we introduce the volume function of i-th component $F_i = F_i(V,T,n_1, \ldots,n_c)$ by the following properties

$$\mu_i(V_2, T, n_1, \ldots, n_c) = \mu_i(V_1, T, n_1, \ldots, n_c) - RT \ln \frac{F_i(V_2, T, n_1, \ldots, n_c)}{F_i(V_1, T, n_1, \ldots, n_c)}, \quad (6)$$

and

$$\lim_{V \to +\infty} \frac{F_i(V, T, n_1, \ldots, n_c)}{V} = 1. \quad (7)$$

Furthermore, we define the volume function coefficient by

$$\Phi_i(V, T, n_1, \ldots, n_c) = \frac{F_i(V, T, n_1, \ldots, n_c)}{V}. \quad (8)$$

Equation 7 then amounts to saying that $\lim_{V \to +\infty} \Phi_i(V,T,n_1,\ldots,n_c) = 1$ for given temperature and moles. The volume function F_i and volume function coefficient Φ_i play analogous roles to fugacity and fugacity coefficients. Comparing (6) with (4), we have

$$RT \ln \frac{F_i(V_2, T, n_1, \ldots, n_c)}{F_i(V_1, T, n_1, \ldots, n_c)} = \int_{V_1}^{V_2} \frac{\partial P}{\partial n_i}(V, T, n_1, \ldots, n_c) dV.$$

Setting $V_1 = V$, the last equation can be rearranged to

$$\ln \frac{F_i(V, T, n_1, \ldots, n_c)}{V} \frac{V}{V_2} \frac{V_2}{F_i(V_2, T, n_1, \ldots, n_c)} = -\frac{1}{RT} \int_{V}^{V_2} \frac{\partial P}{\partial n_i}(V, T, n_1, \ldots, n_c) dV.$$

The above equation can be written as

$$\ln \frac{F_i(V, T, n_1, \ldots, n_c)}{V} = \int_{V}^{V_2} \left[\frac{1}{V} - \frac{1}{RT} \frac{\partial P}{\partial n_i}(V, T, n_1, \ldots, n_c) \right] dV + \ln \frac{F_i(V_2, T, n_1, \ldots, n_c)}{V_2}.$$

Passing $V_2 \to +\infty$, the last term on the right hand side vanishes because of (7), which yields

$$\ln \Phi_i(V, T, n_1, \ldots, n_c) = \int_{V}^{+\infty} \left[\frac{1}{V} - \frac{1}{RT} \frac{\partial P}{\partial n_i}(V, T, n_1, \ldots, n_c) \right] dV. \quad (9)$$

The integral on the right hand side can be evaluated analytically using an equation of state. It follows from (9) that for an ideal gas $F_i(V,T,n_1,\ldots,n_c) = V$, and $\Phi_i(V,T,n_1,\ldots,n_c) = 1$ for any given temperature, moles, and volume. Thus, the volume function coefficient can indicate the degree of nonideality of a component in the mixture. These properties are "volume-based" counterparts of analogous properties of the fugacity and fugacity coefficients with respect to pressure.

Comparing the integral on the right hand side of (9) with the formula for fugacity coefficients found in literature (see e.g., Ref. 3), we note that the relationship between the volume function coefficient and the fugacity coefficient is

$$\Phi_i = \frac{1}{Z\varphi_i},$$

where φ_i denotes the conventional fugacity coefficient and Z is the phase compressibility factor. Z and φ_i must now be expressed in terms of volume, temperature, and moles. In the literature, the Z and φ_i are usually understood as functions of P, T, and composition. However, when Z and φ are to be evaluated for given P, T, and moles, one has to solve the cubic equation to get volume, which may not be unique, and in that case, one has to select one of the roots based on the Gibbs free energy criteria or other methods. In this article, we present an alternative formulation, which uses the volume function coefficients rather than fugacity coefficients. In this formulation, the root-selection problems do not appear because all functions are expressed in terms of volume, temperature, and moles.

The formula for the volume function coefficient Φ_i for the Peng-Robinson equation[9] is presented in the Appendix.

Chemical Potential of a Component in a Real Mixture

In the new framework, we describe the dependency of the chemical potential of a component in a real mixture to the chemical potential in a pure substance. An ideal mixture is the one which obeys

$$\mu_i(V, T, n_1, \ldots, n_c) = \mu_i(V, T, 0, \ldots, 0, n_i, 0, \ldots, 0).$$

To simplify the notation, we will denote the chemical potential of the pure substance i as

$$\mu_i^*(V, T, n_i) = \mu_i(V, T, 0, \ldots, 0, n_i, 0, \ldots, 0),$$

and the volume function in the pure component as

$$F_i^*(V, T, n_i) = F_i(V, T, 0, \ldots, 0, n_i, 0, \ldots, 0).$$

Equation 6 can be written for the mixture as well as for the pure component

$$\mu_i(V,T,n_1,\ldots,n_c) = \mu_i(V_1,T,n_1,\ldots,n_c) - RT\ln\frac{F_i(V,T,n_1,\ldots,n_c)}{F_i(V_1,T,n_1,\ldots,n_c)},$$
$$\mu_i^*(V,T,n_i) = \mu_i^*(V_1,T,n_i) - RT\ln\frac{F_i^*(V,T,n_i)}{F_i^*(V_1,T,n_i)}.$$

Subtracting the second expression from the first above,

$$\mu_i(V,T,n_1,\ldots,n_c) - \mu_i^*(V,T,n_i) = \mu_i(V_1,T,n_1,\ldots,n_c) - \mu_i^*(V_1,T,n_i) - RT\ln\frac{F_i(V,T,n_1,\ldots,n_c)}{F_i(V_1,T,n_1,\ldots,n_c)} - RT\ln\frac{F_i^*(V_1,T,n_i)}{F_i^*(V,T,n_i)}.$$

If the volume V_1 is sufficiently large, the mixture at volume V_1 behaves ideally. Passing $V_1 \to +\infty$, one can derive

$$\mu_i(V,T,n_1,\ldots,n_c) = \mu_i^*(V,T,n_i) - RT\ln\frac{F_i(V,T,n_1,\ldots,n_c)}{F_i^*(V,T,n_i)}. \quad (10)$$

Let us assume that we have a mixture at two states (V',T,n_1', …,n_c') and (V'',T,n_1'',…,n_c''). Our goal is to express the difference of chemical potentials between these two states in terms of the volume functions. Using (10), we derive

$$\mu_i(V',T,n_1',\ldots,n_c') - \mu_i(V'',T,n_1'',\ldots,n_c'') = \mu_i^*(V',T,n_i') - \mu_i^*(V'',T,n_i'') - RT\ln\frac{F_i(V',T,n_1',\ldots,n_c')}{F_i(V'',T,n_1'',\ldots,n_c'')} + RT\ln\frac{F_i^*(V',T,n_i')}{F_i^*(V'',T,n_i'')}.$$

The first two terms on the right hand side can be rewritten as

$$\mu_i^*(V',T,n_i') - \mu_i^*(V'',T,n_i'') = \mu_i^*(V'/n_i',T,1) - \mu_i^*(V''/n_i'',T,1) = -RT\ln\frac{F_i^*(V',T,n_i')}{F_i^*(V'',T,n_i'')}\frac{n_i''}{n_i'},$$

where we take advantage of the fact that the chemical potential is a homogeneous function of order zero and the volume function is a homogeneous function of order one in the volume and moles. Combining the last two equations, we obtain the following key expression for the difference of chemical potentials at two different states written in terms of the volume functions

$$\mu_i(V',T,n_1',\ldots,n_c') - \mu_i(V'',T,n_1'',\ldots,n_c'') = -RT\ln\frac{n_i''}{n_i'}\frac{F_i(V',T,n_1',\ldots,n_c')}{F_i(V'',T,n_1'',\ldots,n_c'')}. \quad (11)$$

Conditions for Two-Phase Equilibrium

Consider a mixture of c components with mole numbers n_1,…,n_c occupying volume V at temperature T. Assuming that the mixture will split into two phases, we want to calculate volumes V' and V'', and mole numbers of each component in each phase n_i' and n_i'' for $i = 1,\ldots,c$, and consequently the pressure. The equilibrium state is derived from the minimization of the total Helmholtz energy of the mixture

$$A = A(V',T,n_1',\ldots,n_c') + A(V'',T,n_1'',\ldots,n_c''),$$

which is subject to the following constraints

$$V' + V'' = V, \quad (12)$$

and

$$n_i' + n_i'' = n_i, \qquad i = 1,\ldots,c. \quad (13)$$

Using the Lagrange multiplier method, one can find the necessary conditions of the phase equilibria

$$P(V',T,n_1',\ldots,n_c') = P(V'',T,n_1'',\ldots,n_c''), \quad (14)$$

and

$$\mu_i(V',T,n_1',\ldots,n_c') = \mu_i(V'',T,n_1'',\ldots,n_c''), \qquad i = 1,\ldots,c, \quad (15)$$

as expected. An equivalent expression of (15) in terms of the volume functions reads as

$$\frac{n_i'}{F_i(V',T,n_1',\ldots,n_c')} = \frac{n_i''}{F_i(V'',T,n_1'',\ldots,n_c'')}. \quad (16)$$

Numerical Algorithm for Two-Phase Flash Computation

In two-phase, we are interested to calculate phase compositions, amounts, and also the pressure of the system. Let us rewrite the two-phase flash Eqs. 12–15 in terms of concentrations and compositions of both phases. We introduce the overall molar concentration $c = n/V$, the phase molar concentrations $c' = n'/V'$ and $c'' = n''/V''$, overall mole fractions $z_i = n_i/n$, and phase mole fractions $x_i' = n_i'/n'$ and $x_i'' = n_i''/n''$, and phase volume fractions $S' = V'/V$, and $S'' = V''/V$, respectively. Using this notation, Eq. 12 transforms to

$$S' + S'' = 1, \quad (17)$$

whereas the mole balance Eq. 13 can be rewritten as

$$c'x_i'S' + c''x_i''S'' = cz_i, \qquad i = 1,\ldots,c. \quad (18)$$

As pressure is an intensive property (homogeneous function of order zero in variables V,n_1,…, n_c), Eq. 14 yields

$$P(1,T,c'x_1',\ldots,c'x_c') = P(1,T,c''x_1'',\ldots,c''x_c''). \quad (19)$$

Finally, the chemical equilibrium Eq. 16 can be written in terms of the volume function coefficients using (11) as

$$\frac{c'x_i'}{\Phi_i(1,T,c'x_1',\ldots,c'x_c')} = \frac{c''x_i''}{\Phi_i(1,T,c''x_1'',\ldots,c''x_c'')}. \quad (20)$$

To solve these equations using the fixed point iteration (also called succesive substitution iteration, SSI), it is convenient to introduce the K_i values by

$$K_i = \frac{x_i''}{x_i'}. \quad (21)$$

From (21) it follows that $x_i'' = K_ix_i'$, which can be substituted into (18) to obtain

Table 1. Properties of the Components for the C_1–nC_5 Mixture Used in Examples 1 and 2

Component	ω_i [−]	T_{crit} [K]	P_{crit} [MPa]	M_w [g mol^{-1}]
C_1	0.011	190.56	4.599	16
nC_5	0.251	469.70	3.37	72.2

The C_1–nC_5 binary interaction coefficient is δ_{C1}–$_{nC5} = 0.041$.

$$x_i' = \frac{z_i}{1+(K_i-1)\alpha}, \qquad x_i'' = \frac{z_i K_i}{1+(K_i-1)\alpha}, \tag{22}$$

where $\alpha = c''S''/c$ is the mole fraction of the double-primed phase. These equations can be used to evaluate phase compositions provided that K_i and α are given. As compositions of both phases in (22) should sum to one, for a given set of K_i values, α can be updated by solving the Rachford-Rice equation[10]

$$\sum_{i=1}^{c}(x_i'' - x_i') = \sum_{i=1}^{c}\frac{(K_i-1)z_i}{1+(K_i-1)\alpha} = 0. \tag{23}$$

Once α and chemical composition of both phases are established, phase molar concentrations and saturations must be determined so that the pressures in both phases are the same. The following system of four equations

$$\begin{gathered} c'S' = c(1-\alpha), \\ c''S'' = c\alpha, \\ S' + S'' = 1, \\ P\left(\tfrac{1}{c'}, T, x_1', \ldots, x_c'\right) = P\left(\tfrac{1}{c''}, T, x_1'', \ldots, x_c''\right), \end{gathered}$$

for the 4 unknowns (c', c'', S'', and S'') can be readily reduced into a single equation for one unknown saturation $S'' \in (0;1)$

$$P\left(\frac{1-S''}{c(1-\alpha)}, T, x_1', \ldots, x_c'\right) = P\left(\frac{S''}{c\alpha}, T, x_1'', \ldots, x_c''\right). \tag{24}$$

For a cubic equation of state, Eq. 24 is an algebraic equation of the fifth order. In theory it may have up to five real roots. In all examples we examined, there was always only one root in the interval (0;1), which could be readily approximated using the bisection method. Other methods, like the Newton method, can be used as well.

Finally, K_i values are updated using (20) as

$$K_i = \frac{x_i''}{x_i'} = \frac{c'\Phi_i\left(1/c'', T, x_1'', \ldots, x_c''\right)}{c''\Phi_i\left(1/c', T, x_1', \ldots, x_c'\right)}.$$

The key steps of the method are summarized in the Algorithm.

Table 2. Overall Properties of the Mixture and Resulting Phase Properties in Two-Phase Flash at Constant Temperature T = 371 K and Volume for Example 1

Property	Unit	Overall mixture	Phase 1	Phase 2
Molar concentration	mol m^{-3}	6307.21	8616.72	4307.03
C_1 mole fraction	–	0.547413	0.388095	0.823458
nC_5 mole fraction	–	0.452587	0.611905	0.176542
Phase volume fraction	–		0.464113	0.535887

Table 3. Overall Properties of the Mixture and Resulting Phase Properties in Two-Phase Flash at Constant Temperature T = 310.95 K and Volume for Example 2

Property	Unit	Overall mixture	Phase 1	Phase 2
Molar concentration	mol m^{-3}	6135.3	10105.5	3177.77
C_1 mole fraction	–	0.489575	0.293471	0.954131
nC_5 mole fraction	–	0.510425	0.706529	0.0458693
Phase volume fraction	–		0.42691	0.57309

The iterations are stopped whenever

$$\max_{i\in\{1,\ldots,c\}}\left|\ln K_i^{n+1} - \ln K_i^{n}\right| < tol = 10^{-12}.$$

Numerical Examples

We have tested the algorithm in several examples of binary and multicomponent mixtures in two-phase. Below we show performance of the method for two binary mixtures and one four-component mixture. Further, we provide two more-complex phase-split computations for a multicomponent reservoir fluid. All examples are motivated by experiments in the PVT cells. In these experiments, the total volume is fixed. A part of this volume is filled by a liquid at some initial pressure P_{ini}. The rest of the volume is filled by a gas at the same initial pressure. When the two fluids are mixed, the pressure changes. The final equilibrium pressure P of the system after mixing results from the VT-flash computation. The correctness of the VT-flash results is checked by performing the PT-flash at the final pressure with the same overall composition and temperature. The agreement was excellent in all cases.

Example 1

In the first example, we investigate two-phase equilibrium for a binary mixture of methane (C_1) and *n*-penthane (nC_5) of total concentration c = 6307.21 mol m^{-3}, with mole fractions z_{C_1} = 0.547413 and z_{nC_5} = 0.452587 at temperature T = 371 K. The condition corresponds to the PVT-cell experiment in which C_1 (34.4% of volume) is placed on the top of nC_5 at the initial pressure P_{ini} = 15 MPa. Parameters of the Peng-Robinson equation of state are presented in Table 1. The algorithm found a solution in 46 iterations. Within each iteration the Rachford-Rice, Eq. 23, was solved by Newton's method with the initial guess α = 0.5. The resulting pressure is P = 10.4653 MPa. The overall mixture and phase-split results are summarized in Table 2. The results were verified by the PT-flash computation performed at the final pressure with the same overall composition and temperature. The PT-flash converged in 45 iterations.

Table 4. Properties of the Components for the Four-Component Mixture Used in Example 3

Component	ω_i [−]	T_{crit} [K]	P_{crit} [MPa]	M_w [g mol^{-1}]
N_2	0.039	126.21	3.39	28
C_1	0.011	190.56	4.599	16
C_3	0.153	369.83	4.248	44.1
nC_{10}	0.489	617.70	2.110	142.3

Table 5. Binary Interaction Coefficients for the Four-Component Mixture Used in Example 3

Component	N_2	C_1	C_3	nC_{10}
N_2	0	0.1	0.1	0.1
C_1	0.1	0	0.036	0.052
C_3	0.1	0.036	0	0
nC_{10}	0.1	0.052	0	0

Example 2

In this example, we compute two-phase equilibrium for a mixture of methane (C_1) and *n*-penthane (nC_5) of total concentration $c = 6135.3$ mol m^{-3}, with mole fractions $z_{C_1} = 0.489575$ and $z_{nC_5} = 0.510425$ at temperature $T = 310.95$ K. The condition corresponds to the PVT-cell experiment in which C_1 (65% of volume) is placed on the top of nC_5 at the initial pressure $P_{ini} = 10.2$ MPa. Parameters of the Peng-Robinson equation of state are presented in Table 1. The algorithm found a solution in 20 iterations. The resulting pressure is $P = 6.95477$ MPa. The overall mixture and split-phase results are summarized in Table 3. The agreement with the PT-flash at the final pressure is excellent. The PT-flash converged in 19 iterations.

Example 3

In Example 3, we compute two-phase equilibrium for a four-component mixture of nitrogen (N_2), methane (C_1), propane (C_3), and *n*-decane (nC_{10}) at temperature $T = 393.15$ K. Here, nitrogen (35% of volume) is placed on the top of a four-component mixture ($z_{N_2} = 0.01$, $z_{C_1} = 0.29$, $z_{C_3} = 0.29$, and $z_{nC_{10}} = 0.41$) at the initial pressure 13.73 MPa. Parameters of the Peng-Robinson equation of state are presented in Tables 4 and 5. The overall molar concentration and overall mole fractions of all components are shown in Table 6. The algorithm found a solution in 25 iterations. The resulting pressure is $P = 14.9502$ MPa. Note the pressure increase due to vaporization. The overall mixture and split-phase results are summarized in Table 6. The results agree with those obtained using the PT-flash at the final pressure. The PT-flash converged in 25 iterations.

Example 4

In Example 4, we compute two two-phase equilibria for a multicomponent oil mixed with nitrogen (N_2), and carbon dioxide (CO_2). The oil is modelled using seven components. The composition of the oil and parameters of the Peng-Robinson equation of state are presented in Tables 7 and 8. The pseudocomponents are defined as PC_1 ($H_2S + C_2 + C_3$), PC_2 (C_4–C_6), and PC_3 (C_7–C_{11}). In both experiments, 50% of volume of the PVT cell is filled by this oil. The initial pressure $P_{ini} = 30.34$ MPa, and the temperature is $T = 413.71$ K. Under these conditions, the oil is in single phase with molar concentration $c_{oil} = 8944.22$ mol m^{-3}. The remaining 50% of volume is filled with either N_2 or CO_2 at the same initial pressure. Addition of gas turns the system into two phase in both cases.

Table 6. Overall Properties of the Mixture and Resulting Phase Properties in Two-Phase Flash at Constant Temperature $T = 393.15$ K and Volume for Example 3

Property	Unit	Overall mixture	Phase 1	Phase 2
Molar concentration	mol m^{-3}	5912.74	6690.98	4795.04
N_2 mole fraction	–	0.2463	0.12944	0.48049
C_1 mole fraction	–	0.2208	0.15509	0.35248
C_3 mole fraction	–	0.2208	0.25349	0.15529
nC_{10} mole fraction	–	0.3121	0.46198	0.01173
Phase volume fraction	–		0.58952	0.41048

Table 7. Composition and Properties of the Components for the Reservoir Fluid Used in Example 4

Component	z_i	ω_i [−]	T_{crit} [K]	P_{crit} [MPa]	M_w [g mol^{-1}]
N_2	0.0003	0.0390	126.21	3.390	28.0
CO_2	0.0140	0.2390	304.14	7.375	44.0
C_1	0.5634	0.0110	190.56	4.599	16.0
PC_1	0.1970	0.1113	333.91	5.329	34.64
PC_2	0.0770	0.2344	456.25	3.445	69.52
PC_3	0.0845	0.4470	590.76	2.376	124.57
C_{12+}	0.0638	0.9125	742.58	1.341	248.30

For the case of N_2, the overall properties of the resulting mixture and phase-split results are summarized in Table 9. The final pressure is $P = 32.66$ MPa. The algorithm found a solution in 33 iterations. The results agree with those obtained using the PT-flash at the final pressure. The PT-flash converged in 34 iterations. Some of the K_i-values in Table 9 are very different from one; the system is far from the critical point.

For the case of CO_2, the overall properties of the resulting mixture and split-phase results are summarized in Table 10. The final pressure is $P = 31.27$ MPa. The algorithm found a solution in 266 iterations. The results agree with those obtained using the PT-flash at the final pressure. The PT-flash converged in 254 iterations. The K_i-values in Table 10 are closer to one. Unlike in the previous case, the mixture is near-critical, which explains the increased number of iterations that are needed to converge using the fixed point iteration method.

Summary and Conclusions

In this work, we have introduced a new thermodynamic function to describe two-phase equilibrium at constant temperature, volume, and moles. The new volume function coefficient replaces the fugacity coefficients that are used in common formulations of two-phase equilibrium at constant temperature and pressure. Unlike the conventional approach, our method can determine uniquely the equilibrium state of a pure substance in two-phase state. The volume-based formulation of two-phase equilibrium in terms of the volume function coefficients has been derived for the Peng-Robinson

Table 8. Binary Interaction Coefficients for the Reservoir Fluid Used in Example 4

Component	N_2	CO_2	C_1	PC_1	PC_2	PC_3	C_{12+}
N_2	0.000	0.000	0.100	0.100	0.100	0.100	0.100
CO_2	0.000	0.000	0.150	0.150	0.150	0.150	0.150
C_1	0.100	0.150	0.000	0.035	0.040	0.049	0.069
PC_1	0.100	0.150	0.035	0.000	0.000	0.000	0.000
PC_2	0.100	0.150	0.040	0.000	0.000	0.000	0.000
PC_3	0.100	0.150	0.049	0.000	0.000	0.000	0.000
C_{12+}	0.100	0.150	0.069	0.000	0.000	0.000	0.000

Table 9. Overall Properties of the Mixture of the Reservoir Fluid from Table 7 (50% of volume) with N_2 at the Initial Pressure P_{ini} = 30.34 MPa and Resulting Phase Properties in Two-Phase Flash at Constant Temperature T = 413.71 K and Volume (Example 4)

Property	Unit	Overall mixture	Phase 1	Phase 2	K_i-values
Molar concentration	mol m^{-3}	8386.44	6877.62	8863.05	
N_2 mole fraction	–	0.466905	0.243471	0.521675	2.14266
CO_2 mole fraction	–	0.007466	0.006159	0.007786	1.26421
C_1 mole fraction	–	0.300435	0.210766	0.322416	1.52973
PC_1 mole fraction	–	0.105051	0.130065	0.098920	0.76054
PC_2 mole fraction	–	0.041061	0.084767	0.030347	0.35801
PC_3 mole fraction	–	0.045060	0.158289	0.017305	0.10932
C_{12+} mole fraction	–	0.034021	0.166484	0.001551	0.00932
Phase volume fraction	–		0.240057	0.759942	

The final pressure is P = 32.66 MPa.

Table 10. Overall Properties of the Mixture of the Reservoir Fluid from Table 7 (50% of volume) with CO_2 at the Initial Pressure P_{ini} = 30.34 MPa and Resulting Phase Properties in Two-Phase Flash at Constant Temperature T = 413.71 K and Volume (Example 4)

Property	Unit	Overall mixture	Phase 1	Phase 2	K_i-values
Molar concentration	mol m^{-3}	10211.55	9168.51	10335.60	
N_2 mole fraction	–	0.000131	0.000103	0.000134	1.303750
CO_2 mole fraction	–	0.568185	0.504174	0.574938	1.140360
C_1 mole fraction	–	0.246739	0.214535	0.250136	1.165950
PC_1 mole fraction	–	0.086275	0.091552	0.085719	0.936288
PC_2 mole fraction	–	0.033722	0.043366	0.032704	0.754150
PC_3 mole fraction	–	0.037006	0.063680	0.034192	0.536942
C_{12+} mole fraction	–	0.027941	0.082591	0.022175	0.268497
Phase volume fraction	–		0.106291	0.893709	

The final pressure is P = 31.27 MPa.

equation of state, but the same concept can be used for other pressure-explicit equations of state as well.

We proposed a numerical algorithm for computation of the phase-split properties, which is based on a combination of the fixed point outer iteration and Newton's method in the inner iteration. To show efficiency of this approach we have performed results of numerical computations of multicomponent mixtures of different complexity. The results indicate that to achieve the same accuracy, the number of iterations of the VT-flash method based on the fixed point iteration is about the same as when using the PT-flash under the same physical conditions. As the final pressure is not known a priori when the volume is constant, the computation of VT-flash using the PT-flash combined with outer iterations, as suggested Refs. 6 and in 7, is necessarily inefficient. Our method provides the correct solution in practically the same number of iterations as one run of the PT-flash at the final pressure.

Acknowledgments

The work was supported by the member companies of the Reservoir Engineering Research Institute, and by the project Mathematical Modelling of Multi-Phase Porous Media Flow 201/08/P567 of the Czech Science Foundation.

Literature Cited

1. Haugen K, Firoozabadi A. Composition at the Interface between multicomponent non-equilibrium phases. *J Chem Phys*. 2009;130: 064707,1–9.
2. Haugen K, Firoozabadi A. Mixing of two nonequilibrium phases in one dimension. *AIChE J*. 2009;55:1930–1936.
3. Firoozabadi A. *Thermodynamics of Hydrocarbon Reservoirs*. New York: McGraw-Hill, 1999.
4. Michelsen ML. The isothermal flash problem. 1. Stability. *Fluid Phase Equilibria*. 1982;9:1–19.
5. Michelsen ML. The isothermal flash problem. 2. Phase-split computation. *Fluid Phase Equilibria*. 1982;9:21–40.
6. Michelsen ML, Mollerup JM. *Thermodynamic Models: Fundamentals and Computational Aspects*. Holte, Denmark: Tie-Line Publications, 2004.
7. Michelsen ML. State function based flash specifications. *Fluid Phase Equilibria*. 1999;158:617–626.
8. Wilson GM. A Modified Redlich-Kwong Equation of State, Application to General Physical Data Calculation, paper No. 15C presented at the 1969 AIChE 65th National Meeting, Cleveland, Ohio, May 4–7, 1969.
9. Peng DE, Robinson DB. A new two-constant equation of state. *Ind Eng Chem Fund*. 1976;15:59–64.
10. Rachford HH, Rice JD. Procedure for use of electronic digital computers in calculating flash vaporization hydrocarbon equilibrium. *Trans Am Institute Mining Metallurg Eng*. 1952;195:327–328.

Appendix: Volume Function Coefficient for Peng-Robinson Equation of State

In this work, we use the Peng-Robinson equation of state[9] in the form

$$P(V,T,n_1,\ldots,n_c) = \frac{nRT}{V-B} - \frac{A}{V^2+2BV-B^2},$$

where R is the universal gas constant, $n = \sum_{i=1}^{c} n_i$ is the total number of moles, and coefficients A and B are given by

$$A=\sum_{i=1}^{c}\sum_{j=1}^{c}n_i n_j a_{ij}, \qquad B=\sum_{i=1}^{c}n_i b_i$$

$$a_{ij}=(1-\delta_{ij})\sqrt{a_i a_j}, \qquad b_i=0.0778\frac{RT_{i,\mathrm{crit}}}{P_{i,\mathrm{crit}}}$$

$$a_i=0.45724\frac{R^2T_{i,\mathrm{crit}}^2}{P_{i,\mathrm{crit}}}\left[1+m_i\left(1-\sqrt{T_r}\right)\right]^2,$$

$$m_i=\begin{cases}0.37464+1.54226\omega_i-0.26992\omega_i^2, & \text{for } \omega_i<0.5,\\ 0.3796+1.485\omega_i-0.1644\omega_i^2+0.01667\omega_i^3 & \text{for } \omega_i\geq 0.5.\end{cases}$$

In these equations, δ_{ij} denotes the binary interaction parameter between the components i and j, $T_{i,\mathrm{crit}}$, $P_{i,\mathrm{crit}}$, and ω_i are the critical temperature, critical pressure, and accentric factor of the i-th component, respectively. The volume function coefficient for the Peng-Robinson equation of state can be found analytically using (9) as

$$\ln\Phi_i=\ln\frac{V-B}{V}-\frac{b_i n}{V-B}+\frac{Ab_i}{BRT}\frac{V}{V^2+2BV-B^2}-\frac{1}{\sqrt{2}BRT}\left[\frac{Ab_i}{2B}-\sum_{j=1}^{c}n_j a_{ij}\right]\ln\left|\frac{V+(1+\sqrt{2})B}{V+(1-\sqrt{2})B}\right|.$$

Manuscript received Apr. 8, 2010, and revision received July 4, 2010.

3.4 [Č3]: Mikyška, J., and Firoozabadi, A., Investigation of Mixture Stability at Given Volume, Temperature, and Number of Moles, Fluid Phase Equilibria, Vol. 321 (May 15, 2012), pp. 1–9, 2012

Fluid Phase Equilibria 321 (2012) 1–9

Contents lists available at SciVerse ScienceDirect

Fluid Phase Equilibria

journal homepage: www.elsevier.com/locate/fluid

Investigation of mixture stability at given volume, temperature, and number of moles

Jiří Mikyška [a], Abbas Firoozabadi [b,c,*]

[a] Czech Technical University in Prague, Faculty of Nuclear Sciences and Physical Engineering, Department of Mathematics, Trojanova 13, 120 00 Prague 2, Czech Republic
[b] Yale University, 9 Hillhouse Avenue, ML 103, New Haven, CT 06511, USA
[c] Reservoir Engineering Research Institute, 595 Lytton Ave., Suite B, Palo Alto, CA 94301, USA

ARTICLE INFO

Article history:
Received 14 November 2011
Received in revised form 23 January 2012
Accepted 25 January 2012
Available online 16 February 2012

Keywords:
Two-phase stability
Constant volume stability
VT-stability
Tangent plane distance function
Helmholtz free energy
Volume function

ABSTRACT

We derive a criterion for phase stability under constant temperature, moles, and volume using the Helmholtz free energy. Using the volume-based formulation, we develop a numerical algorithm to investigate single-phase stability based on the Newton method. We demonstrate robustness and efficiency of the new method in a number of examples in single-phase stability testing.

1. Introduction

Consider a mixture of n components with mole numbers $N_1, \ldots, N_n$ in a closed system of constant volume V at temperature T. We are interested to know whether the mixture is in single-phase or splits into two or more phases. This is the problem of phase stability under constant temperature, moles, and volume (VT-stability). The goal of the constant volume stability analysis is to determine whether a phase is stable at specified volume, temperature, and mole numbers. If the phase is unstable, this procedure may be followed by the equilibrium calculation at constant temperature and volume, in which the final pressure of the mixture in the cell is to be computed together with the compositions and amounts of the split-phases. The latter is the problem of the two-phase phase-split (also called flash) at constant temperature, moles, and volume (VT-flash). The problem has been formulated in a recent paper [1], where a simple iterative algorithm is developed to compute the two-phase equilibrium under constant temperature, volume and moles. VT-stability procedure can be developed to simplify the VT-flash calculation. As the VT-stability algorithm is simpler than VT-flash, it can be performed first. If single-phase is stable, the VT-flash calculation is avoided. This paper is focused on the problem of testing VT-stability only. The application of the VT-stability to provide initial guesses for the VT-flash is an important problem which is currently under investigation.

The phase stability at constant pressure and temperature (PT-stability) is addressed in many references [2–5]. In this approach, pressure, temperature and overall chemical composition are given. Trial phases of various compositions are tested to find if there is a composition for which transfer of a small amount of the trial phase from the initial phase leads to a decrease of the Gibbs free energy. This is usually formulated using the so-called tangent plane distance function D. If a trial phase composition is found for which the function D is negative, the mixture is unstable and the trial phase composition can be used as an initial guess in the two-phase PT-flash [7]. If for all trial phase compositions the value D is non-negative, the mixture is in single-phase. For numerical efficiency, the search for the global minimum of function D [5] in the compositional space is replaced by local minimization using multiple initial guesses [2–4]. Many methods have been developed to locate the minima of function D in the literature cited above and in other papers.

The methods developed for PT-stability may not be corresponding to the VT-flash, in which the pressure is not known a-priori. Michelsen [3] suggested to use the PT-stability algorithm for investigation of the phase stability in other variables specifications (P, S

* Corresponding author at: Reservoir Engineering Research Institute, 595 Lytton Ave, Suite B, Palo Alto, CA 94301, USA. Tel.: +1 650 326 9259.
E-mail addresses: jiri.mikyska@fjfi.cvut.cz (J. Mikyška), abbas.firoozabadi@yale.edu (A. Firoozabadi).

0378-3812/$ – see front matter © 2012 Elsevier B.V. All rights reserved.
doi:10.1016/j.fluid.2012.01.026

or P, H). While these methods should provide the same results, in some special cases, as we will discuss later in the paper, they may not. They may be also differences in numerical efficiency. We have found out that the numerical implementation of the VT-stability using the PT-algorithm at the pressure given by the equation of state may fail to provide correct results. We will show two examples to illustrate this issue. An alternative to the PT-stability will also provide a new option. Therefore, we develop a new 'volume-based' formulation of the phase stability criterion and present a numerical algorithm for testing single-phase stability at constant temperature and volume. Although the VT-stability criterion can be found in Refs. [3,6,8], the working equations for phase stability at constant temperature and volume, to the best of our knowledge, have not appeared in the scientific literature.

The paper is structured as follows. In the first section, we derive conditions for single-phase stability at constant temperature and volume. Then, we reformulate this condition in terms of the volume functions that were introduced previously [1]. A numerical algorithm is suggested for testing VT-stability, and, finally, we present examples of phase stability testing based on the new formulation for a number of mixtures under different conditions.

2. Conditions for phase stability

Consider a mixture of n components with mole numbers $N_1, \ldots, N_n$ occupying volume V at temperature T. The question is whether the system stays in a single phase or splits into two phases. The Helmholtz free energy of a phase is given by

$$A = -PV + \sum_{i=1}^{n} N_i \mu_i, \tag{1}$$

where $P = P(V, T, N_1, \ldots, N_n)$ is the pressure given by a pressure-explicit equation of state, and $\mu_i = \mu_i(V, T, N_1, \ldots, N_n)$ is the chemical potential of the i-th component in the mixture. If the system is in single-phase, then the total Helmholtz free energy of the mixture reads as

$$A^I = A(V, T, N_1, \ldots, N_n), \tag{2}$$

while in the two-phase

$$A^{II} = A(V', T, N_1', \ldots, N_n') + A(V - V', T, N_1 - N_1', \ldots, N_n - N_n'). \tag{3}$$

In Eq. (3) the prime represents the variables of the trial phase. Note that the chemical composition of the trial phase can be quite different from that of the initial phase. Let us assume that if the single phase is unstable, then an arbitrarily small perturbation can turn the system into two-phase. Using the Taylor expansion of the second term of the right hand side of (3) around the point $(V, T, N_1, \ldots, N_n)$, we derive

$$\begin{aligned} A(V - V', T, N_1 - N_1', \ldots, N_n - N_n') &= A(V, T, N_1, \ldots, N_n) \\ &- \frac{\partial A}{\partial V}(V, T, N_1, \ldots, N_n)V' - \sum_{i=1}^{n} \frac{\partial A}{\partial N_i}(V, T, N_1, \ldots, N_n)N_i' \\ &+ R_1(V', T, N_1', \ldots, N_n'), \end{aligned} \tag{4}$$

where $R_1(V', T, N_1', \ldots, N_n')$ denotes the reminder in the Taylor polynomial expansion after the first-order terms. Combining the last equation with (2), and using

$$\frac{\partial A}{\partial V} = -P, \quad \frac{\partial A}{\partial N_i} = \mu_i, \tag{5}$$

we rewrite the change of the Helmholtz free energy from the single-phase to the two-phase state as

$$\begin{aligned} \Delta A = A^{II} - A^I &= A(V', T, N_1', \ldots, N_n') + P(V, T, N_1, \ldots, N_n)V' \\ &- \sum_{i=1}^{n} \mu_i(V, T, N_1, \ldots, N_n)N_i' + R_1(V', T, N_1', \ldots, N_n'). \end{aligned} \tag{6}$$

Using Eq. (1), the last equation can be rewritten as

$$\begin{aligned} \Delta A = &\sum_{i=1}^{n} [\mu_i(V', T, N_1', \ldots, N_n') - \mu_i(V, T, N_1, \ldots, N_n)N_i' \\ &- [P(V', T, N_1', \ldots, N_n') - P(V, T, N_1, \ldots, N_n)]V' \\ &+ R_1(V', T, N_1', \ldots, N_n'). \end{aligned} \tag{7}$$

For sufficiently small perturbations $(V', T, N_1', \ldots, N_n')$ the reminder term cannot change the sign of ΔA, which implies that the single phase is stable if (c.f. [6])

$$\begin{aligned} &\sum_{i=1}^{n} \left[\mu_i(V', T, N_1', \ldots, N_n') - \mu_i(V, T, N_1, \ldots, N_n)\right] N_i' \\ &- [P(V', T, N_1', \ldots, N_n') - P(V, T, N_1, \ldots, N_n)]V' \geq 0 \end{aligned} \tag{8}$$

for all admissible states $(V', T, N_1', \ldots, N_n')$.

3. Different forms of the phase stability criterion

We will rewrite (8) into a more convenient form. Let us introduce the overall molar concentration $c = N/V$, the trial phase molar concentration $c' = N'/V'$, overall mole fractions $z_i = N_i/N$, and trial phase mole fractions $x_i = N_i'/N'$, where $N = \sum_{i=1}^{n} N_i$ and $N' = \sum_{i=1}^{n} N_i'$. Dividing (8) by V' and using the fact that pressure and chemical potentials are homogeneous functions of degree zero in volume and moles, the single-phase is stable if and only if the tangent plane distance function D defined by

$$\begin{aligned} D(T, c'x_1, \ldots, c'x_n) = &\sum_{i=1}^{n} [\mu_i(1, T, c'x_1, \ldots, c'x_n) \\ &- \mu_i(1, T, cz_1, \ldots, cz_n)]c'x_i \\ &- [P(1, T, c'x_1, \ldots, c'x_n) \\ &- P(1, T, cz_1, \ldots, cz_n)] \end{aligned} \tag{9}$$

is nonnegative for all admissible concentrations $(c'x_1, \ldots, c'x_n)$ at temperature T. To see whether a state with a negative value of D exists, it is sufficient to investigate the values of D in the minima. The stationary points of function D are given by

$$\frac{\partial D}{\partial (c'x_j)} = \mu_j' - \mu_j + \sum_{i=1}^{n} \frac{\partial \mu_i'}{\partial N_j'} c'x_i - \frac{\partial P'}{\partial N_j'} = 0, \quad j = 1, \ldots, n. \tag{10}$$

In the equations above, the pressure and chemical potentials are understood as functions of independent variables V', T, and $N_1', \ldots, N_n'$; therefore, the partial derivatives are denoted as $\partial \mu_i'/\partial N_j'$, and $\partial P'/\partial N_j'$, respectively. We use the convention that the primed pressure, chemical potentials and their derivatives are

evaluated at $(1, T, c'x_1, \ldots, c'x_n)$, while the unprimed ones are evaluated at $(1, T, cz_1, \ldots, cz_n)$. From the reciprocity relations

$$\frac{\partial \mu_i'}{\partial N_j'} = \frac{\partial \mu_j'}{\partial N_i'}, \quad \text{and} \quad \frac{\partial P'}{\partial N_j'} = -\frac{\partial \mu_j'}{\partial V'}, \tag{11}$$

we obtain

$$\frac{\partial D}{\partial (c'x_j)} = \mu_j' - \mu_j + \sum_{i=1}^{n} \frac{\partial \mu_j'}{\partial N_i'} c'x_i + \frac{\partial \mu_j'}{\partial V'} = 0, \quad j = 1, \ldots, n. \tag{12}$$

Note that the chemical potentials satisfy

$$\mu_i(\alpha V', T, \alpha N_1', \ldots, \alpha N_n') = \mu_i(V', T, N_1', \ldots, N_n') \tag{13}$$

for all admissible states $(V', T, N_1', \ldots, N_n')$ and $\alpha > 0$ (i.e. μ_i is a homogeneous function of degree zero in variables V' and $N_1', \ldots, N_n'$). Therefore,

$$\sum_{i=1}^{n} \frac{\partial \mu_j'}{\partial N_i'} c'x_i + \frac{\partial \mu_j'}{\partial V'} = 0, \tag{14}$$

and the stationarity conditions (12) simplify to

$$\frac{\partial D}{\partial (c'x_j)} = \mu_j' - \mu_j = 0, \quad j = 1, \ldots, n, \tag{15}$$

which means that in every stationary point of function D, the initial phase and the trial phase are in chemical equilibrium (the chemical potentials of each component in the trial phase and the initial phase are equal). Substituting (15) into (9), the value of D at the stationary point is equal to $P - P'$. If the global minimum of function D is negative, the trial phase will be in chemical equilibrium with the initial phase, but not in mechanical equilibrium. When the trial phase will have higher pressure than the initial phase, the phase split will occur. If the global minimum of function D is zero (trivial solution has zero value of D, so the global minimum of D cannot have a positive value), then the mixture remains in single-phase.

In the development above, the stability criterion (8) was normalized to unit volume of the trial phase, however, it is interesting to mention that other reformulations are also possible. The criterion (8) can also be normalized to unit moles of the trial phase. In this case we define a modification of the D function by

$$D^*(T, c'x_1, \ldots, c'x_n) = \frac{D(T, c'x_1, \ldots, c'x_n)}{c'}. \tag{16}$$

The condition for stationary points of the function D^* reads as

$$\frac{\partial D^*}{\partial (c'x_j)} = \frac{(\mu_j' - \mu_j)c' - D}{c'2} = 0, \quad j = 1, \ldots, n, \tag{17}$$

from which it follows that

$$\mu_j' - \mu_j = \frac{D}{c'} = K, \quad j = 1, \ldots, n, \tag{18}$$

i.e. the difference between chemical potentials in the trial and initial phases has the same value K for all components. Combining (18) with (16) and (9), it can be shown readily that the D^* function in any stationary point is equal to the value K and that the pressures of the trial phase and the initial phase are equal.

As both functions D and D^* have the same signs in any point, the results of stability analysis have to be the same for both functions. However, the locations of minima for the D function are very different from those for D^*. The meaning of stationary point depends on which function is used for stability analysis. This indicates that any recommendation on using the global minimum of any of them as an initial guess for the flash calculation can be considered ad hoc.

4. Limitations of the PT-stability analysis

The discussion above could lead us to the conclusion that to test the single phase stability of a mixture at constant V an T, it is sufficient to perform the conventional PT-stability testing of the mixture using the pressure given by the equation of state for the single phase. Although the conclusion, which has been mentioned in the literature [3], is theoretically correct, we have found out that the common numerical implementations of this approach may not provide correct results. To be specific, the mixtures from Examples 3 and 4 are not VT-stable at certain conditions (see Examples 3 and 4 below), but the PT-stability indicates stability. The reason is that the pressure computed from the equation of state is negative. When P is negative, one cannot use the Wilson correlation to obtain initial guess of K values. Even when we used other initial guesses by assuming various values of positive pressures in the Wilson correlation, the PT-stability predicted that the system is stable. Without good initial guesses, the PT-stability algorithm [2–4] can miss the global minimum of function D and indicate single-phase instead of two-phase. One may argue that if the pressure is negative, the system is unstable without performing flash calculations. Our algorithm would determine phase stability whether the pressure is positive or negative.

Another example when the conventional PT-stability analysis will fail is the situation in which the PT-stability testing is performed on a trivial mixture composed of a single component. In this situation, if the pressure P is higher than the saturation pressure $P^{sat}(T)$ at a given temperature T, the 'mixture' is stable liquid. If pressure P is lower than $P^{sat}(T)$, the 'mixture' is stable gas. Only if $P = P^{sat}(T)$, the 'mixture' can be in two-phase but also in single-phase (saturated liquid or saturated gas). Note that all the latter states are indistinguishable in terms of P and T variables, but can be distinguished using the volume V. Although this issue is typical for pure components only, we would like to have a theory that will treat the real mixtures and the pure components in a unified way. These issues and desirability of an alternative approach to stability have lead us to develop a new 'volume-based' formulation of the phase stability that can address VT-stability directly.

5. Numerical algorithm for testing phase stability

We will derive a numerical procedure for testing single-phase stability at constant temperature, volume, and moles based on the function D. Using the volume functions, which are introduced previously [1], the stationarity conditions (15) for function D can be rewritten as

$$\ln \frac{c'x_i}{cz_i} + \ln \Phi_i(\mathbf{cz}) - \ln \Phi_i(c'\mathrm{x}) = 0, \quad i = 1, \ldots, n, \tag{19}$$

where Φ_i is the volume function of the i-th component and $\mathbf{cz}$ and $\mathbf{c'x}$ denote vectors with components $cz_1, \ldots, cz_n$ and $c'x_1, \ldots, c'x_n$, respectively.

It is tempting to solve the system (19) by the successive substitution method (SSI) defined by

$$c'x_i^{k+1} = cz_i \frac{\Phi_i(c'\mathbf{x}^k)}{\Phi_i(\mathbf{cz})}, \tag{20}$$

where $c'\mathrm{x}^0$ is an initial guess. However, we have found that this approach does not work for the following reasons:

1. The sequence given by (20) does not converge in many cases. Frequently, after several iterations the iterate jumps out of the feasible region (i.e. $c'x_i < 0$ for some $i \in \{1, 2, \ldots, n\}$ or $\sum_{i=1}^{n} b_i c'x_i \geq 1$, where b_i denotes the covolume parameter of the i-th component in the Peng–Robinson equation of state).

2. Even if the sequence (20) converges to a limit, it is not guaranteed that the limit is the correct solution – the global minimum of function D. This is a common problem in local methods which is usually solved by proper initialization of the algorithm, but in case of the SSI method, this does not solve the problem (see the next point).
3. We have seen the cases where the iterates diverge from the correct solution no matter how close the initial guess is to the correct solution. It thus happens that the correct solution is a fixed point of the iteration (20), but the iterates diverge from it rather than converge. In many cases, the algorithm converges to a saddle point of function D rather than (at least local) minimum.
4. The convergence of SSI (if it is achieved) is typically slow. Unlike in PT-stability, the slow convergence is not compensated by the robustness of the method.
5. It is not clear how to choose a stopping criterion. If the iterations are stopped whenever the norm of the increment $\Delta c'x = c'x^{k+1} - c'x^k$ in an iteration is lower than a certain tolerance $\varepsilon_{TOL} > 0$ or if the decrease of the value of D in an iteration is small, there is no guarantee that the error of approximation of $\mathbf{c}'\mathbf{x}$ is small.

Therefore, the system of equations (19) is solved using the Newton–Raphson iterative method. Starting with an initial guess $c'x^0$, in each iteration we find a direction $\Delta c'x^k$ by solving the system

$$\mathbf{J}(c'x^k)\Delta c'x^k = -\mathbf{F}(c'x^k), \tag{21}$$

where the vector $\mathbf{F}$ has the elements

$$F_i(c'x) = \ln \frac{c'x_i}{cz_i} + \ln \Phi_i(\mathbf{cz}) - \ln \Phi_i(c'x), \quad i = 1, \ldots, n, \tag{22}$$

and $\mathbf{J}$ is the Jacobian matrix with elements

$$J_{i,j}(c'x) = \frac{\partial F_i}{\partial (c'x_j)}(c'x) = \frac{\delta_{i,j}}{c'x_j} - \frac{\partial \ln \Phi_i}{\partial (c'x_j)}(c'x), \quad i,j = 1, \ldots, n, \tag{23}$$

where $\delta_{i,j} = 1$ for $i = j$ and $\delta_{i,j} = 0$ for $i \neq j$. After solving for the direction $\Delta c'x^k$, the approximation is updated as

$$c'x^{k+1} = c'x^k + \lambda^k \Delta c'x^k, \tag{24}$$

where $\lambda^k \in (0\,;1\rangle$ is a dumping factor. We set $\lambda^k = 1$ for the first trial. If $c'x^{k+1}$ is outside of the feasible domain, λ^k is halved until the new approximation stays in the feasible domain. This modification of the Newton method (the so-called line search) avoids overshooting and enables to achieve global convergence in the Newton method. This means that the approximations will converge to a stationary point of function D for any initial guess. It should be noted that the property of global convergence is different from the convergence to the global minimum of function D, which, of course, cannot be guaranteed neither by using Newton-Raphson, nor any other local minimization method. The approximations converge to a stationary point, including the local maxima or saddle points. We have observed in many cases that with poor initial guesses the approximations in the Newton–Raphson method converge to a saddle point. Unlike in SSI, the Newton–Raphson iterations always converge to a stationary point if the initial guess is close enough, i.e. there exist basins of attraction around all stationary points. To ensure convergence toward the global minimum of function D, proper initial guesses must be provided.

In PT-stability for vapor-liquid systems, Wilson's correlation [10] usually provides reasonable initial guesses. In VT-stability, this correlation cannot be used directly, because the initial pressure is unknown. One idea could be to use pressure given by equation of state for the initial phase. In some cases, this initial pressure can be negative. Therefore, we propose a robust method for initialization of VT-stability algorithm based on the saturation pressure $P_i^{sat}(T)$ of each component i at temperature T. We will discuss two situations depending on whether the initial phase is considered as liquid- or vapor-like. If the initial phase is liquid-like, then the vapor phase pressure P_{ini} is estimated as

$$P_{ini} = \sum_{i=1}^{n} P_i^{sat}(T) z_i, \tag{25}$$

and the trial (vapor) phase composition is estimated as

$$x_i^0 = \frac{P_i^{sat}}{P_{ini}} z_i, \quad i = 1, \ldots, n. \tag{26}$$

If the initial phase is vapor-like, then we estimate the trial (liquid) phase composition as

$$x_i^0 = \frac{\frac{z_i}{P_i^{sat}}}{\sum_{j=1}^{n} \frac{z_j}{P_j^{sat}}}, \quad i = 1, \ldots, n, \tag{27}$$

and the initial trial (liquid) phase pressure P_{ini} is given by

$$P_{ini} = \sum_{i=1}^{n} P_i^{sat}(T) x_i^0. \tag{28}$$

As we do not know a-priori whether the initial phase is vapor- or liquid-like, both possibilities are tested. The initial concentration c'^0 of the trial phase is evaluated from the equation of state using the estimated trial phase composition $x_i^0 (i = 1, \ldots, n)$ and initial pressure P_{ini}. For multiple roots in the equation of state, we obtain different initial guesses. In case of three different roots, only two of them are accepted and the middle one is disregarded. This way we obtain up to four initial guesses for the Newton method. We have tested this strategy on a number of mixtures (see the Examples) and we have not seen a case for which the global minimum of function D would be missed.

The iterations are stopped when the maximal number of iterations is achieved (500) or when the Euclidian norm of the direction vector is less than a prescribed limit. We use $\|\Delta c'x^k\| < 10^{-7}$ as a stopping criterion in all examples below. For the Newton–Raphson method (and also for any other quadratically convergent method, see e.g. [11]), the norm of the error of $\mathbf{c}'\mathbf{x}$ is approximately equal to the norm of increment $\|\Delta c'x^k\|$ in the vicinity of the stationary point. This is not the case for SSI (and other methods that converge only linearly), in which the small increment does not generally imply a small error of approximation.

6. Numerical examples of VT-stability testing

We have tested the algorithm in several examples of VT-stability testing for binary and multi-component mixtures under different conditions. In all numerical experiments we investigate stability of an n-component mixture with prescribed chemical composition $z_1, \ldots, z_n$ as a function of temperature T and overall molar concentration c. The c, T-space is discretized by a grid with 50×50 vertices. For each point (c, T) of the grid we perform the stability analysis. We provide plots of the value of the global minimum as a function of c and T which allows to detect two-phase stability boundaries. Parameters of the Peng–Robinson equation of state for all components used are presented in Table 1. In most examples we investigate VT-stability of mixtures whose phase-splitting at constant temperature, volume and moles has been investigated in our previous work [1].

Example 1. In the first example we investigate VT-stability for a binary mixture of methane (C_1) and propane (C_3) with mole fractions $z_{C_1} = 0.547413$ and $z_{C_3} = 0.452587$ for temperatures

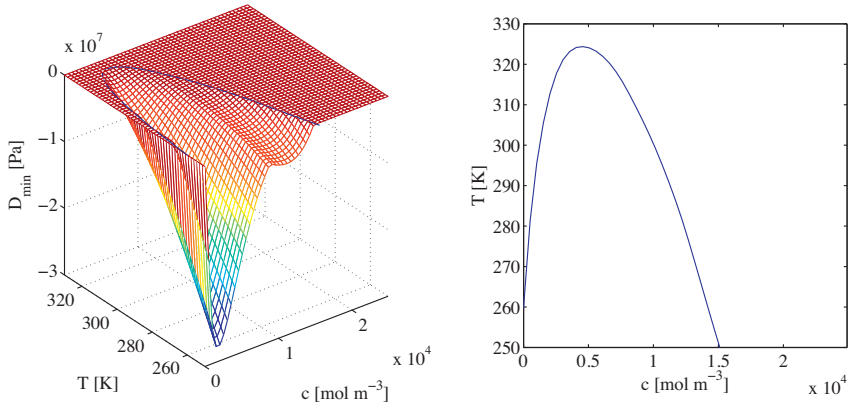

Fig. 1. Global minimum of function D as a function of the overall molar density c and temperature T (left) and boundary between single-phase and two-phase regions in the c, T-space (right). Example 1: binary C_1–C_3 mixture.

$T \in \langle 250\,;330\rangle$ K and the whole range of feasible molar densities. The binary interaction coefficient $\delta_{C_1-C_3} = 0.0365$. The minima of function D for each point and the approximate boundaries of the two-phase region in the c, T-space are presented in Fig. 1.

Example 2. In the second example we investigate VT-stability for a binary mixture of methane (C_1) and normal penthane (nC_5) with mole fractions $z_{C_1} = 0.547413$ and $z_{nC_5} = 0.452587$ for temperatures $T \in \langle 320\,;430\rangle$ K and the whole range of feasible molar densities. The binary interaction coefficient $\delta_{C_1-nC_5} = 0.041$. The minima of function D for each point and the approximate boundaries of the two-phase region in the c, T-space are presented in Fig. 2.

Example 3. In the third example we change the mole fractions in Example 2 and investigate VT-stability for a binary mixture of methane (C_1) and normal penthane (nC_5) with mole fractions $z_{C_1} = 0.489575$ and $z_{nC_5} = 0.510425$ for temperatures $T \in \langle 250\,;450\rangle$ K and the whole range of feasible molar densities. The minima of function D for each point and the approximate boundaries of the two-phase region in the c, T-space are presented in Fig. 3.

Note that for $c = 6135.3$ mol m^{-3} and $T = 310.95$ K, the mixture is unstable, but the PT-stability analysis performed at the pressure provided by the equation of state ($P = -9.93516$ bar) with several initial guesses indicates single-phase. This is an example of one of the issues with the PT-stability analysis discussed above, which justifies the alternative formulation.

Example 4. In the fourth example we investigate VT-stability for a binary mixture of carbon dioxide (CO_2) and normal decane (nC_{10}) with mole fractions $z_{CO_2} = 0.547413$ and $z_{nC_{10}} = 0.452587$ for temperatures $T \in \langle 250\,;650\rangle$ K and the whole range of feasible molar densities. The binary interaction coefficient $\delta_{CO_2-nC_{10}} = 0.15$. The minima of function D for each point and the approximate boundaries of the two-phase region in the c, T-space are presented in Fig. 4. Note that for high molar densities c and low temperatures we can observe a second two-phase region which may correspond to a liquid–liquid two-phase region (provided that the solid phase does not form). As can be seen in Fig. 4, for $c = 6307.21$ mol m^{-3} and $T = 311$ K, the mixture is unstable. This is another example in which the PT-stability fails to provide correct answer because when performed at the pressure given by the equation state ($P = -184.5$ bar), it indicates single phase.

Example 5. In the fifth example we investigate VT-stability for a four-component mixture of nitrogen (N_2), methane (C_1), propane (C_3), and normal decane (nC_{10}) with mole fractions $z_{N_2} = 0.2463$, $z_{C_1} = 0.2208$, $z_{C_3} = 0.2208$, and $z_{nC_{10}} = 0.3121$ for temperatures $T \in \langle 250\,;650\rangle$ K and the whole range of feasible molar densities. The binary interaction coefficients are shown in Table 2. The minima of function D for each point and the approximate boundaries of the two-phase region in the c, T-space are presented in Fig. 5.

Example 6. In the sixth example we investigate VT-stability for a seven-component mixture of nitrogen (N_2), carbon dioxide (CO_2) with a multicomponent oil. The oil is modeled by seven (pseudo)components – N_2, CO_2, methane (C_1), and four hydrocarbon pseudo-components denoted as PC_1 ($H_2S + C_2 + C_3$), PC_2 (C_4–C_6), PC_3 (C_7–C_{11}), and C_{12+}. In this example oil is mixed with nitrogen to obtain a nitrogen-rich mixture with overall composition $z_{N_2} = 0.466905$, $z_{CO_2} = 0.007466$, $z_{C_1} = 0.300435$, $z_{PC_1} = 0.105051$, $z_{PC_2} = 0.041061$, $z_{PC_3} = 0.045060$, and $z_{C_{12+}} = 0.034021$. We investigate VT-stability of this mixture for temperatures $T \in \langle 250\,;650\rangle$ K and the whole range of feasible molar densities. The binary interaction coefficients are shown in Table 3. The minima of function D for each point and the approximate boundaries of the two-phase region in the c, T-space are presented in Fig. 6.

Table 1
Parameters of the Peng–Robinson equation of state for all components used in all examples. PC_1–PC_3 are the pseudocomponents defined in Examples 6 and 7.

Component	$T_{i,crit}$ (K)	$P_{i,crit}$ (MPa)	ω_i (–)	$M_{w,i}$ (g mol^{-1})
CO_2	304.14	7.375	0.2390	44
N_2	126.21	3.390	0.039	28
C_1	190.56	4.599	0.0110	16
C_3	369.83	4.248	0.153	44.1
nC_5	469.70	3.370	0.2510	72.2
nC_{10}	617.70	2.110	0.489	142.28
PC_1	333.91	5.329	0.1113	34.64
PC_2	456.25	3.445	0.2344	69.52
PC_3	590.76	2.376	0.4470	124.57
C_{12+}	742.58	1.341	0.9125	248.30

Table 2
Binary interaction coefficients for the four-component mixture used in Example 5.

Component	N_2	C_1	C_3	nC_{10}
N_2	0	0.1	0.1	0.1
C_1	0.1	0	0.036	0.052
C_3	0.1	0.036	0	0
nC_{10}	0.1	0.052	0	0

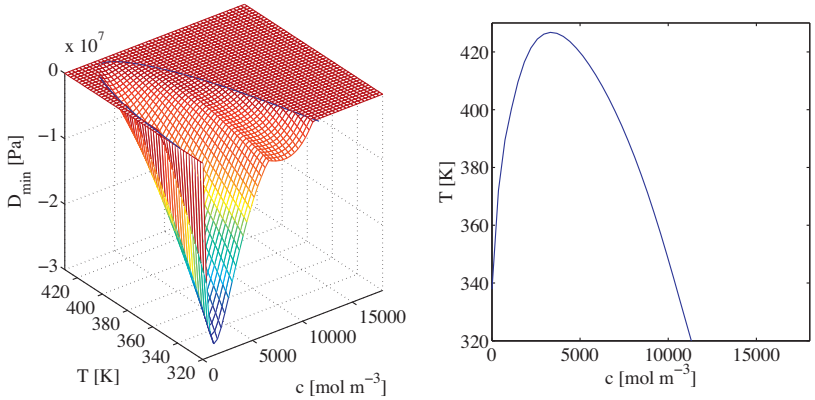

Fig. 2. Global minimum of function D as a function of the overall molar density c and temperature T (left) and boundary between single-phase and two-phase regions in the c, T-space (right). Example 2: binary C_1–nC_5 mixture (mole fractions in the text).

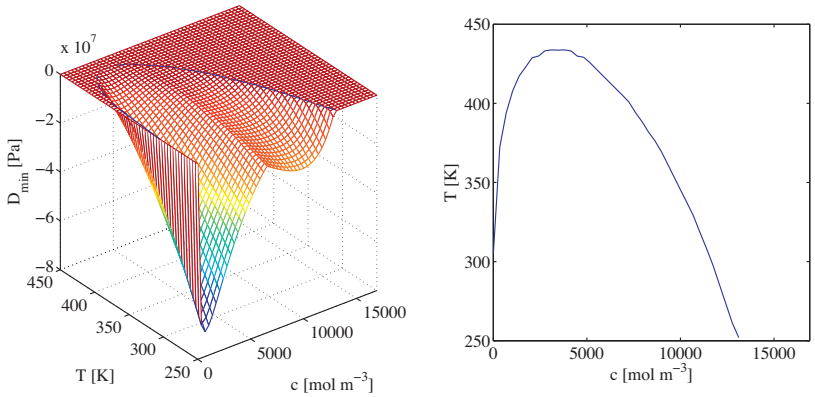

Fig. 3. Global minimum of function D as a function of the overall molar density c and temperature T (left) and boundary between single-phase and two-phase regions in the c, T-space (right). Example 3: binary C_1–nC_5 mixture (mole fractions in the text).

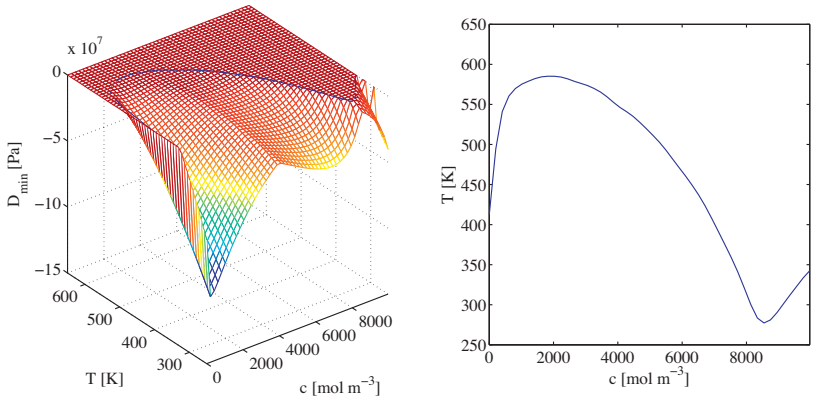

Fig. 4. Global minimum of function D as a function of the overall molar density c and temperature T (left) and boundary between single-phase and two-phase regions in the c, T-space (right). Example 4: binary CO_2–nC_{10} mixture.

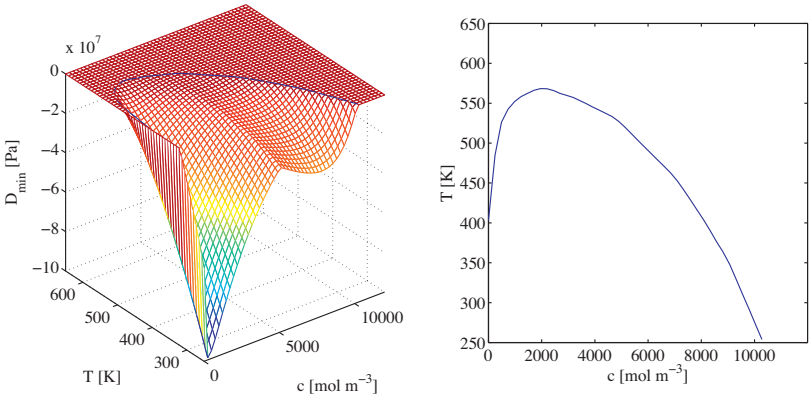

Fig. 5. Global minimum of function D as a function of the overall molar density c and temperature T (left) and boundary between single-phase and two-phase regions in the c, T-space (right). Example 5: 4-component mixture of N_2–C_1–C_3–nC_{10}.

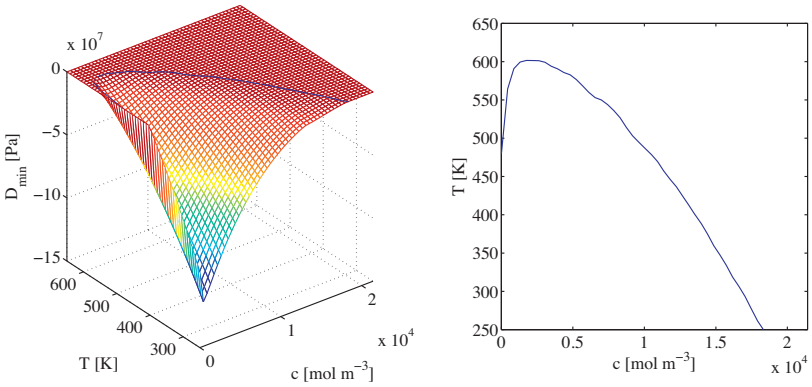

Fig. 6. Global minimum of function D as a function of the overall molar density c and temperature T (left) and boundary between single-phase and two-phase regions in the c, T-space (right). Example 6: 7-component mixture rich in N_2.

Example 7. In the last example we mix the oil from Example 6 with CO_2 so that we obtain a CO_2-rich seven-component mixture with overall composition $z_{N_2} = 0.000131$, $z_{CO_2} = 0.568185$, $z_{C_1} = 0.246739$, $z_{PC_1} = 0.086275$, $z_{PC_2} = 0.033722$, $z_{PC_3} = 0.037006$, and $z_{C_{12+}} = 0.027941$. We investigate VT-stability of this mixture for temperatures $T \in \langle 250\,;\,650 \rangle$ K and the whole range of feasible molar densities. The binary interaction coefficients are shown in Table 3. The minima of function D for each point and the approximate

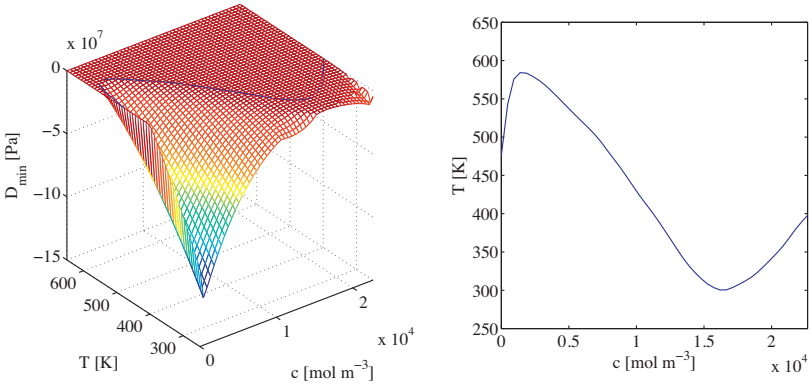

Fig. 7. Global minimum of function D as a function of the overall molar density c and temperature T (left) and boundary between single-phase and two-phase regions in the c, T-space (right). Example 7: 7-component mixture rich in CO_2.

Table 3
Binary interaction coefficients for the reservoir fluids used in Examples 6 and 7.

Component	N_2	CO_2	C_1	PC_1	PC_2	PC_3	C_{12+}
N_2	0.000	0.000	0.100	0.100	0.100	0.100	0.100
CO_2	0.000	0.000	0.150	0.150	0.150	0.150	0.150
C_1	0.100	0.150	0.000	0.035	0.040	0.049	0.069
PC_1	0.100	0.150	0.035	0.000	0.000	0.000	0.000
PC_2	0.100	0.150	0.040	0.000	0.000	0.000	0.000
PC_3	0.100	0.150	0.049	0.000	0.000	0.000	0.000
C_{12+}	0.100	0.150	0.069	0.000	0.000	0.000	0.000

boundaries of the two-phase region in the c, T-space are presented in Fig. 7. We observe again an unstable region in the bottom right corner of Fig. 7 (right) which corresponds to a liquid–liquid two-phase state if the solid phase does not form.

7. Summary and conclusions

In this work we have formulated conditions for the phase stability at constant temperature, volume, and moles. This problem differs significantly from the common problem of stability at constant pressure, because the pressure is not known a-priori. Moreover, the pressures in the initial phase and in the trial phase are not generally the same. We have proposed a simple numerical algorithm for VT-stability testing, which is based on the Newton method with line search. This combination together with a special choice of initial guesses allows robust VT-stability testing. The algorithm has been tested on many mixtures under different conditions of different complexity. In most simulations, the algorithm converges in 10–20 iterations. In seven-components examples, the typical number of Newton iterations is between 20 and 30. In most situations the line search is necessary in the first few iterations of the Newton method only. Once the iterates converge toward the true solution, we observe the quadratic convergence and the line search is not needed any more. In some cases the Newton method does not converge for some initial guesses, but these cases are very rare. If the Newton method does not converge for one initial guess, the other initial guesses converge rapidly. Therefore, we are able to obtain these results using at most four initial guesses for each VT-stability testing. This can not be achieved using the SSI method which breaks down frequently and does not allow to evaluate reliable phase boundaries in the c, T-space as it is for the Newton method.

List of symbols

A	Helmholtz free energy
b_i	covolume parameter of the Peng-Robinson EOS
c	molar concentration
D, D^*	different forms of the tangent plane distance function
$\delta_{i,j}$	Kronecker symbol
δ_{X-Y}	binary interaction coefficient between components X and Y
Φ_i	volume function of the i-th component
i, j	component indices
k	iteration index
μ_i	chemical potential of the i-th component
$M_{w,i}$	molar weight of the i-th component
n	number of components
N_i	mole number of the i-th component
ω_i	accentric factor of the i-th component
P	pressure
$P_{i,crit}$	critical pressure of the it-th component
P_i^{sat}	saturation pressure of the i-th component
P_{ini}	initial pressure
R	universal gas constant
T	absolute temperature
$T_{i,crit}$	critical temperature of the i-th component
V	total volume of the system
x_i	mole fraction of the i-th component in the trial phase
z_i	mole fraction of the i-th component in the initial phase

Acknowledgments

The work was supported by the member companies of the Reservoir Engineering Research Institute, by the project Development of Computer Models of CO_2 Sequestration in the Subsurface P105/11/1507 of the Czech Science Foundation, and by the research direction project MSM6840770010 Applied Mathematics in Technical and Physical Sciences of the Ministry of Education of the Czech Republic.

Appendix A. Volume function coefficient for the Peng–Robinson equation of state

In this work we use the Peng–Robinson equation of state [9] in the form

$$P(V,T,N_1,\ldots,N_n)=\frac{NRT}{V-\mathcal{B}}-\frac{\mathcal{A}}{V^2+2\mathcal{B}V-\mathcal{B}^2},$$

where R is the universal gas constant, $N=\sum_{i=1}^{n}N_i$ is the total mole number, and coefficients $\mathcal{A}$ and $\mathcal{B}$ are given by

$$\mathcal{A}=\sum_{i=1}^{n}\sum_{j=1}^{n}N_iN_ja_{ij},\quad a_{ij}=(1-\delta_{i-j})\sqrt{a_ia_j},\ a_i=0.45724\frac{R^2T_{i,crit}^2}{P_{i,crit}}[1+m_i(1-\sqrt{T_r})]^2,\ m_i=\begin{cases}0.37464+1.54226\omega_i-0.26992\omega_i^2, & \text{for } \omega_i<0.5,\\ 0.3796+1.485\omega_i-0.1644\omega_i^2+0.01667\omega_i^3 & \text{for } \omega_i\geq 0.5\end{cases}.$$

$$\mathcal{B}=\sum_{i=1}^{n}N_ib_i\qquad b_i=0.0778\frac{RT_{i,crit}}{P_{i,crit}}$$

In these equations δ_{i-j} denotes the binary interaction parameter between the components i and j, $T_{i,crit}$, $P_{i,crit}$, and ω_i are the critical temperature, critical pressure, and accentric factor of the i-th component, respectively. Defining the molar densities of the i-th component by $cx_i=N_i/V$, the volume function coefficient for the Peng–Robinson equation of state can be written in terms of molar densities as (for details see [1])

$$ln\,\Phi_i(T,cx_1,\ldots,cx_n)=\ln(1-\mathfrak{B})-\frac{b_ic}{1-\mathfrak{B}}+\frac{\mathfrak{A}b_i}{\mathfrak{B}RT}\frac{1}{1+2\mathfrak{B}-2\mathfrak{B}}$$
$$-\frac{1}{\sqrt{2}\mathfrak{B}RT}\left[\frac{\mathfrak{A}b_i}{2\mathfrak{B}}-\sum_{j=1}^{n}cx_ja_{ij}\right]\ln\left|\frac{1+(1+\sqrt{2})\mathfrak{B}}{1+(1-\sqrt{2})\mathfrak{B}}\right|,\qquad(29)$$

where

$$\mathfrak{A}=\frac{\mathcal{A}}{V^2}=\sum_{i=1}^{n}\sum_{j=1}^{n}cx_icx_ja_{ij},\quad \mathfrak{B}=\frac{\mathcal{B}}{V}=\sum_{i=1}^{n}cx_ib_i.$$

In the text the dependence of the volume function Φ_i on temperature T is not written explicitly, because the temperature is assumed to be constant.

References

[1] J. Mikyška, A. Firoozabadi, AIChE J. 57 (2011) 1897–1904.
[2] A. Firoozabadi, Thermodynamics of Hydrocarbon Reservoirs, McGrew-Hill, 1999.
[3] M.L. Michelsen, Fluid Phase Equilib. 9 (1982) 1–19.

[4] M.L. Michelsen, J.M. Mollerup, Thermodynamic Models: Fundamentals and Computational Aspects, Tie-Line Publications, 2004.
[5] J.Z. Hua, J.F. Brennecke, M.A. Stadtherr, Comput. Chem. Eng. 22 (1998) 1207–1214.
[6] R.A. Heidemann, A.M. Khalil, AIChE J. 22 (1980) 769–779.
[7] M.L. Michelsen, Fluid Phase Equilib. 9 (1982) 21–40.
[8] M.L. Michelsen, Fluid Phase Equilib. 158 (1999) 617–626.
[9] D.E. Peng, D.B. Robinson, Ind. Eng. Chem.: Fundam. 15 (1976) 59–64.
[10] G.M. Wilson, paper No. 15C presented at the 1969 AIChE 65th National Meeting, Cleveland, OH, May 4–7, 1969.
[11] A. Quaternioni, R. Sacco, F. Saleri, Numerical Mathematics, Springer, 2000.

3.5 [Č4]: Jindrová, T., and Mikyška, J., Fast and Robust Algorithm for Calculation of Two-Phase Equilibria at Given Volume, Temperature, and Moles, Fluid Phase Equilibria, Vol. 353 (Sep 15, 2013), pp. 101–114, 2013

Fluid Phase Equilibria 353 (2013) 101–114

Contents lists available at SciVerse ScienceDirect

Fluid Phase Equilibria

journal homepage: www.elsevier.com/locate/fluid

Fast and robust algorithm for calculation of two-phase equilibria at given volume, temperature, and moles

Tereza Jindrová, Jiří Mikyška*

Czech Technical University in Prague, Faculty of Nuclear Sciences and Physical Engineering, Department of Mathematics, Trojanova 13, 120 00 Prague 2, Czech Republic

ARTICLE INFO

Article history:
Received 21 January 2013
Received in revised form 29 May 2013
Accepted 30 May 2013
Available online 14 June 2013

Keywords:
Two-phase equilibrium
Constant volume flash
Helmholtz free energy minimization
Newton–Raphson method
Modified Cholesky factorization

ABSTRACT

We develop a new algorithm for the calculation of phase splitting at constant volume, temperature, and moles. The method is based on the direct minimization of the total Helmholtz free energy of the mixture with respect to the mole- and volume-balance constraints. The algorithm uses the Newton–Raphson minimization method with line-search and modified Cholesky factorization of the Hessian to produce a sequence of states with decreasing values of the total Helmholtz free energy. The algorithm is initialized using an initial guess that is constructed using the results of the constant volume stability testing. The speed and robustness of the algorithm are demonstrated by a number of examples of two-phase equilibrium calculations.

1. Introduction

Consider a closed system of given volume V containing a mixture of n components with mole numbers $N_1, \ldots, N_n$ at temperature T. The goal is to find out if the system is in single phase or splits into phases. If phase splitting occurs, we want to establish composition, densities, and amount of the phases, and eventually, find the equilibrium pressure. The problem of computation of phase equilibria under constant volume, temperature, and moles (the so-called *VT*-flash) is an alternative to the traditional formulation of phase equilibria at constant pressure, temperature, and chemical composition (the so-called *PT*-flash), which has been used in many applications [1–3]. Although the possibility of using alternative variables specifications has been known for a long time, in most applications *PT*-flash has been used to solve the phase equilibrium. To compute phase equilibria under different variables specifications (including *VT*, *PS*, and *PH*), Michelsen [1–4] suggested to use the *PT*-flash algorithm iteratively, trying to find input temperature T and pressure P for the *PT*-flash such that the resulting specification variable (volume V, entropy S, or enthalpy H, respectively) attains the prescribed value. This approach was used in [5] to find the conditions of thermodynamic equilibrium in systems subject to gravitational fields and in [6] to study segregation in centrifugal fields. While this approach allows to reuse existing implementations of *PT*-flash, it is not computationally efficient because many solutions of the *PT*-flash are needed before the equilibrium pressure is found. Another limitation of this approach is that for a pure substance at the saturation pressure, volume is ambiguous (see Example 1 below), and therefore, the nested loop approach must fail to provide correct volume fractions of the split phases. Although the single-component case seems to be a trivial exception, we aim to develop a method that performs equally well for pure substances and mixtures. This motivates our interest in *VT*-based formulation and direct minimization of the total Helmholtz free energy A.

Compared to *PT*-flash, the *VT*-based algorithms for the flash calculation and stability testing have been discussed rarely in the literature. Cabral et al. [7] use the direct minimization of the Helmholtz free energy in problems with various bulk and adsorbed phases. In the *VT*-flash, pressure can become negative during the course of iterations. For this reason, Cabral et al. [7] have evaluated the logarithms of fugacities and pressures using the complex arithmetic. In the *VT*-formulation presented in this paper, the use of complex arithmetic is avoided. This is achieved by expressing the differences of the chemical potentials using the logarithms of volume functions rather than fugacities. The framework of volume functions was developed recently [9] to replace fugacities in the *VT*-based formulations. The first algorithm for the direct calculation of *VT*-flash [9] using the new framework was based on solving the equations of phase equilibria using the succesive substitution iterations (SSI). Numerical examples in [9] demonstrate that the direct calculation of *VT*-flash using SSI can be performed in essentially the same number of iterations as SSI requires in *PT*-flash if applied at the equilibrium pressure. As this pressure is usually not known a-priori

* Corresponding author. Tel.: +420 224358553.
E-mail address: jiri.mikyska@fjfi.cvut.cz (J. Mikyška).

0378-3812/$ – see front matter © 2013 Elsevier B.V. All rights reserved.
http://dx.doi.org/10.1016/j.fluid.2013.05.036

List of notation

Symbol	
A	Helmholtz free energy
b_i	Covolume parameter of the Peng–Robinson EOS
c	Molar concentration
δ_{X-Y}	Binary interaction coefficient between components X and Y
i, j	Component indices
k	Iteration index
μ_i	Chemical potential of the ith component
$M_{w,i}$	Molar weight of the ith component
n	Number of components
N_i	Mole number of the ith component
ω_i	Accentric factor of the ith component
P	Pressure
$P_{i,crit}$	Critical pressure of the ith component
R	Universal gas constant
T	Absolute temperature
$T_{i,crit}$	Critical temperature of the ith component
V	Total volume of the system
z_i	Overall mole fraction of the ith component

(actually, it is one of the results of the *VT*-flash problem), iterative version of the *PT*-flash would require more CPU-time to solve the *VT*-flash problem. Besides its efficiency, there are also other advantages of the *VT*-flash formulation over the *PT*-formulation [11] stemming from the fact that *VT* are the natural variables of pressure-explicit equations of state:

1 As volume is specified and pressure is computed from the equation of state, there is no need to invert the equation of state.
2 As the equation of state is not inverted, the problem of multiple roots of the equation of state is avoided.
3 The algorithm can describe phase splitting in the mixtures as well as in pure components (we will show a specific example of this issue later in this paper).

Although the SSI-algorithm for *VT*-flash works well in many cases, there are several issues to resolve. First, for some problems the SSI algorithm requires too many iterations to converge. Second, if SSI does converge, it does not have to converge to a state corresponding to (at least) a local minimum of the total Helmholtz free energy A. We have found examples, in which the iterates in the SSI-algorithm converge to a state corresponding to the saddle point of A rather than to the point of a minimum of A. In some cases, SSI can converge to the trivial solution although the system should be in two-phase. Providing good initial guesses for the SSI algorithm is another challenge. We have found an example of a binary mixture, for which the iterates in the SSI method diverged from the vicinity of the global minimum of A no matter how close was the initial guess to the point of the global minimum. Recently, we have developed a fast and robust method for testing single-phase stability under constant V and T conditions [10]. This algorithm tests if a small volume of a trial phase with arbitrary density and composition can be split from the initial phase so that the total Helmholtz free energy of the 2-phase system is lower than the energy of the hypothetical single-phase system. If the mixture is stable, the *VT*-flash calculation is avoided. If the mixture splits into phases, the *VT*-stability provides concentrations of a trial phase, which, if taken in a sufficiently small amount from the initial phase, leads to a two-phase system with lower value of A than the hypothetical single phase state. However, the SSI algorithm breaks down if the initial guess from *VT*-stability is used.

To resolve these issues, we have developed a new method for the computation of *VT*-flash which is based on constrained minimization of the total Helmholtz free energy rather than equation solving. The minimization approach allows to solve all the issues mentioned above. As the method is based on the Newton–Raphson iterations, its convergence is fast compared to SSI. Unlike SSI, the new method guarantees that the total Helmholtz free energy of the system decreases in every iteration. Therefore, the method always converges to a state corresponding to a local minimum of A. As we use the results of stability to initialize the iteration, once the stability analysis decides that the system is in two-phase, convergence towards the false trivial solution is avoided.

The paper is structured as follows. In Section 2, we formulate the *VT*-flash problem and derive the equilibrium conditions using the Helmholtz free energy. In Section 3, we describe the new computational algorithm for calculation of phase-equilibria at constant volume, temperature, and moles. In Section 4, we describe construction of the initial guess using the results of *VT*-stability testing. In Section 5, we summarize the essential steps of the algorithm. In Section 6, we present numerical examples showing the performance of the algorithm on several mixtures of different degree of complexity. In Section 7, we discuss the results and draw some conclusions. In Appendix A, we summarize details of the equations of state that were used in the computations.

2. Conditions for phase equilibrium

Consider a mixture of n components with mole numbers $N_1, \ldots, N_n$ occupying volume V at temperature T. Let us assume the system is unstable and splits into two phases. We are interested in calculating volumes of both phases V' and V'', mole numbers of each component in both phases N_i' and N_i'' for $i = 1, \ldots, n$ and the pressure of the system P.

For single-phase systems, the Helmholtz free energy is given by

$$A^I = A(V, T, N_1, \ldots, N_n) = -PV + \sum_{i=1}^{n} N_i \mu_i, \tag{1}$$

where $P = P(V, T, N_1, \ldots, N_n)$ is the pressure given by a pressure-explicit equation of state, and $\mu_i = \mu_i(V, T, N_1, \ldots, N_n)$ is the chemical potential of the ith component in the mixture. For two-phase systems, the total Helmholtz free energy reads as

$$A^{II} = A(V', T, N_1', \ldots, N_n') + A(V'', T, N_1'', \ldots, N_n''). \tag{2}$$

The equilibrium state of the system is the one for which the total Helmholtz free energy increase with respect to the hypothetical single phase system,

$$\Delta A = A(V', T, N_1', \ldots, N_n') + A(V'', T, N_1'', \ldots, N_n'') - A(V, T, N_1, \ldots, N_n), \tag{3}$$

is minimal among all states satisfying the following $(n+1)$ constraints, which express the volume balance and mole balance

$$V' + V'' = V, \tag{4}$$

$$N_i' + N_i'' = N_i, \qquad i = 1, \ldots, n. \tag{5}$$

Using the Lagrange multiplier method, the system of $(n+1)$ necessary conditions of the phase equilibria is derived

$$P(V', T, N_1', \ldots, N_n') = P(V'', T, N_1'', \ldots, N_n''), \tag{6}$$

$$\mu_i(V', T, N_1', \ldots, N_n') = \mu_i(V'', T, N_1'', \ldots, N_n''), \qquad i = 1, \ldots, n. \tag{7}$$

These equations are the basis for equation solving methods like SSI developed in [9]. In this paper, we develop an optimization method, which is based on direct minimization of ΔA subject to the constraints (4) and (5). The same problem could also be formulated

[Č4]: Fluid Phase Equilibria, Vol. 353 (Sep 15, 2013), pp. 101–114, 2013

using the minimization of A rather than ΔA. Obviously, the two formulations yield the same equilibrium states as the last term on the right hand side of (3) is constant. There are two advantages of using ΔA. First, while A can be evaluated up to an unknown additive constant, the expression for ΔA can be evaluated readily from the equation state. Second, ΔA is used in stability testing and the sign of ΔA shows whether a given two-phase split is more stable than the hypothetical single-phase state. This feature helps in the initialization of the algorithm (see Eq. (27) in Section 4).

3. Numerical algorithm for computation of phase equilibrium

We derive a numerical procedure for computing two-phase equilibrium at constant temperature, volume, and moles based on minimization of the total Helmholtz free energy of the two-phase system (3), which is subject to the volume and mole balance constraints (4) and (5).

The constraint equations (4) and (5) can be written in the matrix form with matrix $\mathbb{A} \in \mathrm{R}^{(n+1)\times(2n+2)}$, vector of unknowns $\mathbf{x} \in \mathrm{R}^{2n+2}$ and the vector of right hand side $\mathbf{b} \in \mathrm{R}^{n+1}$ as $\mathbb{A}\mathbf{x} = \mathbf{b}$, or

$$\underbrace{\begin{pmatrix} 1 & & & & 0 & 1 & & & & 0 \\ & 1 & & & 0 & & 1 & & & 0 \\ & & \ddots & & \vdots & & & \ddots & & \vdots \\ & & & & 1 & 0 & & & & 1 & 0 \\ 0 & 0 & \dots & & 0 & 1 & 0 & 0 & \dots & 0 & 1 \end{pmatrix}}_{\mathbb{A}} \underbrace{\begin{pmatrix} N_1' \\ \vdots \\ N_n' \\ V' \\ N_1'' \\ \vdots \\ N_n'' \\ V'' \end{pmatrix}}_{\mathbf{x}} = \underbrace{\begin{pmatrix} N_1 \\ N_2 \\ \vdots \\ N_n \\ V \end{pmatrix}}_{\mathbf{b}}. \tag{8}$$

As the matrix $\mathbb{A}$ has the full rank, the optimization problem with $2n+2$ unknowns and $n+1$ linearly independent linear constraints can be transformed into an unconstrained problem in $2n+2-(n+1) = n+1$ variables. In principle, one could use the constraints to eliminate one set of unknowns (say V'', and $N_1'', \dots, N_n''$) and formulate the problem as an unconstrained optimization problem in the other set of variables (V', and $N_1', \dots, N_n'$). This would lead to a non-symmetric formulation preffering one phase over the other one. This may cause some problems in numerical computation if, for example, one of the phases in the two-phase system occurs in a very small amount. In our method we use a different approach based on the LQ-factorization of matrix $\mathbb{A}$, which can treat all phases in a unified way. The symmetry of our formulation is an advantageous feature that makes the method robust even in these limit situations. The reduction in dimensionality can be performed using two subspaces $\mathcal{Y}$ and $\mathcal{Z}$, where $\mathcal{Y}$ is the $(n+1)$-dimensional subspace of R^{2n+2} spanned by the rows of matrix $\mathbb{A}$ and $\mathcal{Z}$ is $(n+1)$-dimensional subspace of R^{2n+2} of vectors orthogonal to the rows of matrix $\mathbb{A}$. As

$$\mathrm{R}^{2n+2} = \mathcal{Y} \oplus \mathcal{Z}, \tag{9}$$

any $(2n+2)$-dimensional vector $\mathbf{x}$ can be uniquely written as a sum of vectors from $\mathcal{Y}$ and $\mathcal{Z}$ as

$$\mathbf{x} = \mathbb{Y}\mathbf{x}_{\mathcal{Y}} + \mathbb{Z}\mathbf{x}_{\mathcal{Z}}, \tag{10}$$

where $\mathbb{Y}$ and $\mathbb{Z}$ denote matrices from $\mathrm{R}^{(2n+2)\times(n+1)}$ whose columns represent bases of subspaces $\mathcal{Y}$ and $\mathcal{Z}$, respectively, the $(n+1)$-dimensional vector $\mathbf{x}_{\mathcal{Y}}$ is called the range-space part of $\mathbf{x}$, and the $(n+1)$-dimensional vector $\mathbf{x}_{\mathcal{Z}}$ is called the null-space part of $\mathbf{x}$. The solution $\mathbf{x}^*$ of the constrained optimization problem, given by $\mathbf{x}^* = \mathrm{Y}\mathbf{x}_{\mathrm{Y}}^* + \mathrm{Z}\mathbf{x}_{\mathrm{Z}}^*$, is feasible, therefore

$$\mathbb{A}\mathbf{x}^* = \mathbb{A}(\mathbb{Y}\mathbf{x}_{\mathcal{Y}}^* + \mathbb{Z}\mathbf{x}_{\mathcal{Z}}^*) = \mathbf{b}.$$

From the definition of the subspace $\mathcal{Z}$, it follows that $\mathbb{A}\mathbb{Z} = 0$, and

$$\mathbb{A}\mathbb{Y}\mathbf{x}_{\mathcal{Y}}^* = \mathbf{b}.$$

From the definition of subspace $\mathcal{Y}$ it follows that the matrix $\mathbb{A}\mathbb{Y}$ is non-singular, so the vector $\mathbf{x}_{\mathcal{Y}}^*$ is uniquely determined by the previous equation. Similarly, any feasible vector $\mathbf{x}$ must have the same range-space part, that means $\mathbf{x}_{\mathcal{Y}} = \mathbf{x}_{\mathcal{Y}}^*$, and on the contrary, any vector with range-space component $\mathbf{x}_{\mathcal{Y}}^*$ satisfies the constraints of the optimization problem. So the range-space part $\mathbf{x}_{\mathcal{Y}}^*$ of the solution is uniquely determined by the constraints, and only the $(n+1)$-dimensional part $\mathbf{x}_{\mathcal{Z}}^*$ remains unknown.

To represent the null-space $\mathcal{Z}$, we use the LQ-factorization of matrix $\mathbb{A}$ [12]. Let $\mathbb{Q} \in \mathrm{R}^{(2n+2)\times(2n+2)}$ be an orthogonal matrix such that

$$\mathbb{A}\mathbb{Q} = (\mathbb{L} \quad 0), \tag{11}$$

where $\mathbb{L} \in \mathrm{R}^{(n+1)\times(n+1)}$ is a non-singular lower triangular matrix. From this it can be seen that the matrix $\mathbb{Y}$ can be chosen as the first $n+1$ columns of matrix $\mathbb{Q}$ and the matrix $\mathbb{Z}$ can be chosen as the remaining $n+1$ columns of $\mathbb{Q}$, i.e.

$$\mathbb{Q} = (\mathbb{Y} \quad \mathbb{Z}). \tag{12}$$

If we denote the identity matrix in R^{n+1} as $\mathbb{I}_{n+1}$, the matrix $\mathbb{A}$ can be written as $\mathbb{A} = (\begin{smallmatrix} \mathbb{I}_{n+1} & \mathbb{I}_{n+1} \end{smallmatrix})$. The matrices $\mathbb{Y}$ and $\mathbb{Z}$ then read as

$$\mathbb{Y} = \frac{1}{\sqrt{2}}\mathbb{A}^T = \frac{1}{\sqrt{2}}\begin{pmatrix} \mathbb{I}_{n+1} \\ \mathbb{I}_{n+1} \end{pmatrix}, \quad \mathbb{Z} = \frac{1}{\sqrt{2}}\begin{pmatrix} \mathbb{I}_{n+1} \\ -\mathbb{I}_{n+1} \end{pmatrix}. \tag{13}$$

Our algorithm for solving the optimization problem is iterative. Provided that we start from a feasible initial guess $\mathbf{x}^{(0)}$, the algorithm generates a sequence of feasible iterates $\mathbf{x}^{(k)}$. In every iteration, $\mathbf{x}^{(k)}$ is updated as

$$\mathbf{x}^{(k+1)} = \mathbf{x}^{(k)} + \alpha_k \mathbf{d}^{(k)},$$

where $\alpha_k > 0$ denotes the step size and $\mathbf{d}^{(k)}$ denotes the direction vector. Assuming that $\mathbf{x}^{(k)}$ is feasible, we require that $\mathbf{x}^{(k+1)}$ be feasible too. To satisfy this, it is necessary that the direction vector $\mathbf{d}^{(k)}$ be orthogonal to the rows of $\mathbb{A}$, i.e.

$$\mathbb{A}\mathbf{d}^{(k)} = 0, \tag{14}$$

or equivalently

$$\mathbf{d}^{(k)} = \mathbb{Z}\mathbf{d}_{\mathcal{Z}}^{(k)}, \tag{15}$$

for a suitable $(n+1)$-dimensional vector $\mathbf{d}_{\mathcal{Z}}^{(k)}$. It is obvious that the search direction $\mathbf{d}^{(k)}$ is a $(2n+2)$-dimensional vector, which is constructed to lie in a $(n+1)$-dimensional subspace $\mathcal{Z}$. The columns of matrix $\mathbb{Z}$ forming an orthogonal basis of $\mathcal{Z}$ are given by (13), so it remains to determine the vector $\mathbf{d}_{\mathcal{Z}}^{(k)} \in \mathrm{R}^{n+1}$. This way we have transformed the constrained minimization problem to an unconstrained problem in a lower dimension.

To find the vector $\mathbf{d}_{\mathcal{Z}}^{(k)}$, we use the modified Newton method, which is based on the quadratic approximation of function ΔA around the point $\mathbf{x}^{(k)}$. Let us denote by $\mathbf{g}(\mathbf{x})$ the gradient of the

function ΔA. By partial differentiating of ΔA with respect to its variables, we obtain

$$\mathbf{g}(\mathbf{x}) = \nabla(\Delta A)^T = \begin{pmatrix} \mu_1(V', T, N_1', \dots, N_n') \\ \vdots \\ \mu_n(V', T, N_1', \dots, N_n') \\ -P(V', T, N_1', \dots, N_n') \\ \mu_1(V'', T, N_1'', \dots, N_n'') \\ \vdots \\ \mu_n(V'', T, N_1'', \dots, N_n'') \\ -P(V'', T, N_1'', \dots, N_n'') \end{pmatrix}. \tag{16}$$

Next, let us denote by $\mathbb{H}(\mathbf{x})$ the Hessian of the function ΔA obtained in the following block-diagonal form

$$\mathbb{H}(\mathbf{x}) = \nabla^2 \Delta A = \begin{pmatrix} \mathbb{B}' & \mathbb{C}' & & \\ \mathbb{C}'^T & \mathbb{D}' & & \\ & & \mathbb{B}'' & \mathbb{C}'' \\ & & \mathbb{C}''^T & \mathbb{D}'' \end{pmatrix}, \tag{17}$$

where

$$\begin{aligned} &\mathbb{B}' \in \mathrm{R}^{n\times n}, \quad \mathbb{B}'_{ij} = \frac{\partial \mu_i}{\partial N_j'}(V', T, N_1', \dots, N_n'), \\ &\mathbb{B}'' \in \mathrm{R}^{n\times n}, \quad \mathbb{B}''_{ij} = \frac{\partial \mu_i}{\partial N_j''}(V'', T, N_1'', \dots, N_n''), \\ &\mathbb{C}' \in \mathrm{R}^{n}, \quad \mathbb{C}'_{j} = -\frac{\partial P}{\partial N_j'}(V', T, N_1', \dots, N_n'), \\ &\mathbb{C}'' \in \mathrm{R}^{n}, \quad \mathbb{C}''_{j} = -\frac{\partial P}{\partial N_j''}(V'', T, N_1'', \dots, N_n''), \\ &\mathbb{D}' \in \mathrm{R}^{1}, \quad \mathbb{D}' = -\frac{\partial P}{\partial V'}(V', T, N_1', \dots, N_n'), \\ &\mathbb{D}'' \in \mathrm{R}^{1}, \quad \mathbb{D}'' = -\frac{\partial P}{\partial V''}(V'', T, N_1'', \dots, N_n'') \end{aligned}. \tag{}$$

Approximating the function ΔA using the Taylor expansion around the point $\mathbf{x}^{(k)}$ up to the quadratic terms, the search direction $\mathbf{d}^{(k)} = \mathbb{Z}\mathbf{d}_{\mathcal{Z}}^{(k)}$ is found as a solution of the following minimization problem

$$\begin{aligned} &\min_{\mathbf{d}^{(k)}\in \mathrm{R}^{(2n+2)}} \Delta A(\mathbf{x}^{(k)} + \mathbf{d}^{(k)}) = \min_{\mathbf{d}_{\mathcal{Z}}^{(k)}\in \mathrm{R}^{(n+1)}} \Delta A(\mathbf{x}^{(k)} + \mathbb{Z}\mathbf{d}_{\mathcal{Z}}^{(k)}) \\ &\mathbb{A}\mathbf{d}^{(k)} = 0 \\ &\approx \min_{\mathbf{d}_{\mathcal{Z}}^{(k)}\in \mathrm{R}^{(n+1)}} \Delta A(\mathbf{x}^{(k)}) + \mathbf{g}(\mathbf{x}^{(k)})^T \mathbb{Z}\mathbf{d}_{\mathcal{Z}}^{(k)} + \frac{1}{2}(\mathbb{Z}\mathbf{d}_{\mathcal{Z}}^{(k)})^T \mathbb{H}(\mathbf{x}^{(k)})\mathbb{Z}\mathbf{d}_{\mathcal{Z}}^{(k)}. \end{aligned} \tag{18}$$

The vector $\mathbf{d}_{\mathcal{Z}}^{(k)}$ is the argument of minimum of a quadratic function Φ defined as

$$\Phi(\mathbf{d}_{\mathcal{Z}}) = \mathbf{g}(\mathbf{x}^{(k)})^T \mathbb{Z}\mathbf{d}_{\mathcal{Z}} + \frac{1}{2}\mathbf{d}_{\mathcal{Z}}^T \mathbb{Z}^T \mathbb{H}(\mathbf{x}^{(k)})\mathbb{Z}\mathbf{d}_{\mathcal{Z}}.$$

The function Φ has a stationary point if and only if there is a $\mathbf{d}_{\mathcal{Z}}^{(k)}$, for which the gradient of Φ vanishes, i.e.

$$\nabla\Phi(\mathbf{d}_{\mathcal{Z}}^{(k)}) = 0. \tag{19}$$

The stationary point $\mathbf{d}_{\mathcal{Z}}^{(k)}$ is a solution of the following system of equations

$$\mathbb{H}_{\mathcal{Z}}(\mathbf{x}^{(k)})\mathbf{d}_{\mathcal{Z}}^{(k)} = -\mathbf{g}_{\mathcal{Z}}(\mathbf{x}^{(k)}), \tag{20}$$

where $\mathbb{H}_{\mathcal{Z}}(\mathbf{x}^{(k)}) \in \mathrm{R}^{(n+1)\times(n+1)}$ and $\mathbf{g}_{\mathcal{Z}}(\mathbf{x}^{(k)}) \in \mathrm{R}^{n+1}$ are the restrictions of the Hessian and of the gradient vector to the subspace $\mathcal{Z}$ defined as

$$\mathbb{H}_{\mathcal{Z}}(\mathbf{x}^{(k)}) = \mathbb{Z}^T \mathbb{H}(\mathbf{x}^{(k)})\mathbb{Z} \tag{21}$$

and

$$\mathbf{g}_{\mathcal{Z}}(\mathbf{x}^{(k)}) = \mathbb{Z}^T \mathbf{g}(\mathbf{x}^{(k)}). \tag{22}$$

Combining (13), (16), and (17), it follows from (21) and (22) that

$$\mathbb{H}_{\mathcal{Z}}(\mathbf{x}^{(k)}) = \frac{1}{2}\begin{pmatrix} \mathbb{B} & \mathbb{C} \\ \mathbb{C}^T & \mathbb{D} \end{pmatrix}, \tag{23}$$

where

$$\begin{aligned} &\mathbb{B} \in \mathrm{R}^{n\times n}, \mathbb{B}_{ij} = \frac{\partial \mu_i}{\partial N_j'}(V', T, N_1', \dots, N_n') + \frac{\partial \mu_i}{\partial N_j''}(V'', T, N_1'', \dots, N_n''), \\ &\mathbb{C} \in \mathrm{R}^{n}, \mathbb{C}_j = -\frac{\partial P}{\partial N_j'}(V', T, N_1', \dots, N_n') - \frac{\partial P}{\partial N_j''}(V'', T, N_1'', \dots, N_n'') \\ &\mathbb{D} \in \mathrm{R}^{1}, \mathbb{D} = -\frac{\partial P}{\partial V'}(V', T, N_1', \dots, N_n') - \frac{\partial P}{\partial V''}(V'', T, N_1'', \dots, N_n''), \end{aligned}$$

and

$$\mathbf{g}_{\mathcal{Z}}(\mathbf{x}^{(k)}) = \frac{1}{\sqrt{2}}\begin{pmatrix} \mu_1(V', T, N_1', \dots, N_n') - \mu_1(V'', T, N_1'', \dots, N_n'') \\ \vdots \\ \mu_n(V', T, N_1', \dots, N_n') - \mu_n(V'', T, N_1'', \dots, N_n'') \\ -P(V', T, N_1', \dots, N_n') + P(V'', T, N_1'', \dots, N_n'') \end{pmatrix}. \tag{24}$$

Note that the gradient vector in (16) depends on the values of chemical potentials, which are determined up to an arbitrary constant. Unlike in (16), the restricted gradient given by (24) is a function of differences of the chemical potentials between two states whose values can be evaluated uniquely using the equation of state [9]. Unlike in [7], our formulation does not require to use the complex arithmetics.

If $\mathbf{d}_{\mathcal{Z}}^{(k)}$ solves the system of the equations (20) and the matrix $\mathbb{H}_{\mathcal{Z}}$ is positive definite, then the search direction $\mathbf{d}_{\mathcal{Z}}^{(k)}$ is a descent direction. If the matrix of the projected Hessian is not positive definite, then either the quadratic approximation of the function is not bounded from below, or a single minimum does not exist. In this

case, it is necessary to modify the direction $\mathbf{d}_{\mathcal{Z}}^{(k)}$. If the matrix $\mathbb{H}_{\mathcal{Z}}$ is indefinite, then the vector $\mathbf{d}_{\mathcal{Z}}^{(k)}$ is found as a solution of a modified system of the equations

$$\widehat{\mathbb{H}_{\mathcal{Z}}}(\mathbf{x}^{(k)})\mathbf{d}_{\mathcal{Z}}^{(k)} = -\mathbf{g}_{\mathcal{Z}}(\mathbf{x}^{(k)}), \tag{25}$$

where $\widehat{\mathbb{H}_{\mathcal{Z}}}(\mathbf{x}^{(k)})$ is a positive definite matrix obtained by the modified Cholesky decomposition of the matrix $\mathbb{H}_{\mathcal{Z}}(\mathbf{x}^{(k)})$. In this algorithm the usual Cholesky factorization is performed to decompose matrix $\mathbb{H}_{\mathcal{Z}}(\mathbf{x}^{(k)})$ into the product $\mathbb{L}\mathbb{L}^T$ where $\mathbb{L}$ is a lower triangular matrix. If a negative element appears on the diagonal of $\mathbb{L}$ during the Cholesky factorization, a suitable value is added to this element to ensure its positivity in the final decomposition. This way we obtain the Cholesky factorization of a positive definite matrix $\widehat{\mathbb{H}_{\mathcal{Z}}}(\mathbf{x}^{(k)})$, which is used instead of matrix $\mathbb{H}_{\mathcal{Z}}(\mathbf{x}^{(k)})$ in (25) to determine the direction $\mathbf{d}_{\mathcal{Z}}^{(k)}$ in the Newton method. This modification of the Newton method ensures that the obtained direction is a descent direction. Therefore, for a sufficiently small step size $\alpha_k > 0$, the decrease of ΔA can be guaranteed. The following line-search technique can be used to find the step size α_k. First, we put $\alpha_k = 1$ and test if $\Delta A(\mathbf{x}^{(k)} + \mathbf{d}^{(k)}) < \Delta A(\mathbf{x}^{(k)})$. If this condition is satisfied, we set $\mathbf{x}^{(k+1)} = \mathbf{x}^{(k)} + \mathbf{d}^{(k)}$. If the condition is violated, we halve the value of α_k until the condition $\Delta A(\mathbf{x}^{(k)} + \alpha_k\mathbf{d}^{(k)}) < \Delta A(\mathbf{x}^{(k)})$ is satisfied and then set $\mathbf{x}^{(k+1)} = \mathbf{x}^{(k)} + \alpha_k\mathbf{d}^{(k)}$. This completes a single iteration of the Newton method. The iterations are terminated when a suitable stopping criterion is satisfied or the method continues with the next iteration if needed. In this work, we stop the iterations if (cf. [13])

$$\|\mathbf{d}^{(k)}\|_2 := \left(\sum_{j=1}^{2n+2} \mathbf{d}_j^{(k)2}\right)^{1/2} \leq \varepsilon_{tol} = 10^{-7}. \tag{26}$$

4. Initialization of the *VT*-flash algorithm

To initialize the algorithm, an initial guess $\mathbf{x}^{(0)}$ is needed. We use the *VT*-stability test from [10] before the *VT*-flash calculation to test whether the single phase is stable or not at given volume V, temperature T, and mole numbers $N_1, \ldots, N_n$. Denoting by $c_i = N_i/V$ the overall molar concentrations of all components, the *VT*-stability algorithm tests whether a trial phase with concentrations c_i' can be found such that, if taken in a small amount from the initial phase, the two-phase system will have lower total Helmholtz free energy than the single-phase system. From this, the following criterion of stability at constant volume, temperature, and moles can be derived (see [10] for details). The single phase is stable if

$$\begin{aligned} &D(T, c_1', \ldots, c_n') \\ &= \lim_{V' \to 0+} \frac{\Delta A}{V'} = \sum_{i=1}^{n} [\mu_i(1, T, c_1', \ldots, c_n') - \mu_i(1, T, c_1, \ldots, c_n)]c_i' \\ &\quad -[P(1, T, c_1', \ldots, c_n') - P(1, T, c_1, \ldots, c_n)] \geq 0 \end{aligned} \tag{27}$$

for all admissible states $(T, c_1', \ldots, c_n')$. If this condition is satisfied, the system is in single-phase and the *VT*-flash calculation is avoided (pressure can be computed using the equation of state). In the opposite case, the mixture splits into phases and the *VT*-stability algorithm provides trial phase concentrations c_i' such that $D(T, c_1', \ldots, c_n') < 0$. As $D(T, c_1', \ldots, c_n') = \lim_{V' \to 0+} \Delta A/V' < 0$, we can use the bisection method to find a small volume $V' > 0$ such that $\Delta A < 0$ for a state in which one phase is the trial phase with volume V' and mole numbers $N_i' = c_i'V'$ and the other phase properties V'' and N_i'' are computed such that (4) and (5) hold. This way we construct a two-phase state with lower total Helmholtz free energy than the initial single-phase state. As the *VT*-flash algorithm guarantees to decrease the total Helmholtz free energy in every iteration, the possibility of convergence toward the trivial solution is excluded.

5. Algorithm of the modified Newton method for *VT*-flash

Now, we are ready to summarize the essential steps of our algorithm.

Step 1 Let $N_1, \ldots, N_n$, V and $T > 0$ be given. Set the number of iterations $k = 0$. Get an initial feasible solution $\mathbf{x}^{(0)} \in \mathrm{R}^{2n+2}$ from the *VT*-stability algorithm

$$\mathbf{x}^{(0)} = \begin{pmatrix} N_1' \\ \vdots \\ N_n' \\ V' \\ N_1'' \\ \vdots \\ N_n'' \\ V'' \end{pmatrix}. \tag{28}$$

Step 2 Assemble the Hessian $\mathbb{H}_{\mathcal{Z}}(\mathbf{x}^{(k)})$ and the gradient $\mathbf{g}_{\mathcal{Z}}(\mathbf{x}^{(k)})$ of ΔA in the kth iteration projected to the subspace $\mathcal{Z}$ using (23) and (24).

Step 3 Compute the projected step direction $\mathbf{d}_{\mathcal{Z}}^{(k)} \in \mathrm{R}^{n+1}$, and the feasible direction $\mathbf{d}^{(k)} \in \mathrm{R}^{2n+2}$ by

$$\mathbb{H}_{\mathcal{Z}}(\mathbf{x}^{(k)})\mathbf{d}_{\mathcal{Z}}^{(k)} = -\mathbf{g}_{\mathcal{Z}}(\mathbf{x}^{(k)}), \tag{29}$$

$$\mathbf{d}^{(k)} = \mathbb{Z}\mathbf{d}_{\mathcal{Z}}^{(k)}. \tag{30}$$

If the matrix $\mathbb{H}_{\mathcal{Z}}(\mathbf{x}^{(k)})$ is not positive definite, find the vector $\mathbf{d}_{\mathcal{Z}}^{(k)}$ by solving a modified system of equations

$$\widehat{\mathbb{H}_{\mathcal{Z}}}(\mathbf{x}^{(k)})\mathbf{d}_{\mathcal{Z}}^{(k)} = -\mathbf{g}_{\mathcal{Z}}(\mathbf{x}^{(k)}), \tag{31}$$

where $\widehat{\mathbb{H}_{\mathcal{Z}}}(\mathbf{x}^{(k)})$ is a positive definite matrix obtained from the modified Cholesky factorization of matrix $\mathbb{H}_{\mathcal{Z}}(\mathbf{x}^{(k)})$.

Step 4 Determine the step length $\alpha_k > 0$ for the kth iteration satisfying

$$\Delta A(\mathbf{x}^{(k)} + \alpha_k\mathbf{d}^{(k)}) < \Delta A(\mathbf{x}^{(k)}). \tag{32}$$

First, set the step length to $\alpha_k = 1$ and test if the condition (32) holds. If not, use the bisection method to find a value of α_k satisfying (32).

Step 5 Update the approximation as

$$\mathbf{x}^{(k+1)} = \mathbf{x}^{(k)} + \alpha_k\mathbf{d}^{(k)}. \tag{33}$$

Step 6 Test the convergence using (26). If needed, increase k by 1 and go to Step 2. If not needed, the algorithm ends up with the solution $\mathbf{x}^{(k+1)}$.

6. Numerical examples of *VT*-flash calculations

We have tested the algorithm in several examples for binary and multi-component mixtures under different conditions. First, we have tested the *VT*-flash algorithm on all examples of mixtures from [9]. The new algorithm converged well in all cases and provided the same solutions as those reported in [9]. In all cases the

Table 1
Numbers of iterations for the VT-flash algorithm developed in this paper and the succesive substitution iteration (SSI) from [9] for five mixtures investigated in [9]. Example numbers refer to Examples in [9]. The detailed description of the mixtures and conditions can be found in [9].

Number of iterations	VT-flash (this work)	VT-flash SSI [9]
Example 1	6	46
Example 2	6	20
Example 3	6	25
Example 4 (with N_2)	6	33
Example 4 (with CO_2)	6	266

Table 2
Parameters of the Peng–Robinson and CPA equations of state for all components used in all examples.

Component	$T_{i,crit}$ [K]	$P_{i,crit}$ [MPa]	ω_i	$M_{w,i}$ [kg kmol^{-1}]
H_2O	647.29	22.09	0.3440	18.01528
CO_2	304.14	7.375	0.2390	44.0
N_2	126.21	3.390	0.0390	28.0
C_1	190.56	4.599	0.0110	16.0
C_3	369.83	4.248	0.1530	44.1
nC_5	469.70	3.370	0.2510	72.2
C_6	507.40	3.012	0.2960	86.2
nC_{10}	617.70	2.110	0.4890	142.28

new method needed much less iterations than the SSI method from [9]. The numbers of iterations for both methods are summarized in Table 1.

In the following examples, we simulate isothermal compression of a mixture in a closed cell. The *VT*-stability algorithm from [10] is used to detect the boundary between the stable single-phase and two-phase regions for an interval of temperatures and for the whole range of admissible molar concentrations c. For a selected temperature T, we change the overall molar concentration c and provide results of the *VT*-flash calculations for the mixture at temperature T and molar concentrations $c_i = cz_i$. We present six examples of different complexity. In Examples 1–5, we use the Peng–Robinson equastion of state. Parameters of the Peng–Robinson equation of state for all components used are presented in Table 2. For Example 6, we use the Cubic-Plus-Association (CPA) equation of state. Details for both the equations of state can be found in Appendix A.

Note that in the following examples *VT*-flash algorithm is used to evaluate amount and properties of the split phases, generally denoted as phase 1 and phase 2. We have not attempted to perform any phase identification or post processing of the results. Therefore, the numbering of the phases depends solely on the result of the minimization procedure. In some figures we can observe swapping of the two-phases at certain points but this effect has no physical significance.

Example 1

In the first example, we investigate two-phase equilibrium for pure carbon dioxide (CO_2). The approximate boundary between the single-phase and two-phase domains in the c, T-space obtained from *VT*-stability analysis is shown in Fig. 1 (left). As shown in Fig. 1 (left), at temperature $T = 280$ K the mixture occurs in single-phase for low enough molar densities. During isothermal compression, at moderate molar concentrations the mixture splits into two phases, while at high molar densities (higher than 20 kmol m^{-3}) the mixture becomes single-phase again. We show the saturations (volume fractions) of both phases and mass densities of both phases as functions of the overall molar density c in Fig. 2. The equilibrium pressure for each overall molar concentration c is presented in Fig. 1 (right).

Note that within the two-phase region (between points A and B in Fig. 1 (right)), the pressure is constant and equal to the saturation pressure P_{sat} corresponding to the temperature $T = 280$ K. All these states occur at the same pressure P, temperature T, and mole number N. Therefore, *PT*-stability and *PT*-flash cannot distinguish between these states. As these states have different volumes, the *VT*-based formulation can distinguish between them. This example shows that the variables P, T, N are not equivalent to V, T, N in the sense that specifying the volume, temperature and moles uniquely determines the equilibrium state of the system. This is not the case of the P, T, N formulation in which all two-phase states and both saturated gas (point A in Fig. 1 (right)) and saturated liquid (point B in Fig. 1 (right)) occur at the same values of P, T, N.

There are also other advantages of the volume-based formulations. Consider applying *PT*-stability and *PT*-flash to a pure component system at temperature T and pressures $P_1 = P_{sat}(T) + \varepsilon$ and $P_2 = P_{sat}(T) - \varepsilon$, where $\varepsilon > 0$ is an arbitrarily small number. For both cases, the system is in single-phase. For P_1 we have an almost saturated liquid with molar concentration c_1, for P_2 we have an almost saturated gas with molar concentration $c_2 < c_1$. While the difference of pressures $P_1 - P_2$ is very small, the difference in concentrations $c_1 - c_2$ may be large, i.e. although the pressure change is small, the volume of the system changes a lot. The discontinuous jump in volume associated with a small change in pressure may

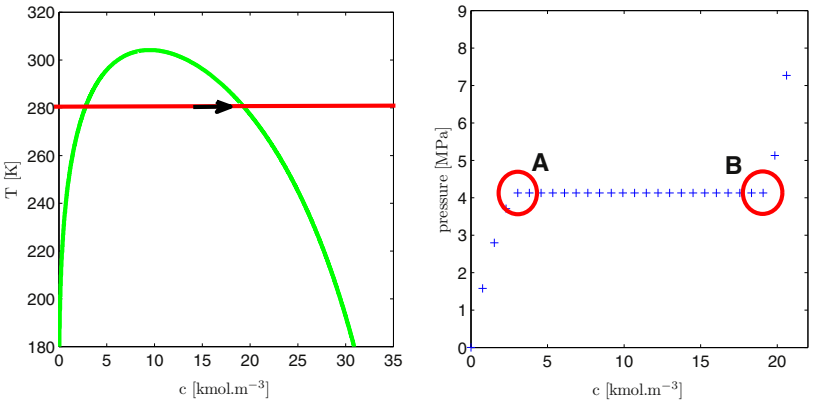

Fig. 1. Approximate boundary between the single-phase and two-phase domains in the c, T-space (left). The arrow indicates the compression at constant temperature $T = 280$ K. Equilibrium pressure as a function of the overall molar density c at $T = 280$ K (right). Example 1: pure CO_2.

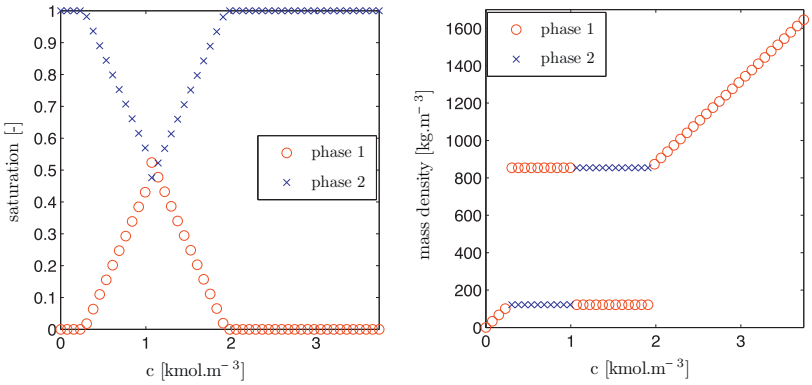

Fig. 2. Saturations (left) and mass densities (right) of both phases as functions of the overall molar density c. Example 1: pure CO_2 at $T = 280$ K.

cause convergence problems in numerical methods applied to the solution of the *PT*-flash. On the other hand, in the *VT*-formulation, the equilibrium pressure is a continuous function of the total volume of the system (cf. Fig. 1 (right)).

Example 2

In the second example, we investigate two-phase equilibrium for a binary mixture of methane (C_1) and normal pentane (nC_5) with mole fractions $z_{C_1} = 0.547413$ and $z_{nC_5} = 0.452587$. The binary interaction coefficient $\delta_{C_1-nC_5} = 0.041$. The approximate boundary between the single-phase and two-phase domains in the c, T-space obtained from *VT*-stability analysis is shown in Fig. 3 (left). As shown in Fig. 3 (left), at temperature $T = 371$ K the mixture occurs in single-phase for low molar densities. During isothermal compression, the mixture splits into two phases at moderate molar densities, while at high molar densities (higher than 9 kmol m^{-3}) the mixture becomes single-phase again.

The equilibrium pressure as a function of the overall molar density c is presented in Fig. 3 (right) illustrating a steady rise of the equilibrium pressure during compression, and its substantial increase at molar densities 9 kmol m^{-3} and higher when all gas is depleted. Saturations of both phases and mass densities of both phases as functions of the overall molar density c are presented in Fig. 4. Mole fractions of both components in both phases for each overall molar density c are presented in Fig. 5.

Example 3

In the third example, we investigate two-phase equilibrium for a binary mixture of carbon dioxide (CO_2) and normal decane (nC_{10}) with mole fractions $z_{CO_2} = 0.547413$ and $z_{C_{10}} = 0.452587$. The binary interaction coefficient $\delta_{CO_2-nC_{10}} = 0.150$. The approximate boundary between the single-phase and two-phase domains in the c, T-space obtained from *VT*-stability analysis is shown in Fig. 6 (left). As shown in Fig. 6, when compressing at constant temperature $T = 311$ K, the mixture occurs in two-phase from the lowest molar densities up to approximately 8 kmol m^{-3}, then the mixture becomes single-phase, while at molar densities higher than 9.5 kmol m^{-3} the mixture becomes two-phase again.

The equilibrium pressure as a function of the overall molar density c is presented in Fig. 6 (right) illustrating a steady rise of the equilibrium pressure during compression, and its substantial increase at molar densities 8 kmol m^{-3} and higher when all gas phase is depleted. Saturations of both phases and mass densities of both phases as functions of the overall molar density c are presented in Fig. 7. Mole fractions of both components in both

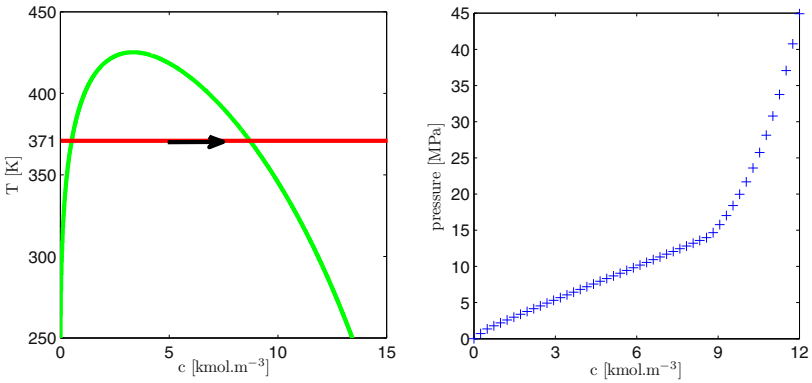

Fig. 3. Approximate boundary between the single-phase and two-phase domains in the c, T-space (left). The arrow indicates the compression at constant temperature $T = 371$ K. Equilibrium pressure as a function of the overall molar density c at $T = 371$ K (right). Example 2: binary C_1–nC_5 mixture ($z_{C_1} = 0.547413$, $z_{nC_5} = 0.452587$).

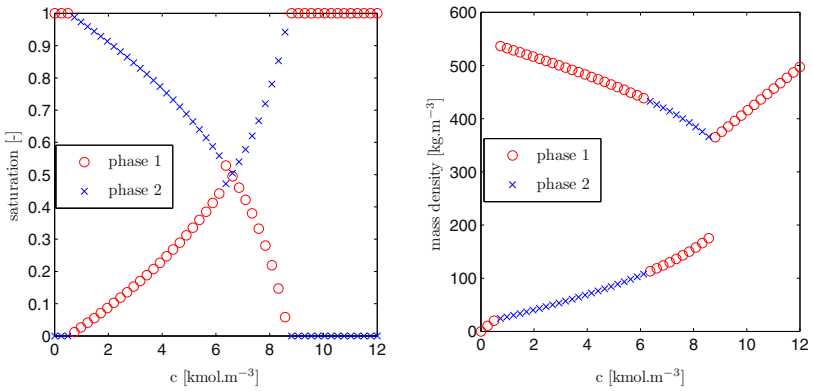

Fig. 4. Saturations (left) and mass densities (right) of both phases as functions of the overall molar density c. Example 2: binary C_1–nC_5 mixture ($z_{C_1} = 0.547413$, $z_{nC_5} = 0.452587$, and $T = 371$ K).

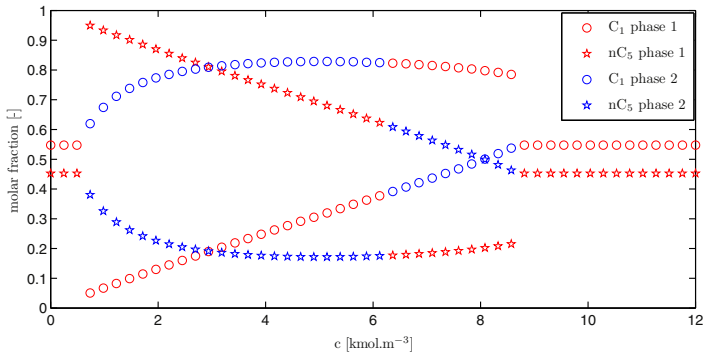

Fig. 5. Molar fractions of both components in both phases as functions of the overall molar density c at $T = 371$ K. Example 2: binary C_1–nC_5 mixture ($z_{C_1} = 0.547413$, $z_{nC_5} = 0.452587$).

phases as functions of the overall molar density c are presented in Fig. 8.

Figs. 6 (left) and 7 (right) suggest that the second two-phase region at high molar densities and low temperatures may correspond to a liquid–liquid two-phase region.

Example 4

In the fourth example, we investigate two-phase equilibrium for a ternary mixture of methane (C_1), hexane (C_6) and normal decane (nC_{10}) with mole fractions $z_{C_1} = 0.405946$, $z_{C_6} = 0.297027$ and

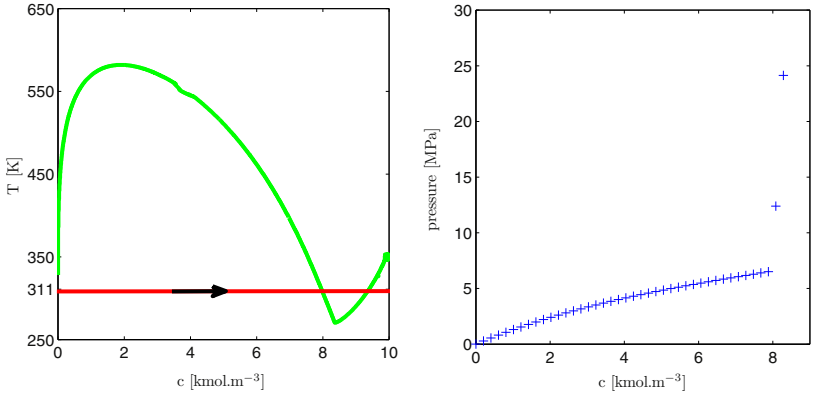

Fig. 6. Approximate boundary between the single-phase and two-phase domains in the c, T-space (left). The arrow indicates the compression at constant temperature $T = 311$ K. Equilibrium pressure as a function of the overall molar density c (right) at $T = 311$ K. Example 3: binary CO_2–nC_{10} mixture ($z_{CO_2} = 0.547413$, $z_{C_{10}} = 0.452587$).

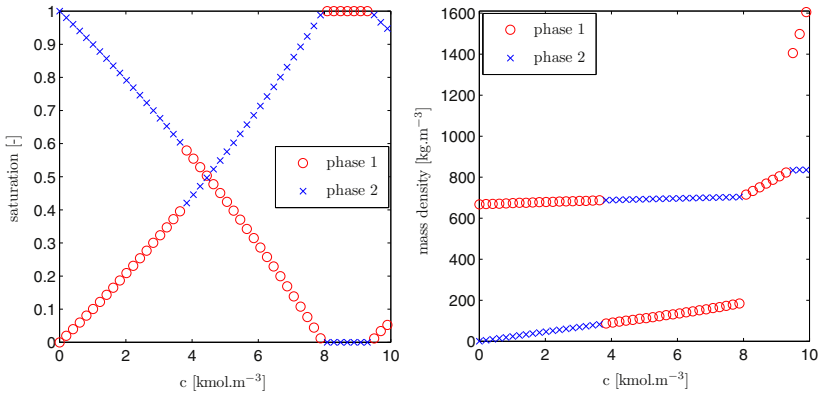

Fig. 7. Saturations (left) and mass densities of both phases as function of the overall molar density c (right). Example 3: binary CO_2–nC_{10} mixture ($z_{CO_2} = 0.547413$, $z_{C_{10}} = 0.452587$, and $T = 311$ K).

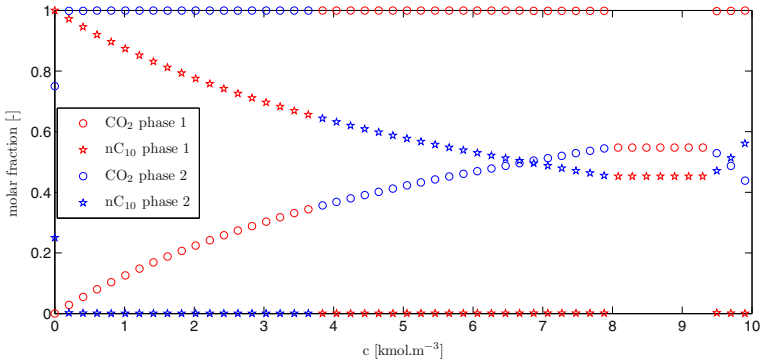

Fig. 8. Molar fractions of both components in both phases as functions of the overall molar density c at $T = 311$ K. Example 3: binary CO_2–nC_{10} mixture ($z_{CO_2} = 0.547413$, $z_{C_{10}} = 0.452587$).

$z_{C_{10}} = 0.297027$. The binary interaction coefficients are presented in Table 3. The approximate boundary between the single-phase and two-phase domains in the c, T-space obtained from VT-stability analysis is shown in Fig. 9 (left). As shown in Fig. 9 (left), at constant temperature $T = 420$ K the mixture occurs in two-phase from the lowest molar densities up to approximately 6.5 kmol m^{-3}, then it becomes single-phase.

The equilibrium pressure as a function of the overall molar density c is presented in Fig. 9 (right) illustrating a steady rise of the equilibrium pressure during compression, and a substantial

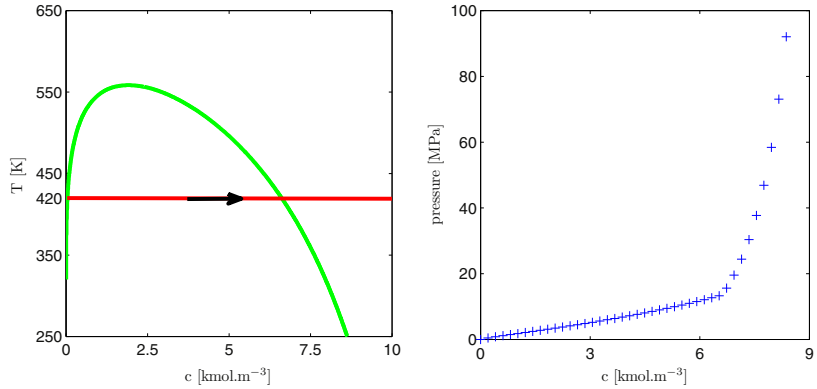

Fig. 9. Approximate boundary between the single-phase and two-phase domains in the c, T-space (left). The arrow indicates the compression at constant temperature $T = 420$ K. The equilibrium pressure as a function of the overall molar density c at $T = 420$ K (right). Example 4: ternary C_1–C_6–nC_{10} mixture ($z_{C_1} = 0.405946$, $z_{C_6} = 0.297027$, $z_{C_{10}} = 0.297027$).

Table 3
Binary interaction coefficients for the ternary mixture used in Example 4.

Component	C_1	C_6	nC_{10}
C_1	0	0.043	0.052
C_6	0.043	0	0
nC_{10}	0.052	0	0

Table 4
Binary interaction coefficients for the four-component mixture used in Example 5.

Component	N_2	C_1	C_3	nC_{10}
N_2	0	0.1	0.1	0.1
C_1	0.1	0	0.036	0.052
C_3	0.1	0.036	0	0
nC_{10}	0.1	0.052	0	0

increase at molar densities 6.5 kmol m^{-3} and higher when all gas phase is depleted. Saturations of both phases and mass densities of both phases as functions of the overall molar density c are presented in Fig. 10. Mole fractions of all components in both phases as functions of the overall molar density c are presented in Fig. 11.

Example 5

In the fifth example, we investigate phase equilibrium for a four-component mixture of nitrogen (N_2), methane (C_1), propane (C_3), and normal decane (nC_{10}) with mole fractions $z_{N_2} = 0.2463$, $z_{C_1} = 0.2208$, $z_{C_3} = 0.2208$, and $z_{nC_{10}} = 0.3121$. The binary interaction coefficients are shown in Table 4. The approximate boundary between the single-phase and two-phase domains in the c, T-space obtained from VT-stability analysis is shown in Fig. 12 (left). As shown in Fig. 12 (left), at constant temperature $T = 393.15$ K the mixture occurs in two-phase from the lowest molar densities up to approximately 8.2 kmol m^{-3}, then it becomes single-phase.

The equilibrium pressure as a function of the overall molar density c is presented in Fig. 12 (right) illustrating a steady rise of the equilibrium pressure during compression, and a substantial increase at molar densities 8.2 kmol m^{-3} and higher when the gas phase is depleted. Saturations of both phases and mass densities of both phases as functions of the overall molar density c are presented in Fig. 13. Mole fractions of all components in both phases as functions of the overall molar density c are presented in Fig. 14.

Example 6

In the sixth example, we investigate phase equilibrium for a binary mixture of water (H_2O) and carbon dioxide (CO_2) with mole fractions $z_{H_2O} = 0.5$ and $z_{CO_2} = 0.5$. The binary interaction

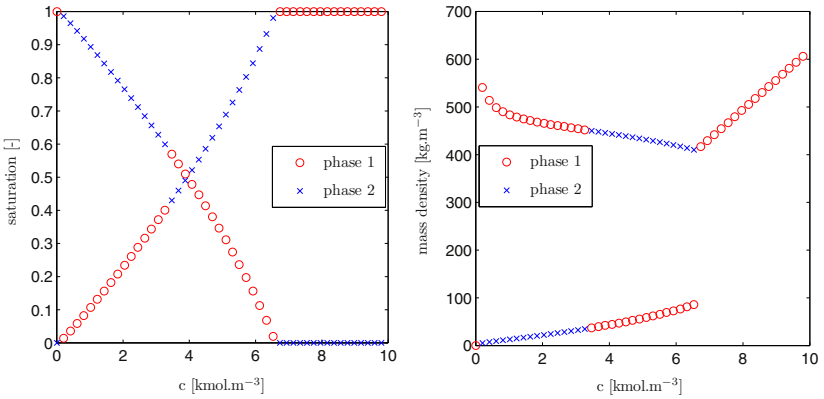

Fig. 10. Saturations (left) and mass densities of both phases (right) as functions of the overall molar density c. Example 4: ternary C_1–C_6–nC_{10} mixture ($z_{C_1} = 0.405946$, $z_{C_6} = 0.297027$, $z_{C_{10}} = 0.297027$, and $T = 420$ K).

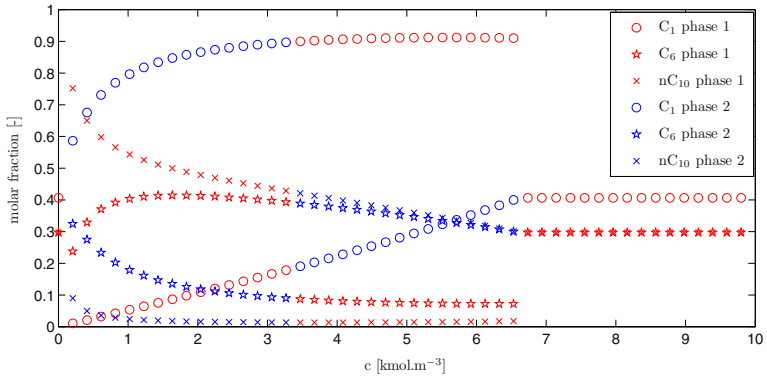

Fig. 11. Molar fractions of all components in both phases as functions of the overall molar density c at $T = 420$ K. Example 4: ternary C_1–C_6–nC_{10} mixture ($z_{C_1} = 0.405946$, $z_{C_6} = 0.297027$ and $z_{C_{10}} = 0.297027$).

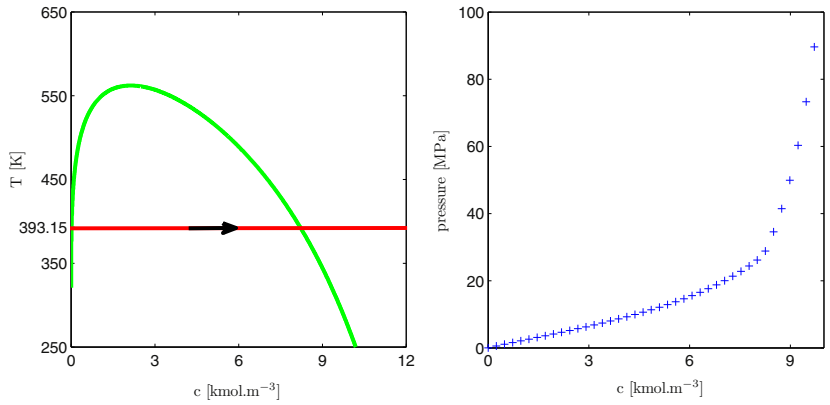

Fig. 12. Approximate boundary between the single-phase and two-phase domains in the c, T-space (left). The arrow indicates the compression at constant temperature $T = 393.15$ K. Equilibrium pressure as a function of the overall molar density c at $T = 393.15$ K (right). Example 5: mixture of N_2–C_1–C_3–nC_{10} ($z_{N_2} = 0.2463$, $z_{C_1} = 0.2208$, $z_{C_3} = 0.2208$, $z_{nC_{10}} = 0.3121$).

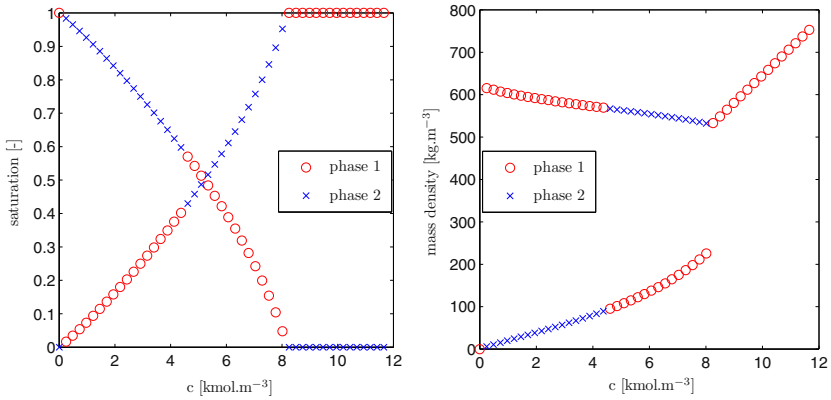

Fig. 13. Saturations (left) and mass densities (right) of both phases as functions of the overall molar density c (right). Example 5: four-component mixture of N_2–C_1–C_3–nC_{10} ($z_{N_2} = 0.2463$, $z_{C_1} = 0.2208$, $z_{C_3} = 0.2208$, $z_{nC_{10}} = 0.3121$, and $T = 393.15$ K).

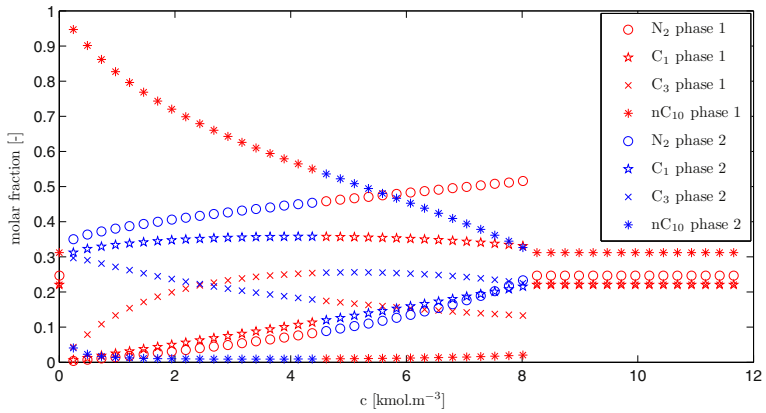

Fig. 14. Molar fractions of all components in both phases as functions of the overall molar density c at $T = 393.15$ K. Example 5: mixture of four-components N_2–C_1–C_3–nC_{10} ($z_{N_2} = 0.2463$, $z_{C_1} = 0.2208$, $z_{C_3} = 0.2208$, $z_{nC_{10}} = 0.3121$).

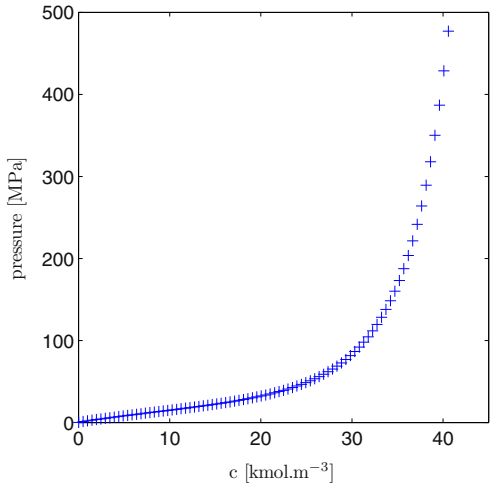

Fig. 15. Equilibrium pressure as a function of the overall molar density c at $T = 413.15$ K. Example 6: binary H_2O–CO_2 mixture ($z_{H_2O} = 0.5$, $z_{CO_2} = 0.5$).

coefficient $\delta_{H_2O-CO_2} = 0.30544$ (for temperature $T = 413.15$ K). The cross association factor used in the CPA equation of state is $s_{CO_2} = 0.083196882$ (for temperature $T = 413.15$ K). As $\delta_{H_2O-CO_2}$ and s_{CO_2} are strongly dependent on temperature, we omit the computation of the stability region for this mixture. For $T = 413.15$ K, the mixture splits in two phases except from very low overall concentrations c.

The equilibrium pressure as a function of the overall molar density c is presented in Fig. 15 (right) illustrating a steady increase of the equilibrium pressure during compression. Saturations of both phases and mass densities of both phases as functions of the overall molar density c are presented in Fig. 16. Mole fractions of both components in both phases as functions of the overall molar density c are presented in Fig. 17. Unlike in previous Examples, we see that the mutual solubility of CO_2 and water is limited.

7. Summary and conclusions

In this work, we have developed a numerical algorithm for the calculation of two-phase equilibria at constant volume, temperature, and moles. The algorithm uses the Newton–Raphson method with line-search for the minimization of the total Helmholtz free energy A of the mixture. The modified Cholesky decomposition of the Hessian matrix ensures the decrease of A in every iteration. The initial guess is constructed using the results of the VT-stability

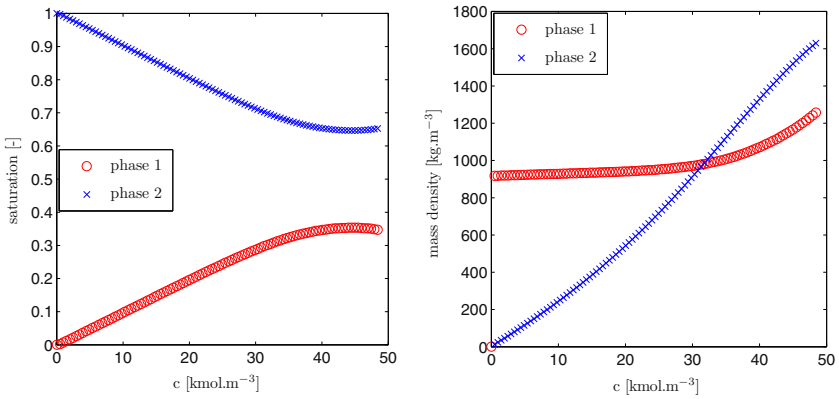

Fig. 16. Saturations (left) and mass densities (right) of both phases as functions of the overall molar density c (right). Example 6: binary H_2O–CO_2 mixture ($z_{H_2O} = 0.5$, $z_{CO_2} = 0.5$, and $T = 413.15$ K).

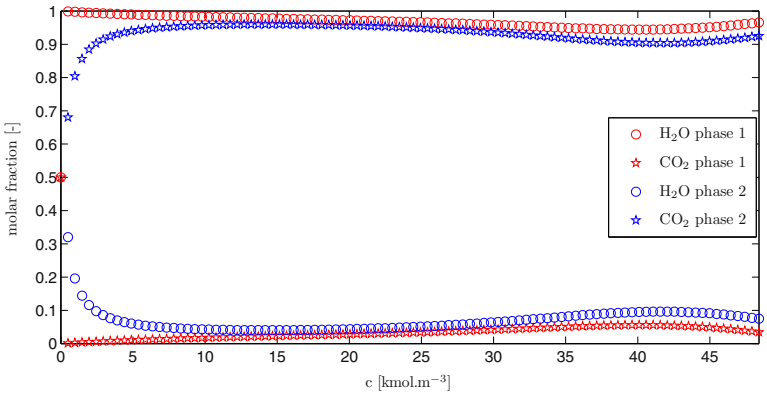

Fig. 17. Molar fractions of both components in both phases as functions of the overall molar density c at $T = 413.15$ K. Example 6: binary H_2O–CO_2 mixture ($z_{H_2O} = 0.5$, $z_{CO_2} = 0.5$).

testing. This approach guarantees that the algorithm always converges to a state of local minimum of A and the possibility of convergence towards the trivial solution is avoided. Compared to the SSI method developed previously in [9], the new algorithm is fast – usually it converges in 6–10 iterations. We have not encountered a case in which the algorithm would not converge. The robustness of our algorithm is documented by the numerous examples provided in this paper. The algorithm was tested on many hydrocarbon mixtures that were described using the Peng–Robinson equation of state and on the H_2O–CO_2 mixture described by the CPA equation of state. We believe that the same approach will be useful for other pressure-explicit equations of state as well.

Acknowledgements

The work was supported by the projects LH12064 Computational Methods in Thermodynamics of Hydrocarbon Mixtures of the Ministry of Education of the Czech Republic, P105/11/1507 Development of Computer Models of CO_2 Sequestration in the Subsurface of the Czech Science Foundation, by the research direction project MSM6840770010 Applied Mathematics in Technical and Physical Sciences of the Ministry of Education of the Czech Republic, and by the project SGS11/161/OHK4/3T/14 Advanced Supercomputing Methods for Implementation of Mathematical Models of the Student Grant Agency of the Czech Technical University in Prague.

Appendix A. Equations of state

In this work we use in Examples 1–5 the Peng–Robinson equation of state [14] in the form

$$P(V,T,N_1,\ldots,N_n)=\frac{NRT}{V-\mathcal{B}}-\frac{\mathcal{A}}{V^2+2\mathcal{B}V-\mathcal{B}^2},$$

where R is the universal gas constant, $N=\sum_{i=1}^{n}N_i$ is the total mole number, and coefficients $\mathcal{A}$ and $\mathcal{B}$ are given by

$$\mathcal{A}=\sum_{i=1}^{n}\sum_{j=1}^{n}N_iN_ja_{ij},$$

$$\mathcal{B}=\sum_{i=1}^{n}N_ib_i,$$

$$a_{ij}=(1-\delta_{i-j})\sqrt{a_ia_j},$$

$$b_i=0.0778\frac{RT_{i,crit}}{P_{i,crit}},$$

$$a_i=0.45724\frac{R^2T_{i,crit}^2}{P_{i,crit}}\left[1+m_i\left(1-\sqrt{T_{r,i}}\right)\right]^2,$$

$$T_{r,i}=\frac{T}{T_{i,crit}},$$

$$m_i=\begin{cases}0.37464+1.54226\omega_i-0.26992\omega_i^2,\\ \text{for } \omega_i<0.5,\\ \\ 0.3796+1.485\omega_i-0.1644\omega_i^2+0.01667\omega_i^3,\\ \text{for } \omega_i\geq 0.5.\end{cases}$$

In these equations δ_{i-j} denotes the binary interaction parameter between the components i and j, $T_{i,crit}$, $P_{i,crit}$, and ω_i are the critical temperature, critical pressure, and accentric factor of the ith component, respectively.

In Example 6 we use for the binary mixture of water (H_2O) and carbon dioxide (CO_2) the Cubic-Plus-Association (CPA) equation of state [15,16]. This equation uses the Peng–Robinson equation of state for the physical interactions and the termodynamic perturbation theory for the bonding of water molecules. We assume that each water molecule has four association sites of two types (mark them α and β), so each type has two sites. We assume the same for each molecule of carbon dioxide, whose association sites can be marked as α' and β'. Let χ_α and χ_β be the mole fractions of water not bonded at site α and β, respectively, and let $\chi_{\alpha'}$ and $\chi_{\beta'}$ be the mole fractions of carbon dioxide not bonded at site α' and β', respectively. Assuming neither cross association nor self association between carbon dioxide molecules, and symmetric cross association between the two sites of different type of water and carbon dioxide, we obtain the following simplified expressions for the symmetric association model

$$\chi_\alpha=\chi_\beta=\chi_w=\frac{1}{1+2(N_w/V)\chi_w\Delta^{\alpha\beta}+2(N_c/V)\chi_c\Delta^{\alpha\beta'}},$$

$$\chi_{\alpha'}=\chi_{\beta'}=\chi_c=\frac{1}{1+2(N_w/V)\chi_c\Delta^{\alpha\beta'}}.$$

In these equations the association strength between molecules of water is given by

$$\Delta^{\alpha\beta}=g\kappa^{\alpha\beta}[\exp(\varepsilon^{\alpha\beta}/k_BT)-1],$$

where k_B is the Boltzmann constant, $\kappa^{\alpha\beta}$ and $\varepsilon^{\alpha\beta}$ are the bonding volume and energy parameters of water, respectively, and g is the contact value of the radial distribution function of hard-sphere mixture that can be approximated as $g=g(\eta)\approx(1-0.5\eta)/(1-\eta)^3$, where $\eta=\mathcal{B}/(4V)$. The association strength between water and carbon dioxide molecules is related to the strength between water molecules as $\Delta^{\alpha\beta'}=s_i\Delta^{\alpha\beta}$ where s_i is the temperature-dependent cross association coefficient which can be determined together with the binary interaction coefficient by fitting the experimental data. As a result, the CPA equation of state for the binary mixture of water and carbon dioxide is given by

$$P(V,T,N_w,N_c)=\frac{NRT}{V-\mathcal{B}}-\frac{\mathcal{A}}{V^2+2\mathcal{B}V-\mathcal{B}^2}+2RT\left(\frac{\eta}{g}\frac{\partial g}{\partial\eta}+1\right)\times\left[\frac{N_w}{V}(\chi_w-1)+\frac{N_c}{V}(\chi_c-1)\right],$$

where R, $\mathcal{A}$ and $\mathcal{B}$ are the parameters from the Peng–Robinson equation of state, N_w and N_c are the mole numbers of water and carbon dioxide, $N=N_w+N_c$, and $\partial g/\partial\eta=(2.5-\eta)/(1-\eta)^4$. The coefficients a_i and b_i for water read as $a_w=a_w^0[1.0+c_1(1-\sqrt{T_{r,w}})+c_2(1-\sqrt{T_{r,w}})^2+c_3(1-\sqrt{T_{r,w}})^3]^2$, $b_w=1.458431489141052\cdot10^{-5}$, where a_w^0, c_1, c_2, c_3 are the parameters of the equation of state given in Table 5.

Table 5
Parameters of the CPA equation of state for the H_2O and CO_2 mixture (the notation is explained in Appendix A).

Symbol	Units	Value
$\kappa^{\alpha\beta}$	[m^3 mol^{-1}]	$1.801506043021089\times10^{-6}$
$\varepsilon^{\alpha\beta}/k_B$	[K]	1738.393603227767
a_w^0	[J m^{-3} mol^{-2}]	0.09627316625476
c_1	–	1.75573246325004
c_2	–	0.00351802110081
c_3	–	−0.27463687473246

References

[1] M.L. Michelsen, Fluid Phase Equilib. 9 (1982) 1–19.
[2] M.L. Michelsen, J.M. Mollerup, Thermodynamic Models: Fundamentals and Computational Aspects, Tie-Line Publications, 2004.
[3] M.L. Michelsen, Fluid Phase Equilib. 9 (1982) 21–40.
[4] M.L. Michelsen, Fluid Phase Equilib. 158 (1999) 617–626.
[5] R.O. Espósito, M. Castier, F.W. Tavares, Chem. Eng. Sci. 55 (2000) 3495–3504.

[6] M. Castier, F.W. Tavares, Chem. Eng. Sci. 60 (2005) 2927–2935.
[7] V.F. Cabral, M. Castier, F.W. Tavares, Chem. Eng. Sci. 60 (2005) 1773–1782.
[9] J. Mikyška, A. Firoozabadi, AIChE J. 57 (2011) 1897–1904.
[10] J. Mikyška, A. Firoozabadi, Fluid Phase Equilib. 321 (2012) 1–9.
[11] S.E. Qui nones-Cisneros, U.K. Deiters, Fluid Phase Equilib. 329 (2012) 22–31.
[12] P.E. Gill, W. Murray, M.H. Wright, Practical Optimization, Academic Press, 1997.
[13] A. Quaternioni, R. Sacco, F. Saleri, Numerical Mathematics, Springer, 2000.
[14] D.E. Peng, D.B. Robinson, Ind. Eng. Chem.: Fundam. 15 (1976) 59–64.
[15] A. Firoozabadi, Thermodynamics of Hydrocarbon Reservoirs, McGrew-Hill, 1999.
[16] Z. Li, A. Firoozabadi, AIChE J. 55 (7) (2009) 1803–1813.

3.6 [Č5]: Polívka, O., and Mikyška, J., Numerical Simulation of Multicomponent Compressible Flow in Porous Medium, Journal of Math-for-Industry, Vol. 3 (2011C-7), pp. 53–60, 2011

Journal of Math-for-Industry, Vol. 3 (2011C-7), pp. 53–60

Math-for-industry
Education & Research Hub

Numerical simulation of multicomponent compressible flow in porous medium

Ondřej Polívka and Jiří Mikyška

Revised on October 25, 2011

Abstract. The paper deals with the numerical modeling of compressible single-phase flow of a mixture composed of several components in a porous medium. The mathematical model is formulated by means of Darcy's law, components continuity equations, constitutive relations, and appropriate initial and boundary conditions. The problem is solved numerically using a combination of the mixed-hybrid finite element method for Darcy's law discretization and the finite volume method for the discretization of the transport equations. This approach provides exact local mass balance. The time discretization is carried out by the Euler method. The resulting large system of nonlinear algebraic equations is solved by the Newton-Raphson iterative method. The dimensions of obtained system of linear algebraic equations are significantly reduced so that they do not depend on the number of mixture components. The convergence of the numerical scheme is verified on two problems of methane injection into a homogeneous 2D reservoir filled with propane which is horizontally or vertically oriented.

Keywords. Mixed-hybrid finite element method, finite volume method, Newton-Raphson method, single-phase compressible multicomponent flow, miscible displacement

1. Introduction

The reliable prediction of transport of multicomponent mixtures in the subsurface is important for many applications including oil recovery or CO_2 sequestration. The traditional approaches use either the fully implicit (fully coupled) method or a sequential method [20, 5]. The fully implicit method is stable, allows for long time steps, but leads to extremely large systems of linear algebraic equations whose size is proportional to the number of components. Alternatively, one can use sequential solution procedures like IMPEC (implicit pressure, explicit concentrations) [13]. In this approach, a pressure equation is formulated by summing up the transport equations [20, 5] or by other method [12, 21, 1]. The pressure equation is solved implicitly using the concentrations from the previous time step. Next, the mole fractions are updated using explicit methods. This procedure allows to reduce the size of the solved system as only pressure is solved implicitly. However, this approach is conditionally stable and the time step has to be chosen prohibitively small in many cases.

In this paper, we deal with the numerical modeling of the compressible single-phase flow of a mixture composed of several components in a porous medium which is suitable for description of multicomponent subsurface transport. We propose a new approach based on a combination of the mixed-hybrid finite element method (MHFEM) and the finite volume method (FVM). Similarly to the implicit schemes, our method leads to large systems of linear algebraic equations, but it is possible to reduce the size of the final system of equations to a size independent on the number of mixture components. Therefore, the solution cost is comparable with the traditional sequential approaches. Unlike in other sequential approaches, no pressure equation has to be formed as pressure is evaluated directly from the equation of state.

The paper is structured as follows. First, we present the mathematical model of the problem. Then, the numerical methods used for derivation of the computational scheme are described together with the proposed computational algorithm. Finally, we present computed numerical results verifying convergence of the numerical scheme.

2. Mathematical model

Let $\Omega \subset \mathbb{R}^2$ be a bounded domain with porosity ϕ [-], and $(0,\tau)$ be the time interval [s]. Consider the single-phase compressible flow of a fluid with N_C components in the domain at a constant temperature T [K]. Neglecting diffusion, the transport of the components is described by the following molar balance equations [12]

$$\frac{\partial(\phi c_i)}{\partial t} + \nabla \cdot (c_i \mathbf{q}) = f_i\,, \quad i = 1, \ldots, N_C\,, \qquad (1)$$
$$c_i = c_i(\mathbf{x}, t)\,, \quad \mathbf{x} \in \Omega\,,\ t \in (0,\tau)\,,$$

where unknown quantities c_i, $i = 1, \ldots, N_C$, are the molar concentrations of the components [mol m^{-3}]. On the

right hand side of equation (1), f_i [mol m^{-3}s^{-1}] denotes the sink/source term. Darcy's velocity $\mathbf{q}$ [m s^{-1}] is given by Darcy's law (see [2])

$$\mathbf{q} = -\mu^{-1}\mathbf{K}(\nabla p - \varrho\mathbf{g})\,, \tag{2}$$

where $\mathbf{K} \in [L^\infty(\Omega)]^{2\times 2}$ is the medium intrinsic permeability [m^2] (generally symmetric and uniformly positive-definite tensor satisfying (B.7)), μ is the viscosity [kg m^{-1}s^{-1}], ∇p denotes a gradient of the pressure p [Pa], $\mathbf{g}$ is the gravitational acceleration vector [m s^{-2}], and ϱ is the fluid density [kg m^{-3}]. Equations (1) and (2) are coupled with constitutive relations expressing dependencies

$$\begin{gathered} p = p\,(c_1,\ldots,c_{N_C},T)\ , \quad \mu = \mu\,(c_1,\ldots,c_{N_C},T)\ , \\ \varrho = \varrho\,(c_1,\ldots,c_{N_C})\ . \end{gathered} \tag{3}$$

In this work, pressure is prescribed by the Peng-Robinson equation of state (PR EOS), while viscosity is given by the Lohrenz-Bray-Clark (LBC) method. Details of relations (3) are presented in Appendix A.

The initial and boundary conditions are given by

$$c_i(\mathbf{x},0) = c_i^0(\mathbf{x})\,, \qquad \mathbf{x}\in\Omega\,,\ i=1,\ldots,N_C\,, \tag{4a}$$

$$c_i(\mathbf{x},t) = c_i^D(\mathbf{x},t)\,, \quad \mathbf{x}\in\Gamma_c(t)\,,\ t\in(0,\tau)\,,\ i=1,\ldots,N_C\,, \tag{4b}$$

$$p(\mathbf{x},t) = p^D(\mathbf{x},t)\,, \quad \mathbf{x}\in\Gamma_p\,,\ t\in(0,\tau)\ , \tag{4c}$$

$$\mathbf{q}(\mathbf{x},t)\cdot\mathbf{n}(\mathbf{x}) = q^N(\mathbf{x},t)\,, \quad \mathbf{x}\in\Gamma_q\,,\ t\in(0,\tau)\ , \tag{4d}$$

where $\mathbf{n}$ is the unit outward normal vector to the boundary $\partial\Omega$. Equations (4c) and (4d) determine the Dirichlet and Neumann boundary conditions on the Γ_p, Γ_q parts of the boundary, respectively, whereas conditions $\Gamma_p\cup\Gamma_q = \partial\Omega$ and $\Gamma_p\cap\Gamma_q = \emptyset$ must be satisfied. The boundary condition (4b) for molar concentration is also the Dirichlet type. The set $\Gamma_c(t)$ denotes the inflow part of the boundary $\partial\Omega$ in time t, i.e.

$$\Gamma_c(t) = \{\mathbf{x}\in\partial\Omega\,|\,\mathbf{q}(\mathbf{x},t)\cdot\mathbf{n}(\mathbf{x}) < 0\}\ .$$

3. Numerical solution

The system of equations (1)–(4) is solved numerically by a combination of the mixed-hybrid finite element method (MHFEM), for Darcy's law (2), and the finite volume method (FVM), for transport equations (1). The subsequent scheme is derived using the Euler method for time discretization and linearized by the Newton-Raphson method (NRM).

We consider a 2D polygonal domain Ω with the boundary $\partial\Omega$ which is covered by a spatial triangulation $\mathcal{T}_\Omega$ consisting of triangles or quadrilaterals. Let us denote K the element of the mesh $\mathcal{T}_\Omega$ with area $|K|$, E the edge of an element with the length $|E|$, N_K the number of elements of the triangulation, and N_E the number of edges of the mesh.

3.1. Discretization of Darcy's law

Darcy's velocity $\mathbf{q}$ can be approximated in the Raviart-Thomas space of the lowest order (RT_K^0) over the element $K\in\mathcal{T}_\Omega$ as

$$\mathbf{q} = \sum_{E\in\partial K} q_{K,E}\mathbf{w}_{K,E}\,, \tag{5}$$

where the coefficient $q_{K,E}$ is the flux of vector function $\mathbf{q}$ through the edge E of the element K with respect to outer normal, and $\mathbf{w}_{K,E}$ represents the piecewise linear RT_K^0–basis function associated with the edge E (see [3, 4, 17] or Appendix B).

By expressing the pressure gradient from Darcy's law (2), we obtain

$$\nabla p = -\mu\mathbf{K}^{-1}\mathbf{q} + \varrho\mathbf{g}\,. \tag{6}$$

Multiplying (6) by the basis function $\mathbf{w}_{K,E}$, integrating over K, taking advantages of the RT_K^0 space (see Appendix B), and using (5) on the right side and the Green theorem on the left side together with the mean value theorem, we derive a discrete form of Darcy's law

$$q_{K,E} = \mu_K^{-1}\left(\alpha_E^K p_K - \sum_{E'\in\partial K}\beta_{E,E'}^K p_{K,E'} + \gamma_E^K\varrho_K\right)\,, \tag{7}$$

for $E\in\partial K$. In equation (7), $\alpha_E^K, \beta_{E,E'}^K$, and γ_E^K are coefficients dependent on the mesh geometry and on the local values of permeability (details in Appendix B); p_K is the cell pressure average; $p_{K,E'}$ is the edge pressure average; and μ_K, ϱ_K denote the mean values of viscosity and density over the cell K, respectively.

The continuity of flux and pressure on the edge E between neighboring elements $K, K'\in\mathcal{T}_\Omega$ can be written as

$$q_{K,E} + q_{K',E} = 0\,, \tag{8}$$

$$p_{K,E} = p_{K',E} =: p_E\,. \tag{9}$$

Boundary conditions (4c), (4d) expressed in a discrete form read as

$$p_{K,E} = p^D(E)\,, \quad \forall E\subset\Gamma_p\,, \tag{10a}$$

$$q_{K,E} = q^N(E)\,, \quad \forall E\subset\Gamma_q\,, \tag{10b}$$

where $p^D(E)$ is the prescribed value of the pressure p averaged on the edge E, and $q^N(E)$ is prescribed flux through the edge E.

The flux can be eliminated by substituting $q_{K,E}$ from (7) into equations (8) and (10b). For further derivation, let us consider time dependent quantities at time t_{n+1} denoted by upper index $n+1$. Then, equations (7)–(10) transform to the following system of N_E linear algebraic equations

$$F_E \equiv \begin{cases} \displaystyle\sum_{K:E\in\partial K}\left(\mu_K^{n+1}\right)^{-1}\Big(\alpha_E^K p_K^{n+1} - \sum_{E'\in\partial K}\beta_{E,E'}^K p_{K,E'}^{n+1} \\ \qquad + \gamma_E^K\varrho_K^{n+1}\Big) = 0\,, \quad \forall E\not\subset\partial\Omega\,, \\ \left(\mu_K^{n+1}\right)^{-1}\Big(\alpha_E^K p_K^{n+1} - \displaystyle\sum_{E'\in\partial K}\beta_{E,E'}^K p_{K,E'}^{n+1} \\ \qquad + \gamma_E^K\varrho_K^{n+1}\Big) - q^N(E) = 0\,, \quad \forall E\subset\Gamma_q\ , \\ p_{K,E}^{n+1} - p^D(E) = 0\,, \quad \forall E\subset\Gamma_p\ . \end{cases} \tag{11}$$

Herein, the symbol $\sum_{K:E\in\partial K}$ denotes the sum over the elements containing edge E. A similar procedure leading to the mixed-hybrid formulation can be found in [16].

3.2. Approximation of the transport equations

Transport equations (1) with the initial and boundary conditions (4) are discretized using the FVM [14]. Integrating (1) over an arbitrary element K from the mesh $\mathcal{T}_\Omega$, and using the Green theorem, we obtain

$$\frac{\mathrm{d}}{\mathrm{d}t}\int_K \phi(\mathbf{x})c_i(\mathbf{x},t) + \int_{\partial K} c_i(\mathbf{x},t)\mathbf{q}(\mathbf{x},t)\cdot\mathbf{n}_{\partial K}(\mathbf{x}) = \int_K f_i(\mathbf{x}),\quad i=1,\dots,N_C. \tag{12}$$

By applying the mean value theorem, and denoting $\phi_K, c_i|_K, f_i|_K$ the averaged values of ϕ, c_i, f_i $(i=1,\dots,N_C)$, respectively, over the cell K, we derive from (12)

$$\frac{\mathrm{d}(\phi_K c_i|_K)}{\mathrm{d}t}|K| + \sum_{E\in\partial K} \widetilde{c_i}|_E \underbrace{\int_E \mathbf{q}\cdot\mathbf{n}_{K,E}}_{=q_{K,E}} = f_i|_K|K|, \tag{13}$$

where $\widetilde{c_i}|_E$ denotes the concentration c_i on the edge E. The integral in (13) is equal to the flux through the edge E from element K (the component of $\mathbf{q}$ in the direction of outward normal to E).

Let us suppose that the porosity does not depend on time. The time derivative of $c_i|_K$ in (13) is approximated by the time difference with a time step Δt_n. Using the Euler method (see [14]), we obtain for every n, all elements $K\in\mathcal{T}_\Omega$, and components $i=1,\dots,N_C$

$$F_{K,i} \equiv \phi_K|K|\frac{c_i|_K^{n+1} - c_i|_K^n}{\Delta t_n} + \sum_{E\in\partial K} \widetilde{c_i}|_E^n\, q_{K,E}^{n+1}\left(p_{K,E}^{n+1}, c_1|_K^{n+1},\dots,c_{N_C}|_K^{n+1}\right) - f_i|_K|K| = 0, \tag{14}$$

where $q_{K,E}^{n+1}$ is given by (7). The value of $\widetilde{c_i}|_E^n$ is chosen from neighboring element in the upwind direction, i.e.

$$\widetilde{c_i}|_E^n = \begin{cases} c_i|_K^n & \text{for} \quad q_{K,E}^{n+1}\geq 0, \\ c_i|_{K'}^n & \text{for} \quad q_{K,E}^{n+1}<0 \ \wedge E\not\subset\partial\Omega : K\cap K' = E, \\ c_i^D|_E^n & \text{for} \quad q_{K,E}^{n+1}<0 \ \wedge E\subset\partial\Omega, \end{cases} \tag{15}$$

where c_i^D represents the concentration of the i-th component on the inflow boundary. Note that the scheme is almost fully implicit – the only term in (14) which is evaluated explicitly is the value of $\widetilde{c_i}|_E^n$.

The initial and boundary conditions (4a) and (4b) are approximated as

$$c_i|_K^0 = c_i^0(K), \qquad \forall K\in\mathcal{T}_\Omega,\ i=1,\dots,N_C, \tag{16a}$$

$$\widetilde{c_i}|_E^n = c_i^D(E,t_n), \quad \forall E\subset\Gamma_c(t),\ i=1,\dots,N_C,\ t_n<\tau. \tag{16b}$$

3.3. Combining the MHFEM and the FVM schemes

Let us use the notation F_E and $F_{K,i}$, for edge $E\in\{1,\dots,N_E\}$, element $K\in\{1,\dots,N_K\}$, and component $i\in\{1,\dots,N_C\}$, the left hand sides of equations (11) and (14) with $q_{K,E}^{n+1}$ substituted from relation (7). The cell averaged values $p_K = p_K(c_1|_K,\dots,c_{N_C}|_K)$, $\varrho_K = \varrho_K(c_1|_K,\dots,c_{N_C}|_K)$, and $\mu_K = \mu_K(c_1|_K,\dots,c_{N_C}|_K)$ are evaluated using constitutive relations (3). The system of $N_E + N_K\times N_C$ equations

$$\mathbf{F} = [F_1,\dots,F_{N_E};\ F_{1,1},\dots,F_{1,N_C},\dots,F_{N_K,1},\dots,F_{N_K,N_C}]^T = \mathbf{0}$$

for unknown molar concentrations $c_1|_K^{n+1},\dots,c_{N_C}|_K^{n+1}$, $K\in\{1,\dots,N_K\}$, and edge averaged pressures p_E^{n+1}, $E\in\{1,\dots,N_E\}$, is a nonlinear system of algebraic equations which we solve using the NRM. The resulting system of linear algebraic equations is shown in Fig. 1, where the sparse Jacobi matrix is unsymmetric, and the unknown vector is represented by corrections of molar concentrations and edge pressures. The nonzero black-coloured values in Fig. 1 are given by partial derivatives

$$(\mathbf{J}_K)_{i,j} = \frac{\partial F_{K,i}}{\partial c_j|_K^{n+1}}, \qquad (\mathbf{J}_{K,E})_i = \frac{\partial F_{K,i}}{\partial p_{K,E}^{n+1}}, \tag{17}$$

$$(\mathbf{J}_{E,K})_j = \frac{\partial F_E}{\partial c_j|_K^{n+1}}, \qquad J_{E,E'} = \frac{\partial F_E}{\partial p_{K,E'}^{n+1}}, \tag{18}$$

where $J_{E,E'}$ is element of the matrix $\mathbf{J}_{E,E'}$ and $i,j = 1,\dots,N_C$; $K=1,\dots,N_K$; $E,E'=1,\dots,N_E$. The partial derivatives in (17) can be evaluated analytically using (3), (11), and (14).

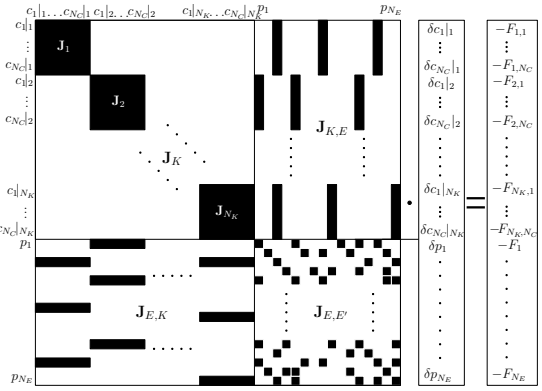

Figure 1: Structure of the system of linear algebraic equations in the NRM.

The size of the system in Fig. 1 can be reduced by inverting the $\mathbf{J}_K$ blocks for all K (the inversion is possible since the blocks are diagonally dominant for small time steps) and eliminating vectors $\mathbf{J}_{E,K}$ for all E,K. Then, we derive

a system of N_E equations for N_E corrections of pressures p_E

$$\sum_{K:E\in\partial K}\sum_{E'\in\partial K}\left(J_{E,E'}-\mathbf{J}_{E,K}\mathbf{J}_K^{-1}\mathbf{J}_{K,E'}\right)\delta p_{E'} = \sum_{K:E\in\partial K}\mathbf{J}_{E,K}\mathbf{J}_K^{-1}\mathbf{F}|_K - F_E\,, \quad (19)$$

where $E=1,\dots,N_E$, $\mathbf{F}|_K=[F_{K,1},\dots,F_{K,N_C}]^T$. Once δp_E are computed, corrections of concentrations $\Delta\mathbf{c}|_K=[\delta c_1|_K,\dots,\delta c_{N_C}|_K]^T$ on each cell K can be evaluated by solving

$$\Delta\mathbf{c}|_K=-\mathbf{J}_K^{-1}\left(\mathbf{F}|_K+\sum_{E'\in\partial K}\delta p_{E'}\,\mathbf{J}_{K,E'}\right), \quad (20)$$

for $K=1,\dots,N_K$. The corrections δp_E and $\delta c_i|_K$ for all edges, components, and elements obtained in an iteration of the NRM are added to the values p_E^{n+1} and $c_i|_K^{n+1}$ from the previous iteration. The iteration process stops if the condition

$$\left\|[\delta c_1|_1,\dots,\delta c_{N_C}|_{N_K},\delta p_1,\dots,\delta p_{N_E}]^T\right\|<\varepsilon \quad (21)$$

is satisfied for a chosen $\varepsilon>0$ (see [19]).

4. Computational algorithm

Numerical solution can be computed in the following steps:

1. Initialize geometry, physical and chemical parameters, and molar concentrations from initial condition; generate a domain triangulation.
2. Calculate pressures p_K on each element using the PR EOS from initial molar concentrations, then evaluate all edge pressures p_E by averaging p_K on neighboring elements.
3. Repeat until the predetermined final time is reached ($t_n<\tau$):
   (a) Repeat the NRM iterations until a convergence criterion is satisfied:
      i. Compute viscosities μ_K^{n+1} on each cell using the LBC method (A.7).
      ii. Compute densities ϱ_K^{n+1} on each cell using (A.3).
      iii. Calculate pressures p_K^{n+1} on each element using the PR EOS (A.1).
      iv. Assemble and solve the system (19) for edge pressure corrections δp_E.
      v. Calculate molar concentration corrections $\delta c_i|_K$ for each component and each element from (20).
      vi. Add the corrections δp_E and $\delta c_i|_K$ to p_E^{n+1} and $c_i|_K^{n+1}$, respectively, check the convergence (21).
   (b) Continue to the next time level ($n\to n+1$).

In steps i.–iii. μ_K^{n+1}, ϱ_K^{n+1}, and p_K^{n+1} are computed using the data from the last available Newton iteration. In the first iteration, data from the previous time step are used.

5. Numerical results

Let us consider a 2D square domain $50\times50\,\mathrm{m}^2$ which represents a cut of a propane reservoir with porosity $\phi=0.2$ and isotropic permeability $\mathbf{K}=k=10^{-14}\,\mathrm{m}^2$ at initial pressure $p=5\cdot10^6\,\mathrm{Pa}$ and temperature $T=397\,\mathrm{K}$ in a horizontal or vertical position. In the left bottom corner of the reservoir, methane is injected and in the right top corner, the mixture of methane and propane is produced (Fig. 2). The injection rate $f_1|_K$ is $2.643\cdot10^{-2}/|K|\ \mathrm{mol\,m^{-3}s^{-1}}$, where $|K|$ is the area of the corner grid element. Physical-chemical properties of the mixture are summarized in Table 1. In all examples the initial data are chosen so that the mixture stays in the single-phase state. The boundary of the domain is impermeable except the outflow corner, where pressure $p=5\cdot10^6\,\mathrm{Pa}$ is maintained. The computational grid with $2\times m\times m$ elements is shown in Fig. 2 (where $m=10$). Parameter ε from the NRM convergence criterion (21) was chosen 10^{-6} for all computations. The system of equations (19) was solved using UMFPACK [6, 7, 8, 9].

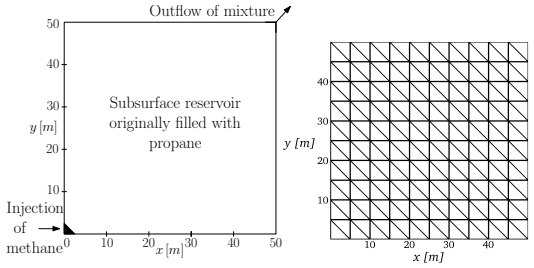

Figure 2: A scheme of simulated reservoir and a structure of the computational grid.

i (component)	p_{ci} [Pa]	T_{ci} [K]
1 (CH_4)	$4.58373\cdot10^6$	$1.89743\cdot10^2$
2 (C_3H_8)	$4.248\cdot10^6$	$3.6983\cdot10^2$
i (component)	V_{ci} [$\mathrm{m^3mol^{-1}}$]	M_i [$\mathrm{kg\,mol^{-1}}$]
1 (CH_4)	$9.897054\cdot10^{-5}$	$1.62077\cdot10^{-2}$
2 (C_3H_8)	$2.000001\cdot10^{-4}$	$4.40962\cdot10^{-2}$
i (component)	ω_i [-]	δ_{i1} [-]	δ_{i2} [-]
1 (CH_4)	$1.14272\cdot10^{-2}$	0	0.0365
2 (C_3H_8)	$1.53\cdot10^{-1}$	0.0365	0

Table 1: Relevant parameters of the PR EOS (see Appendix A) for methane CH_4 and propane C_3H_8. Volume translation is not used.

5.1. Convergence analysis in horizontal case

We will test convergence of the numerical scheme, derived in section 3, using a pseudoanalytical solution – the numerical solution computed on the finest grid $m=160$

($2\times160\times160$ grid cells). Experimental order of convergence (EOC) will be computed between grids $m = 10$, $m = 20$, and $m = 40$ using the L^1, L^2, and L^∞ consistent norms for errors E_m in comparison with the solution on the grid $m = 160$. The error is computed on the finest grid by projecting the solutions from the coarser grids to the finest grid and using the linear interpolation. The time step for the solution $m = 160$ is chosen constant $\Delta t = 750\,\mathrm{s}$. For the solutions on coarser grids, Δt is 4 times larger with each mesh refinement ($\Delta t \sim m^{-2}$), i.e. $\Delta t = 12000\,\mathrm{s}$ for $m = 40$, $\Delta t = 48000\,\mathrm{s}$ for $m = 20$, and $\Delta t = 192000\,\mathrm{s}$ for $m = 10$. The EOC in a norm $\|.\|_\nu$ is given by

$$\mathrm{EOC}_\nu = \frac{\ln \|E_{m_1}\|_\nu - \ln \|E_{m_2}\|_\nu}{\ln m_2 - \ln m_1},$$

where E_{m_1} and E_{m_2} are the numerical solution errors on the grids with parameters m_1 and m_2, respectively.

The convergence analysis is, at first, performed on a problem of injection of methane into a horizontal propane reservoir (i.e. no gravity is considered). The EOC and errors for the situation at time $\tau = 6 \cdot 10^6\,\mathrm{s}$ are included in Table 2. The next Table 3 contains the data from time $\tau = 2.4 \cdot 10^7\,\mathrm{s}$, and a comparison of the solutions on the individual grids at this time is depicted in Fig. 3.

Grid (m)	$\|E_m\|_1$	EOC_1	$\|E_m\|_2$	EOC_2
10	$1.1025 \cdot 10^5$	0.6223	$6.5336 \cdot 10^3$	0.5086
20	$7.1621 \cdot 10^4$	0.8179	$4.5922 \cdot 10^3$	0.6814
40	$4.0627 \cdot 10^4$		$2.8635 \cdot 10^3$	

Grid (m)	$\|E_m\|_\infty$	EOC_∞
10	$1.1204 \cdot 10^3$	0.5077
20	$7.8804 \cdot 10^2$	0.5298
40	$5.4584 \cdot 10^2$	

Table 2: Experimental orders of convergence and errors of methane concentration c_1, $g = 0$, at time $\tau = 6 \cdot 10^6\,\mathrm{s}$ compared with the numerical solution on the grid $m = 160$ ($2 \times m \times m$ elements) and time step $\Delta t = 750\,\mathrm{s}$. On coarser grids, $\Delta t \sim m^{-2}$.

Grid (m)	$\|E_m\|_1$	EOC_1	$\|E_m\|_2$	EOC_2
10	$3.4079 \cdot 10^5$	0.6514	$1.109 \cdot 10^4$	0.5273
20	$2.1697 \cdot 10^5$	0.833	$7.6948 \cdot 10^3$	0.6814
40	$1.218 \cdot 10^5$		$4.7982 \cdot 10^3$	

Grid (m)	$\|E_m\|_\infty$	EOC_∞
10	$1.0485 \cdot 10^3$	0.584
20	$6.9948 \cdot 10^2$	0.4748
40	$5.0333 \cdot 10^2$	

Table 3: Experimental orders of convergence and errors of methane concentration c_1, $g = 0$, at time $\tau = 2.4 \cdot 10^7\,\mathrm{s}$ compared with the numerical solution on the grid $m = 160$ ($2 \times m \times m$ elements) and time step $\Delta t = 750\,\mathrm{s}$. On coarser grids, $\Delta t \sim m^{-2}$.

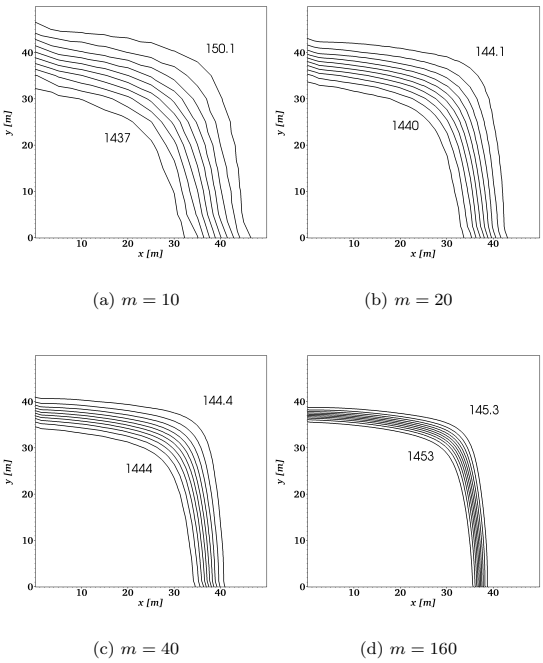

(a) $m = 10$ (b) $m = 20$

(c) $m = 40$ (d) $m = 160$

Figure 3: Contours of methane concentration c_1 at $\tau = 2.4 \cdot 10^7\,\mathrm{s}$ on different grids for Table 3. Isolines are distributed uniformly between the two displayed values.

5.2. Convergence analysis in vertical case

Similarly as in the previous part, we perform the convergence analysis on the problem of methane injection into a vertically oriented 2D propane reservoir. We use the same domain with boundary and data set as in the previous case, but this time, gravity effect is assumed ($g = 9.81\,\mathrm{m\,s^{-2}}$). Pressure $5 \cdot 10^6\,\mathrm{Pa}$ is fixed in the right upper corner of the domain. We present the errors in L^1 and L^2 norm. In Table 4, the EOC and errors from time $\tau = 6 \cdot 10^6\,\mathrm{s}$ are shown. Isolines of methane molar concentration are depicted in Fig. 4 on all computational grids. The last Table 5 contains the data from time $\tau = 2.4 \cdot 10^7\,\mathrm{s}$. As we can see, the EOC is lower in the case of the vertical domain with gravity than in the previous case of horizontal domain without gravity (cf. Tables 2 and 3).

Grid (m)	$\|E_m\|_1$	EOC_1	$\|E_m\|_2$	EOC_2
10	$1.3433 \cdot 10^5$	0.5973	$8.644 \cdot 10^3$	0.4441
20	$8.8787 \cdot 10^4$	0.7717	$6.3535 \cdot 10^3$	0.59
40	$5.2006 \cdot 10^4$		$4.2211 \cdot 10^3$	

Table 4: Experimental orders of convergence and errors of methane concentration c_1, $g = 9.81\,\mathrm{m\,s^{-2}}$, at time $\tau = 6 \cdot 10^6\,\mathrm{s}$ compared with the numerical solution on the grid $m = 160$ ($2 \times m \times m$ elements) and time step $\Delta t = 750\,\mathrm{s}$. On coarser grids, $\Delta t \sim m^{-2}$.

Grid (m)	$\|E_m\|_1$	EOC_1	$\|E_m\|_2$	EOC_2
10	$6.5964 \cdot 10^5$		$2.2368 \cdot 10^4$	
20	$5.0932 \cdot 10^5$	0.3731	$1.8978 \cdot 10^4$	0.2371
40	$3.7703 \cdot 10^5$	0.4339	$1.5975 \cdot 10^4$	0.2485

Table 5: Experimental orders of convergence and errors of methane concentration c_1, $g = 9.81\,\mathrm{m\,s^{-2}}$, at time $\tau = 2.4 \cdot 10^7$ s compared with the numerical solution on the grid $m = 160$ ($2 \times m \times m$ elements) and time step $\Delta t = 750$ s. On coarser grids, $\Delta t \sim m^{-2}$.

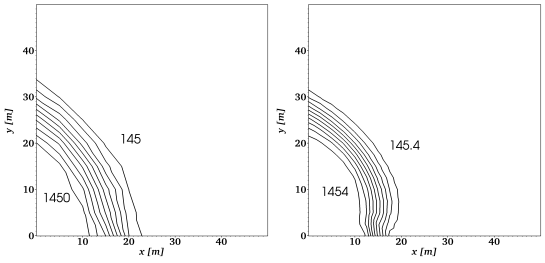

(a) $m = 10$ (b) $m = 20$

(c) $m = 40$ (d) $m = 160$

Figure 4: Contours of methane concentration c_1 at $\tau = 6 \cdot 10^6$ s on different grids for Table 4. Isolines are distributed uniformly between the two displayed values.

CPU-times for the simulation of the horizontal and vertical domain on particular grids can be found in Table 6.

Grid (m)	$g = 0$: CPU-time [s]	$g \neq 0$: CPU-time [s]
10	35	30
20	207	218
40	1976	2378
80	73538	35633
160	436365	554308

Table 6: Computational times for solutions computed on different grids on Dual-Core AMD Opteron(tm) Processor 2216, 2400 MHz (single core used), cache size 1 MB, and total memory 8 GB.

6. Conclusion

In this work, we have developed a new numerical scheme based on a combination of the MHFEM and FVM for simulation of single-phase compressible multicomponent flow in a porous medium. Unlike in traditional approaches, we evaluate the pressure directly from the equation of state. The system of nonlinear algebraic equations obtained by combining the MHFEM, FVM, and using the Euler method is linearized by the Newton-Raphson method. The size of the resulting system of linear algebraic equations depends on the number of mixture components. Therefore, we proposed a technique reducing significantly the system into a size that is independent on the number of mixture components. Consequently, computational costs are comparable with traditional sequential approaches. Although we tested the numerical model for two components, the advantage of this approach is expected to be larger in the more components case. Our method provides exact local mass balance (up to the non-linear solver error) which is important for solving problems especially in a heterogeneous medium. Convergence of the numerical scheme was successfully verified by evaluating the experimental order of convergence on two problems of methane injection into a horizontal and vertical propane reservoir. In the future work, we would like to improve the current model using the high order methods and to test it on problems involving more than two components.

Appendix A

Peng-Robinson equation of state

In this work, pressure is given by the PR EOS [18, 10] as

$$p = \frac{R\,T \sum\limits_{i=1}^{N_C} c_i}{1 - \sum\limits_{i=1}^{N_C} b_i\,c_i} - \frac{\sum\limits_{i=1}^{N_C}\sum\limits_{j=1}^{N_C} a_{ij}\,c_i\,c_j}{1 + 2\sum\limits_{i=1}^{N_C} b_i\,c_i - \left(\sum\limits_{i=1}^{N_C} b_i\,c_i\right)^2}\,. \quad \text{(A.1)}$$

In equation (A.1), $R = 8.314472\,\mathrm{J K^{-1} mol^{-1}}$ is the universal gas constant, T the temperature [K], and

$$a_{ij} = (1 - \delta_{ij})\sqrt{a_i a_j}\,, \quad a_i = \frac{0.45724\,R^2\,T_{ci}^2}{p_{ci}}\,\alpha_i\,,$$
$$\alpha_i = \Big(1 + \big(0.37464 + 1.54226\,\omega_i - 0.26992\,\omega_i^2\big)\cdot$$
$$\cdot\Big(1 - \sqrt{T_{ri}}\Big)\Big)^2\,, \quad T_{ri} = \frac{T}{T_{ci}}\,, \quad b_i = \frac{0.07780\,R\,T_{ci}}{p_{ci}}\,, \quad \text{(A.2)}$$

where δ_{ij} is the binary interaction coefficient [-]; T_{ci}, p_{ci}, ω_i, T_{ri} are the critical temperature, critical pressure, acentric factor [-], reduced temperature [-], respectively – all corresponding to the i-th component.

Density computation

The density-molar concentrations relation, according to [11], reads as

$$\varrho = \sum_{i=1}^{N_C} M_i\, c_i\,, \tag{A.3}$$

where M_i is the molar weight of the i-th component $[\mathrm{kg\,mol^{-1}}]$.

Lohrenz-Bray-Clark model for viscosity

In the numerical computations, the model proposed by Lohrenz, Bray, and Clark [15] in 1964 is used for estimation of (dynamic) viscosity of hydrocarbon mixtures. At first, empirical formulas for the viscosity μ_i^0 of low-pressure pure component fluids are evaluated as follows

$$\mu_i^0 = \begin{cases} 34\cdot 10^{-5}\, {T_{ri}}^{0.94}/\xi_i & \text{for } T_{ri} \le 1.5\,, \\ 17.78\cdot 10^{-5}\left(4.58\,T_{ri} - 1.67\right)^{5/8}/\xi_i & \text{for } T_{ri} > 1.5\,, \end{cases} \tag{A.4}$$

where

$$T_{ri} = \frac{T}{T_{ci}}\,, \quad \xi_i = \frac{{T_{ci}}^{1/6}}{{M_i}^{1/2}\,{p_{ci}}^{2/3}}\,, \quad i = 1,\ldots,N_C\,. \tag{A.5}$$

Next, we express the low-pressure viscosity of a mixture of N_C components as

$$\mu^0 = \frac{\sum\limits_{i=1}^{N_C} z_i\,\mu_i^0\,\sqrt{M_i}}{\sum\limits_{i=1}^{N_C} z_i\,\sqrt{M_i}}\,, \tag{A.6}$$

where $z_i = c_i/c$ is the mole fraction of the i-th component. The final viscosity μ of the multicomponent fluid for higher pressures is given by

$$\begin{aligned}\left[\left(\mu-\mu^0\right)\xi + 10^{-4}\right]^{1/4} &= 0.1023 + 0.023364\,c_r + \\ &+ 0.058533\,c_r^2 - 0.040758\,c_r^3 + 0.0093324\,c_r^4\,.\end{aligned} \tag{A.7}$$

In equation (A.7), c_r is called the reduced molar density defined as

$$c_r = c\sum_{i=1}^{N_C} z_i\,V_{ci}\,, \tag{A.8}$$

where V_{ci} is the critical molar volume of the i-th component. The parameter ξ in (A.7) is computable according to

$$\xi = \frac{\left(\sum\limits_{i=1}^{N_C} z_i\,T_{ci}\right)^{1/6}}{\left(\sum\limits_{i=1}^{N_C} z_i\,M_i\right)^{1/2}\left(\sum\limits_{i=1}^{N_C} z_i\,p_{ci}\right)^{2/3}}\,. \tag{A.9}$$

In relations (A.4)–(A.9) the temperatures T and T_{ci} are in Kelvins, molar weights M_i in grams per mole, critical pressures p_{ci} in atmospheres ($1\,\mathrm{atm} = 101325\,\mathrm{Pa}$), critical molar volumes V_{ci} in litres per mole, molar densities c and c_i in moles per litre, and viscosity μ is in the units of centipoise $\left(1\,\mathrm{cP} = 10^{-3}\mathrm{kg\,m^{-1}\,s^{-1}}\right)$.

Appendix B

In this part, we describe details of derivation of discrete Darcy's law (7) using the Raviart-Thomas space. Raviart-Thomas space of the lowest order RT_K^0, over an element K from a triangulation $\mathcal{T}_\Omega$ (consisting of triangles) of the domain Ω, is generated by the basis functions

$$\mathbf{w}_{K,E}(\mathbf{x}) = \frac{1}{2|K|}\left(\mathbf{x} - \mathbf{N}_{K,E}\right)\,, \quad \forall \mathbf{x}\in K\,,\ E\in\partial K\,, \tag{B.1}$$

where $\mathbf{N}_{K,E}\in K$ is a node against edge E. The basis functions (B.1) satisfy the following properties

$$\nabla\cdot\mathbf{w}_{K,E}(\mathbf{x}) = \frac{1}{|K|}\,, \quad \mathbf{w}_{K,E}(\mathbf{x})\cdot\mathbf{n}_{K,E'} = \frac{\delta_{E,E'}}{|E|}\,. \tag{B.2}$$

Multiplying (6) with the basis function $\mathbf{w}_{K,E}$, and integrating over element K, we can write

$$\int_K \nabla p\cdot\mathbf{w}_{K,E'} = -\mu_K\sum_{E\in\partial K} q_{K,E}\int_K \mathbf{K}^{-1}\mathbf{w}_{K,E}\cdot\mathbf{w}_{K,E'} + \\ + \varrho_K\int_K \mathbf{g}\cdot\mathbf{w}_{K,E'}\,, \tag{B.3}$$

where we have used (5) and the mean value theorem. Using the Green theorem, the mean value theorem, and properties (B.2), we obtain

$$\int_K \nabla p\cdot\mathbf{w}_{K,E'} = \sum_{E\in\partial K}\int_E p\,\mathbf{w}_{K,E'}\cdot\mathbf{n}_{K,E} - \int_K p\nabla\cdot\mathbf{w}_{K,E'} = \\ = \underbrace{\frac{1}{|E'|}\int_{E'} p}_{p_{K,E'}} - \underbrace{\frac{1}{|K|}\int_K p}_{p_K}\,. \tag{B.4}$$

Denoting

$$A_{K,E,E'} = \int_K \mathbf{K}^{-1}\mathbf{w}_{K,E}\cdot\mathbf{w}_{K,E'}\,, \quad G_{K,E'} = \int_K \mathbf{g}\cdot\mathbf{w}_{K,E'}\,, \tag{B.5}$$

we combine (B.3) and (B.4) into

$$\mu_K\sum_{E\in\partial K} q_{K,E}A_{K,E,E'} = p_K - p_{K,E'} + \varrho_K G_{K,E'}\,. \tag{B.6}$$

Because $\mathbf{K}$ is uniformly positive-definite (see [16]), i.e.

$$\exists\alpha_0 > 0 : \alpha_0\sum_{i=1}^{2}\xi_i^2 \le \sum_{i,j=1}^{2}\left[K(\mathbf{x})\right]_{i,j}\xi_i\,\xi_j\,,\ \forall\xi\in\mathbb{R}^2\,, \tag{B.7}$$

for almost all $\mathbf{x}\in\Omega$, it is possible to invert the matrix $\mathbf{A}_K = \left(A_{K,E,E'}\right)_{E,E'\in\partial K}$. Multiplying (B.6) in a vector form by $\mathbf{A}_K^{-1}$, we obtain

$$q_{K,E} = \mu_K^{-1}\left(\alpha_E^K p_K - \sum_{E'\in\partial K}\beta_{E,E'}^K p_{K,E'} + \gamma_E^K\varrho_K\right)\,, \tag{B.8}$$

which is Darcy's law (7) with coefficients α_E^K , $\beta_{E,E'}^K$, and γ_E^K given by

$$\alpha_E^K = \sum_{E' \in \partial K} A^{-1}_{K,E,E'} , \quad \beta^K_{E,E'} = A^{-1}_{K,E,E'} , \\ \gamma_E^K = \sum_{E' \in \partial K} A^{-1}_{K,E,E'} G_{K,E'} , \tag{B.9}$$

where $A^{-1}_{K,E,E'}$ is the element of the inverse matrix $\mathbf{A}_K^{-1}$.

Acknowledgements

This research has been supported by the projects Development of Computational Models for Simulation of CO2 Sequestration, P105/11/1507 of the Czech Science Foundation, and Numerical Methods for Multiphase Flow and Transport in Subsurface Environmental Applications, Kontakt ME10009 of Czech Ministry of Education, Youth and Sports.

References

[1] Acs, G., Doleschall, S., Farkas, E.: General Purpose Compositional Model, *Society of Petroleum Engineers Journal*, Vol.: 25, Issue: 4 (1985) 543–553.

[2] Bear, J., Verruijt, A.: Modeling Groundwater Flow and Pollution (1987), D. Reidel Publishing Company, Dordrecht, Holland.

[3] Brezzi, F., Fortin, M.: Mixed and Hybrid Finite Element Methods (1991), Springer-Verlag, New York Inc.

[4] Chavent, G., Roberts, J. E.: A unified physical presentation of mixed, mixed-hybrid finite elements and standard finite difference approximations for the determination of velocities in waterflow problems, *Advances in Water Resources*, 14(6) (1991).

[5] Chen, Z., Huan, G., Ma, Y.: Computational Methods for Multiphase Flows in Porous Media (2006), SIAM, Philadelphia.

[6] Davis, T. A.: A column pre-ordering strategy for the unsymmetric-pattern multifrontal method, *ACM Transactions on Mathematical Software*, vol 30, no. 2 (2004), pp. 165–195.

[7] Davis, T. A.: Algorithm 832: UMFPACK, an unsymmetric-pattern multifrontal method, *ACM Transactions on Mathematical Software*, vol 30, no. 2 (2004), pp. 196–199.

[8] Davis, T. A. and Duff, I. S.: A combined unifrontal/multifrontal method for unsymmetric sparse matrices, *ACM Transactions on Mathematical Software*, vol. 25, no. 1 (1999), pp. 1–19.

[9] Davis, T. A. and Duff, I. S.: An unsymmetric-pattern multifrontal method for sparse LU factorization, *SIAM Journal on Matrix Analysis and Applications*, vol 18, no. 1 (1997), pp. 140–158.

[10] Firoozabadi, A.: Thermodynamics of Hydrocarbon Reservoirs (1998), McGraw-Hill, NY.

[11] Holzbecher, E. O.: Modeling Density-Driven Flow in Porous Media: Principles, Numerics, Software (1998), Springer-Verlag, Berlin.

[12] Hoteit, H., Firoozabadi, A.: Multicomponent Fluid Flow by Discontinuous Galerkin and Mixed Methods in Unfractured and Fractured Media, *Water Resources Research* (2005), 41, W11412, doi:10.1029/2005WR004339.

[13] Huyakorn, P. S., Pinder, G. F.: Computational Methods in Subsurface Flow (1983), Academic Press, Inc., New York.

[14] Leveque, R. J.: Finite Volume Methods for Hyperbolic Problems (2002), Cambridge University Press, Cambridge.

[15] Lohrenz, J., Bray, B. G., Clark, C. R.: Calculating Viscosities of Reservoir Fluids From Their Compositions, *Journal of Petroleum Technology* Oct. (1964) 1171–1176.

[16] Maryška, J., Rozložník M., Tůma M.: Mixed-hybrid finite element approximation of the potential fluid flow problem, *Journal of Computational and Applied Mathematics* 63 (1995), 383–392.

[17] Mikyška, J., Firoozabadi, A.: Implementation of higher-order methods for robust and efficient compositional simulation, *Journal of Computational Physics* 229 (2010) 2898–2913.

[18] Peng, D. Y., Robinson, D. B.: A New Two-Constant Equation of State, *Industrial and Engineering Chemistry: Fundamentals 15* (1976) 59–64.

[19] Quarteroni, A., Sacco, R., Saleri, F.: Numerical Mathematics (2000), Springer-Verlag, New York.

[20] Russel, T. F., Wheeler, M. F.: Finite Element and Finite Difference Methods for Continuous Flows in Porous Media in: *The Mathematics of Reservoir Simulation, Frontiers in Applied Mathematics* (1983) 35–106, SIAM, Philadelphia.

[21] Young, L. C., Stephenson, R. E.: A Generalized Compositional Approach for Reservoir Simulation, *Society of Petroleum Engineers Journal*, Vol.: 23, Issue: 5 (1983) 727–742.

Ondřej Polívka and Jiří Mikyška
Department of Mathematics, Faculty of Nuclear Sciences and Physical Engineering, Czech Technical University in Prague, Trojanova 13, 120 00 Praha 2, Czech Republic
E-mail: ondrej.polivka(at)fjfi.cvut.cz
jiri.mikyska(at)fjfi.cvut.cz

3.7 [Č6]: Polívka, O., and Mikyška, J., Compositional Modeling in Porous Media using Constant Volume Flash and Flux Computation without the Need for Phase Identification, Journal of Computational Physics 272: 149–169, 2014

Journal of Computational Physics 272 (2014) 149–169

Contents lists available at ScienceDirect

Journal of Computational Physics

www.elsevier.com/locate/jcp

Compositional modeling in porous media using constant volume flash and flux computation without the need for phase identification

Ondřej Polívka, Jiří Mikyška *

Department of Mathematics, Faculty of Nuclear Sciences and Physical Engineering, Czech Technical University in Prague, Trojanova 13, 120 00 Prague 2, Czech Republic

ARTICLE INFO

Article history:
Received 2 July 2013
Received in revised form 24 February 2014
Accepted 11 April 2014
Available online 24 April 2014

Keywords:
Compositional simulation without phase identification
Mixed-hybrid finite element method
Finite volume method
Phase-by-phase upwinding
Constant-volume phase splitting
Pressure computation

ABSTRACT

The paper deals with the numerical solution of a compositional model describing compressible two-phase flow of a mixture composed of several components in porous media with species transfer between the phases. The mathematical model is formulated by means of the extended Darcy's laws for all phases, components continuity equations, constitutive relations, and appropriate initial and boundary conditions. The splitting of components among the phases is described using a new formulation of the local thermodynamic equilibrium which uses volume, temperature, and moles as specification variables. The problem is solved numerically using a combination of the mixed-hybrid finite element method for the total flux discretization and the finite volume method for the discretization of transport equations. A new approach to numerical flux approximation is proposed, which does not require the phase identification and determination of correspondence between the phases on adjacent elements. The time discretization is carried out by the backward Euler method. The resulting large system of nonlinear algebraic equations is solved by the Newton–Raphson iterative method. We provide eight examples of different complexity to show reliability and robustness of our approach.

1. Introduction

Mathematical models of gas injection into oil reservoirs play an important role in solving problems in enhanced oil recovery or CO_2 sequestration. These models have to describe transport of a mixture composed of several chemical components in a porous medium. Depending on the local thermodynamic conditions, the mixture can remain in a single phase or can split into two (or more) phases. In this work, we investigate models in which components splitting among the phases is described by means of the equilibrium thermodynamics (i.e. we adopt the assumption of the local thermodynamic equilibrium).

Let us briefly review the formulation of currently available compositional models, discuss several issues inherent to this formulation, and common ways of solving these issues. Traditionally, compositional models are formulated using a set of mass or mole balance equations for each component of the mixture in which phase velocities are given by the extended version of Darcy's law [5,13,14,24]. Phases are assumed to be compressible; their behavior is described by an equation of

* Corresponding author. Tel.: +420 224 358 553.
E-mail addresses: ondrej.polivka@fjfi.cvut.cz (O. Polívka), jiri.mikyska@fjfi.cvut.cz (J. Mikyška).

http://dx.doi.org/10.1016/j.jcp.2014.04.029
0021-9991/

state, e.g. the Peng–Robinson [30] or other equation of state, of the general pressure-explicit form $P = P(V, T, N_1, \ldots, N_{n_c})$, where P denotes the pressure, V is the volume, T is the temperature, and $N_1, \ldots, N_{n_c}$ are the mole numbers of the n_c components of the mixture. Using the assumption of the local thermodynamic equilibrium, the splitting of components between the phases is described by the equality of chemical potentials or fugacities of every component in both phases [12]. The fugacities are considered to be known functions of P, T, and chemical composition, which can be derived from the equation of state [12,23]. Therefore, for a given specification of P, T, and chemical composition, the stability algorithms [21, 12] can decide whether the single-phase mixture is stable or not. If the mixture is unstable, PT-flash algorithms are applied to compute the two-phase equilibrium at given P and T [22,12]. To the best of our knowledge, all available formulations of compositional models use this PT-based (constant pressure and temperature) approach to phase equilibrium computation.

No matter how wide-spread the use of the PT-based formulations of the phase stability and phase equilibria is, this approach has some limitations. First, it has been already noticed in [26,16] that specification of P, T, and overall mole numbers (or mole fractions) does not always determine the equilibrium state of the system uniquely. For example, if we have 1 mole of pure water at $P = 1$ atm and $T = 100\,^{\circ}\mathrm{C}$, one cannot tell whether it is a saturated liquid, a saturated gas, or a two-phase mixture of both. Although all these states correspond to the same values of pressure, temperature, and moles, these states are not the same as they differ in total volume of the mixture. Note that this situation can happen in the compositional simulation if, for example, during fast injection of a pure component into a reservoir, the injected component displaces all other components from the injection cell. It is certainly desirable to have a robust model formulation which will not crash in this situation. Let us also mention that the problem of non-uniqueness of the equilibrium state at given P, T, and $N_1, \ldots, N_{n_c}$ is not limited to pure components. We have observed the same problem in many multi-component mixtures in three phases [15].

Another complication inherent to the PT-based flash equilibrium formulations is the fact that in compositional simulation the pressure is not known a-priori. Actually, pressure field is one of the unknowns that has to be computed by the simulator. Unlike concentrations, there is no balance equation describing evolution of the pressure field. Instead, pressure is given implicitly by solving the whole system of equations. In the literature, two approaches to pressure computation in compositional simulation are available. In the first approach of Ács et al. [1], an evolution partial differential equation for pressure is formed by combining the evolution equations for overall concentrations in a suitable way. This extra equation can be solved to get the pressure field. Pressure computation is then followed by the update of concentrations using the transport equations, typically in an IMPEC (implicit pressure, explicit concentrations) manner [11,28]. As we have one more equations than unknowns, the system is overdetermined, and we have two ways to evaluate the overall concentration of the mixture – either by summing the updated overall molar concentrations of the components or by performing the PT-flash on the mixture at the predicted pressure. Due to numerical discretization errors, the two values of concentration are not the same and the mass-balance error occurs. This error can be reduced by reducing the time step. Therefore, this mass-balance error has been used as one of the criteria for the time step selection [14,34]. Let us also mention that to assemble the pressure equation, coefficients of the total two-phase compressibility and total partial molar volumes of all components have to be evaluated [12], which requires additional algebraic manipulations. An alternative approach to pressure computation is the approach of Young and Stephenson [35], in which pressure update is formed using the linearization of the transport equations with respect to selected primary variables. This approach can also be adopted in the IMPEC manner and its application also requires considerable algebraic manipulation. Moreover, the correct selection of the primary variables can be tricky as phases can appear/disappear during the simulation.

Both issues mentioned above can be overcome by using an alternative variables specification for the stability and flash equilibrium computations. By specifying volume, temperature, and moles (or temperature and overall molar concentrations of all components), the equilibrium state of the system is uniquely determined [26]. This approach requires using variables V, T, and N_i $(i = 1, \ldots, n_c)$ rather than the conventional set P, T, and composition. The reformulation of the state functions like chemical potentials in terms of the new variables has been carried out in [26] and VT-based stability and flash algorithm have been derived in [26,27,16]. Within the new framework, the problem of non-uniqueness of the equilibrium state does not appear. The VT-based formulations can also be used for pressure computation because, once the temperature and overall molar concentrations are specified, equilibrium pressure is one of the outcomes of the VT-flash calculation.

In this work, we develop a new formulation of the compositional model which uses the VT-stability and VT-flash equilibrium calculation for pressure evaluation. The approach has several desirable features following from the fact that volume, temperature, and moles are the natural variables of the equation of state. In the conventional PT-flash, pressure has to be found a-priori using some of the above mentioned methods [1,35], and volume has to be computed by inverting the equation of state. The cubic equations of state may have up to three roots, from which the correct one has to be selected. Usually, the root with the lowest value of the Gibbs free energy is used [12]. In the VT-based algorithm, volume of the cell is known a-priori and pressure can be evaluated directly without the need to invert the equation of state once the resulting phase split has been computed using the VT-flash algorithm. The need for the root selection procedure is thus avoided. This feature can be even more attractive when non-cubic equation of state (like the cubic plus association equation of state) are used as in these equations number of roots is not known a-priori [18].

The approach suggested in this paper also addresses one issue not related to the VT-flash that is usually overlooked in the literature. In all formulations used for gas injection into oil reservoirs we are aware of, one usually distinguishes two phases – one of them labeled as gas and the other one labeled as liquid. In many situations of practical importance this distinction can be done easily using the phase densities, viscosities or other physical properties of the fluids. When

computing the phase fluxes across the cell boundaries, the gas phase properties on both sides of the interface are used to compute the gas phase flux across the interface between the two cells. Similarly liquid properties on both sides of the interface are used to compute the flux of the liquid phase over the interface. It is tacitly assumed that it is always possible to find out the phase identity – i.e. decide which one of the two equilibrium phases is the gas and which one is the liquid so that the correct pairing of the corresponding phases at the interface between the two grid cells is performed. This approach runs into difficulties when investigating mixtures close to the critical point where both split-phases are very similar [12]. Moreover, above the critical point, the supercritical fluids have some properties similar to liquids while other properties are similar to gases. Selection of the phase identity is then often matter of an ad-hoc procedure. It is also not clear how to compute phase fluxes between two cells with different number of phases – e.g. with one phase on one side and two phases on the other side – or between the cells which are both single-phase but one of them contains liquid and the other one gas.

Therefore, we suggest a new formulation of components fluxes in the compositional model and a special version of the upwind technique for the flux approximation which avoids the need for the phase identification. The numerical flux proposed in this work is locally conservative, does not depend on any phase identification, and solves the problem of connection of fluxes between the cells with different number of phases on both sides in a natural way. This method also helps to develop a correct formulation of the boundary conditions and avoids certain complexities encountered in our previous work [24].

The paper is structured as follows. In Section 2, the mathematical model is formulated by means of partial differential equations representing the conservation laws, Darcy's laws, and by means of the conditions of local thermodynamic equilibrium in the VT-settings. We define several fluxes and derive some relations between them. Then, the compositional model is formulated and appropriate initial and boundary conditions are prescribed. In Section 3, the system of equations is solved numerically using the Mixed-Hybrid Finite Element Method (MHFEM) for the Darcy's law discretization, and the Finite Volume Method (FVM) for the components transport equations discretization. We also describe details of the numerical flux approximation. A fully implicit scheme is derived and linearized using the Newton–Raphson iterative method (NRM). In Section 4, we summarize the essential steps of the computational algorithm. In Section 5, we present examples of computations using the new approach. In Section 6, we summarize essential features of the method and draw some conclusions. In Appendices A and B, we provide details of the equation of state used in the calculation, and details of the derivation of the MHFEM.

2. Mathematical model

2.1. Transport equations

Consider two-phase compressible flow of a mixture composed of n_c components in a porous medium with porosity ϕ [–] at a constant temperature T [K]. Neglecting diffusion and capillarity, the transport of the components can be described by the following molar balance equations [24]

$$\frac{\partial(\phi c_i)}{\partial t} + \nabla \cdot \left(\sum_\alpha c_{\alpha,i} \mathbf{v}_\alpha \right) = F_i, \quad i = 1, \ldots, n_c, \tag{1}$$

where $\sum_\alpha$ sums over all phases, c_i is the overall molar concentration of component i [mol m^{-3}], $c_{\alpha,i}$ is the molar concentration of component i in phase α [mol m^{-3}], and F_i is the sink or source term [mol m^{-3} s^{-1}]. The phase velocity $\mathbf{v}_\alpha$ is given by the extended Darcy's law

$$\mathbf{v}_\alpha = -\lambda_\alpha \mathbf{K}(\nabla p - \varrho_\alpha \mathbf{g}), \quad \lambda_\alpha = \frac{k_{r\alpha}}{\mu_\alpha}, \tag{2}$$

where $\mathbf{K} = \mathbf{K}(\mathbf{x})$ is the medium intrinsic permeability [m^2], p is the pressure [Pa], $\varrho_\alpha = \sum_{i=1}^{n_c} c_{\alpha,i} M_i$ is the density of fluid in phase α (M_i is the molar weight of component i [kg mol^{-1}]), and $\mathbf{g}$ is the gravitational acceleration vector [m s^{-2}]. The α-phase mobility λ_α is given by the ratio of the α-phase relative permeability $k_{r\alpha}$ [–] and α-phase dynamic viscosity μ_α [kg m^{-1} s^{-1}]. The α-phase relative permeability depends on its saturation S_α [–] as

$$k_{r\alpha} = k_{r\alpha}(S_\alpha), \tag{3}$$

and

$$\mu_\alpha = \mu_\alpha(T, c_{\alpha,1}, \ldots, c_{\alpha,n_c}) \tag{4}$$

is computed using the Lohrenz–Bray–Clark method [19].

2.2. VT-stability and phase-split calculation

Depending on the local thermodynamic conditions at each point, the mixture can be in a single phase or split into two phases. To test whether the phase splitting occurs, we use a constant volume phase stability test described in [27]. Assuming that temperature $T > 0$ and the overall molar concentrations $c_1, \dots, c_{n_c}$ are known, this algorithm tests if splitting of a small amount of a trial phase with arbitrary concentrations $c'_1, \dots, c'_{n_c}$ from the initial phase can decrease the total Helmholtz free energy of the system. If such a trial phase cannot be found, then the single phase is stable, $c_{\alpha,i} = c_i$, $S_\alpha = 1$, and pressure is given by an equation of state of the form

$$p = p(T, c_1, \dots, c_{n_c}). \tag{5}$$

In this work, we use the Peng–Robinson equation of state, which is detailed in Appendix A.

If the VT-stability indicates that the system is in two phases, the splitting of components among the phases is given by the following phase equilibrium conditions [26]

$$\sum_\alpha c_{\alpha,i} S_\alpha = c_i, \qquad \sum_\alpha S_\alpha = 1, \tag{6a}$$

$$p(T, c_{\alpha,1}, \dots, c_{\alpha,n_c}) = p(T, c_{\beta,1}, \dots, c_{\beta,n_c}), \quad \forall \alpha \neq \beta, \tag{6b}$$

$$\widetilde{\mu}_i(T, c_{\alpha,1}, \dots, c_{\alpha,n_c}) = \widetilde{\mu}_i(T, c_{\beta,1}, \dots, c_{\beta,n_c}), \quad \forall \alpha \neq \beta, \ \forall i = 1, \dots, n_c. \tag{6c}$$

Eqs. (6) express the balance of mass and volume (6a), mechanical equilibrium (6b), and chemical equilibrium (6c) in which $\widetilde{\mu}_i$ denotes the chemical potential of component i. Details of relations (6b) and (6c) can be found in Appendix A.

The system of equations (6) represents a set of non-linear algebraic equations. If the temperature T and overall molar concentrations $c_1, \dots, c_{n_c}$ are specified, solving (6) will provide molar concentrations of all components in both phases $c_{\alpha,i}$ and phase saturations S_α. Once the system (6) is resolved, the equilibrium pressure p can be determined readily using the equation of state as

$$p = p(T, c_{\alpha,1}, \dots, c_{\alpha,n_c}), \tag{7}$$

where α is any of the split-phases. The value of pressure does not depend on the selection of α because in equilibrium, pressures in both phases are the same, see (6b).

2.3. Definition of several fluxes

Let us define the i-th component flux in the α-phase $\mathbf{q}_{\alpha,i}$ and the total α-phase flux $\mathbf{q}_\alpha$ as

$$\mathbf{q}_{\alpha,i} = c_{\alpha,i} \mathbf{v}_\alpha, \tag{8a}$$

$$\mathbf{q}_\alpha = \sum_{i=1}^{n_c} \mathbf{q}_{\alpha,i} = c_\alpha \mathbf{v}_\alpha, \tag{8b}$$

where $c_\alpha = \sum_{i=1}^{n_c} c_{\alpha,i}$ is the total α-phase concentration. By summing over all phases in (8), we can calculate the total component flux $\mathbf{q}_i$ and the total flux $\mathbf{q}$ as

$$\mathbf{q}_i = \sum_\alpha \mathbf{q}_{\alpha,i} = \sum_\alpha c_{\alpha,i} \mathbf{v}_\alpha, \tag{9a}$$

$$\mathbf{q} = \sum_\alpha \mathbf{q}_\alpha = \sum_\alpha c_\alpha \mathbf{v}_\alpha. \tag{9b}$$

For further derivation of the numerical scheme, we need to express the phase velocity $\mathbf{v}_\alpha$ using the total flux $\mathbf{q}$. By substituting (2) into (9b), Darcy's law for the total flux can be formulated as

$$\mathbf{q} = -\sum_\alpha c_\alpha \lambda_\alpha \mathbf{K} (\nabla p - \widetilde{\varrho} \mathbf{g}), \tag{10}$$

where

$$\widetilde{\varrho} = \frac{\sum_\alpha c_\alpha \lambda_\alpha \varrho_\alpha}{\sum_\alpha c_\alpha \lambda_\alpha} \tag{11}$$

is an average density. Note that although λ_α can vanish when $S_\alpha \to 0$, the sum $\sum_\alpha c_\alpha \lambda_\alpha$ is always positive, so the division in (11) is permissible. By inverting $\mathbf{K}$ (which is invertible since (B.7) holds) in (10), the pressure gradient is given by

$$\nabla p = -\frac{\mathbf{K}^{-1} \mathbf{q}}{\sum_\alpha c_\alpha \lambda_\alpha} + \widetilde{\varrho} \mathbf{g}. \tag{12}$$

Combining (12) and (2), we have

$$\mathbf{v}_\alpha = \frac{\lambda_\alpha}{\sum_\beta c_\beta \lambda_\beta}\left(\mathbf{q} - \sum_\beta c_\beta \lambda_\beta (\varrho_\beta - \varrho_\alpha)\mathbf{K}\mathbf{g}\right). \tag{13}$$

Then, using (8a) and (13), $\mathbf{q}_{\alpha,i}$ can be evaluated as

$$\mathbf{q}_{\alpha,i} = \frac{c_{\alpha,i}\lambda_\alpha}{\sum_\beta c_\beta \lambda_\beta}\left(\mathbf{q} - \sum_\beta c_\beta \lambda_\beta (\varrho_\beta - \varrho_\alpha)\mathbf{K}\mathbf{g}\right), \tag{14}$$

and the total component flux (combining (9a) and (13)) as

$$\mathbf{q}_i = \sum_\alpha \frac{c_{\alpha,i}\lambda_\alpha}{\sum_\beta c_\beta \lambda_\beta}\left(\mathbf{q} - \sum_\beta c_\beta \lambda_\beta (\varrho_\beta - \varrho_\alpha)\mathbf{K}\mathbf{g}\right). \tag{15}$$

2.4. Model formulation

Let $\Omega \subset \mathbb{R}^d$ ($d \in \mathbb{N}$) be a bounded domain and I be a time interval. In $\Omega \times I$, we solve for $c_i = c_i(\mathbf{x}, t)$ the following equations which can be obtained from the transport equations (1) and (9a)

$$\frac{\partial(\phi c_i)}{\partial t} + \nabla \cdot \mathbf{q}_i = F_i, \quad i = 1, \ldots, n_c, \tag{16}$$

where $\mathbf{q}_i$ is given by (15), and $\mathbf{q}$ is given by (10). The molar concentrations $c_{\alpha,i}$ and saturations S_α are related to the overall molar concentrations c_i by (6) from which we also determine the pressure (see Section 2.2). Relative permeabilities and viscosities are given by (3) and (4). For this system of equations, we impose the following initial and boundary conditions

$$c_i(\mathbf{x}, 0) = c_i^0(\mathbf{x}), \quad \mathbf{x} \in \Omega,\ i = 1, \ldots, n_c, \tag{17a}$$

$$p(\mathbf{x}, t) = p^D(\mathbf{x}, t), \quad \mathbf{x} \in \Gamma_p,\ t \in I, \tag{17b}$$

$$\mathbf{q}_i(\mathbf{x}, t) \cdot \mathbf{n}(\mathbf{x}) = 0, \quad \mathbf{x} \in \Gamma_q,\ t \in I,\ i = 1, \ldots, n_c, \tag{17c}$$

where $\mathbf{n}$ is the unit outward normal vector to the boundary $\partial\Omega$, $\Gamma_p \cup \Gamma_q = \partial\Omega$, and $\Gamma_p \cap \Gamma_q = \emptyset$. Initial values of molar concentrations are given by (17a), whereas (17b) is the Dirichlet boundary condition prescribing the pressure p_D on Γ_p, and (17c) is zero Neumann boundary condition representing impermeable boundary on Γ_q. We assume that Γ_p is the outflow boundary, so no boundary condition for concentration has to be imposed.

3. Numerical scheme

The system of equations (16), (6), and (17) is solved numerically by a combination of the MHFEM for the total flux discretization, and the FVM for the transport equations discretization. The system is linearized using the NRM. The local number of phases on every element is determined by testing the single-phase stability at constant temperature and overall molar concentrations using the constant volume stability algorithm described in [27]. In two-phase elements, the splitting of components among the phases is computed using the VT-flash algorithm from [26]. Once the phase state (i.e. single-phase or two-phase) of every element and the phase splitting in two-phase elements have been established, pressure is computed explicitly using the equation of state.

We consider a 2D polygonal domain Ω with the boundary $\partial\Omega$ which is covered by a conforming triangulation $\mathcal{T}_\Omega$. Let us denote K the element of the mesh $\mathcal{T}_\Omega$ with area $|K|$, E the edge of an element with the length $|E|$, n_k the number of elements of the triangulation, and n_e the number of edges of the mesh.

3.1. Discretization of the total flux

The total flux $\mathbf{q}$ is approximated locally in the Raviart–Thomas space of the lowest order ($\mathrm{RT}_0(K)$) over the element $K \in \mathcal{T}_\Omega$ [3] as

$$\mathbf{q}|_K = \sum_{E \in \partial K} q_{K,E}\mathbf{w}_{K,E}, \tag{18}$$

where the coefficient $q_{K,E}$ is the numerical flux of vector function $\mathbf{q}$ through the edge E on the element K with respect to the outer normal, and $\mathbf{w}_{K,E}$ represents the piecewise linear $\mathrm{RT}_0(K)$-basis function associated with the edge E (see Appendix B).

Multiplying relation (12) by the basis function $\mathbf{w}_{K,E}$, integrating over the element K, and using the $\mathrm{RT}_0(K)$ properties described in details in Appendix B, we obtain a discrete form of Darcy's law for the total flux (10) as follows

$$q_{K,E} = \sum_{\alpha\in\Pi(K)} c_{\alpha,K}\lambda_{\alpha,K}\left(\alpha_E^K p_K - \sum_{E'\in\partial K}\beta_{E,E'}^K \widehat{p}_{K,E'} + \gamma_E^K \widetilde{\varrho}_K\right), \quad E\in\partial K. \tag{19}$$

In Eq. (19), $\Pi(K)$ denotes all phases on element K. The coefficients α_E^K, $\beta_{E,E'}^K$ and γ_E^K dependent on the mesh geometry and on the local values of the medium permeability are detailed in Appendix B. Further, p_K denotes the cell pressure average, $\widehat{p}_{K,E'}$ is the edge pressure average, $c_{\alpha,K}$, $\lambda_{\alpha,K}$, $\widetilde{\varrho}_K$ are the mean values of concentration and mobility of phase α, and average density on element K. The cell-averaged quantities are functions of the overall molar concentrations and temperature at element K; their evaluation is described in Section 3.3.

The continuity of normal component of the total flux and pressure on the edge E between neighboring elements $K, K'\in\mathcal{T}_\Omega$ can be written as

$$q_{K,E} + q_{K',E} = 0, \tag{20}$$

$$\widehat{p}_{K,E} = \widehat{p}_{K',E} =: \widehat{p}_E. \tag{21}$$

The boundary conditions (17b), (17c) are discretized as

$$\widehat{p}_E = p^D(E), \quad \forall E\subset\Gamma_p, \tag{22a}$$

$$q_{K,E} = 0, \quad \forall E, K : E\subset\Gamma_q,\ E\in\partial K, \tag{22b}$$

where $p^D(E)$ is the prescribed value of pressure p averaged on the edge E.

The numerical flux can be eliminated by substituting $q_{K,E}$ from (19) into (20) and (22b). For further derivation, let us consider time dependent quantities at time t_{n+1} denoted by upper index $n+1$. Then, Eqs. (19)–(22) can be transformed to the following system of n_e linear algebraic equations $\mathcal{F}_E = 0$, where

$$\mathcal{F}_E = \begin{cases} \sum\limits_{K:E\in\partial K}\Big(\sum\limits_{\alpha\in\Pi(K)} c_{\alpha,K}^{n+1}\lambda_{\alpha,K}^{n+1}\Big)\Big(\alpha_E^K p_K^{n+1} - \sum\limits_{E'\in\partial K}\beta_{E,E'}^K\widehat{p}_{E'}^{n+1} + \gamma_E^K\widetilde{\varrho}_K^{n+1}\Big), & \forall E\not\subset\Gamma_p, \\ \widehat{p}_E^{n+1} - p^D(E), & \forall E\subset\Gamma_p. \end{cases} \tag{23}$$

Herein, the symbol $\sum\limits_{K:E\in\partial K}$ denotes the sum over the elements adjacent to the edge E.

3.2. Approximation of the transport equations

The transport equations (16) with the initial and boundary conditions (17) are discretized by the FVM [17]. Integrating (16) over an arbitrary element $K\in\mathcal{T}_\Omega$ and using Green's theorem, we have

$$\frac{\mathrm{d}}{\mathrm{d}t}\int_K \phi(\mathbf{x})c_i(\mathbf{x},t) + \int_{\partial K}\mathbf{q}_i(\mathbf{x},t)\cdot\mathbf{n}_{\partial K}(\mathbf{x}) = \int_K F_i(\mathbf{x}), \quad i = 1,\dots,n_c. \tag{24}$$

Applying the mean value theorem on (24), and denoting $\phi_K, c_{i,K}, F_{i,K}$, the averaged values of ϕ, c_i, F_i $(i = 1,\dots,n_c)$ over the cell K, respectively, the semi-discrete form of (16) reads as

$$\frac{\mathrm{d}(\phi_K c_{i,K})}{\mathrm{d}t}|K| + \sum_{E\in\partial K} q_{i,K,E} = F_{i,K}|K|, \tag{25}$$

where $q_{i,K,E}$ is a numerical approximation of $\int_E \mathbf{q}_i\cdot\mathbf{n}_{K,E}$ for $E\in\partial K$. The numerical flux $q_{i,K,E}$ is evaluated by the following upwind technique

$$q_{i,K,E} = \begin{cases} \sum\limits_{\alpha\in\Pi(K,E)^+} q_{\alpha,i,K,E} - \sum\limits_{\beta\in\Pi(K',E)^+} q_{\beta,i,K',E}, & \forall E\notin\partial\Omega, \\ \sum\limits_{\alpha\in\Pi(K,E)^+} q_{\alpha,i,K,E}, & \forall E\in\Gamma_p, \\ 0, & \forall E\in\Gamma_q, \end{cases} \tag{26}$$

where $\Pi(K,E)^+ = \{\alpha\in\Pi(K)\mid q_{\alpha,i,K,E} > 0\}$ for $E\in\partial K$, and $q_{\alpha,i,K,E}$ is (14) written in a discrete form as

$$q_{\alpha,i,K,E} = \frac{c_{\alpha,i,K}\lambda_{\alpha,K}}{\sum\limits_{\beta\in\Pi(K)} c_{\beta,K}\lambda_{\beta,K}}\left(q_{K,E} - \sum_{\beta\in\Pi(K)} c_{\beta,K}\lambda_{\beta,K}(\varrho_{\beta,K} - \varrho_{\alpha,K})\gamma_E^K\right). \tag{27}$$

Notice that (26) is an approximation of (15), where we sum over the phases on the edge E taking only the outflowing phases into account. This method ensures that no phase identification or phase interconnection between neighboring elements is necessary, and the total component fluxes are balanced on each inner edge. In (27), $q_{K,E}$ is given by (19), $c_{\alpha,i,K}$

and $S_{\alpha,K}$ are computed locally on each element by VT-flash (see Section 2.2), and from them, $c_{\alpha,K}$, $\lambda_{\alpha,K}$, and $\varrho_{\alpha,K}$ are evaluated.

Assuming that the porosity does not depend on time, the time derivative of $c_{i,K}$ in (25) is approximated by the time difference with a time step Δt_n. Using Euler's method [17], we obtain for every n, all $K \in \mathcal{T}_\Omega$, and $i = 1, \dots, n_c$ Eq. (25) in a form $\mathcal{F}_{K,i} = 0$, where

$$\mathcal{F}_{K,i} = \phi_K |K| \frac{c_{i,K}^{n+1} - c_{i,K}^{n}}{\Delta t_n} + \sum_{E \in \partial K} q_{i,K,E}^{n+1} - F_{i,K}|K|, \tag{28}$$

where $q_{i,K,E}$ is given by (26). Note that scheme (28) is fully implicit.

The initial conditions (17a) are approximated as

$$c_{i,K}^0 = c_i^0(K), \quad \forall K \in \mathcal{T}_\Omega,\ i = 1, \dots, n_c, \tag{29}$$

where $c_i^0(K)$ denotes the average value of c_i^0 on element K.

3.3. Assembling the final scheme

In Eqs. (23) and (28), we have denoted $\mathcal{F}_E$ and $\mathcal{F}_{K,i}$, (for the edge $E \in \{1, \dots, n_e\}$, element $K \in \{1, \dots, n_k\}$, and component $i \in \{1, \dots, n_c\}$) the expressions which represent the components of a vector $\boldsymbol{\mathcal{F}}$. To evaluate coefficients $c_{\alpha,K}^{n+1}$, $\lambda_{\alpha,K}^{n+1}$, $\widetilde{\varrho}_K^{n+1}$ that are needed in (23) and also other element-averaged quantities depending on phase splitting required in (26)–(28), we perform the VT-flash calculation on element K using the cell-averaged values $c_{1,K}^{n+1}, \dots, c_{n_c,K}^{n+1}$, and temperature T. The cell average pressure p_K^{n+1} is also given implicitly by the result of the VT-flash at given $c_{1,K}^{n+1}, \dots, c_{n_c,K}^{n+1}$, and temperature T as described in Section 2.2. Using the NRM, we therefore solve a nonlinear system of algebraic equations of $n_k \cdot n_c + n_e$ equations

$$\boldsymbol{\mathcal{F}} = [\mathcal{F}_{1,1}, \dots, \mathcal{F}_{1,n_c}, \dots, \mathcal{F}_{n_k,1}, \dots, \mathcal{F}_{n_k,n_c}; \mathcal{F}_1, \dots, \mathcal{F}_{n_e}]^T = \mathbf{0} \tag{30}$$

for unknown primary variables – overall molar concentrations $c_{1,K}^{n+1}, \dots, c_{n_c,K}^{n+1}$, $K \in \{1, \dots, n_k\}$, and pressures on edges $\widehat{p}_E^{n+1}$, $E \in \{1, \dots, n_e\}$. In each iteration of the NRM, we solve the following linear system of algebraic equations

$$\mathbf{J}\boldsymbol{\delta} = -\boldsymbol{\mathcal{F}}. \tag{31}$$

The Jacobian matrix $\mathbf{J}$ of system (31) is sparse and nonsymmetric. The matrix is divided into 4 blocks whose elements can be evaluated analytically using the following relations

$$(\mathbf{J}_{K,K'})_{i,j} = \frac{\partial \mathcal{F}_{K,i}}{\partial c_{j,K'}^{n+1}}, \qquad (\mathbf{J}_{K,E})_i = \frac{\partial \mathcal{F}_{K,i}}{\partial \widehat{p}_E^{n+1}}, \qquad (\mathbf{J}_{E,K})_j = \frac{\partial \mathcal{F}_E}{\partial c_{j,K}^{n+1}}, \qquad J_{E,E'} = \frac{\partial \mathcal{F}_E}{\partial \widehat{p}_{E'}^{n+1}}, \tag{32}$$

where $J_{E,E'}$ is an element of the matrix $\mathbf{J}_{E,E'}$, $i, j = 1, \dots, n_c$; $K, K' = 1, \dots, n_k$; $E, E' = 1, \dots, n_e$. The vector of solutions $\boldsymbol{\delta}$ contains the corrections of molar concentrations $\delta c_{i,K}^{n+1}$ and pressures on the edges $\delta \widehat{p}_E^{n+1}$, which are computed in each NRM iteration and added to the values of $c_{i,K}^{n+1}$ and $\widehat{p}_E^{n+1}$ given from the previous iteration. The iteration procedure ends when the condition

$$\|\boldsymbol{\mathcal{F}}\| < \varepsilon \tag{33}$$

is satisfied for a chosen $\varepsilon > 0$ [33]. The robustness of the NRM is increased by using the line-search technique [33]. If the NRM cannot converge in 10 iterations or if the line-search does not lead to the reduction of $\|\boldsymbol{\mathcal{F}}\|$ in 10 iterations, the time step is restarted and the value Δt_n is halved. If the NRM converges in less than 4 iterations, the time step is accepted and the next time step size is increased ($\Delta t_{n+1} = 1.2 \Delta t_n$).

Let us point out that the linearization is performed with respect to the overall molar concentrations on each element and traces of pressure on every edge of the triangulation. These variables are persistent – i.e. well defined independently of whether a given element is in a single phase or two phases. The derivatives in (32) are also well defined in both single phase and two phases. Therefore, our scheme performs well in both cases and no primary variables switching is needed for treating phase appearance/disappearance (cf. [2,6,29]). As the discretization of the transport equations is based on the approximation of the total component flux, the connection between the elements with different number of phases is treated in a natural way.

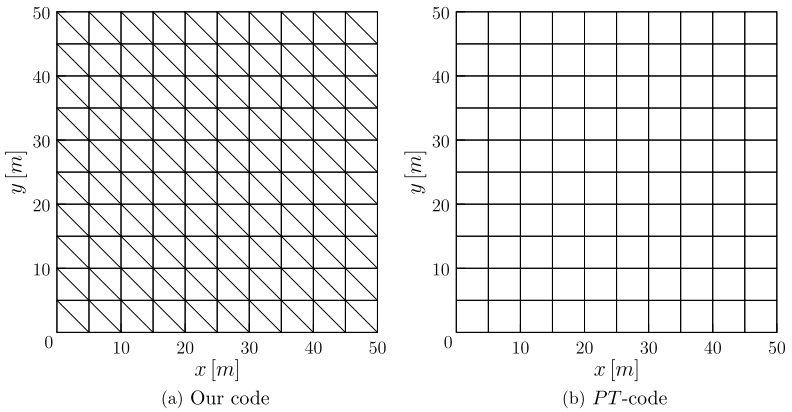

Fig. 1. Structures of the computational grid in our code and PT-code.

4. Computational algorithm

Numerical solution can be computed in the following steps:

1. Initialize the geometry, physical and chemical parameters, and molar concentrations, generate a domain triangulation.
2. Calculate pressures p_K on each element using the equation of state (A.1) and initial molar concentrations, then initialize all edge pressures $\widehat{p}_E$ by averaging p_K on neighboring elements.
3. Repeat until the predetermined final time is reached ($t_n \in I$):
   (a) Repeat the NRM iterations until the convergence criterion (33) is satisfied:
      i. Perform the stability and flash calculations (see Section 2.2) to obtain a number of phases and their compositions locally on all elements.
      ii. Evaluate phase mobilities $\lambda_{\alpha,K}^{n+1}$ using (2), (3), and (4) on each element.
      iii. For each K, compute the cell-averaged pressures p_K^{n+1} using (5) or (6b) depending on the phase state (see Section 2.2), and average densities $\widetilde{\varrho}_K^{n+1}$ using (11).
      iv. Evaluate the total fluxes $q_{K,E}^{n+1}$ using (19) and phase fluxes $q_{\alpha,i,K,E}^{n+1}$ using (27).
      v. Assemble and solve the system (31) for corrections of molar concentrations $\delta c_{i,K}^{n+1}$ and pressures $\delta\widehat{p}_E^{n+1}$ simultaneously.
      vi. Add corrections $\delta c_{i,K}^{n+1}$ and $\delta\widehat{p}_E^{n+1}$ to $c_{i,K}^{n+1}$ and $\widehat{p}_E^{n+1}$, respectively, check the convergence criterion (33).
   (b) Continue to the next time level ($n \to n+1$).

In steps i.–iii. $c_{\alpha,K}^{n+1}$, $\lambda_{\alpha,K}^{n+1}$, $\widetilde{\varrho}_K^{n+1}$, and p_K^{n+1} are computed using the data from the last available Newton iteration. In the first iteration, data from the previous time step are used.

5. Numerical results

In this section, we present results of compositional simulations of gas injections into reservoirs filled with different mixtures using the numerical scheme described above. We compute the flow in a 2D square reservoir 50×50 m^2 with porosity $\phi = 0.2$ and isotropic permeability $\mathbf{K} = k = 9.87 \times 10^{-15}$ m^2 (i.e. 10 mD) if not specified otherwise. Structure of the computational grid with $2 \times 10 \times 10$ elements is shown in Fig. 1(a). Parameter ε from the NRM convergence criterion (33) was chosen 10^{-6} for all computations. The systems of linear algebraic equations were solved using the direct solver UMFPACK [7–10]. All our results were computed on a grid of $2 \times 40 \times 40$ elements except for the simulations serving for the convergence verification. Our calculations were performed on Six-Core AMD Opteron(tm) Processor 2427 at 2.2 GHz and 32 GB memory. Only VT-flash calculations were performed in parallel. The rest of the computation was sequential.

In the following parts, the numerical simulations are computed for different mixtures, and validated with results computed using an other code. The other code uses the method of Ács et al. [1] to decouple pressure computation and the update of concentrations. While the pressure equation is treated semi implicitly using the MHFEM, the update of concentrations is performed explicitly using the first order FVM upwind scheme. The phase splitting is solved using the conventional PT-flash, and the phase identification is performed using the densities of the split phases. Details of the scheme can be found in [13,14,24]. In the following, we denote this code as PT-code. Note that in [24] a higher order scheme is used for computations. In this paper, we compare our results with those obtained by the first order (MHFEM–FVM) variant of the scheme [24] on a rectangular grid with structure shown in Fig. 1(b). Examples 1 and 2 correspond to Examples 3 and 4

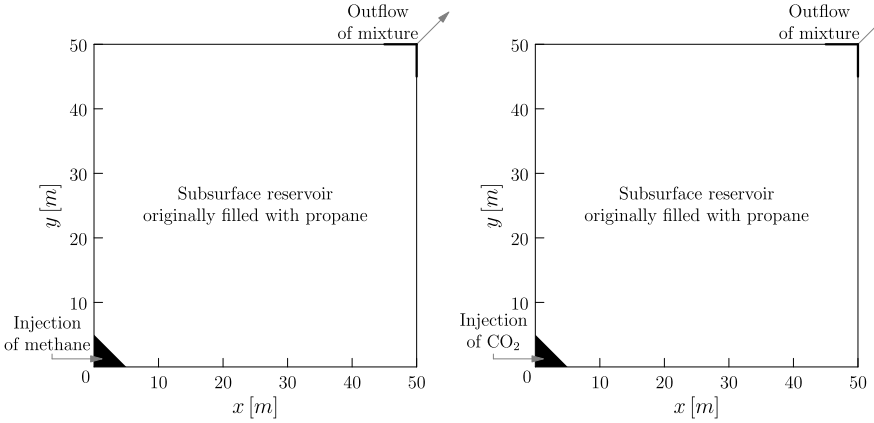

(a) Examples 1 and 2 (b) Examples 3 and 4

Fig. 2. Outlines of the simulated reservoirs for Examples 1–4.

Table 1
Relevant parameters of the Peng–Robinson equation of state (A.1) for Examples 1 and 2. Volume translation is not used.

i (component)	p_{ci} [MPa]	T_{ci} [K]	V_{ci} [$m^3\,mol^{-1}$]	M_i [$g\,mol^{-1}$]	ω_i [–]	δ_{i1} [–]	δ_{i2} [–]
1 (C_1)	4.58373	189.743	9.897054×10^{-5}	16.2077	1.14272×10^{-2}	0	0.0365
2 (C_3)	4.248	369.83	2×10^{-4}	44.0962	0.153	0.0365	0

in [24]. Examples 3 and 4 are inspired by Example 2 in [25]. Examples 6 and 7 correspond to Examples 6 and 5 in [24]. Example 8 demonstrates a case in which the traditional PT-based approach fails.

5.1. Injection of methane into propane

Let us consider a cut through a propane reservoir at initial pressure $p = 6.9$ MPa and temperature $T = 311$ K. In the left bottom corner of the reservoir, methane is injected, and in the right upper corner, the mixture of methane and propane is produced (Fig. 2(a)). The injection rate of methane is 42.5 m^2/day at pressure 1 atm (0.101325 MPa) and temperature 293 K. The parameters of the Peng–Robinson equation of state for both components of the mixture are summarized in Table 1. In these settings, both methane and propane are single-phase but when mixed, the mixture can split into two phases. The boundary of the domain is impermeable except for the outflow corner where pressure $p = 6.9$ MPa is maintained. Relative permeability depends linearly on saturation as $k_{r\alpha}(S_\alpha) = S_\alpha$ for each phase α.

Example 1. First, we simulate injection of methane into a horizontal reservoir (i.e. with zero gravity) originally filled with propane. Isolines of methane overall molar fraction $c_1/(\sum_{i=1}^{2} c_i)$ at three different times are shown in Fig. 3. The value of molar fraction nearest to the injection corner is 0.95, and with each isoline towards the outflow corner the value decreases by 0.1. The mixture stays in the single phase in the major part of the domain, but, in the mixing zone, the two-phase region develops (visualized by gray color). The computation to $t = 1.71$ years lasted 13.1 hours. To validate our results, the problem was computed also by the PT-code. The obtained result at $t = 1.14$ years is depicted in Fig. 3(d) (indication of the two-phase region was unavailable in the PT-code). The result is similar to the one in Fig. 3(b).

In this example, we also verify convergence of the numerical scheme. In the single-phase case, an analytical solution for a special problem is available. The experimental convergence analysis of the MHFEM–FVM for this problem can be found in [32]. As, to the best of our knowledge, there is no analytical solution for the two-phase case available, we use a pseudoanalytical solution, i.e. the numerical solution computed on the finest grid of 8192 elements, for the convergence analysis. Experimental orders of convergence (EOC) are computed between neighboring grids $m = 2 \times 2 \times 2$, $2 \times 4 \times 4$, $2 \times 8 \times 8$, $2 \times 16 \times 16$, and $2 \times 32 \times 32$ using the L^1 and L^2 consistent norms for errors E_m of methane concentrations and cell-averaged pressures in comparison with the solution obtained on the grid $2 \times 64 \times 64$. The errors are computed on the finest grid by projecting the solutions from the coarser grids to the finest grid. The time step for the pseudoanalytical solution is chosen constant $\Delta t = 195.3125$ s. For the solutions on coarser grids, Δt is 4 times larger with each mesh refinement ($\Delta t \sim m^{-1}$), i.e. $\Delta t = 781.25$ s for the solution computed on 2048 elements, $\Delta t = 3125$ s for 512 elements, $\Delta t = 12\,500$ s for 128 elements, $\Delta t = 50\,000$ s for 32 elements, and $\Delta t = 200\,000$ s for 8 elements. The EOC in a norm $\|.\|_\nu$ is given by

$$\mathrm{EOC}_\nu = \frac{\ln \|E_{m_1}\|_\nu - \ln \|E_{m_2}\|_\nu}{\ln m_2 - \ln m_1},$$

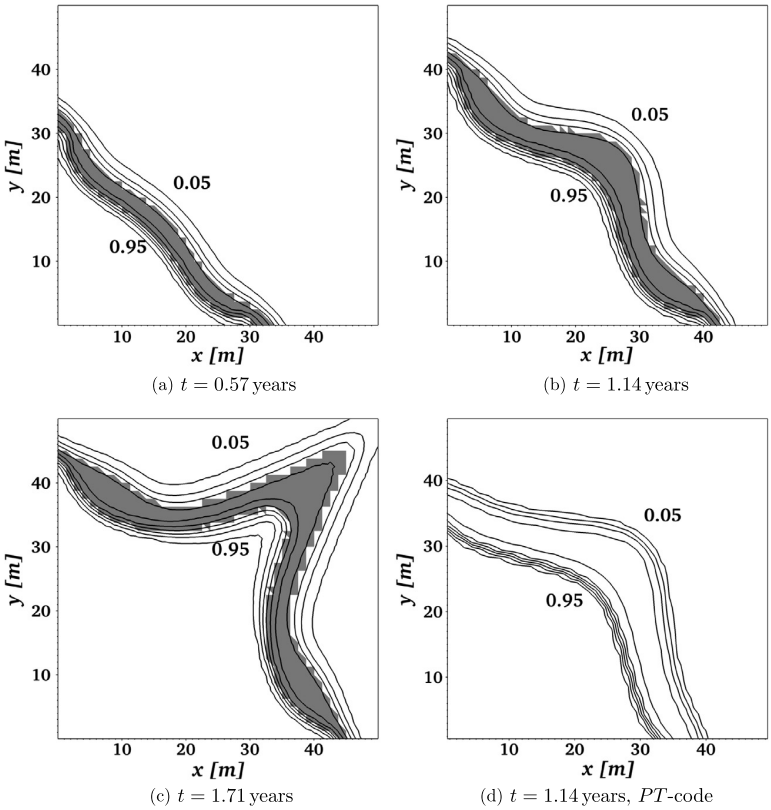

(a) $t = 0.57$ years (b) $t = 1.14$ years

(c) $t = 1.71$ years (d) $t = 1.14$ years, PT-code

Fig. 3. Isolines of methane overall molar fraction and the two-phase region (gray color) at different times. Contours are distributed uniformly between the two printed values. The solution is computed on the triangular grid $2 \times 40 \times 40$; (d) is computed on 40×40 rectangles using the PT-code (the two-phase region is not indicated here): Example 1.

Table 2
Experimental orders of convergence and errors of methane concentration c_1 at time $t = 0.48$ years for grids of m elements compared with the numerical solution on the grid of 8192 elements and the time step $\Delta t = 195.3125$ s. On coarser grids, $\Delta t \sim m^{-1}$.

m	$\|E_m\|_1$	EOC_1	$\|E_m\|_2$	EOC_2
8	7.3988×10^5		3.3186×10^4	
		0.4588		0.2532
32	5.3833×10^5		2.7844×10^4	
		0.6912		0.5809
128	3.3342×10^5		1.8615×10^4	
		0.4082		0.1114
512	2.5125×10^5		1.7232×10^4	
		0.6679		0.3603
2048	1.5814×10^5		1.3424×10^4	

where E_{m_1} and E_{m_2} are the numerical solution errors for the grids containing m_1 and m_2 elements, respectively. The EOC and L^1 and L^2 errors of methane concentrations and cell-averaged pressures for the situation at time $t = 0.48$ years are included in Table 2 and Table 3. EOC of concentrations in L^1 norm are approximately 0.5, which is expected for the first order upwind FVM on hyperbolic problems with discontinuous solutions [17]. A comparison of the solutions on the individual grids using methane overall molar fractions at this time is depicted in Fig. 4.

Example 2. In the next example, we simulate the methane injection into a vertical reservoir (i.e. with gravity) originally filled with propane. In Fig. 5 isolines of methane overall molar fraction $c_1/(\sum_{i=1}^{2} c_i)$ at different times are depicted. The value of molar fraction nearest to the injection corner is 0.95, and with each isoline towards the outflow corner the value decreases by 0.1. As in Example 1, the fluid is in the single phase in the whole reservoir except for the mixing zone where the mixture occurs also in two phases as indicated by gray color. The computation to $t = 1.14$ years lasted 13.2 hours. To validate our results, the problem was computed also by the PT-code. The obtained result at $t = 1.14$ years is depicted in Fig. 5(d) (indication of the two-phase region was unavailable in the PT-code). The result differs slightly from ours in Fig. 5(c). The zone between 0.95 and 0.05 isoline is narrower in Fig. 5(d), however, we observed an incorrect pressure in the

Table 3
Experimental orders of convergence and errors of pressure p_K at time $t = 0.48$ years for grids of m elements compared with the numerical solution on the grid of 8192 elements and the time step $\Delta t = 195.3125$ s. On coarser grids, $\Delta t \sim m^{-1}$.

m	$\|E_m\|_1$	EOC_1	$\|E_m\|_2$	EOC_2
8	3.0257×10^8	0.1283	6.0661×10^6	0.1301
32	2.7682×10^8	0.3544	5.5430×10^6	0.3550
128	2.1652×10^8	0.6859	4.3339×10^6	0.6866
512	1.3459×10^8	1.0166	2.6928×10^6	1.0166
2048	6.6528×10^7		1.3310×10^6	

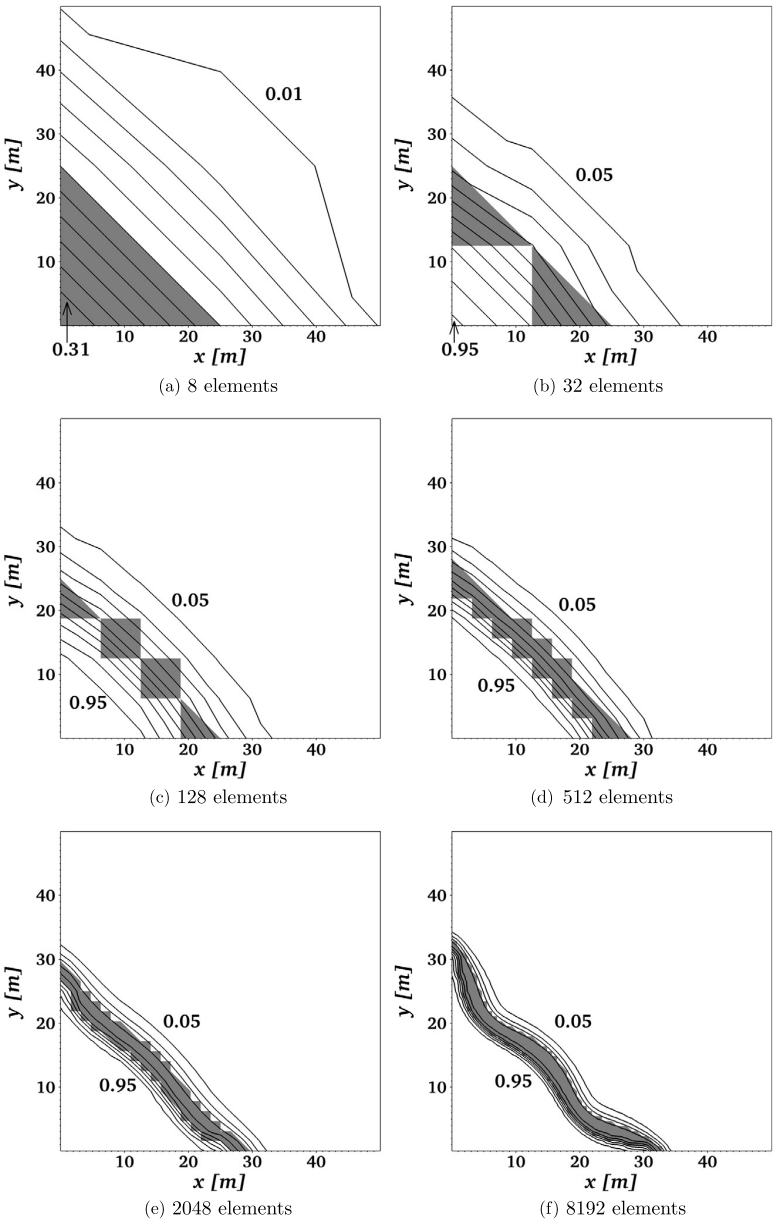

(a) 8 elements (b) 32 elements

(c) 128 elements (d) 512 elements

(e) 2048 elements (f) 8192 elements

Fig. 4. Isolines of methane overall molar fraction and the two-phase region (gray color) computed on different grids at time $t = 0.48$ years. Contours are distributed uniformly between the two printed values. Solutions are computed on the triangular grid: Example 1.

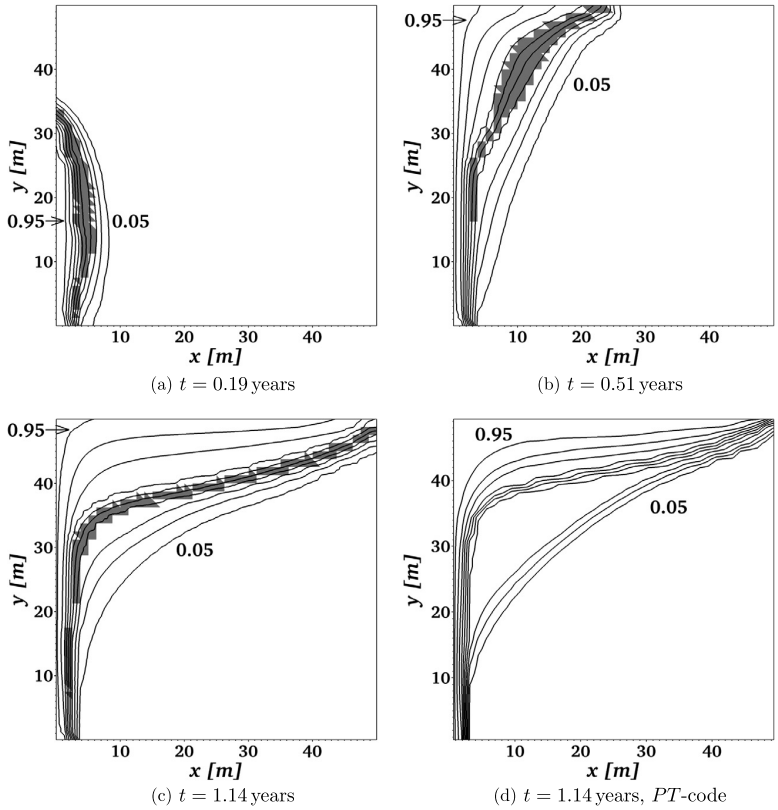

(a) $t = 0.19$ years (b) $t = 0.51$ years

(c) $t = 1.14$ years (d) $t = 1.14$ years, PT-code

Fig. 5. Isolines of methane overall molar fraction and the two-phase region (gray color) at different times. Contours are distributed uniformly between the two printed values. The solution is computed on the triangular grid $2 \times 40 \times 40$; (d) is computed on 40×40 rectangles using the PT-code (the two-phase region is not indicated here): Example 2.

Table 4
Relevant parameters of the Peng–Robinson equation of state (A.1) for Examples 3, 4, and 8. Volume translation is not used.

i (component)	p_{ci} [MPa]	T_{ci} [K]	V_{ci} [m^3 mol^{-1}]	M_i [g mol^{-1}]	ω_i [–]	δ_{i1} [–]	δ_{i2} [–]
1 (CO_2)	7.375	304.14	9.416×10^{-5}	44	0.239	0	0.15
2 (C_3)	4.248	369.83	2×10^{-4}	44.0962	0.153	0.15	0

outflowing element in the right upper corner of the domain in this result. Instead of a value close to 6.9 MPa (at the corner edges, there is prescribed exactly 6.9 MPa), which was observed in our result, there was 6.68 MPa in the result obtained by the PT-code. The lower pressure in the outflowing corner implies higher velocities, which can explain the difference in the molar fractions.

5.2. Injection of CO_2 into propane

Let us consider a cut through a propane reservoir at initial pressure $p = 2.5$ MPa and temperature $T = 311$ K. In the left bottom corner of the reservoir, CO_2 is injected, and in the right upper corner, the mixture of CO_2 and propane is produced (Fig. 2(b)). The injection rate of CO_2 is 42.5 m^2/day at pressure 1 atm and temperature 293 K. The parameters of the Peng–Robinson equation of state for both components of the mixture are summarized in Table 4. In these settings, the mixture can stay in the single phase or split into two phases. The boundary of the domain is impermeable except for the outflow corner where pressure $p = 2.5$ MPa is maintained. Relative permeability depends linearly on saturation as $k_{r\alpha}(S_\alpha) = S_\alpha$ for each phase α.

Example 3. In Fig. 6, a simulation of CO_2 injection into a horizontal reservoir originally filled with propane is shown. Isolines of CO_2 overall molar fraction $c_1/(\sum_{i=1}^{2} c_i)$ are distributed uniformly between the two displayed values of 0.95 and 0.05. The mixture stays in the single phase in the majority of the domain, only in the zone where the molar fractions are greater than

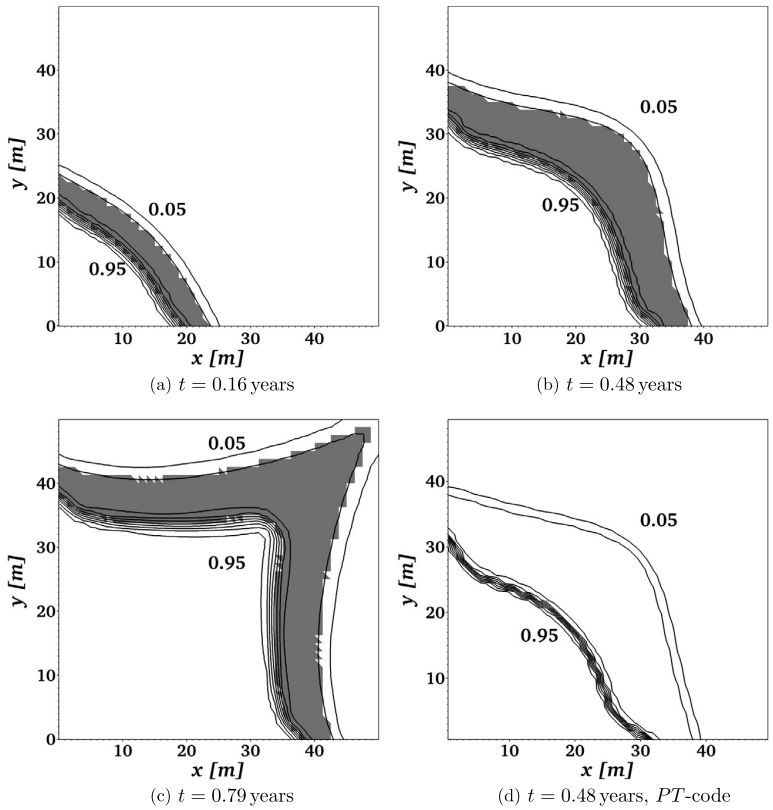

Fig. 6. Isolines of CO_2 overall molar fraction and the two-phase region (gray color) at different times. Contours are distributed uniformly between the two printed values. The solution is computed on the triangular grid $2 \times 40 \times 40$; (d) is computed on 40×40 rectangles using the PT-code (the two-phase region is not indicated here): Example 3.

0.05 and less than 0.95, the two-phase region (colored in gray) appears. The computation to $t = 0.79$ years lasted 6.4 hours. To validate our results, the problem was computed also by the PT-code. The zone between 0.95 and 0.05 isolines in the obtained result at $t = 0.48$ years depicted in Fig. 6(d) (indication of the two-phase region was unavailable in the PT-code) is slightly wider than the one in Fig. 6(b) computed by our code.

Example 4. In this example, we simulate the CO_2 injection into a vertical propane reservoir. Uniformly distributed contours of CO_2 overall molar fractions $c_1/(\sum_{i=1}^{2} c_i)$ between 0.95 and 0.05 are visualized in Fig. 7. The single-phase mixture occupies a major part of the domain during the simulation but in the mixing zone a two-phase domain (gray color) also develops. At time $t = 0.55$ years, we observed that there were the most two-phase elements of the whole simulation. Afterwards, the number of two-phase elements decreases. The computation to $t = 0.79$ years lasted 8.8 hours. To validate our results, the problem was computed also by the PT-code. The obtained result at $t = 0.48$ years is depicted in Fig. 7(d) (indication of the two-phase region was unavailable in the PT-code). The result differs from ours in Fig. 7(b), however, we observed an incorrect pressure in the outflowing element in the right upper corner of the domain in this result. Instead of a value close to 2.5 MPa (at the corner edges, there is prescribed exactly 2.5 MPa), which was observed in our result (2.51 MPa), there was 2.27 MPa in the other result. The lower pressure in the outflowing corner can cause different velocities, which explains the difference in the molar fractions. In the injection corner, the pressure was 2.53 MPa in the result obtained by the PT-code, while we observed 2.97 MPa in our result.

5.3. Injection of CO_2 into oil

In the third problem, let us consider a cut through an oil (8-component hydrocarbon mixture) reservoir at initial pressure $p = 27.6$ MPa and temperature $T = 403.15$ K. The initial overall molar fractions in the reservoir can be found in Table 5. CO_2 is injected in one corner of the reservoir, and the mixture of CO_2 and oil is produced in the opposite corner. The injection rate of CO_2 is 133.33 m^2/day at pressure 1 atm and temperature 293 K. The parameters of the Peng–Robinson equation of state for all components of the mixture are summarized in Table 6. In these settings, the mixture can stay in the single

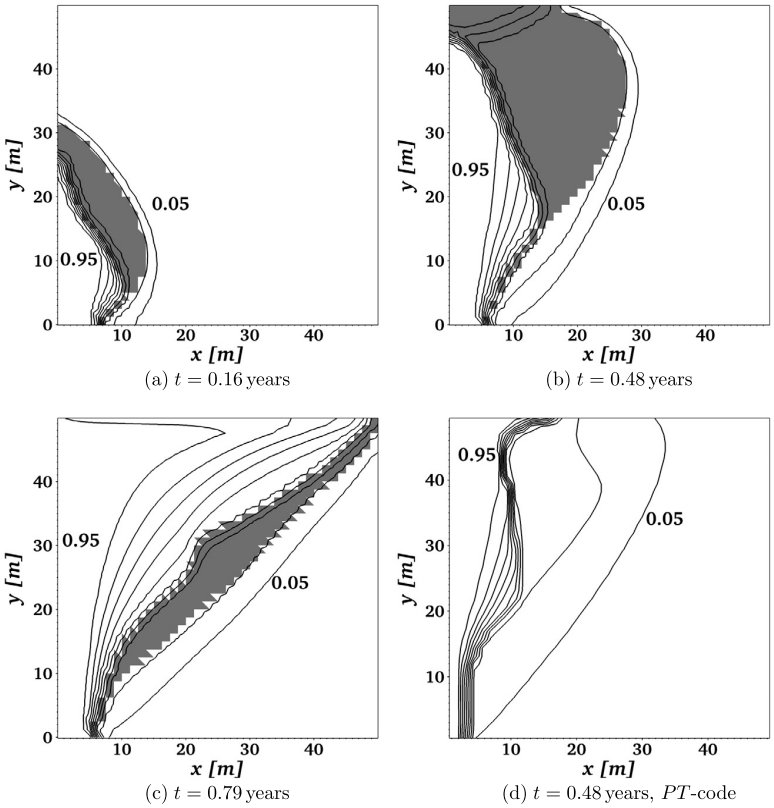

Fig. 7. Isolines of CO_2 overall molar fraction and the two-phase region (gray color) at different times. Contours are distributed uniformly between the two printed values. The solution is computed on the triangular grid $2 \times 40 \times 40$; (d) is computed on 40×40 rectangles using the PT-code (the two-phase region is not indicated here): Example 4.

Table 5
The initial overall molar fractions in the reservoir.

Component	CO_2	N_2	C_1	C_2–C_3	C_4–C_5	C_6–C_{10}	C_{11}–C_{24}	C_{25+}
Overall molar fraction	0.0086	0.0028	0.4451	0.1207	0.0505	0.1328	0.1660	0.0735

Table 6
Relevant parameters of the Peng–Robinson equation of state (A.1) for Examples 5, 6, and 7. Volume translation is not used.

i (component)	p_{ci} [MPa]	T_{ci} [K]	V_{ci} [$m^3\,mol^{-1}$]	M_i [$g\,mol^{-1}$]	ω_i [–]	δ_{i1} [–]	δ_{i2} [–]	δ_{i3} [–]	δ_{i4} [–]	δ_{i5} [–]	δ_{i6} [–]	δ_{i7} [–]	δ_{i8} [–]
1 (CO_2)	7.375	304.14	9.416×10^{-5}	44	0.239	0	0	0.15	0.15	0.15	0.15	0.15	0.08
2 (N_2)	3.39	126.21	8.988×10^{-5}	28	0.039	0	0	0.1	0.1	0.1	0.1	0.1	0.1
3 (C_1)	4.599	190.56	9.84×10^{-5}	16	0.011	0.15	0.1	0	0.0346	0.0392	0.0469	0.0635	0.1052
4 (C_2–C_3)	4.654	327.81	1.6571×10^{-4}	34.96	0.11783	0.15	0.1	0.0346	0	0	0	0	0
5 (C_4–C_5)	3.609	435.62	2.7522×10^{-4}	62.98	0.21032	0.15	0.1	0.0392	0	0	0	0	0
6 (C_6–C_{10})	2.504	574.42	4.6839×10^{-4}	110.21	0.41752	0.15	0.1	0.0469	0	0	0	0	0
7 (C_{11}–C_{24})	1.502	708.95	9.3876×10^{-4}	211.91	0.66317	0.15	0.1	0.0635	0	0	0	0	0
8 (C_{25+})	0.76	891.47	1.9298×10^{-3}	462.79	1.7276	0.08	0.1	0.1052	0	0	0	0	0

phase or split into two phases. The boundary of the domain is impermeable except for the outflow corner where pressure $p = 27.6$ MPa is maintained. Relative permeability depends quadratically on saturation as $k_{r\alpha}(S_\alpha) = S_\alpha^2$ for each phase α.

To validate our results, the following examples were computed also by the PT-code as in the previous simulations, but we have not included the results obtained by the PT-code for the sake of brevity.

Example 5. In Fig. 9, a simulation of CO_2 injection in the left bottom corner of a horizontal reservoir originally filled with oil is shown. In the right upper corner, the mixture is produced. The reservoir is outlined in Fig. 8(a). In each of the 6

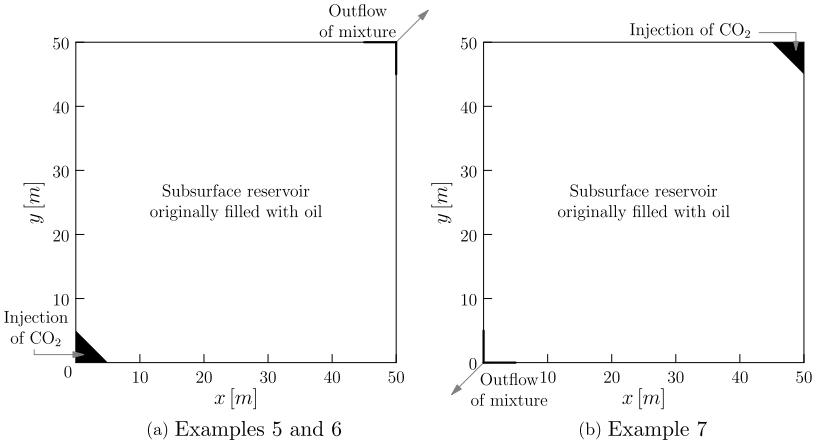

(a) Examples 5 and 6 (b) Example 7

Fig. 8. Outlines of the simulated reservoirs for Examples 5–7.

plots, isolines of the overall molar fraction $c_i/(\sum_{i=1}^{8} c_i)$ are visualized for 1 of the 8 components at time $t = 1.36$ years. Contours are distributed uniformly between the displayed values. In each figure the two-phase region is colored in gray color. In comparison with Examples 1–4, the two-phase region occupies a major part of the domain. The computation to $t = 1.36$ years lasted 57.8 hours.

Example 6. This example is similar to Example 5, but this time we simulate injection of CO_2 into a vertical oil reservoir. CO_2 is injected in the left bottom corner and the mixture is produced in the right upper corner (as outlined in Fig. 8(a)). Results of the simulation at time $t = 1.36$ years are shown in Fig. 10 using the isolines of the overall molar fractions $c_i/(\sum_{i=1}^{8} c_i)$ of 6 selected components, and the two-phase region is colored in gray. As in Example 5, also here, the two-phase region occupies a large part of the reservoir. The computation to $t = 1.36$ years lasted 96.7 hours.

Example 7. In this example, we compute the injection of CO_2 in the right upper corner of the vertical reservoir, whereas the mixture outflows in the left bottom corner (see Fig. 8(b)). Fig. 11 shows results of the simulation at time $t = 1.36$ years. Isolines of the overall molar fraction $c_i/(\sum_{i=1}^{8} c_i)$ are visualized for the same components as in Examples 5 and 6. Again, the gray-colored two-phase region is spread over a significant part of the reservoir. The computation to $t = 1.36$ years lasted 75.3 hours.

5.4. CO_2 close to the saturation pressure

Example 8. In the last example, we simulate an isothermal injection of CO_2 into a reservoir that is filled with pure gas CO_2 at temperature $T = 280$ K and $p = 4$ MPa. Note that the saturated vapor pressure of CO_2 at 280 K is 4.13 MPa. CO_2 is injected in the left bottom corner of the reservoir and produced in the right upper corner. The injection rate is 42.5 m^2/day at pressure 1 atm and temperature 293 K. The parameters of the Peng–Robinson equation of state for CO_2 are summarized in Table 4 (first line). The medium has a low permeability $\mathbf{K} = k = 9.87 \times 10^{-17}$ m^2 (i.e. 0.1 mD) and porosity $\phi = 0.2$. The boundary of the domain is impermeable except for the outflow corner where pressure $p = 4$ MPa is maintained. Relative permeability depends linearly on saturation as $k_{r\alpha}(S_\alpha) = S_\alpha$ for each phase α.

Due to the injection, the pressure in the vicinity of the injection point rises above the value of the saturation pressure and the liquid CO_2 phase should appear. Fig. 12 shows the result of our code at four different times. The computation to $t = 10.14$ years lasted 4.6 hours. The liquid CO_2 with density approximately 873 kg m^{-3} displaces the vapor with density approximately 118 kg m^{-3}. The two-phase elements (gray) correspond well with the dashed isoline of the saturation pressure (see Fig. 12). The PT-code (based on [13,14,24]) used for this simulation crashes due to the problem with the phase identification. This problem shows the advantages of the VT-based formulation which does not require the phase identification.

6. Summary and conclusions

We have developed a new formulation of the compositional model for the reservoir simulation. The new feature of the model is that it uses computation of phase equilibria at constant temperature and volume rather than pressure. Compared to the traditional PT-based formulation, the new formulation in terms of VT is not only more robust, but also provides a convenient and natural way for the pressure computation. In the new formulation, the equation of state does not have to be

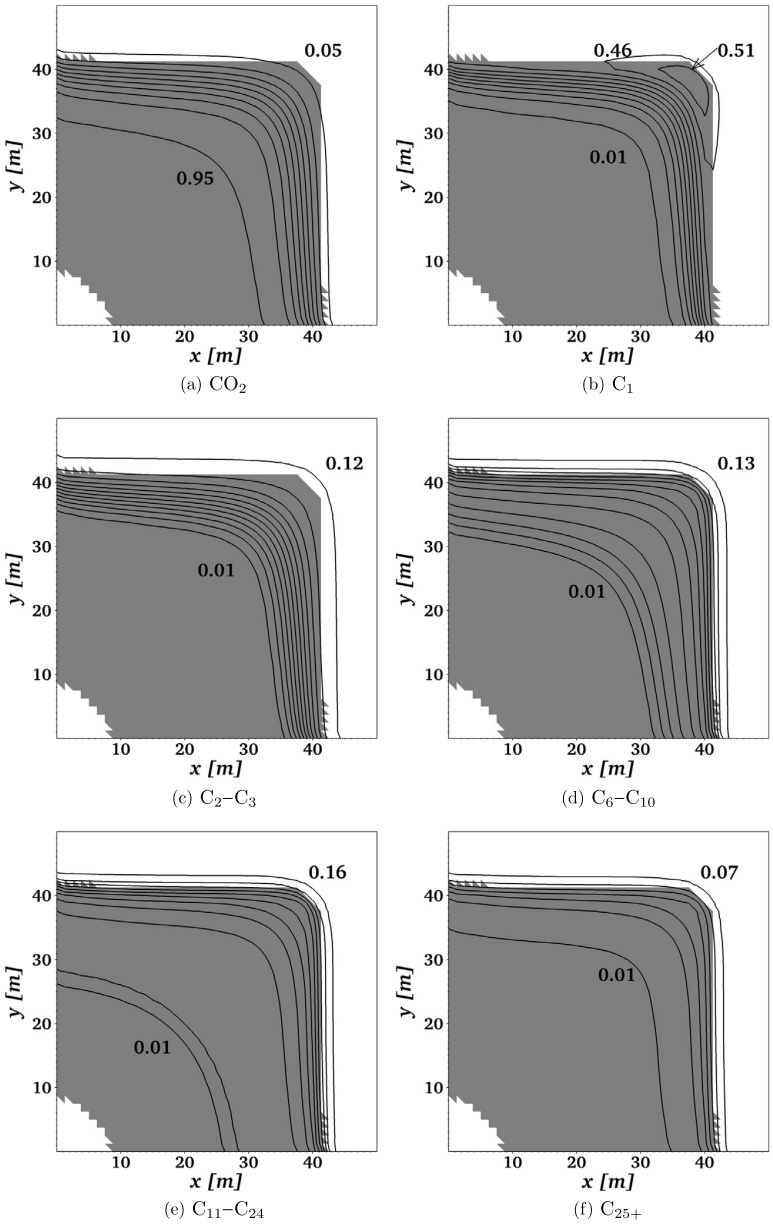

(a) CO_2 (b) C_1

(c) C_2–C_3 (d) C_6–C_{10}

(e) C_{11}–C_{24} (f) C_{25+}

Fig. 9. Isolines of the overall molar fractions and the two-phase region (gray color) at $t = 1.36$ years. Contours are distributed uniformly between the two printed values. The solution is computed on the triangular grid $2 \times 40 \times 40$: Example 5.

inverted, and thus the root selection problem does not appear. We have tested the model on eight examples involving binary and multicomponent mixtures described by the Peng–Robinson equation of state. We expect that the same approach can be used for other pressure-explicit equations of state as well. Moreover, we expect that the advantage of the fact that there is no need for inversion in the equation of state will appear to be beneficial for simulations using non-cubic equations of state. These equations of state can describe correctly association in the mixtures involving polar components (e.g. $CO_2 + H_2O$) and, thus, have important applications in problems related to carbon sequestration [18,16]. Extension of our approach to these equations of state is a subject of current research.

We have discretized the model using a combination of the MHFEM and FVM for the computation of two-phase compressible flow of a mixture in porous media in 2D. In comparison with the traditional approaches, our approximation of the component flux between elements does not depend on the phase identification and pairing of phases between elements.

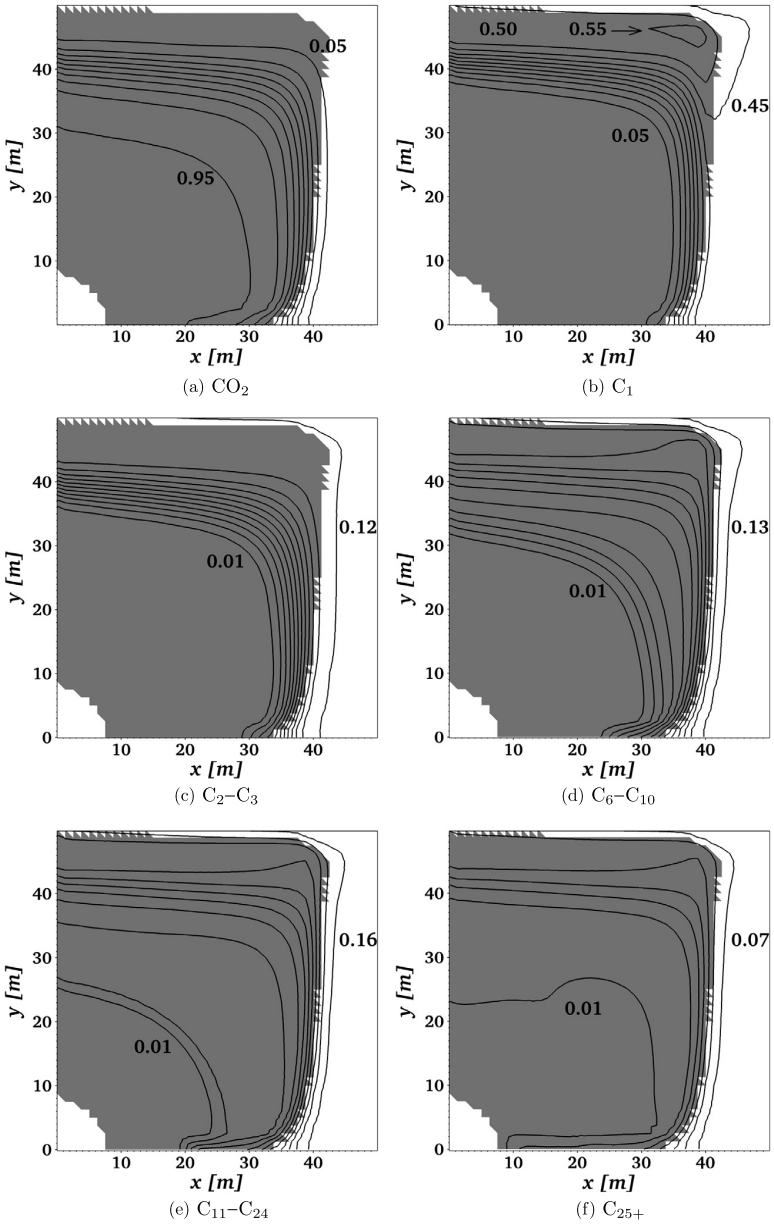

(a) CO_2 (b) C_1

(c) C_2–C_3 (d) C_6–C_{10}

(e) C_{11}–C_{24} (f) C_{25+}

Fig. 10. Isolines of the overall molar fractions and the two-phase region (gray color) at $t = 1.36$ years. Contours are distributed uniformly between the two printed values. The solution is computed on the triangular grid $2 \times 40 \times 40$: Example 6.

This feature of the model will be also advantageous in problems related to carbon sequestration as typically CO_2 is injected into the reservoir in the supercritical state.

Our method is fully coupled, fully implicit and is therefore much more expensive in comparison with the decoupled (sequential) IMPEC approaches. In this work, we focused on the robustness of the formulation rather than the CPU costs. We believe that the robustness of the VT-flash and flux evaluation which does not depend on the phase identification can be exploited also in the sequential schemes. Development of such schemes is another subject of our current research.

Many questions related to the new formulation remain open, e.g. how to include diffusion or capillarity in the VT-based model. For example, capillarity in the compositional simulation has traditionally been formulated using the extension of the concepts developed in the immiscible flow. Here, the VT-based formulation seems to be of great advantage with respect to PT, but currently available theories of capillarity rely heavily on the phase identification. We believe that the model

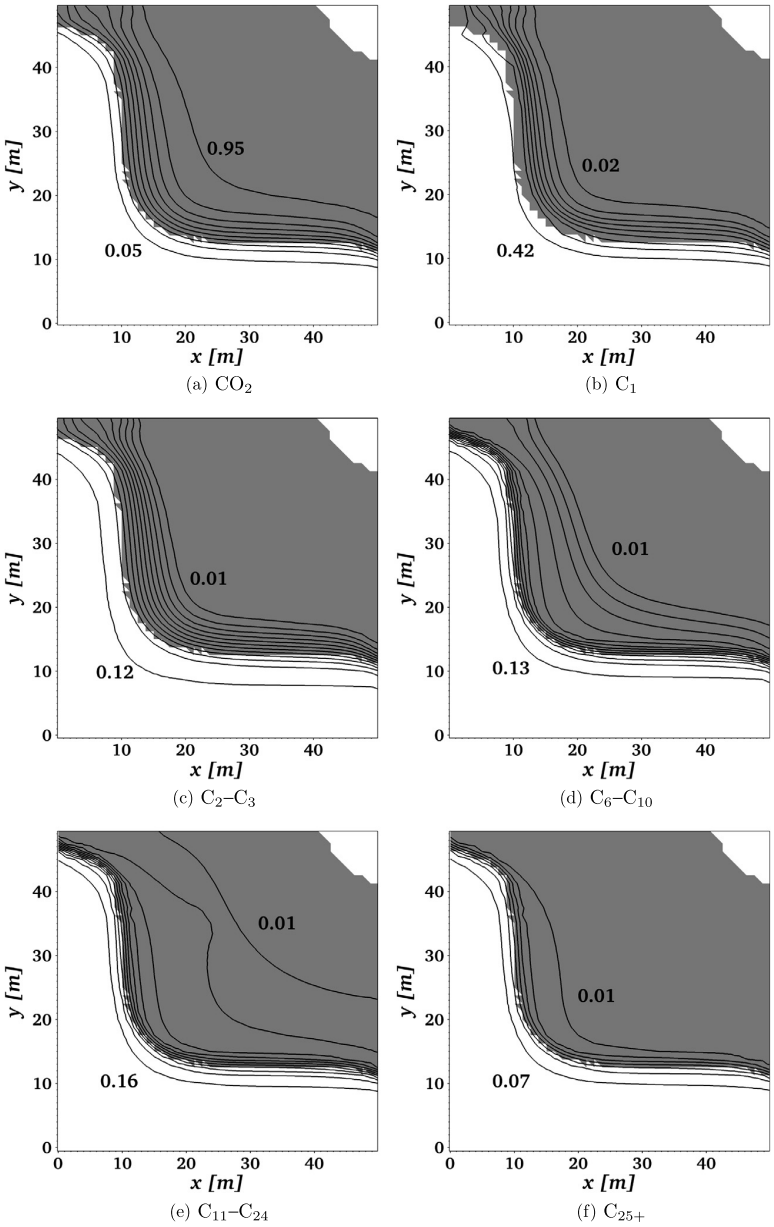

(a) CO_2 (b) C_1

(c) C_2–C_3 (d) C_6–C_{10}

(e) C_{11}–C_{24} (f) C_{25+}

Fig. 11. Isolines of the overall molar fractions and the two-phase region (gray color) at $t = 1.36$ years. Contours are distributed uniformly between the two printed values. The solution is computed on the triangular grid $2 \times 40 \times 40$: Example 7.

concept proposed in this paper can be extended to include capillarity and diffusion, although this may require a non-trivial revision of basic concepts and the way we usually describe these phenomena. Development of such extensions is subject of our future research.

Acknowledgements

This work has been supported by the project P105/11/1507 Development of Computational Models for Simulation of CO2 Sequestration of the Czech Science Foundation and by the project KONTAKT II LH 12064 Computational Methods in Thermodynamics of Hydrocarbon Mixtures of the Ministry of Education, Youth and Sport of the Czech Republic.

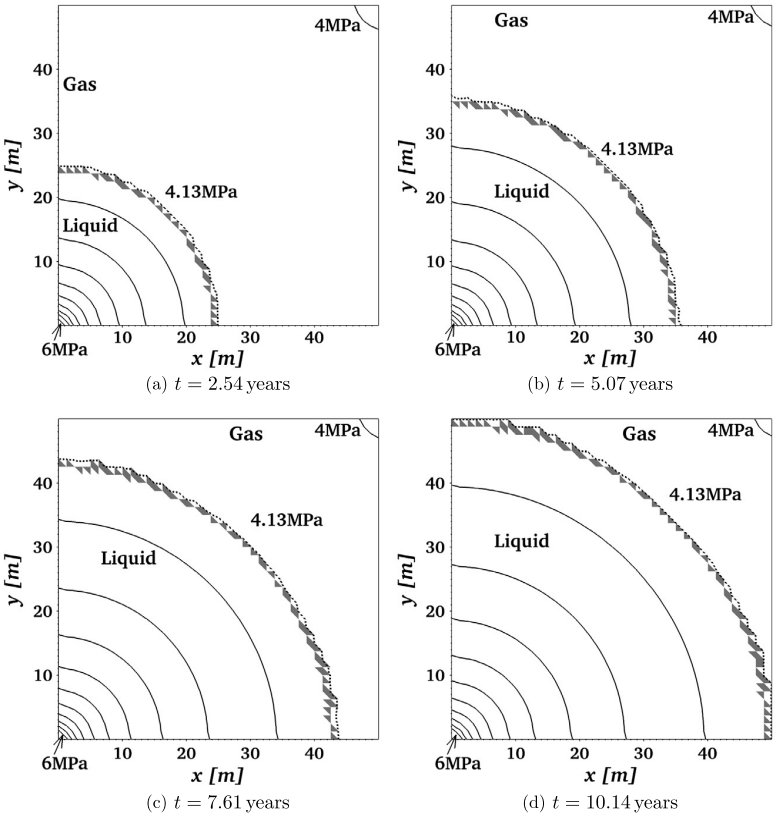

(a) $t = 2.54$ years (b) $t = 5.07$ years

(c) $t = 7.61$ years (d) $t = 10.14$ years

Fig. 12. Isolines of the cell-averaged pressure p_K and the two-phase elements (gray color) at different times. Solid contours are distributed uniformly between the two printed values. Dashed contours represent the saturation pressure and separates the liquid and gas zones. The solution is computed on the triangular grid $2 \times 40 \times 40$: Example 8.

Appendix A. Details of the constitutive relations

Pressure in (6b) is given by the Peng–Robinson equation of state [30,12,26,27] as

$$p(T, c_1, \ldots, c_{n_c}) = \frac{RT \sum_{i=1}^{n_c} c_i}{1 - \sum_{i=1}^{n_c} b_i c_i} - \frac{\sum_{i=1}^{n_c} \sum_{j=1}^{n_c} a_{ij} c_i c_j}{1 + 2 \sum_{i=1}^{n_c} b_i c_i - (\sum_{i=1}^{n_c} b_i c_i)^2}. \tag{A.1}$$

In Eq. (A.1), $R = 8.314472\ \mathrm{J\,K^{-1}\,mol^{-1}}$ is the universal gas constant and

$$\begin{aligned} a_{ij} &= (1 - \delta_{ij})\sqrt{a_i a_j}, \qquad a_i = 0.45724 \frac{R^2 {T_{ci}}^2}{p_{ci}} \left[1 + m_i (1 - \sqrt{T_{ri}})\right]^2, \\ m_i &= \begin{cases} 0.37464 + 1.54226\omega_i - 0.26992\omega_i^2 & \text{for } \omega_i < 0.5, \\ 0.3796 + 1.485\omega_i - 0.1644\omega_i^2 + 0.01667\omega_i^3 & \text{for } \omega_i \geq 0.5, \end{cases} \\ T_{ri} &= \frac{T}{T_{ci}}, \qquad b_i = 0.0778 \frac{RT_{ci}}{p_{ci}}, \end{aligned} \tag{A.2}$$

where δ_{ij} is the binary interaction coefficient [–]; T_{ci}, p_{ci}, ω_i, T_{ri} are the critical temperature [K], critical pressure [Pa], acentric factor [–], reduced temperature [–], respectively – all corresponding to the i-th component.

The condition of chemical equilibrium (6c) can be rewritten in terms of the volume function coefficients, which were introduced in [26] to replace fugacities in the VT-based formulations. The equivalent condition to (6c) reads as

$$\frac{c_{\alpha,i}}{\varphi_i(T, c_{\alpha,1}, \ldots, c_{\alpha,n_c})} = \frac{c_{\beta,i}}{\varphi_i(T, c_{\beta,1}, \ldots, c_{\beta,n_c})}, \quad \forall \alpha \neq \beta,\ \forall i = 1, \ldots, n_c, \tag{A.3}$$

where the volume function coefficient φ_i for the Peng–Robinson equation of state reads as

$$\begin{aligned}&\ln\varphi_i(T,c_1,\dots,c_{n_c})\\&=\ln\left(1-\sum_{j=1}^{n_c}b_jc_j\right)-\frac{b_i\sum_{j=1}^{n_c}c_j}{1-\sum_{j=1}^{n_c}b_jc_j}+\frac{b_i\sum_{j=1}^{n_c}\sum_{k=1}^{n_c}a_{jk}c_jc_k}{RT\sum_{j=1}^{n_c}b_jc_j(1+2\sum_{j=1}^{n_c}b_jc_j-(\sum_{j=1}^{n_c}b_jc_j)^2)}\\&\quad-\frac{1}{\sqrt{2}RT\sum_{j=1}^{n_c}b_jc_j}\left(\frac{b_i\sum_{j=1}^{n_c}\sum_{k=1}^{n_c}a_{jk}c_jc_k}{2\sum_{j=1}^{n_c}b_jc_j}-\sum_{j=1}^{n_c}a_{ij}c_j\right)\ln\left|\frac{1+(1+\sqrt{2})\sum_{j=1}^{n_c}b_jc_j}{1+(1-\sqrt{2})\sum_{j=1}^{n_c}b_jc_j}\right|.\end{aligned}\tag{A.4}$$

Details of the definition and basic properties of the volume functions and volume function coefficients as well as derivation of the last formula can be found in [26].

Appendix B. Raviart–Thomas basis functions and details of the MHFEM

In this part, we describe details of derivation of discrete Darcy's law (19) using the Raviart–Thomas space [3,4,31,24]. The Raviart–Thomas space of the lowest order $\mathrm{RT}_0(K)$, over an element K from a triangulation $\mathcal{T}_\Omega$ (consisting of triangles) of the domain Ω, is generated by the basis functions

$$\mathbf{w}_{K,E}(\mathbf{x})=\frac{1}{2|K|}(\mathbf{x}-\mathbf{N}_{K,E}),\quad \forall\mathbf{x}\in K,\ E\in\partial K,\tag{B.1}$$

where $\mathbf{N}_{K,E}\in K$ is a node against edge E. The basis functions (B.1) satisfy the following properties

$$\nabla\cdot\mathbf{w}_{K,E}(\mathbf{x})=\frac{1}{|K|},\qquad \mathbf{w}_{K,E}(\mathbf{x})\cdot\mathbf{n}_{K,E'}=\frac{\delta_{E,E'}}{|E|}.\tag{B.2}$$

Multiplying (12) with the basis function $\mathbf{w}_{K,E}$, and integrating over element K, we can write

$$\int_K\nabla p\cdot\mathbf{w}_{K,E'}=-\Big(\sum_{\alpha\in\Pi(K)}c_{\alpha,K}\lambda_{\alpha,K}\Big)^{-1}\sum_{E\in\partial K}q_{K,E}\int_K\mathbf{K}^{-1}\mathbf{w}_{K,E}\cdot\mathbf{w}_{K,E'}+\widetilde{Q}_K\int_K\mathbf{g}\cdot\mathbf{w}_{K,E'},\tag{B.3}$$

where we have used (18), the mean value theorem, and $\Pi(K)$ denotes all phases on element K. On the other hand, using the Green theorem, the mean value theorem, and properties (B.2), we obtain

$$\int_K\nabla p\cdot\mathbf{w}_{K,E'}=\sum_{E\in\partial K}\int_E p\mathbf{w}_{K,E'}\cdot\mathbf{n}_{K,E}-\int_K p\nabla\cdot\mathbf{w}_{K,E'}=\frac{1}{|E'|}\int_{E'}p-\frac{1}{|K|}\int_K p.\tag{B.4}$$

Denoting

$$\begin{aligned}&A_{K,E,E'}=\int_K\mathbf{K}^{-1}\mathbf{w}_{K,E}\cdot\mathbf{w}_{K,E'},\qquad G_{K,E'}=\int_K\mathbf{g}\cdot\mathbf{w}_{K,E'},\\&\widehat{p}_{K,E'}=\frac{1}{|E'|}\int_{E'}p,\qquad p_K=\frac{1}{|K|}\int_K p,\end{aligned}\tag{B.5}$$

we combine (B.3) and (B.4) into

$$\Big(\sum_{\alpha\in\Pi(K)}c_{\alpha,K}\lambda_{\alpha,K}\Big)^{-1}\sum_{E\in\partial K}q_{K,E}A_{K,E,E'}=p_K-\widehat{p}_{K,E'}+\widetilde{Q}_KG_{K,E'}.\tag{B.6}$$

Assuming that $\mathbf{K}$ is a uniformly positive-definite tensor (see [20]), i.e.

$$\exists\alpha_0>0:\quad \alpha_0\sum_{i=1}^d\xi_i^2\leqslant\sum_{i,j=1}^d\big[\mathbf{K}(\mathbf{x})\big]_{i,j}\xi_i\xi_j,\quad\forall\boldsymbol{\xi}\in\mathbb{R}^d,\tag{B.7}$$

for almost all $\mathbf{x}\in\Omega$, it is possible to invert the matrix $\mathbf{A}_K=(A_{K,E,E'})_{E,E'\in\partial K}$. Multiplying (B.6) in a vector form by $\mathbf{A}_K^{-1}$, we obtain for $K\in\mathcal{T}_\Omega$ and $E\in\partial K$

$$q_{K,E} = \sum_{\alpha \in \Pi(K)} c_{\alpha,K} \lambda_{\alpha,K} \left(\alpha_E^K p_K - \sum_{E' \in \partial K} \beta_{E,E'}^K \widehat{p}_{K,E'} + \gamma_E^K \widetilde{\varrho}_K \right), \tag{B.8}$$

which is Darcy's law (19) with coefficients α_E^K, $\beta_{E,E'}^K$, and γ_E^K given by

$$\alpha_E^K = \sum_{E' \in \partial K} A^{-1}_{K,E,E'}, \qquad \beta_{E,E'}^K = A^{-1}_{K,E,E'}, \qquad \gamma_E^K = \sum_{E' \in \partial K} A^{-1}_{K,E,E'} G_{K,E'}, \tag{B.9}$$

where $A^{-1}_{K,E,E'}$ is the element of the inverse matrix $\mathbf{A}_K^{-1}$.

References

[1] G. Ács, S. Doleschall, É. Farkas, General purpose compositional model, SPE J. 25 (4) (1985) 543–553 (SPE-10515-PA).
[2] A. Bourgeat, M. Jurak, F. Smaï, On persistent primary variables for numerical modeling of gas migration in a nuclear waste repository, Comput. Geosci. 17 (2) (2013) 287–305.
[3] F. Brezzi, M. Fortin, Mixed and Hybrid Finite Element Methods, Springer-Verlag, New York Inc., 1991.
[4] G. Chavent, J.E. Roberts, A unified physical presentation of mixed, mixed-hybrid finite elements and standard finite difference approximations for the determination of velocities in waterflow problems, Adv. Water Resour. 14 (6) (1991) 329–348.
[5] Z. Chen, G. Huan, Y. Ma, Computational Methods for Multiphase Flows in Porous Media, SIAM, Philadelphia, 2006.
[6] H. Class, R. Helmig, P. Bastian, Numerical simulation of non-isothermal multiphase multicomponent processes in porous media. 1. An efficient solution technique, Adv. Water Resour. 25 (5) (2002) 533–550.
[7] T.A. Davis, A column pre-ordering strategy for the unsymmetric-pattern multifrontal method, ACM Trans. Math. Softw. 30 (2) (2004) 165–195.
[8] T.A. Davis, Algorithm 832: UMFPACK, an unsymmetric-pattern multifrontal method, ACM Trans. Math. Softw. 30 (2) (2004) 196–199.
[9] T.A. Davis, I.S. Duff, A combined unifrontal/multifrontal method for unsymmetric sparse matrices, ACM Trans. Math. Softw. 25 (1) (1999) 1–19.
[10] T.A. Davis, I.S. Duff, An unsymmetric-pattern multifrontal method for sparse LU factorization, SIAM J. Matrix Anal. Appl. 18 (1) (1997) 140–158.
[11] M. Delshad, S.G. Thomas, M.F. Wheeler, Parallel numerical reservoir simulations of nonisothermal compositional flow and chemistry, SPE J. 16 (2) (2011) 239–248.
[12] A. Firoozabadi, Thermodynamics of Hydrocarbon Reservoirs, McGraw–Hill, NY, 1998.
[13] H. Hoteit, A. Firoozabadi, Multicomponent fluid flow by discontinuous Galerkin and mixed methods in unfractured and fractured media, Water Resour. Res. 41 (2005), http://dx.doi.org/10.1029/2005WR004339, W11412.
[14] H. Hoteit, A. Firoozabadi, Compositional modeling by the combined discontinuous Galerkin and mixed methods, SPE J. (March 2006) 19–34.
[15] T. Jindrová, Computational methods in thermodynamics of multicomponent mixtures, Master thesis, Department of Mathematics, Faculty of Nuclear Sciences and Physical Engineering, Czech Technical University in Prague, 2013.
[16] T. Jindrová, J. Mikyška, Fast and robust algorithm for calculation of two-phase equilibria at given volume, temperature, and moles, Fluid Phase Equilib. 353 (2013) 101–114.
[17] R.J. Leveque, Finite Volume Methods for Hyperbolic Problems, Cambridge University Press, Cambridge, 2002.
[18] Z. Li, A. Firoozabadi, Cubic-plus-association equation of state for water-containing mixtures: is "cross association" Necessary? AIChE J. 56 (7) (2009) 1803–1813.
[19] J. Lohrenz, B.G. Bray, C.R. Clark, Calculating viscosities of reservoir fluids from their compositions, J. Pet. Technol. (Oct. 1964) 1171–1176.
[20] J. Maryška, M. Rozložník, M. Tůma, Mixed-hybrid finite element approximation of the potential fluid flow problem, J. Comput. Appl. Math. 63 (1995) 383–392.
[21] M.L. Michelsen, The isothermal flash problem. 1. Stability, Fluid Phase Equilib. 9 (1) (1982) 1–19.
[22] M.L. Michelsen, The isothermal flash problem. 2. Phase split calculation, Fluid Phase Equilib. 9 (1) (1982) 21–40.
[23] M.L. Michelsen, J.M. Mollerup, Thermodynamic Models: Fundamentals and Computational Aspects, Tie-Line Publications, 2004.
[24] J. Mikyška, A. Firoozabadi, Implementation of higher-order methods for robust and efficient compositional simulation, J. Comput. Phys. 229 (2010) 2898–2913.
[25] J. Mikyška, A. Firoozabadi, Application of high-resolution methods in compositional simulations, Proc. Comput. Sci. 4 (2011) 928–937.
[26] J. Mikyška, A. Firoozabadi, A new thermodynamic function for phase-splitting at constant temperature, moles, and volume, AIChE J. 57 (7) (2011) 1897–1904.
[27] J. Mikyška, A. Firoozabadi, Investigation of mixture stability at given volume, temperature, and number of moles, Fluid Phase Equilib. 321 (2012) 1–9.
[28] J. Moortgat, S. Sun, A. Firoozabadi, Compositional modeling of three-phase flow with gravity using higher-order finite element methods, Water Resour. Res. 47 (2011), http://dx.doi.org/10.1029/2010WR009801, W05511.
[29] R. Neumann, P. Bastian, O. Ippisch, Modeling and simulation of two-phase two-component flow with disappearing nonwetting phase, Comput. Geosci. 17 (2013) 139–149.
[30] D.Y. Peng, D.B. Robinson, A new two-constant equation of state, Ind. Eng. Chem. Fundam. 15 (1976) 59–64.
[31] O. Polívka, J. Mikyška, Numerical simulation of multicomponent compressible flow in porous medium, J. Math. Ind. 3 (2011) 53–60, JMI2011C-7.
[32] O. Polívka, J. Mikyška, Combined mixed-hybrid finite element-finite volume scheme for computation of multicomponent compressible flow in porous media, in: Numerical Mathematics and Advanced Applications 2011, Proceedings of ENUMATH 2011, Springer-Verlag, Berlin, Heidelberg, 2013, pp. 559–567.
[33] A. Quarteroni, R. Sacco, F. Saleri, Numerical Mathematics, Springer-Verlag, New York, 2000.
[34] S. Sun, A. Firoozabadi, J. Kou, Numerical modeling of two-phase binary fluid mixing using mixed finite elements, Comput. Geosci. 16 (4) (2012) 1101–1124.
[35] L.C. Young, R.E. Stephenson, A generalized compositional approach for reservoir simulation, SPE J. 23 (5) (1983) 727–742.

Literatura

[1] Ackerer, P., Younes, A. (2007), Efficient approximations for the simulation of density driven flow in porous media, *Advances in Water Resources*, 31:15–27.

[2] Ács, G., Doleschall, S., Farkas, É. (1985), General Purpose Compositional Model, *SPE Journal*, 25(4): 543–553. SPE-10515-PA.

[3] Azis, K., Settari, A. (1979), *Petroleum Reservoir Simulation*, Applied Science Publishers Ltd., London.

[4] Baker, L. E., Kraemer, D. L. (1980), Critical points and saturation pressure calculations for multicomponent systems, *SPE Journal*, February: 15–24.

[5] Bear, J., Verruijt, A. (1987), *Modeling Groundwater Flow and Pollution*, D. Reidel Publishing Company, Dordrecht, Holland.

[6] Bourgeat, A., Jurak, M., Smaï, F. (2013), On persistent primary variables for numerical modeling of gas migration in a nuclear waste repository. *Computational Geosciences*, 17(2): 287–305.

[7] Brdička, R., Dvořák, J. (1977), *Základy fysikální chemie*, Academia, Praha.

[8] Brezzi, F., Fortin, M. (1991), *Mixed and Hybrid Finite Element Methods*, Springer, New York.

[9] Cabral, V.F., Castier, M., Tavares, F.W. (2005), Thermodynamic equilibrium in systems with multiple adsorbed and bulk phases, *Chemical Engineering Science*, 60(6), 1773–1782.

[10] Castier, M., Tavares, F.W. (2005), Centrifugation equilibrium of natural gas, *Chemical Engineering Science*, 60(11), 2927–2935.

[11] Castier, M. (2009), Solution of the isochoric-isoenergetic flash problem by direct entropy maximization, *Fluid Phase Equilibria*, 276:7–17.

[12] Chavent, G., Jaffré, J. (1986), *Mathematical Models and Finite Elements for Reservoir Simulation*, North-Holland, Amsterdam.

[13] Chavent, G., Roberts, J.E. (1991), A unified physical presentation of mixed, mixed-hybrid finite elements and standard finite difference approximations for the determination of velocities in waterflow problems, *Advances in Water Resources*, 14(6): 329–348.

[14] Chen, Z., Cockburn, B., Jerome, J., W., and Shu, C.-W. (1995), Mixed-RKDG Finite Element Methods for the 2-D Hydrodynamic Model for Semiconductor Device Simulation, *VLSI Design*, 3(2):145–158.

[15] Chen, Z., Ewing, R. E. (1997), *From Single-Phase To Compositional Flow: Applicability Of Mixed Finite Elements*, in Transport in Porous Media, 225–242.

[16] Chen, Z., Ma Y., Huan, G. (2006), *Computational Methods for Multiphase Flows in Porous Media*, SIAM, Philadelphia.

[17] Class, H., Helmig, R., Bastian, P. (2002), Numerical simulation of non-isothermal multiphase multicomponent processes in porous media.: 1. An efficient solution technique, *Advance in Water Resources*, 25(5), 533–550.

[18] Coats, K. H. (1980), An equation of state compositional model, *SPE Journal*, October:363–376.

[19] Coats, K. H. (1982), Reservoir Simulation: State of the Art, *Journal of Petroleum Technology*, August:1633–1642.

[20] Coats, K. H., Thomas, L.K., Pierson, R. G. (1998), Compositional and Black Oil Reservoir Simulation, *SPE Reservoir Evaluation & Engineering*, August: 372–379.

[21] Cockburn, B., Shu, C.-W. (2001), Runge-Kutta Discontinuous Galerkin Methods for Convection Dominated Problems, *Journal of Scientific Computing*, 16(3):173–261.

[22] Darcy, H. (1856), *Les Fontaines Publiques de la Ville de Dijon*, Victor Dalmond, Paris.

[23] Davis, T. A. (2004), A column pre-ordering strategy for the unsymmetric-pattern multifrontal method, *ACM Transactions on Mathematical Software*, 30(2), 165–195.

[24] Davis, T. A. (2004), Algorithm 832: UMFPACK, an unsymmetric-pattern multifrontal method, *ACM Transactions on Mathematical Software*, 30(2), 196–199.

[25] Davis, T. A., Duff, I. S. (1999), A combined unifrontal/multifrontal method for unsymmetric sparse matrices, *ACM Transactions on Mathematical Software*, 25(1), 1–19.

[26] Davis, T. A., Duff, I. S. (1997), An unsymmetric pattern multifrontal method for sparse LU factorization, *SIAM Journal on Matrix Analysis and Applications*, 18(1), 140–158.

[27] Delshad, M., Thomas, S.G., Wheeler, M.F. (2011), Parallel numerical reservoir simulations of nonisothermal compositional flow and chemistry, *SPE Journal*, 16(2), 239–248.

[28] Espósito, R.O., Castier, M., Tavares, F.W., (2000), Calculations of thermodynamic equilibrium in systems subject to gravitational fields, *Chemical Engineering Science*, 55(17), 3495–3504.

[29] Feistauer, M., Felcman, J., Straškraba, I. (2003), *Mathematical and Computational Methods for Compressible Flow*, Clarendon Press, Oxford.

[30] Firoozabadi, A. (1999), *Thermodynamics of Hydrocarbon Reservoirs*, McGraw-Hill, New York.

[31] Gill, P.E., Murray, W., Wright, M.H. (1997), *Practical Optimization*, Academic Press.

[32] Hansen, E. (1992), *Global Optimization using Interval Analysis*, Marcel-Dekker, New York.

[33] Haugen K., Firoozabadi A. (2009), Composition at the interface between multicomponent non-equilibrium phases, *Journal of Chemical Physics*, 130:064707,1–9.

[34] Haugen K., Firoozabadi A. (2009), Mixing of two nonequilibrium phases in one dimension, *AIChE Journal*, 55:1930–1936.

[35] Heidemann, R. A. (1975), The criteria for thermodynamic stability, *AIChE Journal*, 21(4): 824–826.

[36] Heidemann, R. A., Khalil, A. M. (1980), The calculation of critical points, *AIChE Journal*, 5:769–779.

[37] Heidemann, R. A. (1983), Computation of high pressure phase equilibria, *Fluid Phase Equilibria*, 14: 55–78.

[38] Holzbecher, E. O. (1988), *Modeling Density-Driven Flow in Porous Media: Principles, Numerics, Software*, Springer-Verlag, Berlin.

[39] Hoteit, H., Ackerer, P., Mosé, R., Erhel, J., Phillipe, B. (2004), New two-dimensional slope limiters for discontinuous Galerkin methods on arbitrary meshes, *International Journal for Numerical Methods in Engineering*, 61:2566–2593.

[40] Hoteit, H., Firoozabadi, A. (2005), Multicomponent fluid flow by discontinuous Galerkin and mixed methods in unfractured and fractured media, *Water Resources Research*, 41 W11412, doi:10.1029/2005WR004339.

[41] Hoteit, H., Firoozabadi, A. (2006), Compositional Modeling by the Combined Discontinuous Galerkin and Mixed Methods, *SPE Journal*, March 2006.

[42] Hoteit, H., Firoozabadi, A. (2006), Compositional Modeling of Discrete-Fractured Media Without Transfer Fuctions by the Discontinuous Galerkin and Mixed Methods, *SPE Journal*, September:341–352.

[43] Hoteit, H., Firoozabadi, A. (2006), Simple Phase Stability-Testing Algorithm in the Reduction Method, *AIChE Journal*, 52(8):2909–2920.

[44] Hoteit, H., Firoozabadi, A. (2009), Numerical Modeling of Diffusion in Fractured Media for Gas-Injection and -Recycling Schemes, *SPE Journal*, June:323-337.

[45] Hua, J. Z., Brennecke, J. F., Stadtherr, M. A. (1996), Reliable Computation of Phase Stability Using Interval Analysis: Cubic Equation of State Models, *Comput. Chem. Eng.*, 22, 1207-1214.

[46] Hua, J. Z., Brennecke, J., Stadtherr, M. A. (1998), Enhanced interval analysis for phase stability: Cubic equation of state models, *Ind. Eng. Chem. Res.* 37:1519–1527.

[47] Huyakorn, P. S., Pinder, G. F. (1983), *Computational Methods in Subsurface Flow*, Academic Press, Inc., New York.

[48] Jindrová, T. (2013), *Computational Methods in Thermodynamics of Multicomponent Mixtures*. Master thesis at the Department of Mathematics, Faculty of Nuclear Sciences and Physical Engineering, Czech Technical University in Prague.

[49] Jindrová, T., Mikyška, J. (2014), General Algorithm for Multiphase Equilibria Calculation at Given Volume, Temperature, and Moles, submitted.

[50] Kearfott, R. B. (1989), *Interval arithmetic methods for non-linear systems and non-linear optimization: An outline and status*, in: Sharda, R., Golden, B. L., Wasil, E., Balci, O., Stewart, W. (Eds.): Impact of Recent Computer Advances on Operations Research, Elsevier:533–542.

[51] Kearfott, R. B. (1990), Interval arithmetic techniques in the computational solution of nonlinear systems of equations: Introduction, examples, and comparisons, *Lectures in Applied Mathematics*, 26: 337–357.

[52] Kearfott, R. B. (1996), *Rigorous Global Search: Continuous Problem*, Kluwer Academic Publishers, Dordrecht, The Netherlands.

[53] van Leer, B. (1973), Towards the ultimate conservative difference scheme I. The quest of monotonicity, *Springer Lecture Notes Phys.*, 18, 163–168.

[54] van Leer, B. (1974), Towards the ultimate conservative difference scheme II. Monotonicity and conservation combined in a second order scheme, *J. Comput. Phys.*, 14, 361–370.

[55] van Leer, B. (1977a), Towards the ultimate conservative difference scheme III. Upstream-centered finite-difference schemes for ideal compressible flow, *J. Comput. Phys.*, 23, 263–275.

[56] van Leer, B. (1977b), Towards the ultimate conservative difference scheme IV. A new approch to numerical convection, *J. Comput. Phys.*, 23, 276–299.

[57] van Leer, B. (1979), Towards the ultimate conservative difference scheme V. A second order sequel to Godunov's method, *J. Comput. Phys.*, 32, 101–136.

[58] Leveque, R., J. (2002), *Finite Volume Methods for Hyperbolic Problems*, Cambridge Texts in Applied Mathematics, Cambridge University Press.

[59] Li, Z., and Firoozabadi, A. (2009), Cubic-plus-association (CPA) Equation of State for Water-containing Mixtures: Is 'Cross association' Necessary? *AIChE Journal*, 55:7, 1803–1813.

[60] Lohrenz, J., Bray, B., Clark R. (1964), Calculating viscosities of reservoir fluids from their compositions, *Journal of Petroleum Technology*, 16, 1171–1176.

[61] Maryška, J., Rozložník, M., Tůma, M. (1995), Mixed-hybrid finite element approximation of the potential fluid flow problem, *Journal of Computational and Applied Mathematics*, 63: 383–392.

[62] Michelsen, M.-L. (1982), The Isothermal Flash Problem. 1. Stability, *Fluid Phase Equilibria*, 9(1), 1–19.

[63] Michelsen, M.-L. (1982), The Isothermal Flash Problem. 2. Phase Split Calculation, *Fluid Phase Equilibria*, 9(1), 21–40.

[64] Michelsen M.-L. (1999), State function based flash specifications, *Fluid Phase Equilibria*, 158:617–626.

[65] Michelsen, M.-L., Mollerup, J.-M. (2004), *Thermodynamic Models: Fundamentals and Computational Aspects*, Tie-Line Publications.

[66] Mikyška, J., Firoozabadi, A. (2011), Application of high-resolution methods in compositional simulations, *Procedia Computer Science* 4, 928–937.

[67] Monteagudo, J., E., P., and Firoozabadi, A. (2007), Control-Volume Model for Simulation of Water Injection in Fractured Media: Incorporating Matrix Heterogeneity and Reservoir Wettability Effects, *SPE Journal*, September 2007.

[68] Monteagudo, J. E. P., Firoozabadi, A. (2007), Comparison of fully implicit and IMPES formulations for simulation of water injection in fractured and unfractured media, *International Journal for Numerical Methods in Engineering*, 69:698–728.

[69] Moore, R. E. (1966), *Interval Analysis*, Prentice-Hall, Englewood Cliffs, New Jersey.

[70] Moore, R. E., Kearfott, R. B., Cloud, M. J. (2009), *Introduction to Interval Analysis*, SIAM, Philadelphia.

[71] Moortgat, J., Sun, S., Firoozabadi, A. (2011), Compositional modeling of three-phase flow with gravity using higher-order finite element methods, *Water Resources Research*, 47, http://dx.doi.org/10.1029/2010WR009801, W05511.

[72] Nagarajan, N. R., Cullick, A. S., Griewank, A. (1991), New strategy for phase equilibrium and critical point calculations by thermodynamic energy analysis. Part I. Stability analysis and flash, *Fluid Phase Equilibria* 62:191–211.

[73] Nagarajan, N. R., Cullick, A. S., Griewank, A. (1991), New strategy for phase equilibrium and critical point calculations by thermodynamic energy analysis. Part II. Critical point calculations, *Fluid Phase Equilibria* 62:211–223.

[74] Nasrabadi, H., Hoteit, H., Firoozabadi, A. (2006), An analysis of species separation in a thermogravitational column filled with a porous medium, *Transport in Porous Media*, 67:473–486.

[75] Neaumaier, A. (1990), *Interval methods for systems of equations*, Cambridge University Press, Cambridge.

[76] Neumann, R., Bastian, P., Ippisch, O. (2013), Modeling and simulation of two-phase two-component flow with disappearing nonwetting phase, *Computational Geosciences*, 17:139–149.

[77] Novák, J. P., Růžička, V., jr., Malijevský, A., Matouš, J., Linek, J. (1985), The DAN method for calculation of vapour-liquid equilibria using an equation of state; flash calculation, *Collection of Czechoslovak Chemical Communications*, 50:23-32.

[78] Pappa, G. D., Perakis, C., Tsimpanogiannis, I. N., Voutsas, E. C. (2009), Thermodynamic modeling of the vapor-liquid equilibrium of the CO_2-H_2O mixture, *Fluid Phase Equilibria*, 284:56–63.

[79] Pasad, G. V., Venkatarathnam, G. (1999), A method for avoiding trivial roots in isothermal flash calculations using cubic equations of state, *Industrial & Engineering Chemistry Research* 38(9):3530–3534.

[80] Peaceman, D. W. (1977), *Fundamentals of Numerical Reservoir Simulation*, Elsevier, New York.

[81] Peng, D.-Y.; Robinson, D., B. (1976), A New Two-Constant Equation of State, *Ind. Eng. Chem., Fundam.*, 15(1): 59–64.

[82] Perakis, C., Voutsas, E., Magoulas, K., Tassios, D. (2006), Thermodynamic modeling of the vapor-liquid equilibrium of the water/ethanol/CO_2 system, *Fluid Phase Equilibria*, 243:142–150.

[83] Poling, B. E., Grens II E. A., Prausnitz J. M. (1981), Thermodynamic Properties from a Cubic Equation of State: Avoiding Trivial Roots and Spurious Derivatives, *Ind. Eng. Chem. Proc. Des. Dev.*, 20(1):127–130.

[84] Polívka, O., Mikyška, J. (2013), Combined mixed-hybrid finite element-finite volume scheme for computation of multicomponent compressible flow in porous media, *in: Numerical Mathematics and Advanced Applications 2011, Proceedings of ENUMATH 2011*, Springer-Verlag, Berlin, Heidelberg, 559–567.

[85] Quarteroni, A., Sacco, R., Saleri, F. (2000), *Numerical Mathematics*, Springer-Verlag, New York.

[86] Quiñones-Cisneros, S.E., Deiters, U.K. (2012), An efficient algorithm for the calculation of phase envelopes of fluid mixtures, *Fluid Phase Equilibria* 329(15), 22–31.

[87] Rachford H.-H., Rice J.D. (1952), Procedure for use of electronic digital computers in calculating flash vaporization hydrocarbon equilibrium, *Trans Am Institute Mining Metallurg Eng.*, 195:327–328.

[88] Raviart, P., Thomas, J. (1977), *A Mixed Hybrid Finite Element Method for the Second Order Eliiptic Problem, Lect. Notes Math. Ser., vol. 606,* Springer, New York.

[89] Russel, T. F., Wheeler, M. F. (1983), *Finite Element and Finite Difference Methods for Continuous Flows in Porous Media*, in The Mathematics of Reservoir Simulation, Frontiers in Applied Mathematics, 35–106, SIAM, Philadelphia.

[90] Saber, N., Shaw, J. M. (2008), Rapid and robust phase behaviour stability analysis using global optimization, *Fluid Phase Equilibria*, 264:137–146.

[91] Sammon, P., H. (1988), An Analysis of Upstream Differencing, *SPE Reservoir Engineering*, August 1988, 1053–1056.

[92] Souza, A. T., Cardozo-Filho, L., Wolff, F., Guirardello, R. (2006), Application of interval analysis for Gibbs and Helmholtz free energy global minimization in phase stability analysis, *Brazilian Journal of Chemical Engineering*, 23(1):117–124.

[93] Sun, S., Firoozabadi, A., Kou, J. (2012), Numerical modeling of two-phase binary fluid mixing using mixed finite elements, *Computational Geosciences*, 16(4), 1101–1124.

[94] Trangenstein, J. A., Bell, J. B. (1989), Mathematical structure of compositional reservoir simulation, *SIAM Journal on Scientific and Statistical Computing*, 10(5), 817–845.

[95] Watts, J. W. (1986), A compositional formulation of the pressure and saturation equations, *SPE Reservoir Engineering*, 1:243–252.

[96] Wilson G.-M. (1969), A Modified Redlich-Kwong Equation of State, Application to General Physical Data Calculation, *paper No. 15C presented at the 1969 AIChE 65th National Meeting, Cleveland, Ohio, May 4–7, 1969*.

[97] Younes, A., Ackerer, P., Lehmann, F. (2006), A new mass lumping scheme for the mixed hybrid finite element method, *Int. J. Numer. Meth. Engng*, 67:89–107.

[98] Younes, A., Fahs, M., Ahmed, S. (2009), Solving density driven flow problems with efficient spatial discretizations and higher-order time integration methods, *Advances in Water Resources*, 32:340–352.

[99] Young, L.-C., Stephenson, R. E. (1983), A Generalized Compositional Approach for Reservoir Simulation, *SPE Journal*, 23(5), 727–742.